WATER IN SILICATE GLASSES

Thesis by

Lynn Alison Silver

In Partial Fulfillment of the Requirements

for the Degree of

Doctor of Philosophy

California Institute of Technology

Pasadena, California

1988

(Submitted August 27, 1987)

Acknowledgements

The work included in this thesis was completed with the help of Dr. P. Dobson, Dr. G. Fine, Dr. H. Eckert, Phil Ihinger, Dr. S. Newman and Paula Rosener. I would like to express my thanks to Prof. A. Boettcher, Prof. S. Epstein and Prof. P. Wyllie for the use of their laboratories; to Dr. K. Burke for financial support for work completed at the Johnson Space Center; and to Paul Hawley for his help with the preparation of this document.

I have enjoyed and benefited from daily interactions with Dr. J. Beckett, Jen Blank, Dr. M. Carroll, Dr. G. Mattioli, Greg Miller and Prof. G. Rossman. I would like to thank my husband John and my parents for their support and encouragement especially on those numerous occasions when the end seemed to be nowhere in sight.

I also want to thank my thesis advisor, Ed Stolper, Professor of Geology, for all his help and for all he has taught me; I hope that I will enjoy my future scientific pursuits as much as he does his.

This work was supported by NSF Grants EAR-8212765, EAR-8417434 and EAR-8618229 and by the donors of the Petroleum Research Fund, administered by the American Chemical Society (Grant 17737-AC2).

Abstract

The speciation of water in a variety of hydrous silicate glasses, including simple and rhyolitic compositions, synthesized over a range of experimental conditions with up to 11 weight percent water has been determined using infrared spectroscopy. This technique has been calibrated with a series of standard glasses and provides a precise and accurate method for determining the concentrations of molecular water and hydroxyl groups in these glasses.

For all the compositions studied, most of the water is dissolved as hydroxyl groups at total water contents less than 3-4 weight percent; at higher total water contents, molecular water becomes the dominant species. For total water contents above 3-4 weight percent, the amount of water dissolved as hydroxyl groups is approximately constant at about 2 weight percent and additional water is incorporated as molecular water. Although there are small but measurable differences in the ratio of molecular water to hydroxyl groups at a given total water content among these silicate glasses, the speciation of water is similar over this range of composition. The trends in the concentrations of the H-bearing species in the hydrous glasses included in this study are similar to those observed in other silicate glasses using either infrared or NMR spectroscopy.

The effects of pressure and temperature on the speciation of water in albitic glasses have been investigated. The ratio of molecular water to hydroxyl groups at a given total water content is independent of the pressure and temperature of equilibration for albitic glasses synthesized in rapidly quenching piston cylinder apparatus at

temperatures greater than 1000°C and pressures greater than 8 kbar. For hydrous glasses quenched from melts cooled at slower rates (i.e., in internally heated or in air-quench cold seal pressure vessels), there is an increase in the ratio of molecular water to hydroxyl group content that probably reflects reequilibration of the melt to lower temperatures during slow cooling.

Molecular water and hydroxyl group concentrations in glasses provide information on the dissolution mechanisms of water in silicate liquids. Several mixing models involving homogeneous equilibria of the form $H_2O + O = 2OH$ among melt species have been explored for albitic melts. These models can account for the measured species concentrations if the effects of non-ideal behavior or mixing of polymerized units are included, or by allowing for the presence of several different types of anhydrous species.

A thermodynamic model for hydrous albitic melts has been developed based on the assumption that the activity of water in the melt is equal to the mole fraction of molecular water determined by infrared spectroscopy. This model can account for the position of the water-saturated solidus of crystalline albite, the pressure and temperature dependence of the solubility of water in albitic melt, and the volumes of hydrous albitic melts. To the extent that it is successful, this approach provides a direct link between measured species concentrations in hydrous albitic glasses and the macroscopic thermodynamic properties of the albite-water system.

The approach taken in modelling the thermodynamics of hydrous albitic melts has been generalized to other silicate compositions.

Spectroscopic measurements of species concentrations in rhyolitic and simple silicate glasses quenched from melts equilibrated with water vapor provide important constraints on the thermodynamic properties of these melt-water systems. In particular, the assumption that the activity of water is equal to the mole fraction of molecular water has been tested in detail and shown to be a valid approximation for a range of hydrous silicate melts and the partial molar volume of water in these systems has been constrained. Thus, the results of this study provide a useful thermodynamic description of hydrous melts that can be readily applied to other melt-water systems for which spectroscopic measurements of the H-bearing species are available.

Preface

The first three chapters of this thesis comprise a revised version of a paper submitted to Journal of Petrology. Chapters 4 and 5 are a condensed version of a paper soon to be submitted. Appendices 3-5 are other papers that I was involved with while at Caltech: Appendix 3 is a paper from Journal of Geology and is referred to in the text as Silver & Stolper (1985); Appendix 4 is a published paper in Geochimica Cosmochimica Acta and is referred to in the text as McMillan et al. (1983); and Appendix 5 is the final version of a paper to be submitted to Journal of Chemical Physics and is referred to in the text as Eckert et al. (1987b).

Table of Contents

Introduction

Experimental petrologists have studied the influence of water on the physical and chemical properties of hydrous silicate melts for more than fifty years (Goranson, 1931, 1936). Despite the enormous volume of literature devoted to this subject, interest in these problems has not waned, as evidenced by the fact that in just the past two years there have been four new publications reporting on the effects of water on phase equilibria in hydrous albitic melts alone (Goldsmith & Jenkins, 1985; Hamilton & Oxtoby, 1986; Blamart et al., 1986; Richet et al., 1986). Although the early studies have stood up to a remarkable degree, it is not surprising that petrologists have returned again and again to investigate the effects of water on the physical and chemical properties of silicate melts given the abundant evidence of the importance of water in the evolution of terrestrial igneous systems.

Until recently, experimental investigations of water-bearing melts have focused on their bulk, macroscopic properties; for example, measurements of water solubility and of the effects of water pressure on solid-liquid phase equilibria, or of the effects of dissolved water on transport properties such as viscosity, electrical conductivity, and diffusivities of water and other components in hydrous melts and glasses (e.g., Burnham, 1975, 1979; Watson, 1981; Takata et al., 1981; Karsten et al., 1982). Although they provide ample documentation of the influence of water on the properties of silicate melts and have been widely used to constrain thermodynamic models of hydrous silicate melts, these studies give few direct insights into the molecular level interactions that take place when water dissolves in molten silicates.

In recent years, petrologists have turned increasingly to spectroscopic studies of hydrous glasses to provide such insights and to understand better how water affects the physical and chemical properties of magmas. In particular, infrared spectroscopy on water-bearing glasses can be used to distinguish between water that is dissolved as molecules of water and that dissolved as hydroxyl groups in silicate glasses and can provide a quantitative method for determining the concentrations of these hydrous species. In addition, spectroscopic studies of H-bearing species in hydrous systems can provide information on their motional properties and the changes in the silicate framework accompanying the dissolution of water can be ascertained (Bartholomew et al., 1980; Bartholomew & Schreurs, 1980; Wu, 1980; Mysen et al., 1980; Mysen & Virgo, 1980, 1986a,b; Stolper, 1982a; McMillan et al., 1983, 1986; McMillan & Remmele, 1986; Eckert et al., 1987a,b; Farnan et al., 1987).

In this thesis, I report the results of an investigation of the speciation of water in a variety of hydrous silicate glasses quenched from melts equilibrated over a range of pressures and temperatures using infrared spectroscopy. The spectroscopic measurements of species concentrations in these glasses are used to develop thermodynamic models for hydrous silicate liquids that are based on the assumption that the activity of water is equal to the mole fraction of molecular water determined spectroscopically. These models are discussed in detail for hydrous albitic melts and then generalized to a variety of melt compositions. To the extent that the approach taken in this study is successful, it provides a direct and quantitative link between

measurements of microscopic characteristics of silicate melts -- that is, of species concentrations -- and descriptions of their macroscopic physical and chemical properties.

In Chapter 1, the infrared spectroscopic technique is used to measure the concentrations of molecular water and hydroxyl groups in hydrous albitic glasses synthesized under various conditions with up to 11 weight percent water. The effects of pressure, temperature and cooling rates on the speciation of water in these glasses is also investigated.

In Chapter 2, the spectroscopic measurements of the concentrations of molecular water and OH groups in albitic glasses are used to constrain four mixing models involving the homogeneous equilibria among melt species of the form $H_2O + O = OH$. These models are considered with the view that if the species concentrations predicted by these models can account for the spectroscopic data, then they may provide insights into the dissolution mechanisms for water in silicate melts.

In Chapter 3, a thermodynamic model of the heterogeneous equilibria between melt, vapor, and crystalline albite following the approach outlined in Stolper (1982b) and Silver & Stolper (1985) is developed. The variations in the concentrations of molecular water as a function of the total dissolved water content provide a basis for rationalizing phase equilibria, such as water solubility and the freezing-point depression in the albite-water system.

In Chapter 4, the speciation of water in a variety of silicate glasses is investigated and the influence of bulk composition is discussed. In Chapter 5, the approach used in modelling the

thermodynamic properties of hydrous albitic melts, based on the approximation that the activity of water is equal to the mole fraction of molecular water, is applied to other melt compositions. Spectroscopic measurements of molecular water contents in hydrous glasses quenched from water-saturated melts are used to evaluate the validity of this activity-composition model and to constrain the thermodynamic properties of these melt-water systems.

Chapter 1. The Speciation of Water in Albitic Glasses

In this chapter, the calibration of the infrared spectroscopic technique, based on determination of the extinction coefficients of the infrared absorbance bands in glasses due to the presence of dissolved molecules of water and hydroxyl groups, is used to measure the concentrations of molecular water and OH groups in hydrous albitic glasses synthesized under various conditions. This study comprises two sets of experiments: the synthesis of hydrous albitic glasses in (1) piston cylinder apparatus at pressures between 8 and 25 kbar and temperatures between 1000 and 1600°C, and (2) internally heated pressure vessels at pressures between 1 and 7 kbar and temperatures between 950 and 1150°C. The effects of pressure, temperature and cooling rates on the speciation of water are also discussed.

Experimental Methods

The starting materials used in this study were glasses prepared from crystalline Amelia albite or a synthetic oxide mixture of albite composition. Amelia albite was ground in agate to a powder under ethanol and then dried at 800°C and 1 atm for 24 h to remove any hydrocarbon residue; the powdered albite was melted in air at 1 atm and 1300°C and quenched to glass; the glass was then finely ground and heated at 800°C as described above. The synthetic oxide mixture was prepared by grinding appropriate amounts of Na_2CO_3, Al_2O_3, and SiO_2 (Johnson-Matthey SpecPure Reagents) in agate under ethanol for 6 h; this mixture was then melted in air at 1200°C for 1 h and quenched to glass; the glass was ground under ethanol and heated as described above. Both batches of starting materials were stored over dessicant.

Major element concentrations were measured on selected glass samples by electron microprobe to assess glass homogeneity, to verify glass compositions and to determine the extent of sodium loss during the drying process. The glasses were analyzed with a JEOL 733 electron microprobe, with an accelerating voltage of 15 KV, a beam current of 5 nA, and a 20-25 micron spot size. The analyses are listed in Table 1.

Hydrous glasses were synthesized by quenching from melts held at elevated pressure and temperature. Most of the glass samples were synthesized in a piston cylinder apparatus at Caltech. The powdered starting materials together with known amounts of triply-distilled deionized H_2O were weighed into Pt capsules, which were then sealed by arc-welding. These capsules were run in a 0.5-inch solid-media piston cylinder apparatus using a NaCl or talc cell with a pyrex sleeve at pressures between 8 and 25 kbar and temperatures between 1000 and 1600°C (see Fine & Stolper, 1985, for experimental details). In all but one case, the capsules were held at constant pressure and temperature for the duration of the run; one experiment (ABC-34) was held at 13 kbar, 1200°C for 0.5 h, then the pressure was decreased to 8 kbar, and the sample was held at this lower pressure for 2 h. At the end of most experiments, the power was shut off and the run cooled at a rate of 150-200°C/s to 100°C (unless otherwise noted). Several runs were cooled at controlled cooling rates (0.3-2.5°C/s) using a Eurotherm Model 125 programmer. All of the run conditions are listed in Table 2.

Two samples (JRH-1, JRH-2) were synthesized in a piston cylinder apparatus in Professor Holloway's laboratory at the Arizona State University and are described in McMillan et al. (1983). Several samples

Table 1. Anhydrous glass compositions

TABLE 1

Anhydrous Glass compositions[1]

	Amelia Albite	Synthetic Albite
SiO_2	68.05	70.19
Al_2O_3	19.98	19.18
FeO	0.03	0
CaO	0.16	0
K_2O	0.18	0
Na_2O	11.60	10.63
TOTAL	100	100

Notes:
1. Reported values are based on average of 10 individual electron microprobe analyses per sample, and are given in weight percent.

Table 2. Hydrous albitic glasses: Piston cylinder experiments

TABLE 2 Hydrous albitic glasses: Piston cylinder experiments[1]

SAMPLE #	starting material	P (kb)	T (C)	time (min)	amt H2O added	Density[2] (g/l)		H2O,mol wt %	OH wt %	H2O,tot[4] sum(wt%)	H2O (total) (wt%)		REMARKS[6]	mole fractions[7] X(B)	X(H2O)	X(OH)
ABC-34	Am.ab	8	1200	120	7	2400	e	3.23	2.04	5.27			c,f	0.092	0.056	0.071
AVS-4	syn.ab	10	1000	130	20[5]	2425	h	0.75	1.54	2.29			f	0.041	0.013	0.055
JIH 1	syn.gel	10	1200	240	5	2391	e	2.29	1.99	4.29			a,c	0.075	0.040	0.070
JIH 2	syn.gel	10	1200	240	10	2350	e	4.38	1.92	6.30			a,c	0.109	0.076	0.066
ALB-3378	fused ab	15	1100	120	5	2410	d	2.67	1.98	4.65	4.76* (.14),	4.6**(.23)	b,f,u	0.081	0.047	0.069
ALB-3403	fused ab	15	1100	30	8	2320	e	4.55	2.01	6.56		6.8**(.34)	b,f,u	0.113	0.079	0.069
LMS-26	Am.ab	15	1200	120	6	2385	h	2.45	2.02	4.47			f	0.079	0.043	0.071
ALB-3388	fused ab	15	1225	120	3	2430	d	1.26	1.74	3.00	2.9* (.06),	2.9**(.15)	b,f,u	0.053	0.022	0.062
ALB-3399	fused ab	15	1350	30	1	2475	d	0.13	0.85	0.98			b,f,u	0.018	0.002	0.031
LMS-27	Am.ab	15	1400	120	3	2490	h	0.00	0.10	0.10			c,f	0.002	0.000	0.004
A1003	syn.ab	15	1400	130	7	2490	e	0.00	0.10	0.10			f	0.002	0.000	0.004
A1009	Am.ab	15	1400	80	3	2425	h	0.71	1.50	2.22			c,f	0.040	0.013	0.054
A1010	Am.ab	15	1400	75	5	2410	h	1.20	1.77	2.97			c,f	0.053	0.021	0.063
LMS-19	Am.ab	15	1400	120	5	2410	h	1.84	1.90	3.74			c,x	0.066	0.033	0.067
LMS-20	Am.ab	15	1400	120	7	2400	e	1.99	1.96	3.95			c,w	0.070	0.035	0.069
LMS-11	Am.ab	15	1400	120	5	2400	h	1.94	2.05	3.99			c,f	0.070	0.034	0.072
LMS-9	Am.ab	15	1400	120	5	2400	e	2.04	2.06	4.11			c,z	0.072	0.036	0.073
LMS-18	Am.ab	15	1400	120	5	2385	h	2.33	2.14	4.48			f,c,y	0.079	0.041	0.075
A1012	Am.ab	15	1400	120	16[5]	2375	e	2.66	2.02	4.68			c	0.082	0.047	0.071
A1008	Am.ab	15	1400	85	6	2367	h	3.59	2.08	5.67			c,f	0.099	0.062	0.072
A1011	Am.ab	15	1400	153	11	2330	h	4.58	2.20	6.78			f	0.117	0.079	0.076
LMS-22	Am.ab	15	1400	120	8	2325	h	4.69	2.30	6.99			f	0.120	0.081	0.079
LMS-23	Am.ab	15	1400	120	8	2300	e	6.00	2.40	8.41			c	0.143	0.102	0.082
LMS-21	Am.ab	15	1400	120	9	2280	e	7.40	2.26	9.65			c	0.163	0.125	0.076
LMS-29	Am.ab	15	1600	45	7	2420	h	1.19	1.71	2.90			f	0.052	0.021	0.061
AVS-7	syn.ab	19	1000	130	19[5]	2325	e	5.11	2.35	7.46			c	0.128	0.088	0.081
ABC-22	Am.ab	20	1400	180	4	2475	e	0.00	0.18	0.18			f	0.003	0.000	0.006
ABC-12	Am.ab	20	1400	437	2	2475	h	0.00	0.21	0.21			f	0.004	0.000	0.008
ABC-10	Am.ab	20	1400	437	4	2475	h	0.00	0.27	0.27			c,f	0.005	0.000	0.010
ABC-21	Am.ab	20	1400	120	1	2475	d	0.07	0.74	0.81	0.96* (.02),	1.05**(.05)	b,f,u	0.015	0.001	0.027
CAB-1	Am.ab	20	1400	314	5	2456	d	0.15	0.84	0.99			c	0.018	0.003	0.030
CAB-5	Am.ab	20	1400	300	1	2490	d	0.16	0.86	1.02	0.88* (.03)	**	c	0.018	0.003	0.031
ABC-26	Am.ab	20	1400	120	1	2480	d	0.16	0.90	1.06	1.04 (.02),	0.99 (.05)	f	0.019	0.003	0.033
ABC-23	Am.ab	20	1400	120	3	2465	e	0.37	1.25	1.62			b,f	0.029	0.007	0.045
ABC-20	Am.ab	20	1400	120	2	2460	h	0.85	1.56	2.41		2.22**(.11)	b,f,u	0.043	0.015	0.056
ABC-13	Am.ab	20	1400	336	3	2435	h	0.96	1.68	2.64	2.54* (.07)		f	0.047	0.017	0.060
CAB-2	Am.ab	20	1400	314	3	2454	d	0.94	1.71	2.65			c,f	0.047	0.017	0.061
CAB-3	Am.ab	20	1400	314	7	2392	d	1.59	1.97	3.55			c,f	0.063	0.028	0.070
CAB-4	Am.ab	20	1400	330	6	2419	d	2.57	2.08	4.65			c,f	0.082	0.045	0.073
ABC-11	Am.ab	20	1400	336	7	2385	h	2.86	2.08	4.94	4.93* (.2)		c,f	0.086	0.050	0.073
A101	syn.ab	20	1400	275	5	2375	e	3.08	1.95	5.03			c	0.088	0.054	0.068
ABC-9	Am.ab	20	1400	365	6	2385	h	3.00	2.12	5.12	4.94* (.14)		f	0.089	0.052	0.074
ABC-14	Am.ab	20	1400	390	8	2325	h	4.56	2.27	6.83	6.90* (.14)		c,f	0.118	0.079	0.078
CAB-6	Am.ab	20	1400	300	10	2328	d	5.10	2.23	7.34			c,f	0.126	0.088	0.077
ABC-15	Am.ab	20	1500	240	8	2335	h	4.32	2.14	6.47			f	0.112	0.075	0.074
ABC-17	Am.ab	20	1600	140	6	2460	h	0.12	0.90	1.02			f	0.018	0.002	0.032
A100	syn.ab	25	1400	240	5	2410	e	2.00	2.01	4.01			c	0.071	0.035	0.071

Notes:
(1) epsilon values: e(5218 cm-1)=1.67, e(4485 cm-1)=1.13 l/mol-cm
(2) Density measurements: h= made with heavy liquids (error: 25 g/l)
d=density measured with Berman balance (error: 10-20 g/l)
e=density estimated (error: 30 g/l)
(3) * total H2O contents measured by H2 manometry
** total H2O contents measured by NMR
(4) total H2O contents determined from sum of molecular H2O and OH,
reported H2O content is average of several analyses
(5) amount of water added sufficient to saturate sample
(6) a=samples synthesized at ASU, u=samples synthesized at UCLA, b=used boron nitride assemblies
Infrared spectra taken with: c=Cary 17 spectrometer, f=Nicolet FTIR spectrometer
Cooling rate = 150 deg/s, unless indicated: w=0.27 C/s, x=0.54 C/s, y=1.11 C/s, z=2.5 C/s
(7) mole fractions calculated as follows:
X(B)=mole fraction of H2O,total = (wt%H2O/18)/(wt%H2O/18+(100-wt%H2O)/32.78)
X(H2O)=mole fraction of molecular H2O = (wt%H2O,mol/18)/(wt%H2O/18+(100-wt%H2O)/32.78)
X(OH)=mole fraction of hydroxyl = 2(X(B)-X(H2O,mol))

were synthesized in Professor Boettcher's laboratory at the University of California, Los Angeles, in a one-inch piston cylinder apparatus, using a NaCl and boron nitride (BN) assembly (ALB-3378, ALB-3388, ALB-3399, ALB-3403, ABC-20, ABC-21) or a NaCl and fired pyrophyllite assembly (ABC-26). Synthesis conditions for all of these samples are described in Table 2.

Several samples were synthesized in internally heated pressure vessels (IHPV). Powdered starting materials were sealed in Pt or Au capsules with known amounts of triply-distilled water and held at pressures between 1 and 7 kbar and temperatures between 1000 and 1150°C in a 3/4-inch bore IHPV at the Johnson Space Center, using the setup described by Holloway (1971). The pressure medium was Ar gas and the temperature was controlled using a Pt-10%Rh vs. Pt thermocouple. At the conclusion of the run, the power was shut off, and the run cooled isobarically at 180-240°C/min. The run conditions are listed in Table 3. Sample A78-56 is from Dr. John Delaney (synthesized in an IHPV in Professor Holloway's laboratory) and has been previously reported on by Stolper (1982a), and the run conditions are listed in Table 3.

Doubly-polished thin sections of the run products were prepared for the infrared spectroscopic work as described by Newman et al. (1986). The sample thicknesses were measured using a digital dial indicator. Pellets were prepared for selected samples by pressing 0.5 mg finely ground glass mixed with 200 mg KBr into a disc; transmission spectra in the mid-infrared region were obtained on these pellets. For most samples, glass densities were measured on bubble-free glass fragments using a Berman balance and weighing in air and in toluene, or by a

Table 3. Hydrous albitic glasses:

Internally heated pressure vessel experiments

TABLE 3 Hydrous albitic glasses: IHPV experiments [1]

SAMPLE #	starting material	P (kb)	T (C)	Time (hrs.)	amt H2O added [5]	Density (g/l) [2]	H2O,mol (wt %)	OH (wt %)	H2O,tot (wt %) [3]	REMARKS [4,6,7]	mole fractions [8] X(B)	X(H2O)	X(OH)
G 1	Am.ab	0.99	1150	23	12.8	2475 e	0.00	0.21	0.21	c,j,leaked,xtl	0.004	0.000	0.008
G 2	Am.ab	0.99	1150	23	11.75	2410 d	2.49	1.66	4.15	c,j,ex H2O	0.073	0.044	0.057
Ab 12	Am.ab	2.00	1150	144	13.9	2345 e	4.33	1.94	6.28	c,j,bb-free	0.109	0.076	0.065
Ab 12	Am.ab	2.00	1150	144	13.9	2345 e	4.46	1.87	6.33	c,j,bb-rich	0.109	0.078	0.062
G 3	Am.ab	2.03	1150	22	9.6	2435 e	1.35	1.57	2.92	c,j,ex v	0.052	0.024	0.055
G 5	Am.ab	2.28	1150	19	3.3	2475 e	0.00	0.13	0.13	c,j,gl,bb	0.002	0.000	0.005
G 4	Am.ab	2.28	1150	19	12.7	2410 e	2.49	1.75	4.24	c,j,leaked,xtl	0.075	0.044	0.060
G 4	Am.ab	2.28	1150	19	12.7	2410 e	2.70	1.94	4.64	c,j,leaked,xtl	0.081	0.048	0.066
A78-56	syn. gel	3.00	950			2300 h	4.89	1.98	6.87	c,f,a	0.118	0.085	0.066
G 6	Am.ab	3.68	1150	24	13.1	2290 e	6.54	2.18	8.72	c,j,ex v	0.148	0.113	0.070
G 7	Am.ab	3.68	1150	24	12.2	2264 h	7.34	2.11	9.45	c,j,ex H2O,bb	0.160	0.126	0.067
G 7	Am.ab	3.68	1150	24	12.2	2264 h	7.53	2.23	9.76	c,j,ex H2O,bb	0.164	0.129	0.071
F 3	syn.ab	4.97	1000	5	3.1	2354 d	1.63	1.91	3.54	c,j,	0.063	0.029	0.067
F 4	syn.ab	4.97	1000	6	7.1	2282 d	5.19	2.29	7.48	c,j,few bb	0.128	0.091	0.075
G 8	Am.ab	5.00	1150	24	12.9	2415 e	2.23	1.92	4.15	c,j,ex v,few bb	0.073	0.040	0.066
Ab 2	Am.ab	5.00	1150	144	4.7	2410 e	2.79	1.75	4.53	c,j,bb-rich	0.080	0.050	0.060
Ab 2	Am.ab	5.00	1150	144	4.7	2410 e	2.80	1.79	4.59	c,j,bb-free	0.080	0.050	0.061
Ab 3	Am.ab	5.00	1150	144	7	2365 e	4.01	1.79	5.80	c,j,bb-free	0.101	0.071	0.060
Ab 6	Am.ab	5.00	1150	144	14.4	2300 e	6.39	1.55	7.94	c,j,bb-free	0.136	0.111	0.050
Ab 5	Am.ab	5.00	1150	144	9.8	2300 e	6.27	2.00	8.27	c,j,few bb	0.141	0.109	0.065
Ab 6	Am.ab	5.00	1150	144	14.4	2300 e	7.36	1.43	8.79	c,j,bb-rich	0.149	0.126	0.046
G 10a	Am.ab	5.00	1150	24	12.6	2260 e	7.90	1.87	9.77	c,j,gl,bb-rich	0.165	0.135	0.059
G 10x	Am.ab	5.00	1150	24	12.6	2260 e	7.99	2.05	10.04	c,j,gl+xtls	0.169	0.136	0.065
F 8	syn.ab	5.03	1000	7	8.9	2300 d	5.60	1.86	7.46	c,j,	0.128	0.097	0.061
F 8	syn.ab	5.03	1000	7	8.9	2301 d	6.40	1.79	8.19	c,j,bb-rich	0.140	0.111	0.058
F 8	syn.ab	5.03	1000	7	8.9	2301 d	6.40	1.86	8.26	c,j,few bb	0.141	0.111	0.060
F 8	syn.ab	5.03	1000	7	8.9	2301 d	6.60	1.98	8.58	c,j,bb-free	0.146	0.114	0.064
G 11	Am.ab	7.00	1150	24	14.3	2260 e	8.19	1.95	10.14	c,j,ex H2O,bb	0.170	0.140	0.061
G 9	Am.ab	7.00	1150	24	12.7	2260 e	8.41	2.04	10.45	c,j,ex H2O,xtl,gl+bb	0.175	0.143	0.064
G 9	Am.ab	7.00	1150	24	12.7	2260 e	8.44	2.77	11.21	c,j,bb	0.187	0.144	0.086

Notes: (1) epsilon values: e(5218 cm-1)=1.67 l/mol-cm, e(4485 cm-1)=1.13 l/mol-cm
(2) Densities measurements: h=heavy liquids, d=Berman balance (error: 25 g/l)
e=densities estimated (error: 40 g/l)
(3) Total water contents determined from sum of molecular H2O and OH
(4) Infrared spectra taken using:c=Cary 17 spectrophotometer,f=FTIR
for samples containing bubbles, several spots were analyzed to assess differences in H2O contents
(5) amount of water added sufficient to saturate sample , except for A78-56, Ab2, Ab3, F3, F4, and G5
(6) Samples synthesized at: a=ASU, j=Johnson Space Center
(7) bb=bubbles, ex v=vapor escaped when charge opened, gl=glass, xtl=charge was partly crystalline
(8) mole fraction calculation, see footnote, TABLE 2

float-sink method using heavy liquids of known density. For samples that contained bubbles, densities were estimated by comparison with samples with similar water contents for which the densities had been measured.

Transmission infrared spectra were taken using either a Cary 17 (2500-8000 cm^{-1}) or a Nicolet 60SX FTIR spectrophotometer (400-8000 cm^{-1}). The Nicolet FTIR uses a W source, CaF_2 beamsplitter and an InSb detector (1850-8000 cm^{-1}) and a Globar source, KBr beamsplitter and a $HgCdTe_2$ detector (400-5000 cm^{-1}), with a resolution of 2-4 cm^{-1}, a mirror velocity of 1.57 cm/s, and 512-2048 scans.

Total water contents for nine albitic glasses were determined by the hydrogen manometric technique described by Newman et al. (1986). Total water contents of six samples were determined by nuclear magnetic resonance (NMR) spectroscopy, using the method described by Eckert et al. (1987b).

Infrared Spectroscopy

Band Assignments

Infrared spectra (1500-3800 cm^{-1}): Figure 1 shows the infrared absorption spectrum (1400-3800 cm^{-1}) of a hydrous albitic glass (5.1 wt % H_2O[1]). The two bands of interest in this region peak at 1635 and 3530 cm^{-1}. The band assignments were reviewed by Newman et al. (1986) for rhyolitic glasses: the band at 1635 cm^{-1} is the fundamental bending mode of H_2O molecules; the broad band at 3530 cm^{-1} is due to

---

1. Reported water contents in this section were determined by infrared spectroscopy as described below.

Figure 1. Infrared absorption spectrum of albitic glass, ABC-9, with 5.1 wt % H_2O. Sample thickness is 36 microns. The dashed line represents the spectrum of anhydrous albite glass, scaled to 36 microns.

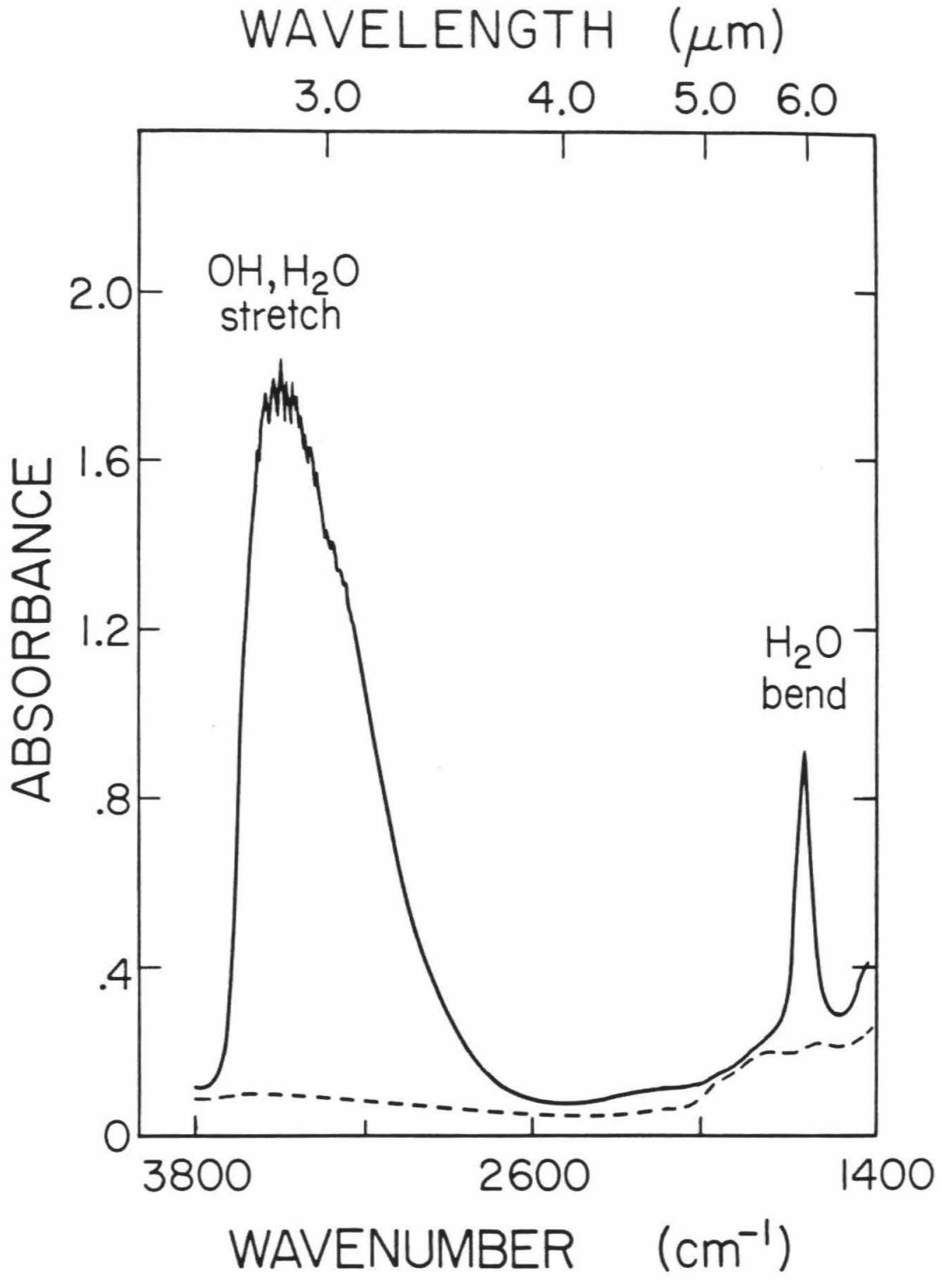
WAVELENGTH (μm)
3.0
4.0
5.0
6.0
OH, H2O
stretch
H2O
bend
ABSORBANCE
2.0
1.6
1.2
.8
.4
0
3800
2600
1400
WAVENUMBER (cm-1)

fundamental OH stretching vibrations. The exact positions of these bands are displaced slightly in albitic glasses relative to rhyolitic glasses, which have absorption maxima at 1630 and 3570 cm^{-1} (Newman et al., 1986). The weak bands observed near 1800 and 1600 cm^{-1} in the anhydrous glass shown in Fig. 1 are due to vibrations of the aluminosilicate network and are unrelated to the hydrogen content.

Figure 2 shows the spectra (2400-4000 cm^{-1}) of five albitic glasses with water contents ranging from 0.1 to 5.1 wt %. The breadth and asymmetry of the band at 3530 cm^{-1} reflects the distribution of hydrogen-bond strengths of the hydroxyl and H_2O groups dissolved in the glasses (Scholze, 1959; Paterson, 1982). The intensity of this band increases with increasing water content with no significant change in band shape over this range of water contents. Although McMillan & Remmele (1986) noted the presence of an additional component at 3450 cm^{-1} in the infrared spectra of silica glasses with high water contents, the infrared spectra (this work) and Raman spectra (McMillan et al., 1983; Mysen & Virgo, 1986b) of hydrous albitic glasses do not show this feature. There is, however, a subtle change in the shape of the 3530 cm^{-1} band with increasing water content: the band becomes narrower in glasses with total water contents greater than 2 wt %. This feature is illustrated in Fig. 3, which compares the 3530 cm^{-1} band shapes of two samples containing 0.1 and 3.55 wt % H_2O, scaled to a constant height at maximum intensity. The band for the sample with the higher water content is narrower than the low water content sample in both the high and low wavenumber regions.

Figure 2. Infrared spectra showing the OH-stretch band for five albitic glasses spanning a range of total water contents. All the samples have been scaled to a constant thickness of 35 microns, and are arranged in order of increasing water content from bottom to top of the figure. Samples shown are LAS-27 (0.1 wt % H_2O), ABC-17 (1.02 wt % H_2O), LAS-29 (2.97 wt % H_2O), CAB-3 (3.55 wt % H_2O), and ABC-9 (5.12 wt % H_2O).

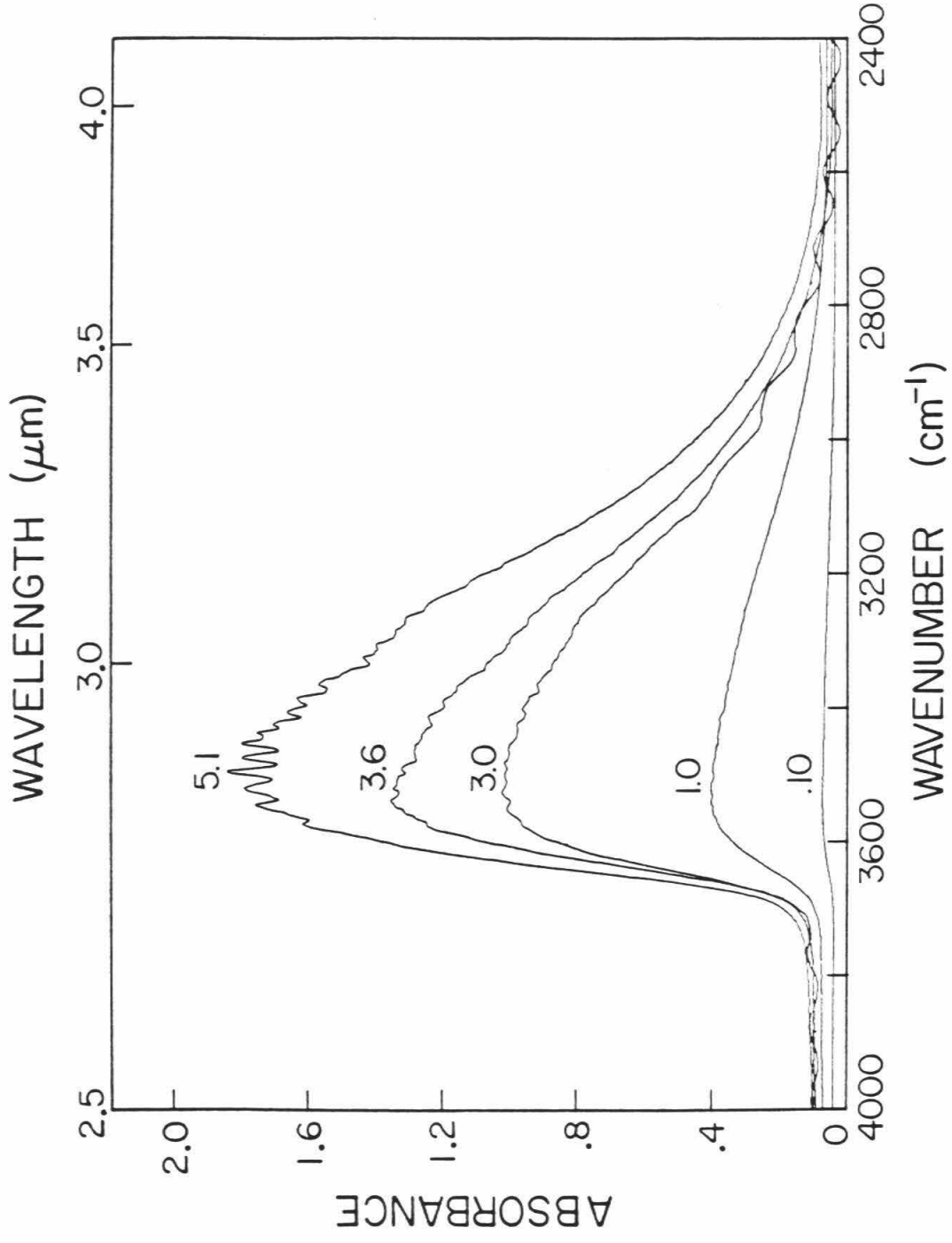
WAVELENGTH (μm)
2.5
3.0
3.5
4.0
ABSORBANCE
2.0
1.6
1.2
.8
.4
0
5.1
3.6
3.0
1.0
.10
4000
3600
3200
2800
2400
WAVENUMBER (cm⁻¹)

Figure 3. Infrared spectra showing the OH-stretch of two albitic glasses with 0.1 (LAS-27) and 3.55 (CAB-3) wt % H_2O. Both spectra have been scaled to the same height at maximum intensity. This band is narrower at both the low and high wavenumber regions in the sample with the higher total water content.

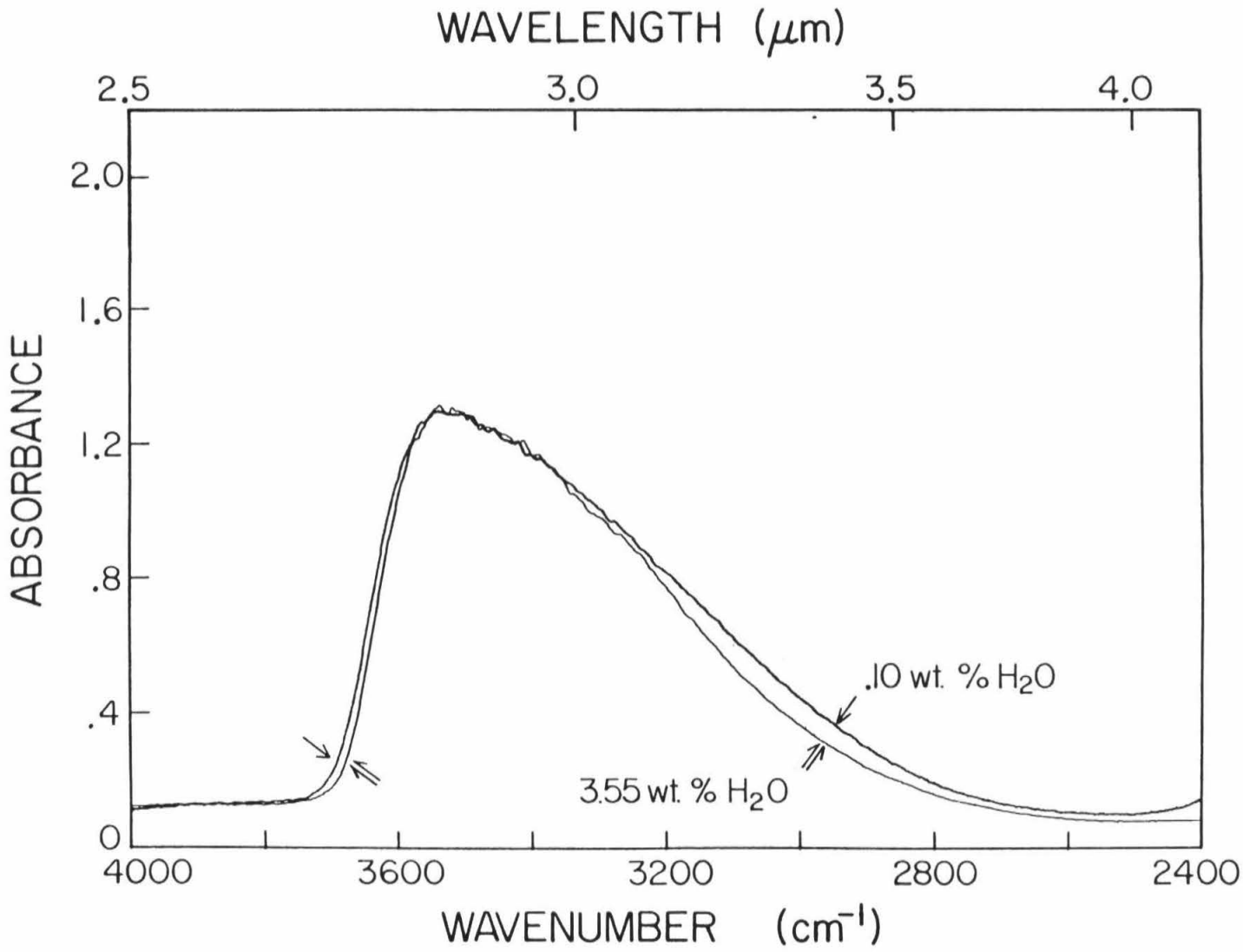
WAVELENGTH (μm)
2.5
3.0
3.5
4.0
2.0
1.6
1.2
.8
.4
0
ABSORBANCE
.10 wt. % H2O
3.55 wt. % H2O
4000
3600
3200
2800
2400
WAVENUMBER (cm-1)

Near-infrared spectra (3800-7600 cm^{-1}): There are four bands of interest in the near-infrared region (Fig. 4). Band assignments are reviewed by Newman et al. (1986) for hydrous rhyolitic glasses. The absorption at 7030 cm^{-1} is the first overtone of the fundamental OH stretching vibration at 3530 cm^{-1}. The band at 5218 cm^{-1} is a combination bend + stretch mode of H_2O molecules. The absorption coefficient of this band is linearly correlated with that of the 1635 cm^{-1} band, with a correlation coefficient of 0.99. The band at 4485 cm^{-1} is a combination mode for Si-OH and Al-OH groups, and other X-OH species may also contribute here. The absorption at 4000 cm^{-1} correlates with total water content (Stolper, 1982a, Fig. 8). Acocella et al. (1984) suggested that the absorption at 4000 cm^{-1} is correlated with the molecular water content (i.e., the intensity of the 5200 cm^{-1} band), but I have found that for hydrous albitic glasses in which only hydroxyl groups were detected, there is measurable intensity at 4000 cm^{-1}. Thus, the interpretation of Stolper (1982a) that both molecular water and hydroxyl groups contribute to this absorption is preferred.

For hydrous albitic glasses with total water contents < 2 wt % that were synthesized using BN-bearing furnace assemblies, the spectra show absorptions at 4125 and 5030 cm^{-1}. The assignment of the 5030 cm^{-1} band is unknown. The band at 4125 cm^{-1} may be due to the presence of dissolved molecular H_2, which has a Raman-active fundamental stretching vibration at 4125 cm^{-1} that has been observed in H-bearing albitic glasses by Raman spectroscopy (Luth et al., 1987). The $^{11}B/^{30}Si$ ratio of sample ABC-21 was determined by ion-microprobe by Dr. I. Hutcheon and indicates a boron content of ~0.3 wt %. In view of the enhanced boron

Figure 4. Near-infrared spectra of four albitic glasses with total water contents up to 7.3 wt.% H_2O, all scaled to a thickness of 300 microns. The samples are arranged in order of increasing water content from bottom to top, and have been offset from each other by 0.04 absorbance units to avoid overlap. Note the continuous increase in intensities of the 5218 and 7030 cm^{-1} bands with increasing water content, whereas the intensity of the 4485 cm^{-1} band increases for water contents up to 4 wt % H_2O, and then remains constant. Samples shown are ABC-17 (1.02 wt % H_2O), A1009 (2.22 wt % H_2O), ABC-9 (5.12 wt % H_2O), and CAB-6 (7.34 wt % H_2O).

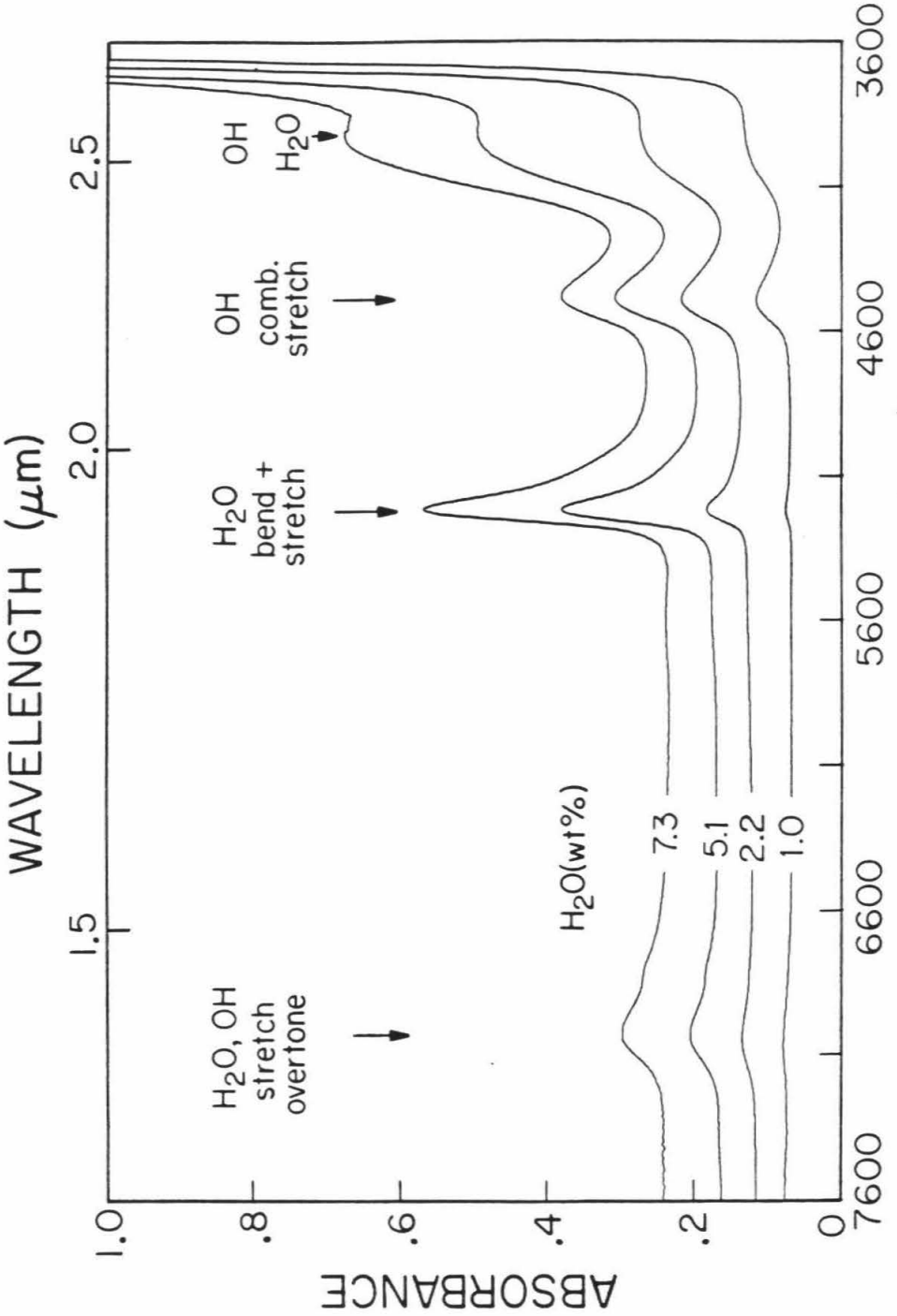
WAVELENGTH (μm)
1.5
2.0
2.5
H2O, OH stretch overtone
H2O bend + stretch
OH comb. stretch
OH
H2O
H2O(wt%)
7.3
5.1
2.2
1.0
ABSORBANCE
1.0
.8
.6
.4
.2
0
7600
6600
5600
4600
3600
WAVENUMBER (cm-1)

content of this experiment, the results of syntheses in BN-bearing assemblies in piston cylinder apparatus should be used with caution. Experiments that utilized BN assemblies are indicated in Table 2.

The near-infrared bands in hydrous albitic glasses are displaced slightly relative to their positions in hydrous rhyolitic and silica glasses. In rhyolitic glasses, the band locations are at 4510, 5240, and 7080 cm^{-1} (Newman et al., 1986). In silica glass the combination mode for Si-OH occurs at 4520 cm^{-1} (L.A. Silver, unpub. results), shifted slightly relative to its position in albitic glasses. There is, however, significant overlap of the bands. The combination mode due to molecular water occurs at 5270 cm^{-1} and the first overtone of the OH stretching fundamental occurs at 7210 cm^{-1} in silica glass (L.A. Silver, unpub. results); both of these modes are shifted to higher energies relative to their locations in albitic glass.

Figure 4 shows the near-infrared spectra (3600-7600 cm^{-1}) of four albitic glasses with water contents ranging from 1.02 to 7.34 wt %. With increasing water content, the bands at 4000, 5218, and 7030 cm^{-1} all increase in intensity. The band at 4485 cm^{-1} increases in intensity with increasing water content up to ~4 wt % total H_2O and then remains approximately constant in intensity at higher total water contents. A low-intensity band appears at high water contents at ~5600 cm^{-1} (not visible in Fig. 4); its intensity appears to be correlated with that of the molecular water band at 5218 cm^{-1}. The assignment of this band is unclear; however, a similar band occurs in the spectrum of liquid water at 5634 cm^{-1} (see Stolper, 1982a, Fig. 12).

The 7030 cm^{-1} overtone of the OH-stretching vibration changes shape

with increasing water content. Figure 5 shows the spectra of five albitic glasses arranged with increasing water contents up to 7.34 wt % in the region 6400-7400 cm^{-1}. There is a distinct shoulder at 6850 cm^{-1} in glasses containing >2.5 wt % H_2O that becomes more pronounced at higher water contents. There is no comparable feature at ~3425 cm^{-1} (i.e., one-half the frequency of this shoulder). A similar feature in the spectra of opals has been attributed to clustering of water molecules (Langer & Flörke, 1974). This feature may thus indicate the onset of clustering of H_2O molecules in the water-rich samples in which most of the water is present as water molecules.

The band at 7030 cm^{-1} is much narrower than twice the band width of the fundamental mode at 3530 cm^{-1}; that is, little overtone intensity is contributed by the strongly hydrogen-bonded OH groups with fundamental stretching frequencies between ~2600 to 3100 cm^{-1}. This is not unexpected given the demonstration by Adams & Douglas (1959) that in hydrous glasses and minerals of a wide variety of compositions, the overtone near 7100 cm^{-1} does not appear when there is strong association, i.e., strongly hydrogen-bonded OH groups.

Mid-infrared spectra (600-1500 cm^{-1}): Figure 6 shows the powder infrared spectra (600-1500 cm^{-1}) of one anhydrous albitic glass and four hydrous albitic glasses embedded in KBr. All of the spectra have been scaled to a constant height of the 1030 cm^{-1} band. It is difficult to use these spectra to obtain quantitative information because of the uncertainties associated with adsorbed water and variable particle size due to uneven grinding. However, in a qualitative way, these spectra permit the identification of important features in this region and are

Figure 5. Infrared spectra showing the first overtone of the OH-stretch band for five albitic glasses with total water contents between 0.8 and 7.3 wt.% H_2O, scaled to a thickness of 300 microns. The samples are arranged in order of increasing water from bottom to top to illustrate the development of the shoulder near 6850 cm^{-1}. Samples shown are ABC-21 (0.81 wt % H_2O), A1009 (2.22 wt % H_2O), A1010 (2.97 wt % H_2O), ABC-9 (5.12 wt % H_2O), and CAB-6 (7.34 wt % H_2O).

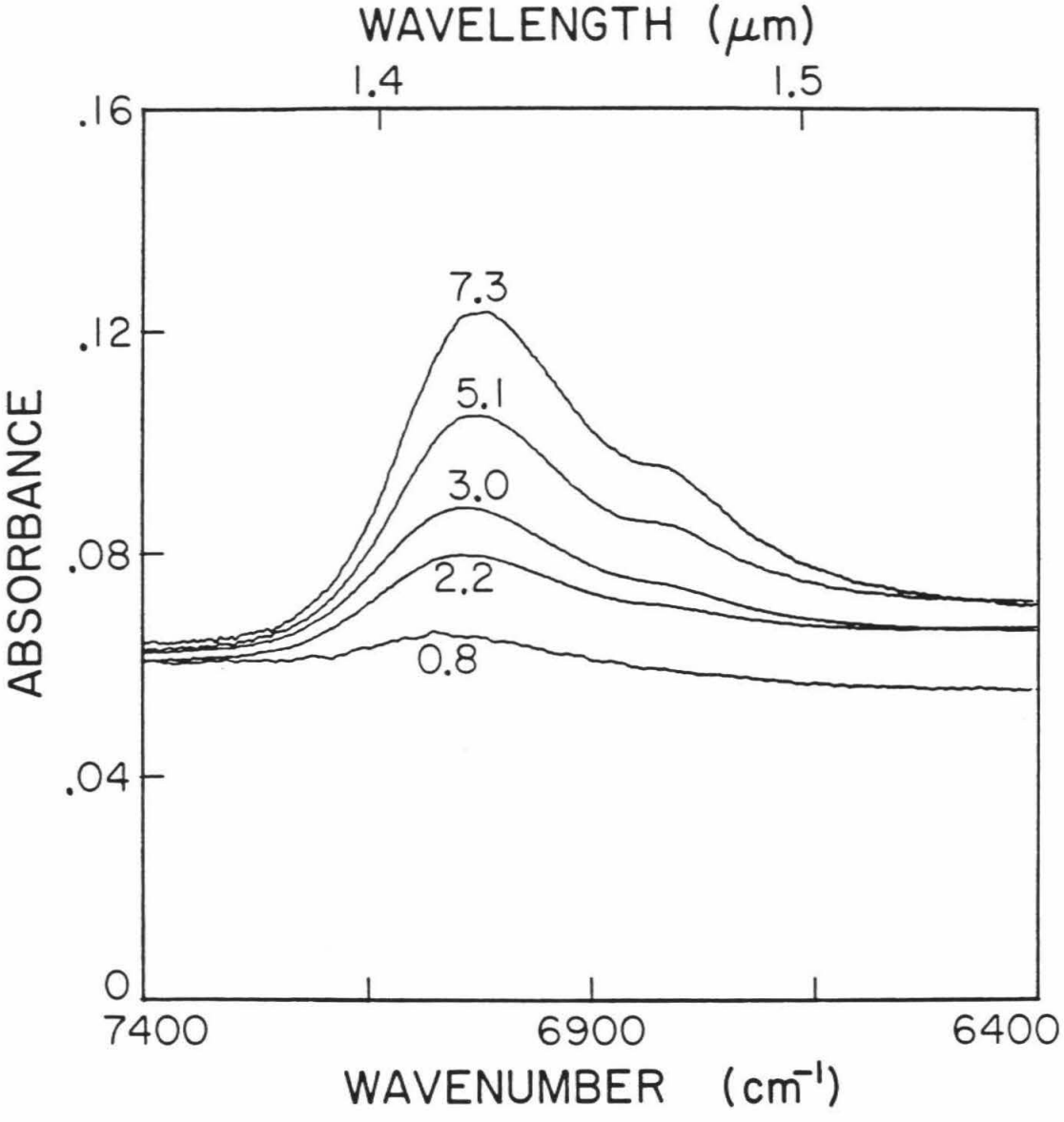
WAVELENGTH (μm)
1.4
1.5
.16
.12
.08
.04
0
ABSORBANCE
7.3
5.1
3.0
2.2
0.8
7400
6900
6400
WAVENUMBER (cm⁻¹)

Figure 6. Infrared spectra of one anhydrous albitic glass and four hydrous albitic glasses with total water contents ranging from 4 to 7 wt % H_2O. Spectra were obtained on disks made by pressing 0.5 mg of finely ground glass into 200 mg of KBr. All the spectra have been scaled to the same height of the 1030 cm^{-1} band, and have been offset by 0.1 absorbance units for clarity. The height of the shoulder at 900 cm^{-1} (noted by the arrow) remains approximately constant relative to the height of the 1000 cm^{-1} band for the samples with total water contents > 4 wt %. Samples shown are LAS-20 (3.95 wt % H_2O), JRH-1 (4.32 wt % H_2O), JRH-2 (6.3 wt % H_2O) and LAS-22 (6.99 wt % H_2O).

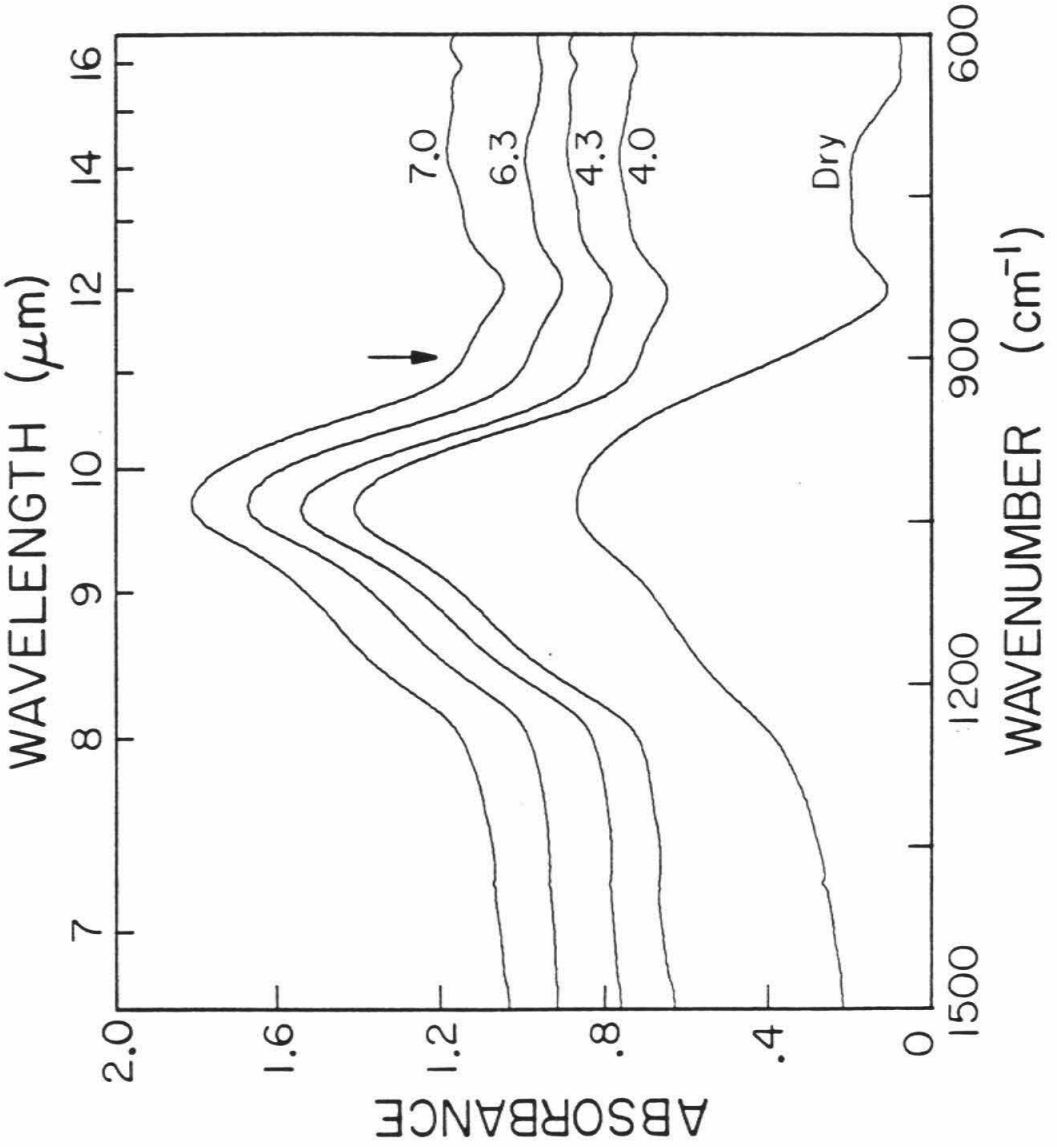
WAVELENGTH (μm)
7
8
9
10
12
14
16
2.0
1.6
1.2
.8
.4
0
ABSORBANCE
1500
1200
900
600
WAVENUMBER (cm⁻¹)
7.0
6.3
4.3
4.0
Dry

comparable to Raman spectra obtained for this region (McMillan et al., 1983).

All of the glasses show a group of broad bands between 850 and 1200 cm^{-1}, with a maximum intensity at 1030-1040 cm^{-1}. The bands in this region have been assigned based on Raman spectra to the symmetric stretching vibrations of tetrahedra associated with 1 to 4 nonbridging oxygens (McMillan et al., 1982) and may also include deformation vibrations of Al-O-H and Si-O-H groups near 1075 cm^{-1} (McMillan et al., 1983).

There is a well-developed shoulder at 900 cm^{-1} that appears in the infrared spectra of hydrous albitic glasses, but is absent from the spectra of dry albitic glass; this band might be due to Si,Al-OH vibrations and may be the mode that, in combination with the OH stretch at ~3500 cm^{-1} is responsible for the Si,Al-OH mode at 4485 cm^{-1} (see above). The 900 cm^{-1} band has roughly a constant intensity relative to the height of the 1030 cm^{-1} band in the hydrous glass spectra illustrated in Fig. 6; as discussed above, the 4485 cm^{-1} band also has roughly a constant intensity for total water contents greater than about 4 weight percent.

The assignment of the 900 cm^{-1} band is not well-established. A similar band has been observed in Raman spectra of hydrous albitic glasses (Mysen et al., 1980; McMillan et al., 1983; Mysen & Virgo, 1986b) and there are at least three different interpretations of it. In hydrous silica glass, there is a Raman and infrared band at 970 cm^{-1}, assigned to Si-OH stretching vibrations (Stolen & Walrafen, 1976). The absence in hydrous albitic glass of a distinct band at 970 cm^{-1} (i.e.,

corresponding to Si-OH groups), and the appearance of the band at 900 cm^{-1} led Remmele et al. (1986) to suggest that the latter band is due to Al-OH groups and that most or all of the hydroxyls in albitic glass are Al-OH. Mysen et al. (1980) deconvolved Raman spectra of hydrous albitic glasses and assigned a band near 880 cm^{-1} to the symmetric O-Si,Al-O stretching vibration and a band near 980 cm^{-1} to the Si-OH stretch. No bands were assigned to Al-OH. Subsequently, Mysen & Virgo (1986b) deconvolved the Raman spectra of hydrous albitic glasses into a second set of bands with locations and assignments differing from their earlier work. This time, no bands assigned to Si-OH or Al-OH vibrations were resolved, but they inferred the presence of Al- and Na-OH groups in hydrous albitic glasses based on mass-balance considerations. Although the interpretation of Remmele et al. (1986) is preferred, at present, the band assignments in this region of the spectra of hydrous albitic glasses are not firmly understood.

Band intensities

Band intensities (i.e., peak heights) were measured for the 4485, 5218 and 7030 cm^{-1} bands for most of the hydrous albitic glasses that were studied. For the 1635 and 3530 cm^{-1} bands, the band intensities are harder to measure unless the samples are very thin or the water concentrations are low, so only selected samples were measured at these frequencies. For the 1635 cm^{-1} band, the band intensities were measured after numerical subtraction of the spectrum of an anhydrous albite glass scaled to the thickness of the water-bearing glass. Integral absorbance measurements (i.e., the area under the absorption peak) were obtained by

numerical integration after background subtraction. Backgrounds for the near-infrared and 3530 cm^{-1} bands were obtained either by estimating a baseline tangent to the spectrum between the minimum on either side of the absorbance band or by generating a computer-fit polynomial baseline. Both methods are arbitrary, but yield similar results and are reproducible. Measured band intensities and integral absorbance measurements are reported in Table 4. Precisions of band intensities are estimated to be on the order of a few percent based on repeated analyses of individual samples, similar to the results of Newman et al. (1986).

The validity of Lambert's law (i.e, that absorbance is proportional to sample thickness) for these samples was confirmed by measuring band intensities on several pieces of the same sample ground to different thicknesses. Figure 7 shows the absorbances of the 4485 and 5218 cm^{-1} bands as functions of sample thickness for three glasses with water contents ranging from 2.64 to 6.83 wt %. The close correspondence of the data shown in Fig. 7 to 45° lines demonstrates that adsorbed water does not contribute significantly to the band intensities in these samples. Although not shown, a similar relationship holds for the 7030 cm^{-1} band. These bands can thus be used to determine quantitatively the concentrations of OH groups and molecular H_2O, provided the appropriate values for the extinction coefficients are used. Band intensities are reproducible on samples stored in laboratory air for over five years.

Either the peak height or the integral absorbance determinations can be used for quantitative analysis of the species concentrations. There is a linear relationship between the absorbance and integral

Table 4. Infrared absorbance data

TABLE 4

	Near-infrared Bands							Infrared bands					
		5218 cm-1		4485 cm-1		7030 cm-1		3530 cm-1			1636 cm-1		
Sample #	thickness (cm)	Abs	Int Abs (cm-1)	Abs	Int Abs (cm-1)	Abs	Int Abs (cm-1)	thickness (cm)	Abs	Int Abs (cm-1)	thickness (cm)	Abs	Int Abs (cm-1)
LAS-27	0.0561	0.000	0.0	0.009	1.6	0.001	0.65	0.0561	0.600	302			
AL003	0.1143	0.000	0.0	0.018	3.1	0.002	0.88	0.1143	1.134	567			
ABC-12	0.0317	0.000	0.0	0.011	1.5	0.002	0.42	0.0317	0.630	313			
ABC-10	0.0212	0.000		0.009				0.0212	0.638	319			
ABC-17	0.0217	0.006	0.7	0.030	5.4	0.005	1.23	0.0088	0.832	423	0.0217	0.158	11.6
AL009	0.0563	0.099	15.0	0.132	25.0	0.032	9.34						
AVS-4	0.0118	0.020	2.6	0.027	4.4	0.007	2.20				0.0118	0.550	31.8
ABC-13	0.0397	0.086	13.1	0.101	19.5	0.026	7.70				0.0110	0.688	44.1
CAB-2	0.0074	0.017	2.1	0.019	3.0	0.004	1.58	0.0074	1.720	919	0.0074	0.460	24.6
LAS-29	0.0238	0.063	9.4	0.062	10.8	0.018	5.40	0.0029	0.784	380	0.0029	0.258	15.9
AL010	0.1054	0.287	45.6	0.282	55.6	0.087	25.27						
CAB-3	0.0033	0.012		0.009		0.003		0.0033	1.195	563	0.0033	0.360	20.2
LAS-11	0.0173	0.075	13.0	0.053	10.8	0.016	5.62						
LAS-18	0.0084	0.043	6.5	0.027	5.6	0.01	3.10				0.0084	1.023	68.4
LAS-26	0.1307	0.706	112.5	0.394	76.7	0.156	45.16						
CAU-4	0.0315	0.181	28.7	0.099	18.9	0.038	11.31						
ABC-11	0.0153	0.096	16.0	0.049	9.7	0.021	6.75						
ABC-9	0.0320	0.211	33.9	0.101	20.0	0.041	12.23	0.0036	1.660	799	0.0036	0.66	42.0
AL008	0.0818	0.642	104.5	0.252	48.7	0.123	36.60						
ABC-15	0.0075	0.069	10.9	0.024	3.9	0.012	3.55						
ABC-14	0.0295	0.288	47.2	0.095	18.8	0.051	15.81						
AR8-56	0.0233	0.241	38.2	0.066	12.3	0.044	11.61				0.0025	0.813	51.2
LAS-22	0.0192	0.194	31.3	0.064	12.8	0.028	8.00						
CAB-6	0.0265	0.0291	48.3	0.086	17.0	0.051	15.32						

Figure 7. Absorbance (peak height at maximum intensity) of the 4485 and 5218 cm^{-1} bands as a function of sample thickness (cm) for three albitic glasses with water contents between 2.65 and 6.83 wt % H_2O. The 45° lines demonstrate that the Beer-Lambert relation is valid up to 6.83 wt % H_2O for these two bands. Samples shown are ABC-13 (2.64 wt % H_2O), ABC-9 (5.12 wt % H_2O) and ABC-14 (6.83 wt % H_2O).

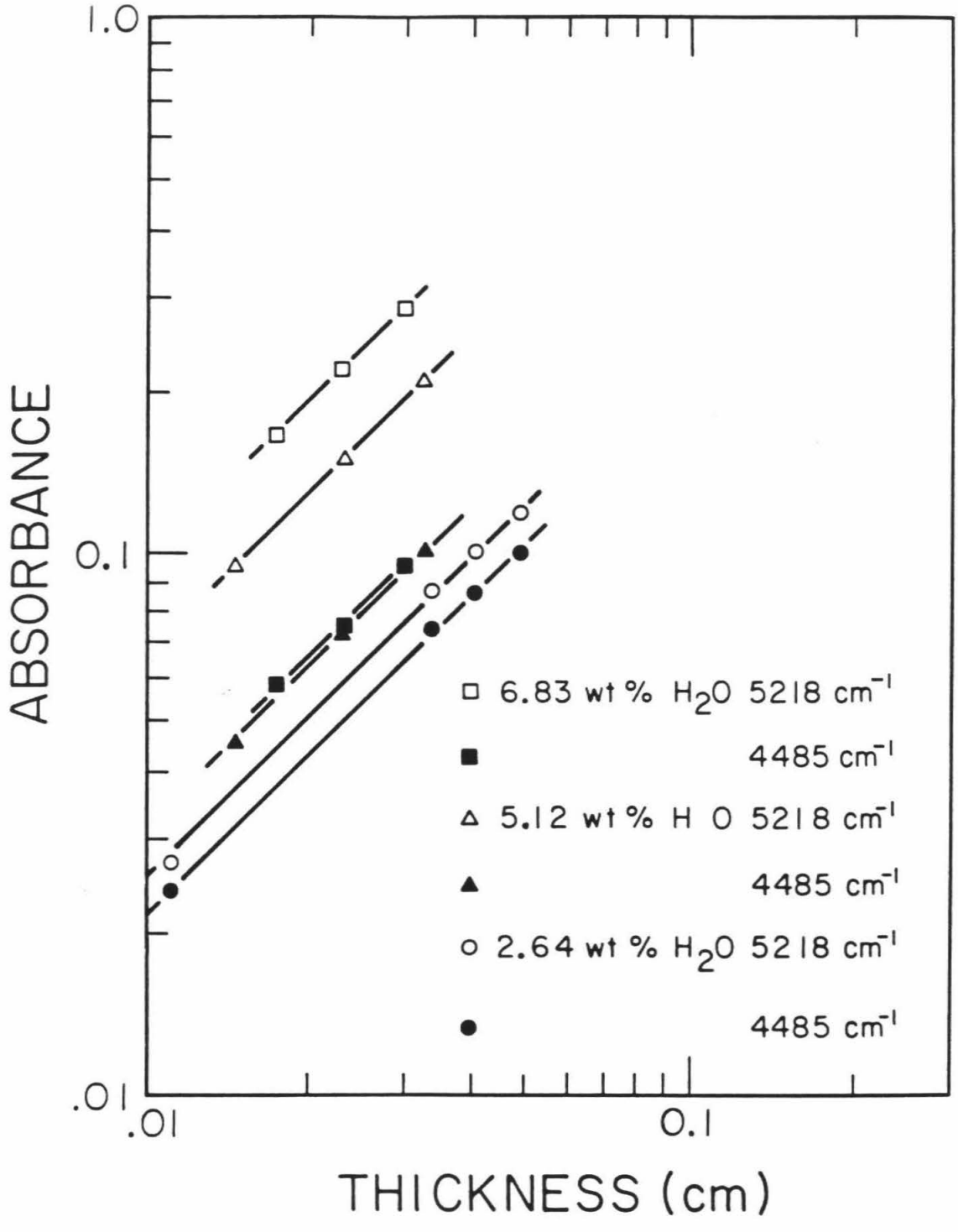
1.0
0.1
.01
.01
0.1
ABSORBANCE
THICKNESS (cm)
6.83 wt % H2O 5218 cm-1
4485 cm-1
5.12 wt % H O 5218 cm-1
4485 cm-1
2.64 wt % H2O 5218 cm-1
4485 cm-1

absorbance measurements for both the 4485 and 5218 cm^{-1} bands, both with correlation coefficients (r) of 0.999. A linear relationship between the absorbance and integral absorbance is also observed for the 7030, 1635 and 3530 cm^{-1} bands, with r = 0.998, 0.999 and 0.990, respectively. Since there is no obvious advantage to using the integral absorbance measurements instead of peak heights, peak heights have been used for the quantitative work.

Determination of extinction coefficients

According to Beer's law, the concentration of a particular H-bearing species (given as the weight fraction of water that would be released from the sample if all of the hydrogen dissolved as this species were converted to H_2O) that gives rise to an infrared absorption is directly proportional to the intensity of that band (Abs) and inversely proportional to the sample thickness (d) and the glass density (ρ):

$$\text{concentration} = \frac{\text{Abs} \times 18.015}{d \times \rho \times \varepsilon} \qquad (1)$$

where ε is the extinction coefficient or molar absorptivity, which is a function of composition, and must be determined for each band of interest. I first determined values of the extinction coefficients for the 4485 and 5218 cm^{-1} bands for hydrous albitic glass following the method of Stolper (1982a) and Newman et al. (1986): The total dissolved water contents of a suite of glasses were determined by hydrogen manometry and/or ^1H NMR spectroscopy. The absorbances of the 5218 and 4485 cm^{-1} bands were measured on the same samples. A weighted linear least-squares regression method was then used to solve for the

extinction coefficients of these two infrared bands (Table 5). As described in Newman et al. (1986), the procedure assumes that the extinction coefficients do not vary over the range of water contents studied and that there are only two hydrogen-bearing species present in the glasses, such that the total water content of the glass can be obtained by summing the amount of molecular H_2O (from the 5218 cm^{-1} band) and the amount of water dissolved as hydroxyl groups (from the 4485 cm^{-1} band).

Six samples were used for the calibration with water contents ranging from 1.02 to 6.83 wt % and exactly the same glass fragments were used for the manometric, NMR and infrared measurements. Figure 8 shows the total water content determined by summing the amounts of OH groups (4485 cm^{-1} band) and molecular H_2O (5218 cm^{-1} band) calculated from the infrared measurements (based on the best-fit extinction coefficients) vs. the total water content determined by the manometric or NMR technique. The excellent correspondence between these methods suggests that the assumption of constant ε is valid for this range of water contents. Also shown in Fig. 8 is sample A78-56 from Dr. J. Delaney for which the total water content (6.85 wt % H_2O) had been determined by H_2 manometry by Professor P. Knauth. The water content I determined by infrared spectroscopy for this sample using the best-fit extinction coefficients (6.87 wt % H_2O) reproduces Knauth's manometric result and provides an independent test of the validity of this method.

Extinction coefficients were determined for the 1635, 3530, and 7030 cm^{-1} bands based on the values for the 4485 and 5218 cm^{-1} bands, using the method described by Newman et al. (1986). Integral extinction

Table 5. Extinction coefficients for albitic glass

TABLE 5

Extinction coefficients for albitic glass

Wavenumber (cm^{-1})	Species	ε (l/mol-cm)	ε^* (l/mol-cm^2)
4485	OH	1.13 ± 0.04	219 ± 8
5218	H_2O	1.67 ± 0.06	268 ± 9
7030	OH,H_2O	0.20 ± 0.002	59 ± 0.5
3530	OH,H_2O	70 ± 2	35,000 ± 500
1636	H_2O	49 ± 2	3,081 ± 143

Figure 8. Total water contents obtained by infrared spectroscopy by summing the concentrations of molecular H_2O (5218 cm^{-1} band) and OH groups (4485 cm^{-1} band) versus total water content determined by H_2 manometry or NMR spectroscopy. Open symbols represent samples that were synthesized in BN-free assemblies; filled symbols represent samples synthesized in BN-bearing assemblies; * represents sample A78-56 from Dr. J Delaney. Estimated errors are indicated by error bars. The molar extinction coefficients are given in Table 5. Synthesis conditions of all of the glasses are listed in Table 2, except for A78-56 (Table 3) Samples shown are ABC-21, CAB-5, ABC-26, ABC-20, ABC-13, ALB-3388, ALB-3378, ABC-11, ABC-9, ALB-3403, A78-56, and ABC-14.

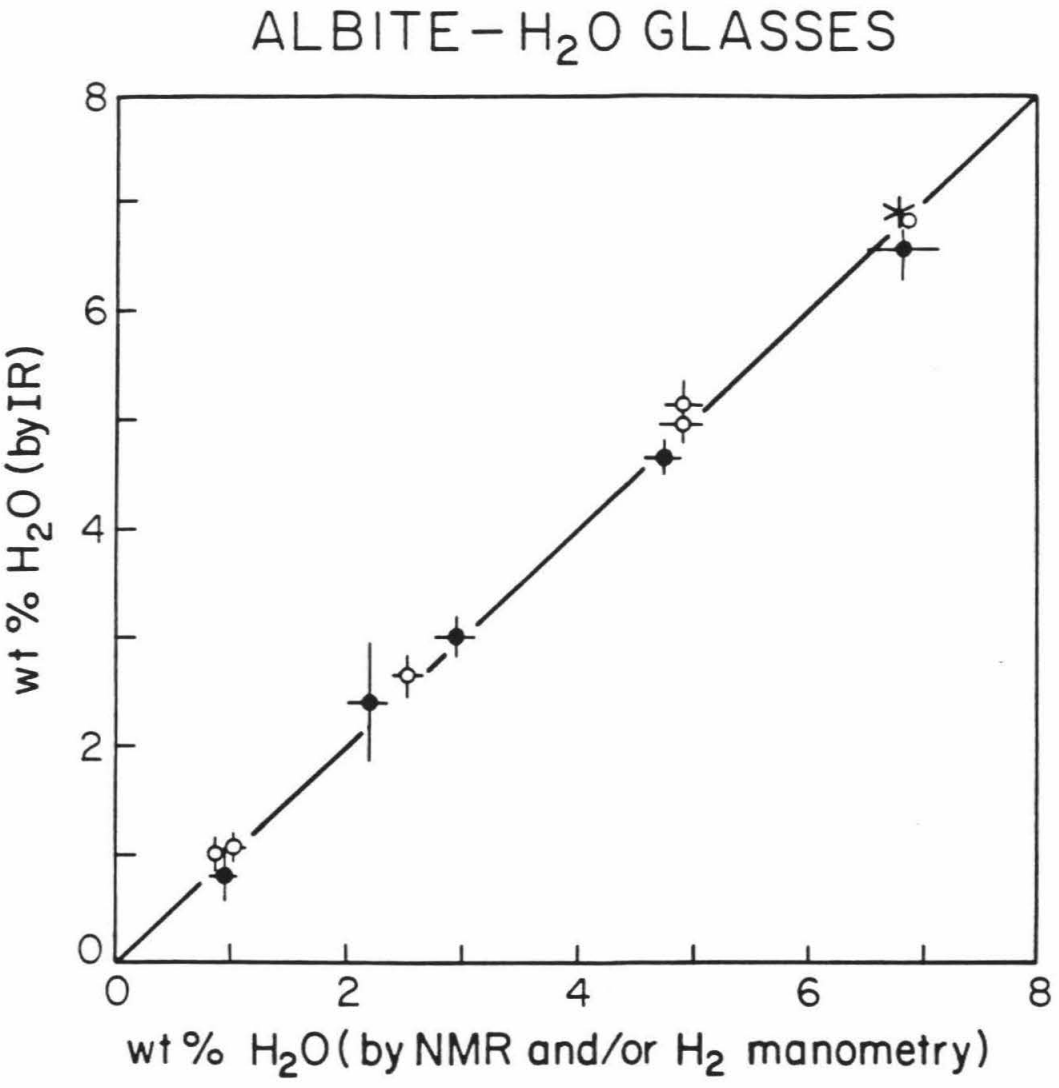
ALBITE – H_2O GLASSES
wt % H_2O (by IR)
wt % H_2O (by NMR and/or H_2 manometry)
0
2
4
6
8

coefficients were also determined for each band based on the best-fit ratio of area to peak height for each band. The values for all of the extinction and integral extinction coefficients determined in this study are listed in Table 5.

The extinction coefficient for the 5218 cm^{-1} band in hydrous albitic glasses is similar to the value determined for the equivalent absorption in hydrous rhyolitic glasses, whereas for the 4485 cm^{-1} band, the extinction coefficient for albitic glasses is smaller than for its counterpart in rhyolitic glass.

The bands at 3530 and 7030 cm^{-1} have contributions from water dissolved as molecular water and hydroxyl groups. Consequently, the molar absorptivities may vary with total water content as the relative proportion of molecular H_2O and OH changes. Extinction coefficients for the OH and molecular H_2O species were fit separately for these bands following Newman et al. (1986). However, for each of these bands, the extinction coefficients for the OH and molecular H_2O species are similar. Thus, only a single extinction coefficient for each of these bands is reported in Table 5. This contrasts with the case for rhyolitic glasses, where, for both the 3550 and 7100 cm^{-1} bands, the extinction coefficient of the OH species is almost twice that of the molecular H_2O species.

As noted above, the low-water glasses synthesized in BN-bearing assemblies have measurable intensity at 4125 cm^{-1}, which could be due to the presence of molecular H_2 or to a boron-bearing species. I determined the total water contents of six glasses that were synthesized in BN-bearing assemblies by NMR and/or H_2 manometry and also determined,

by infrared spectroscopy, the amounts of water dissolved as hydroxyl and molecular water from the 4485 and 5218 cm^{-1} bands. These samples were not, however, included in the calibration because of the possible existence of an additional H-bearing species, but the best fit extinction coefficients for the 4485 and 5218 cm^{-1} bands are basically identical whether or not glasses synthesized in BN assemblies are included in the regression. As shown in Fig. 8, for each sample synthesized in BN-bearing assemblies, the calculated total water content determined from the sum of the molecular water and OH contents is typically low, but within 0.3 wt % of the value determined for the same sample by hydrogen manometry or NMR. Thus, if the band at 4125 cm^{-1} is in fact a H-bearing species, its concentration is small, though perhaps not negligible.

Newman et al. (1986) calibrated the infrared technique for rhyolitic glasses with water contents up to 2 wt %. In this study, I have demonstrated that infrared spectroscopy can be used quantitatively for determining total water contents and species concentrations in albitic glasses up to a total water content of at least 7 wt %. Over this concentration range, infrared spectroscopy offers a non-destructive method for measuring total water contents and hydrogen-bearing species concentrations in albitic glasses that is comparable to the most precise techniques currently available. With the FTIR spectrometer, spots on the order of a few tens of microns in diameter can be routinely analysed, making the technique ideal for experimental studies.

It is often supposed in phase equilibrium studies that the amount of water loaded into the capsule is a good measure of the actual amount

present during the experiment. Inspection of Tables 2 and 3 indicates that the analyzed water contents are generally less than the amount expected based on the weight of water placed in the capsule. This appears to be true for samples included in this investigation regardless of the laboratory in which they were synthesized. Investigations that rely only on the nominal water content of a sample, without confirmation by an independent technique (e.g., Mysen & Virgo, 1986a) may not be truly quantitative.

The Speciation of Water in Albitic Glasses

Using the calibrations described in the previous section, I determined the concentrations of hydroxyl groups and molecular water dissolved in hydrous albitic glass synthesized at a variety of pressures and temperatures. Total dissolved water contents (up to 11.2 wt %) and species concentrations are listed in Tables 2 and 3. Figures 9 and 10 show the concentrations of water dissolved as molecular H_2O and OH as functions of total water content up to 11 wt % for samples quenched from melts equilbrated at 15-20 kbar and 1350-1400°C (Fig. 9) and for glasses quenched from melts equilibrated at other conditions in the range 8-25 kbar and 1000-1600°C (Fig. 10). Also shown are best-fits to the data in Fig. 9 (see Appendix 1 for fitting procedure). All of the samples shown in Figs. 9 and 10 were synthesized in piston cylinder apparatus (Table 2).

At low total water contents, most of the water is dissolved as hydroxyl groups, but the amount of molecular water increases progressively as the total water content increases. At about 4 wt %

Figure 9. The concentrations of water dissolved as molecules of water (open symbols) and as OH groups (filled symbols) as functions of total water content for albitic glasses with total water contents up to 9.6 wt % H_2O. The samples were synthesized in piston cylinder apparatus at 15-20 kbar and 1350-1400°C; run conditions are given in Table 2. The species concentrations and total water contents were determined by infrared spectroscopy based on the best-fit values for the extinction coefficients (Table 5). The solid curves represent a best fit to this data (see the caption for Fig. 13 for best fit parameters).

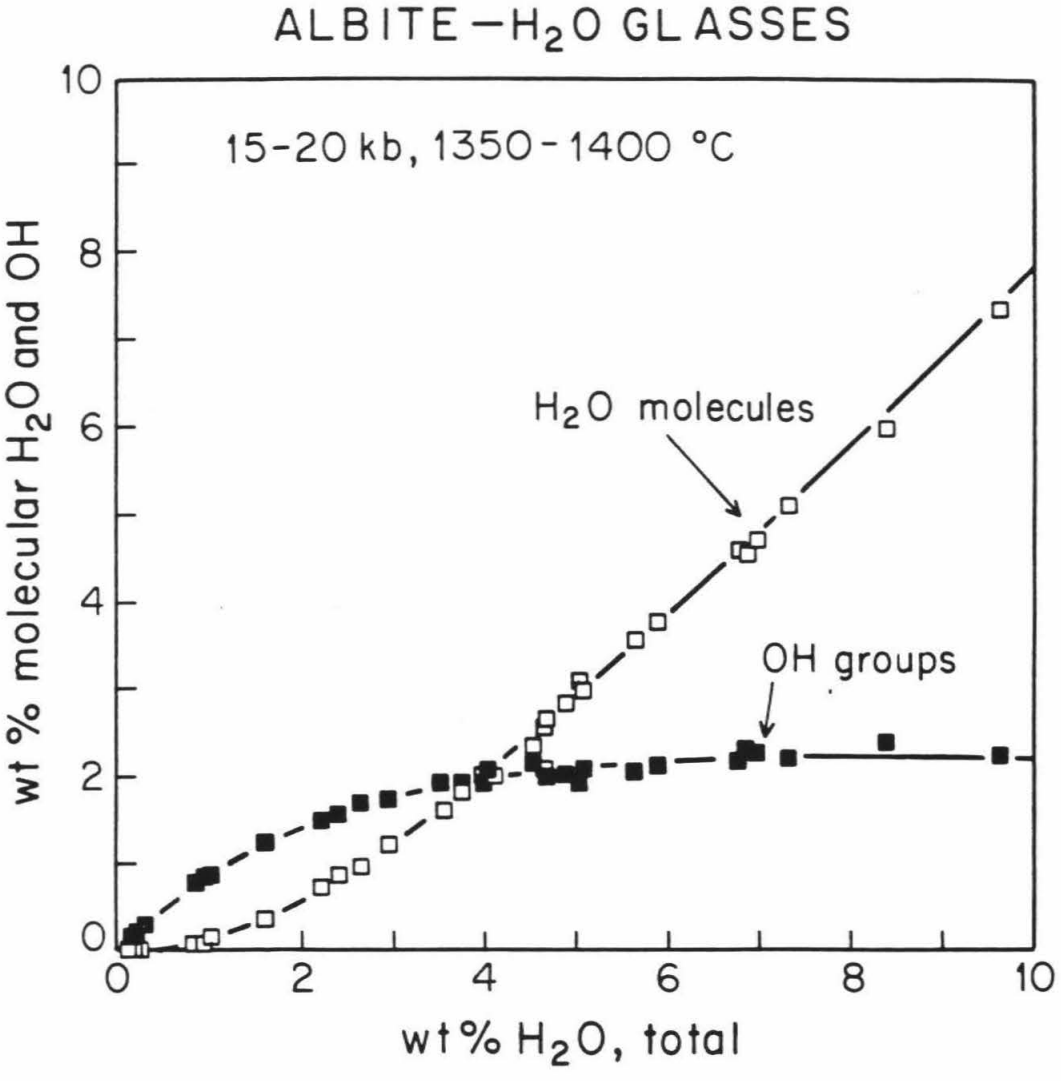
ALBITE—H_2O GLASSES
15-20 kb, 1350-1400 °C
H_2O molecules
OH groups
wt % molecular H_2O and OH
wt % H_2O, total
0
2
4
6
8
10

Figure 10. The concentrations of water dissolved as molecules of water (open symbols) and as hydroxyl groups (filled symbols) as functions of total water content for hydrous glasses synthesized in piston cylinder apparatus at experimental conditions other than 1350-1400°C and 15-20 kbar, together with a best-fit to the data shown in Fig. 9. Run conditions for all the samples are noted in the legend and are listed in Table 2.

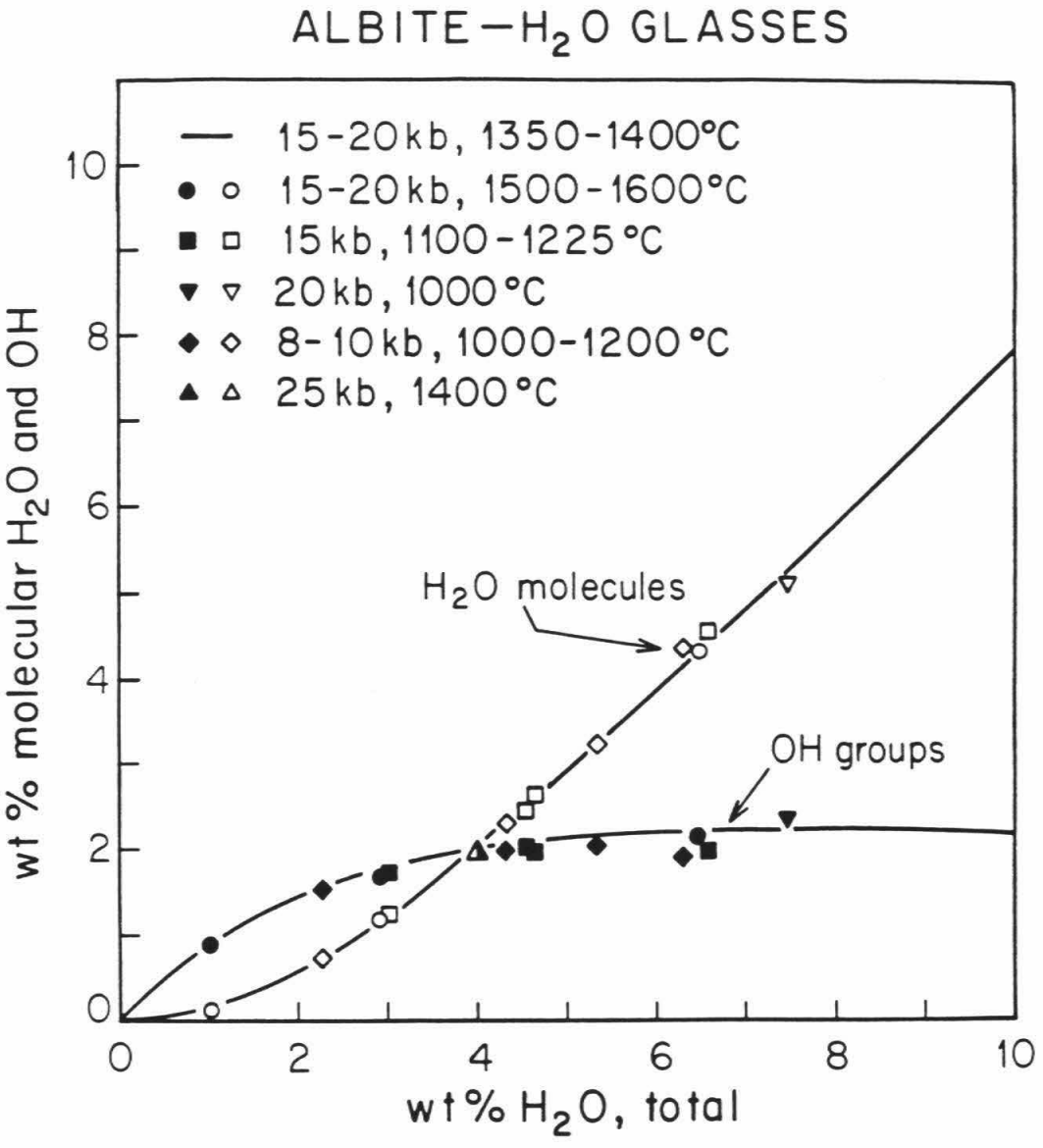
ALBITE—H2O GLASSES
15-20kb, 1350-1400°C
15-20kb, 1500-1600°C
15kb, 1100-1225°C
20kb, 1000°C
8-10kb, 1000-1200°C
25kb, 1400°C
H2O molecules
OH groups
wt % molecular H2O and OH
wt % H2O, total
0
2
4
6
8
10

total water, equal amounts of water are dissolved as hydroxyl groups and as H_2O molecules. At higher water contents, the OH concentration levels off and remains at approximately a constant value; i.e., beyond this point, essentially all additional water is incorporated as molecular H_2O. Although the position at which equal amounts of water are dissolved as OH groups and H_2O groups differs from composition to composition, the trends for albitic glass are essentially identical in shape to those observed for a complex "hydrosilicate" glass (Bartholomew et al., 1980), Na-silicate glass (Acocella et al., 1984), rhyolitic glass (Newman et al., 1986, 1987), orthoclase glass and the 1 atm silica-anorthite-wollastonite eutectic composition (Chapter 4).

I also determined the speciation of water in albitic glass for glasses quenched from melts equilibrated in IHPV at 1-7 kbar and 950-1150°C. The species concentrations and total water contents were determined by infrared spectroscopy and are listed in Table 3. Figure 11 compares the concentrations of water dissolved as molecular water and OH groups as a function of total water up to 11.2 wt % for these samples with the fit to the data from the samples synthesized in piston cylinder apparatus. Again, the OH concentration levels off with increasing total water content, but in comparison with the data from piston cylinder syntheses, there is more scatter and the OH concentration levels off at about 1.9 wt % instead of 2.1 wt % H_2O. As discussed below, the differences between the experiments conducted in IHPV and in piston cylinder apparatus can be attributed to the slower quenching rates of IHPV.

The well-defined trends in the concentrations of molecular H_2O and

Figure 11. The concentrations of water dissolved as molecules of H_2O (open symbols) and as OH groups (filled symbols) as functions of total water contents up to 11.2 wt % H_2O for glasses synthesized in IHPVs at P=1-7 kbar and T=950-1150°C, together with a best-fit to the data shown in Fig. 9. The smaller symbols represent those samples for which the infrared spectra were obtained on regions that contained bubbles.

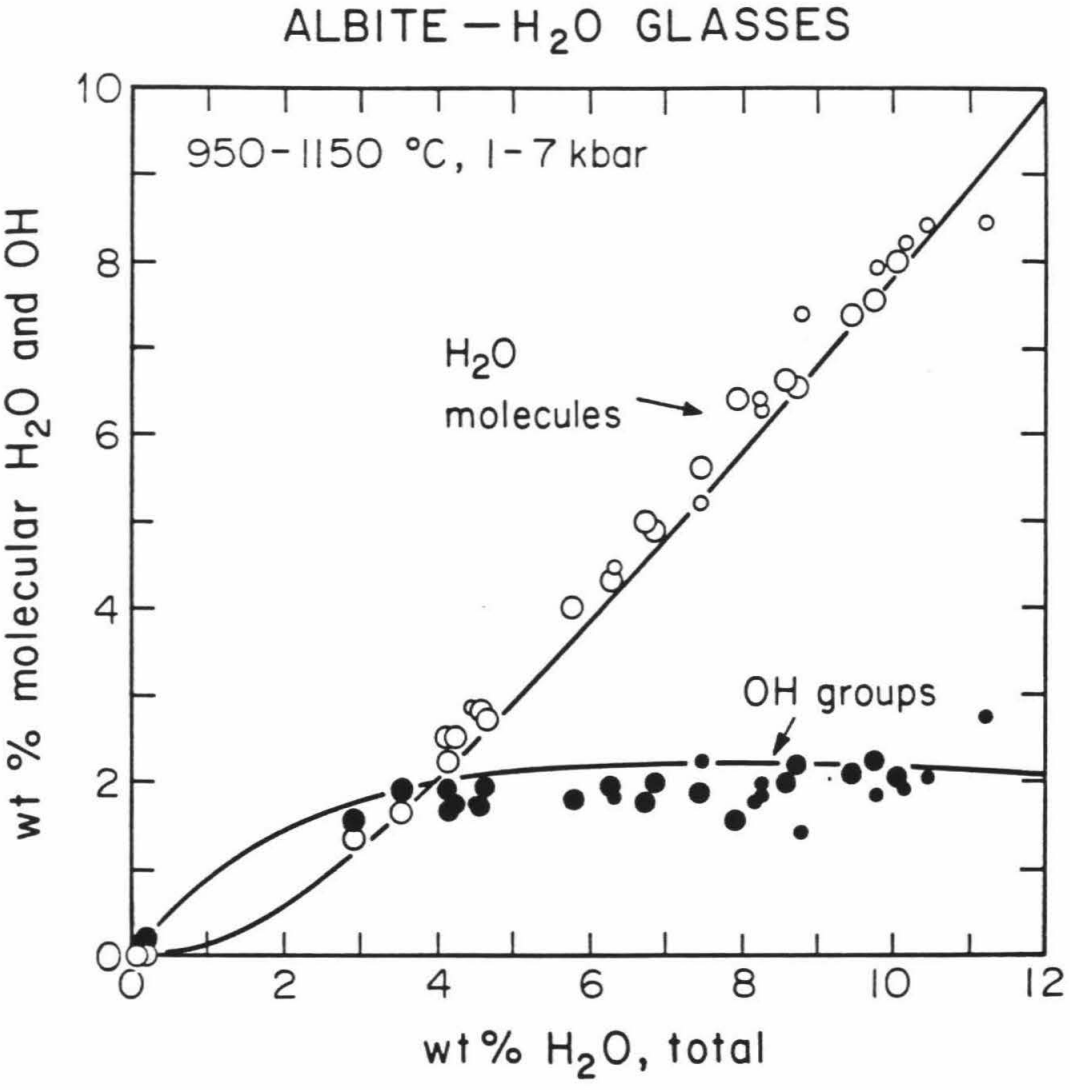
ALBITE — H_2O GLASSES
950-1150 °C, 1-7 kbar
H_2O molecules
OH groups
wt % molecular H_2O and OH
wt % H_2O, total
0
2
4
6
8
10
12

OH groups as a function of total water content for all of these glasses, synthesized over a wide range of experimental conditions, illustrate the lack of a major dependence of the speciation of water on pressure and temperature. As discussed below and by Newman et al. (1987) for rhyolitic glasses, there is probably a minor increase in molecular water relative to hydroxyl groups with decreasing temperature at low temperature. As will be shown in Chapter 2, these observations can be used to constrain the thermodynamic properties of hydrous melts.

Several of the albitic glasses have an absorption near 2350 cm^{-1}, which is due to the fundamental bending mode of molecular CO_2 (Fine & Stolper, 1985) and is probably caused by adsorption of atmospheric CO_2 onto the starting materials. The total amount of dissolved molecular CO_2 is always $\leq$0.35 wt % based on the extinction coefficient for this band determined by Fine & Stolper (1985). The molecular H_2O/OH ratios for glasses with and without CO_2 at a given total water content are indistinguishable, indicating that the presence of small amounts of CO_2 does not have a significant effect on the speciation of water.

The effects of quenching

The molecular water detected in these glasses is structurally-bound, not in fluid inclusions or bubbles, based on several lines of evidence. The glasses synthesized in piston cylinder apparatus are optically clear and generally completely free of bubbles. In optically clear areas of glasses containing up to 7 wt % total water, no bubbles were seen with a scanning electron microscope, with a resolution of 100-200Å. Professor J. Christie of the University of California examined a

glass with a total water content of 7 wt % (LAS-22) by transmission electron microscopy with a resolution of ~30Å and detected no features indicating clustering of water molecules. Infrared spectra taken on optically clear hydrous glasses at liquid N_2 temperatures do not show ice bands (Stolper, 1982a; L.A. Silver, unpub. results); ice bands are observed in the spectra of visibly bubbly samples when they are frozen (Stolper, 1982a). In rhyolitic glasses with up to 5 wt % total D_2O, NMR spectra confirm that very little of the water (if any) is present as a free fluid phase, i.e., in inclusions (Eckert et al., 1987a). The ^1H NMR spectra of two hydrous albitic glasses from this study and a variety of other bubble-free hydrous silicate glasses with up to 9 wt % H_2O provide similar constraints on the state of water in these in glasses (Eckert et al., 1987b).

There can be little doubt that molecular water and hydroxyl groups coexist stably in hydrous silicate liquids and that the presence of molecular water in glasses is not an artifact of quenching or cooling. The fundamental bending mode of H_2O molecules at 1630 cm^{-1} was observed in the high temperature (850°C) spectrum of a rhyolitic obsidian (Aines et al., 1983). The intensity of this band showed a small inverse dependence on the temperature at which the spectrum was taken. The fact that molecular water persists in this rhyolite at temperatures above its glass transition indicates that its presence in glasses quenched from melts held at high temperatures and pressures is not simply a result of cooling. In addition, the reversible dependence of the concentrations of molecular H_2O and OH groups on temperature whether observed in situ (Aines et al., 1983) or in glasses quenched from temperatures between

400 and 650°C (Stolper et al., 1983; Newman et al., 1987) is not readily reconcilable with quenching effects.

Since rhyolitic glasses exhibit a small, but measurable, temperature dependence of the relative concentrations of molecular H_2O and OH at low temperatures, such that the OH content increases with increasing temperature, it is possible that the ratio of molecular H_2O to OH of glasses synthesized from melts equilibrated at high temperatures could increase as the melt reequilibrates to low temperatures. To address this possibility, several samples of albite with 3.7-4.5 wt % total H_2O were held at 15 kbar and 1400°C for 2 h, and then cooled at rates of 2.5 to 0.28°C/s. For this range of cooling rates, the relative concentrations of OH groups and molecular H_2O at a constant total water content are independent of cooling history and indistinguishable from glasses quenched as rapidly as possible (i.e., 150-200°C/s; Table 2). However, the glasses synthesized in IHPV show erratic, generally higher ratios of molecular H_2O to OH than those synthesized in piston cylinder apparatus. The differences between the two sets of experiments cannot be due to the typically lower equilibration temperatures and pressures of the samples synthesized in IHPV because similar effects are not observed in the data obtained for glasses with similar total water contents (samples JRH-1, JRH-2, ABC-34, AVS-4) synthesized in piston cylinder apparatus over a comparable temperature and pressure range (1000-1200°C, 8-10 kbar). These results indicate that the differences in species concentrations probably reflect the slower quenching rates in the IHPV.

The results obtained for albitic glasses synthesized in piston cylinder apparatus at temperatures between 1000-1600°C do not show any temperature dependence of the speciation of water over this temperature range. This contrasts with the behavior described above for hydrous rhyolitic glasses at temperatures up to 850°C and could reflect a change in the temperature dependence of the equilibria between the hydrous species between low and high temperature. Alternatively, it could indicate that even the molecular water to hydroxyl ratios of the glasses quenched from melts in piston cylinder apparatuses increase on quenching. The slower cooling rates in IHPV would in this case result in reequilibration of the melt to even lower temperature. However, as shown in Chapter 2, extrapolation of the observed low temperature dependence of equilibria between H_2O and OH to high temperatures does not predict a large variation in the speciation of water between 1000 and 1600°C and would not change the conclusions presented here.

Comparison with other studies

The trends in the speciation of water in hydrous albitic glasses presented in this work are similar to results obtained from infrared (Bartholomew et al., 1980; Stolper, 1982a; Acocella et al., 1984; Stolper & Silver, 1985) and NMR (Bartholomew & Schreurs, 1980; Eckert et al., 1987a,b; Farnan et al., 1987) spectroscopic studies of other hydrous silicate glass compositions synthesized at various conditions. In particular, the ^1H MAS-NMR studies of Eckert et al. (1987b) included some of the samples synthesized as part of this study, and yield very similar results to those reported here, based on a completely

independent method. The exact value at which the OH content levels off as total water content increases varies with the bulk composition of the silicate (Stolper & Silver, 1985, see Chapter 4), but the levelling off and the progressive increase in the ratio of molecular H_2O to OH with total water content appear to be robust, reproducible phenomena.

In contrast to the consistency and reproducibility of the results based on infrared and NMR spectroscopies, Raman spectroscopic studies of hydrous glasses have yielded inconsistent results when results of different laboratories, or even successive reports from a single laboratory, are compared. The early studies on hydrous glasses using Raman spectroscopy failed to detect any intensity near 1600 cm^{-1} (Mysen et al., 1980; Mysen & Virgo, 1980) and led to the conclusion, in contrast with published infrared results (Orlova, 1962; Ernsberger, 1977), that water dissolves in silicate melts only as OH groups. Later, McMillan et al. (1983) observed a small band near 1600 cm^{-1} in the Raman spectra of hydrous albitic glasses that they assigned to molecular H_2O, confirming the results of the previous infrared studies; recently, Mysen & Virgo (1986a) confirmed the results of McMillan et al. (1983).

Detection of molecular water in glasses by Raman spectroscopy is difficult because of the low Raman cross-section of molecular water; this is the reason water is a commonly used solvent for the Raman study of other molecules. Given the difficulty in detecting this species by Raman spectroscopy, it would not be expected to be the optimum technique for quantitative measurement of its concentration.

Other factors also make quantitative measurements of species concentrations in glasses by Raman spectroscopy difficult. Foremost

among them is the difficulty in normalizing band intensities. In the case of the infrared measurements reported in this paper, I measure the intensity of a band and normalize it to the thickness of the sample. Using Beer's law and constant extinction coefficients, if the intensity per thickness (the "absorption coefficient") in one sample is twice that of another, then the concentration of the absorbing species in the first glass is twice that in the second. For the Raman spectra of glasses, there is typically no such convenient normalization procedure. Ideally, one band due to a major species whose concentration is invariant over the range of samples studied could be used for normalization (i.e., all other band intensities would be scaled to the intensity of this band). However, in silicate glasses covering a substantial compositional range, it is not generally possible to identify such an invariant band, and in any case, band assignments are so poorly known that even if a species could be postulated to be invariant, it would be difficult to confidently associate it with a specific band. Consequently, normalization procedures that have been adopted are necessarily ad hoc (Seifert et al., 1981; Mysen et al., 1982). Also, in contrast to the infrared studies reported here, where bands are well separated from each other, deconvolution procedures are required in the Raman studies to obtain band intensities and these involve a variety of assumptions about band shapes, location, and number that diminish the precision of the results.

Despite these difficulties, Mysen & Virgo (1986a) attempted to use Raman spectroscopy to measure quantitatively the concentrations of molecular water and hydroxyl groups in hydrous silica glass. They

concluded that hydroxyl groups are the dominant species of dissolved water for total water contents up to 10 wt %, that the ratio of molecular water to hydroxyl groups decreases with increasing water content in the 4-10 wt % water range, and that molecular water (not hydroxyl) group concentrations are approximately constant over this concentration range. These conclusions are quite different from those reached in this study for albitic glass and by others for silicate glasses, including silica, based on infrared and NMR spectroscopies. Recently, Farnan et al. (1987) used cross-polarization NMR to determine the concentration of hydroxyl groups as a function of total water content for hydrous silica glasses with 2.5 and 8.7 wt % H_2O. They found that molecular water is the dominant species at high total water contents and that the molecular H_2O to OH ratio increases with total water content, in agreement with the data presented here for albitic glasses. In addition, my own preliminary work on silica glasses with up to about 10 wt % water, based on the infrared intensities of the 4520 and 5270 cm^{-1} bands, also indicates a behavior for silica that is similar to that observed for all other glasses studied by infrared spectroscopy.

It is not possible to be certain of the cause of the discrepancies between the conclusions based on infrared and NMR spectroscopies versus those based on Raman spectroscopy. However, it must be an analytical problem and not, as suggested by Mysen & Virgo (1986a), related in some way to the techniques by which the glasses were prepared. Their samples and the samples from this study were synthesized by identical techniques, and, as demonstrated above, equilibration temperature and

pressure have, at most, minor effects on the results. Mysen & Virgo (1986a) implied that the similarity between the infrared results obtained by several investigators on such a wide range of glasses synthesized over a range of conditions was so surprising given the expectation that they would be different that it cast doubt on the validity of the results. However, there is a stability and reproducibility in the infrared results that provides confidence in the technique and in the quantitative aspects of this work. It has been demonstrated here and elsewhere (Newman et al., 1986; see also Chapter 4) that infrared spectroscopy can yield precise and accurate measurements of total water content when properly calibrated. In contrast, the Raman technique is not, at this point, as internally consistent or quantitatively successful. Until Raman spectroscopy can be demonstrated against independent techniques to be truly quantitative, infrared and NMR spectroscopies will remain the methods of choice for measuring species concentrations in hydrous glasses.

Summary

1. H_2 manometry and NMR spectroscopy have been used to calibrate an infrared spectroscopic method for measuring the concentrations of molecular H_2O and hydroxyl in albitic glasses. This technique offers a precise, accurate and non-destructive method for measuring species concentrations and total water contents in hydrous glasses.

2. The speciation of water in albitic glasses for total water contents up to about 11 wt % has been determined by infrared spectroscopy. At low total water contents, most of the water is

dissolved as hydroxyl groups; at total water contents greater than 4 wt %, molecular water becomes the dominant species and the OH groups concentration levels off. These results are in agreement with those obtained by NMR spectroscopic studies of several glasses from this study. The trends in the speciation of water in albitic glasses are similar to those observed in other silicate glass compositions using infrared and NMR spectroscopies.

3. The proportions of molecular H_2O and OH in glasses quenched from melts equilibrated at temperatures in the range 1000-1600°C and pressures between 8 and 25 kbar in piston cylinder apparatus are independent of the P and T of equilibration. However, by comparison, the glasses synthesized in IHPV have a higher ratio of molecular H_2O to OH groups at a given total water content that probably reflects reequilibration of the melt to lower temperatures.

Chapter 2. Thermodynamic Models of Hydrous Albitic Melts

In this chapter, four mixing models involving homogeneous equilibria among melt species that can account for the spectroscopically determined molecular water and hydroxyl group concentrations are illustrated. These models are based on the simple model discussed previously by Stolper (1982a) and Silver & Stolper (1985). One of the goals of this study of the concentrations of water molecules and hydroxyl groups is to see if they can be rationalized in terms of simple considerations of such homogeneous equilibria and, if so, if they can yield insights into the thermodynamics of hydrous silicate melts.

Ideal Mixing of H_2O, OH, and Oxygen in Hydrous Silicate Melt

If water molecules are injected into albitic melt, the water molecules would react with the silicate portion of the melt to generate hydroxyl groups. Although there may be many reactions taking place, this first model represents the simplest model of homogeneous equilibria in hydrous silicate melts. The melt is modelled as an ideal mixture of water molecules, hydroxyl groups, and oxygens that interact according to

$$H_2O, \text{ molecules (melt)} + O \text{ (melt)} = 2OH \text{ (melt)} \qquad (2)$$

(Stolper, 1982b; Silver & Stolper, 1985). The activities (= mole fractions) of these three species are related through the following equilibrium constant:

$$K_1 = \frac{(a^m_{OH})^2}{(a^m_{H_2O,mol})(a^m_O)} = \frac{(X^m_{OH})^2}{(X^m_{H_2O,mol})(X^m_O)} \qquad (3)$$

At any pressure and temperature, K_1 is a constant and the concentrations of the three species can be calculated easily as a function of total

water content and K_1 using the expressions given in Silver & Stolper (1985). This treatment is basically an extension of the treatment developed by Wasserburg (1957) for modelling the thermodynamic properties of silicate melts.

Figure 12 compares the measured concentrations of hydroxyl groups and molecules of water in albitic glasses plotted in terms of their mole fractions with the concentrations expected for a value of $K_1 = 0.17$ given that the melt species mix ideally. The shapes of the model and actual species concentration curves are grossly similar in that the molecular water concentration is concave up when plotted against total water content and the hydroxyl group content is concave down. The agreement between the model and actual concentrations is best at low (< 2 wt %) water contents. At high water contents, however, the constant K_1 model diverges progressively from the measured concentrations as the hydroxyl group concentration levels off more sharply than does the model calculation.

The general correspondence between observed species concentrations and those calculated using the simplest ideal mixing model suggests that it is a useful starting point for development of more complex and realistic models of the homogeneous equilibria of hydrous albitic melts. The ideal mixing model involves several simplifying assumptions, each of which will be relaxed in subsequent sections to illustrate how more complex models can account in detail for the observed species concentrations. The first assumption is that the mixing between species is ideal; i.e., that all possible configurations of water molecules, hydroxyl groups, and oxygen atoms are energetically identical. This

Figure 12. The mole fractions of molecular H_2O (open symbols) and OH groups (filled symbols) in albitic glass as functions of the mole fraction of total water X_B for the glasses shown in Figs. 9 and 10. The solid curve shows the calculated species concentrations based on a simple ideal mixing model with K_1=0.17 (equation 3).

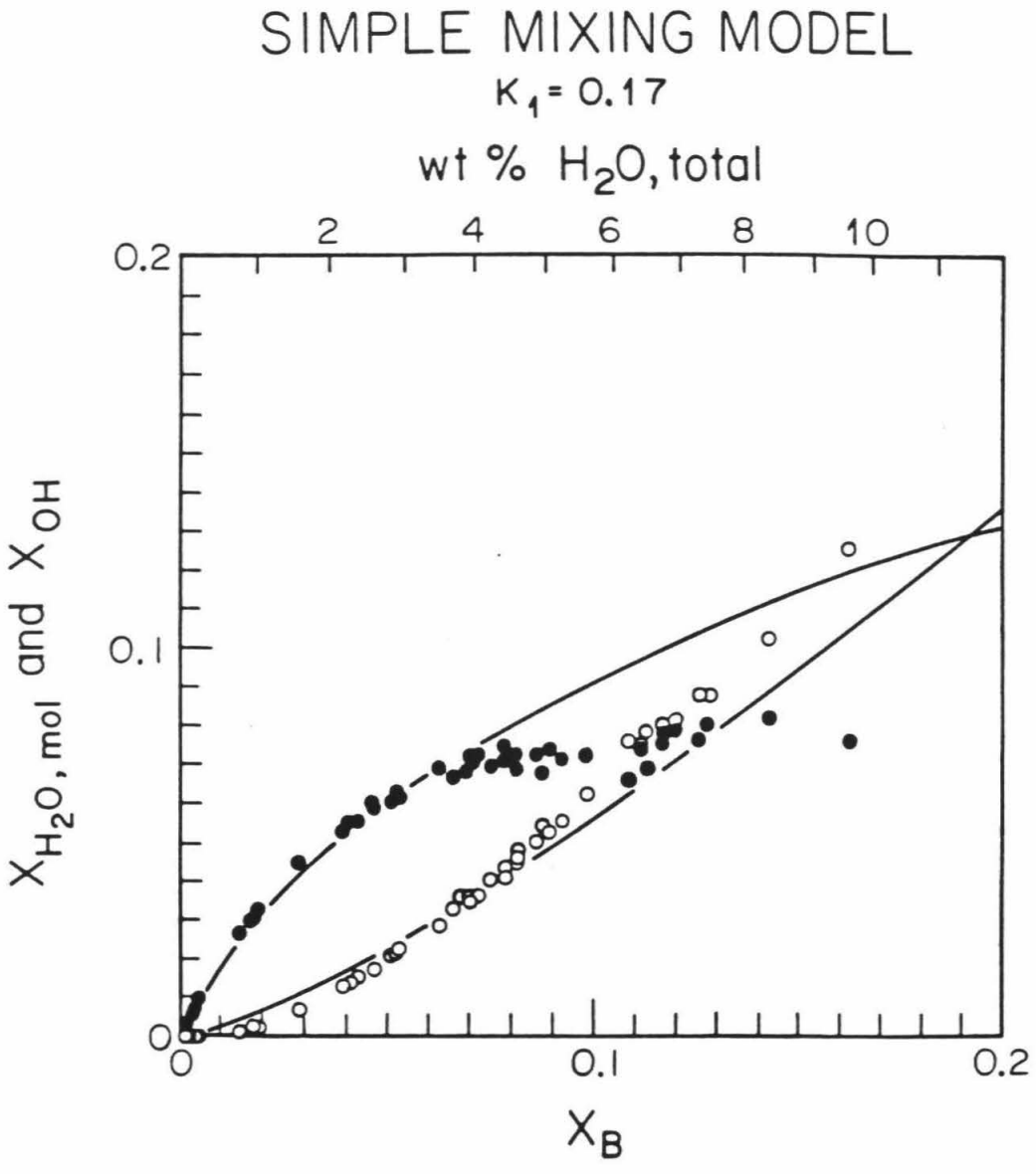
SIMPLE MIXING MODEL
$K_1 = 0.17$
wt % H_2O, total
2
4
6
8
10
0.2
0.1
0
0
0.1
0.2
$X_{H_2O, mol}$ and X_{OH}
X_B

assumption can be relaxed by including non-ideal interactions between the three species. The second assumption is that the entropy of mixing of the melt can be modelled by counting all possible configurations of water molecules, hydroxyl groups, and oxygen atoms assuming that each of these species occupies a single "lattice site" in the sense of quasi-crystalline models of melt structure (Guggenheim, 1952). This assumption can be relaxed by recognizing that polymeric units exist in silicate melts and modelling the configurational entropy accordingly. The final assumption in the simple ideal mixing model is that all of the oxygens in the melt are indistinguishable and equally reactive with water molecules to produce hydroxyl groups; i.e., that only one reaction such as (2) needs to be considered. This is clearly unrealistic in that it is likely that different types of oxygens (e.g., bridging vs. non-bridging vs. free; oxygens between two Al-bearing tetrahedra, two Si-bearing tetrahedra, etc.) should be distinguished and probably react to differing degrees with water molecules. This assumption can be easily relaxed by considering several different, coupled reactions such as (2) each describing interactions with distinguishable oxygen (and/or hydroxyl) types.

Before going on to consider these complexities, it is convenient to discuss the expected effects of pressure and temperature on the concentration of hydrous species in albitic melt in the context of the simple ideal mixing model. The variation in K_1 with pressure is related to ΔV^o_r, the standard state volume change of reaction (2), which, given the assumption of ideal mixing, would be equal to the actual volume change:

$$\frac{d(\ell nK_1)}{dP} = -\frac{\Delta V_r^o}{RT} \qquad (4)$$

The lack of pressure dependence of speciation in albitic glasses between 8 and 25 kbar indicates that the reaction of water molecules with the silicate framework to produce hydroxyl groups in albitic glass results in a negligible change in volume over this pressure range. Analysis of the density and speciation data presented by Acocella et al. (1984) for hydrous Na-silicate glasses leads to a value for the volume change of reaction (2) of -3.4 cc/mole at 1 atm, 25°C.[2] Given this volume change, for a melt with 4.3 wt % water of which 2 wt % is dissolved as hydroxyl groups at 10 kbar and 1200°C, increasing the pressure to 20 kbar would increase the hydroxyl content to only 2.2 wt %. This is a small change, but it should have been detectable. Thus, if there is a volume change for reaction (2) in albitic melt, it is less than about -3 cc/mole. There is no support for the suggestion of Mysen & Virgo (1986a) that the volume change is as large as -6 cc/mole.

The effect of temperature on speciation can be similarly modelled in terms of ΔH_r^o, the standard state enthalpy change of reaction (2), which, given the assumption of ideal mixing is equal to the actual enthalpy change:

$$\frac{d(\ell nK_1)}{d(1/T)} = \frac{\Delta H_r^o}{R} \qquad (5)$$

---

2. Acocella et al. (1984) obtained a similar result if the partial molar volumes they determined are expressed on the same equal oxygen basis used in this study.

By plotting the value of $\ln((X^m_{OH})^2/(X^m_{H_2O,mol} X^m_O))$ based on the measured species concentrations versus 1/T(K) for rhyolitic glasses with about 2 wt % water equilibrated between 300 and 700°C, Stolper et al. (1983) found a value of $\Delta H^o_r \sim 3$ kcal/mole. Assuming this value also applies to albitic melts with higher water contents at high temperature, for a glass containing 4.3 wt % water of which 2 wt % is dissolved as hydroxyl groups at 1000°C, increasing temperature to 1400°C would increase the hydroxyl content to only 2.2 wt %. Even such a small variation should be measurable with the infrared technique, yet it has not been detected in the rapidly quenched piston cylinder runs. Either ΔH^o_r decreases with increasing temperature, water content, or from rhyolitic to albitic glasses, or as discussed above, even the piston cylinder runs reequilibrate on quenching to a lower temperature and none of the temperature dependence of speciation at high temperatures is preserved. In either case, the temperature dependence of speciation at high temperatures is inferred to be small.

Non-Ideal Mixing of H_2O, Hydroxyl, and Oxygen Units

I have chosen to model possible non-ideal interactions between water molecules, hydroxyls, and oxygens using the formalism of a strictly regular ternary solution. This is analogous to the extension by Shaw (1964) of Wasserburg's (1957) model of silicate-water mixtures as ideal mixtures of water molecules and oxygen atoms to include non-ideal behavior. In this treatment, the entropy of mixing is taken to be identical to that in an ideal mixture, but all possible configurations of the three species over the quasi-crystalline lattice sites are not

energetically identical. It can be readily shown that the activities of the three species given these restrictions are (Guggenheim, 1952; Prigogine & Defay, 1954, equation 16.90)

$$a_{H_2O,mol} = X_{H_2O,mol} \exp\{\frac{1}{RT}\,(X_O X_{OH}(W_{H_2O,mol-O} - W_{O-OH} + W_{H_2O,mol-OH}) + X_O^2\, W_{H_2O,mol-O} + X_{OH}^2\, W_{H_2O,mol-OH})\} \quad (6.1)$$

$$a_O = X_O \exp\{\frac{1}{RT}\,(X_{H_2O,mol} X_{OH}(W_{O-OH} - W_{H_2O,mol-OH} + W_{H_2O,mol-O}) + X_{H_2O,mol}^2\, W_{H_2O,mol-O} + X_{OH}^2\, W_{O-OH})\} \quad (6.2)$$

$$a_{OH} = X_{OH} \exp\{\frac{1}{RT}\,(X_{H_2O,mol}\, X_O\, (W_{H_2O,mol-OH} - W_{H_2O,mol-O} + W_{O-OH}) + X_{H_2O,mol}^2\, W_{H_2O,mol-OH} + X_O^2\, W_{O-OH})\} \quad (6.3)$$

where the W_{ij} in units of energy, are the binary interaction parameters. I have assumed that the W_{ij}/RT are independent of pressure and temperature, based on the lack of observable P,T effects on the measured species concentrations. If W_{ij} is positive, i and j atoms will tend to be separated (i.e., i and j atoms will tend to cluster with like atoms) in the mixture compared to the random distribution of an ideal solution; if W_{ij} is negative, i and j atoms will tend to be associated in the mixture compared with an ideal solution. For a strictly regular solution of water molecules, hydroxyls, and oxygens, K_1 (equation 3) defined in terms of the activities given in equation (6) will be

constant at a given temperature and pressure.

Using the activity expressions given above and the relationship between them defined by the definition of K_1, a least-squares technique has been used to determine values of K_1 and the W_{ij} that best fit the measured species concentrations for hydrous albitic glasses (the best fit parameters are given in the caption of Fig. 13). Figure 13 shows that this treatment can indeed account for the observed species distribution in albitic glasses; this is not very surprising given that the fit involves four adjustable parameters. Best fit values for $W_{H_2O,mol-O}$, W_{O-OH}, and $W_{H_2O,mol-OH}$ are negative, indicating in the context of this model that the species do not tend to cluster preferentially with like molecules; this is consistent with the ^1H NMR results of Eckert et al. (1987b), who see no evidence for clustering of OH groups or water molecules. Shaw (1964) also found that a negative value for the H_2O-O interaction parameter was required to fit measured phase equilibria in the albite-H_2O system.

Polymer Mixing Models

In both the ideal and non-ideal mixing models developed above, the entropy of mixing is evaluated by counting the number of possible configurations of H_2O, OH, and oxygens distributed over the sites of a quasi-crystalline lattice. However, in anhydrous albitic melt, oxygen atoms are arranged in linked tetrahedra and thus a more realistic treatment of the entropy of hydrous melts would consider the fact that the mixing units are polymers of a variety of sizes and shapes. In this section, a schematic model that includes the effects of polymerization

Figure 13. Calculation (solid curves) of the mole fractions of molecular H_2O and OH groups in albitic melt as function of the mole fraction of total water, X_B, based on a regular solution model (binary interaction parameters: $W_{H_2O,mol-O}$ = -3.295RT, W_{O-OH} = -6.019RT, $W_{H_2O,mol-OH}$ = -0.572RT) and a value for K_1 of 1.07×10^{-4}. This best fit curve is reproduced in Figs. 9-11. Shown for comparison are the mole fractions of molecular water (open symbols) and OH groups (filled symbols) determined by IR spectroscopy for the samples shown in Figs. 9 and 10. See text for details.

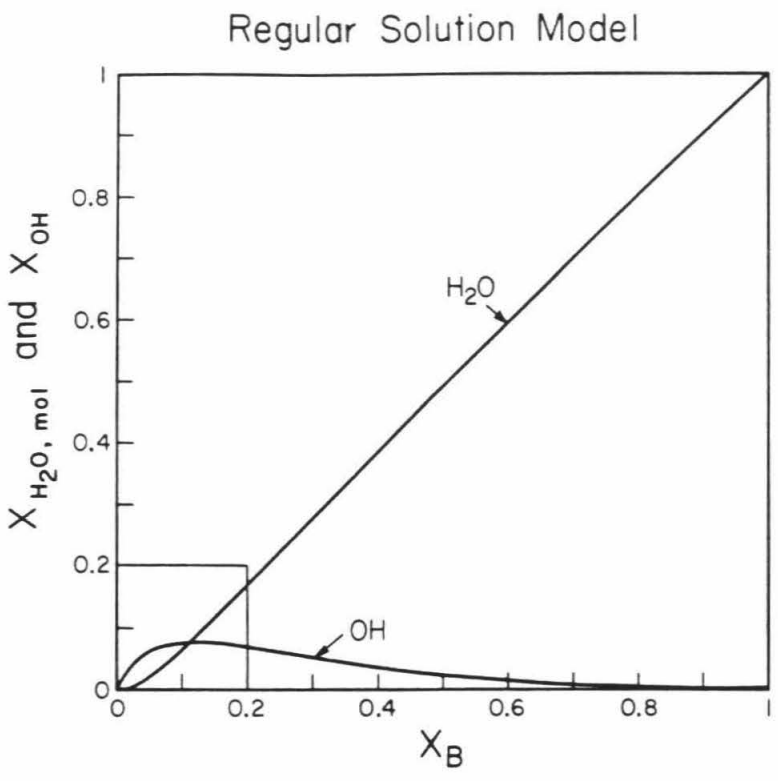
Regular Solution Model
$X_{H_2O,\,mol}$ and X_{OH}
H_2O
OH
X_B
0
0.2
0.4
0.6
0.8
1

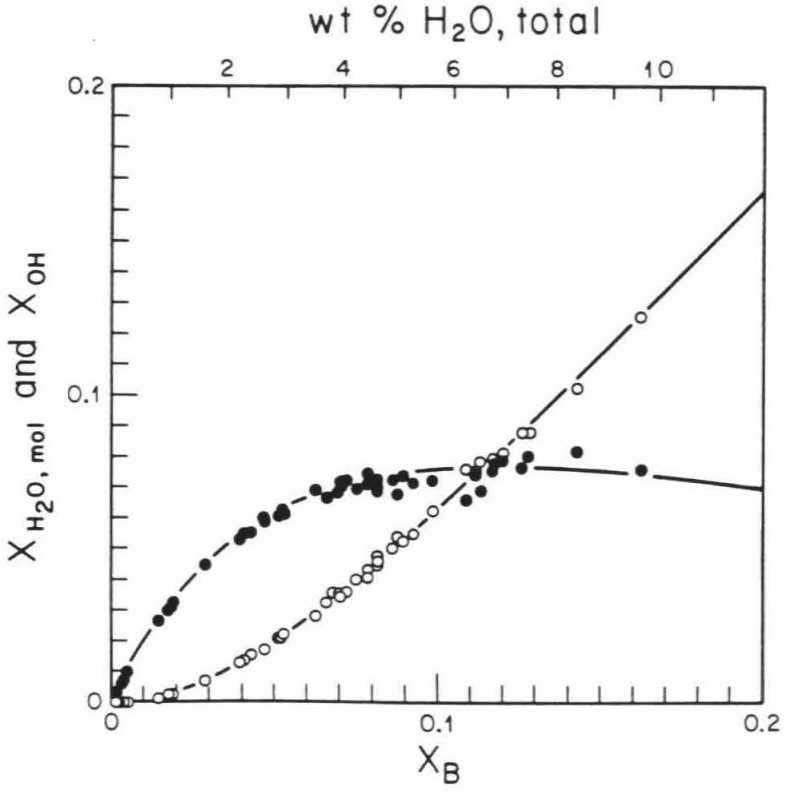
wt % H_2O, total
2
4
6
8
10
$X_{H_2O,\,mol}$ and X_{OH}
X_B
0
0.1
0.2

on the mixing properties of hydrous melts is illustrated.

In this model, the anhydrous melt is composed of chain polymers each consisting of ℓ oxygen atoms. A chain of oxygens can react with a water molecule to produce two smaller chains of length $(\ell+1)/2$, each of which is terminated by a hydroxyl group. The hydrous melt is thus modelled as a mixture of anhydrous polymers of length ℓ, hydroxyl-bearing polymers of length $(\ell+1)/2$, and water molecules. Using Flory's approximation for the entropy of mixing of such polymers and assuming that the enthalpy of mixing is zero, the activities of each of these polymer species is (Guggenheim, 1952; Flory, 1953, equations XIII-12,13,14):

$$a_{H_2O,mol} = v_{H_2O,mol}\exp\{(1 - v_{H_2O,mol}) - \frac{1}{\ell} v_{\ell O} - (\frac{2}{\ell+1}) v_{(\frac{\ell+1}{2})OH}\} \quad (7.1)$$

$$a_{\ell O} = v_{\ell O}\exp\{(1 - v_{\ell O}) - \ell v_{H_2O,mol} - (\frac{2\ell}{\ell+1}) v_{(\frac{\ell+1}{2})OH}\} \quad (7.2)$$

$$a_{(\frac{\ell+1}{2})OH} = v_{(\frac{\ell+1}{2})OH}\exp\{(1 - v_{(\frac{\ell+1}{2})OH}) - (\frac{\ell+1}{2})v_{H_2O,mol} - (\frac{\ell+1}{2\ell})v_{\ell O}\} \quad (7.3)$$

where $v_{H_2O,mol}$, $v_{\ell O}$ and $v_{(\frac{\ell+1}{2})OH}$ are the volume fractions of the three polymers. These can be expressed in terms of the number of lattice sites each polymer occupies:

$$v_{H_2O,mol} = \frac{n_{H_2O,mol}}{N_s} \quad (8.1)$$

$$v_{(\frac{\ell+1}{2})OH} = \frac{(\frac{\ell+1}{2})n_{OH}}{N_s} \quad (8.2)$$

$$v_{\ell O} = \frac{n_O - (\frac{\ell-1}{2})n_{OH}}{N_s} \quad (8.3)$$

where N_S = total number of lattice sites = $n_O + n_{OH} + n_{H_2O,mol}$, and n_O, n_{OH} and $n_{H_2O,mol}$ are as given in Silver & Stolper (1985). The polymer units interact through the following reaction:

$$\text{anhydrous polymer } (\ell \text{ oxygens in length}) + H_2O, \text{ molecules} = \text{H-bearing polymer } (\tfrac{\ell+1}{2} \text{ oxygens in length}) \tag{9}$$

with an equilibrium constant given by

$$K_p = \frac{(a_{(\frac{\ell+1}{2})OH})^2}{(a_{H_2O,mol})(a_{\ell O})} \tag{10}$$

Substitution of the activity and volume fraction expressions from equations (7) and (8) into this equation for K_p yields, after some manipulation, the following relation:

$$K_p = \frac{(v_{(\frac{\ell+1}{2})OH})^2}{(v_{H_2O,mol})(v_{\ell O})} = (\tfrac{\ell+1}{2})^2 \frac{(n_{OH})^2}{(n_{H_2O,mol})(n_O - (\frac{\ell-1}{2})n_{OH})} \tag{11}$$

For a given value of K_p, equation (11) can be solved at a given total water content for the equilibrium concentrations of the dissolved species. As shown in Fig. 14, for large values of ℓ (~20), the model species concentrations are similar to the measured values.

This treatment is highly schematic. The compromises that are implicit in the use of Flory's approximation and the neglect of the effect of polymer shape are discussed in detail in Guggenheim (1952) and Flory (1953), but it appears that to first order the simple treatment is appropriate. It is likely that a range of polymer sizes exist in

Figure 14. Calculation of the hydrous species concentrations as a function of the mole fraction of total water, X_B, for a model based on mixing of molecules of different sizes (equation 11). The solid curves represent the calculated species concentrations for K_p=60 and ℓ=20, where ℓ=length of polymer chain. Also shown for comparison are the mole fractions of the hydrous species concentrations based on IR spectroscopy for the samples in Figs. 9 and 10.

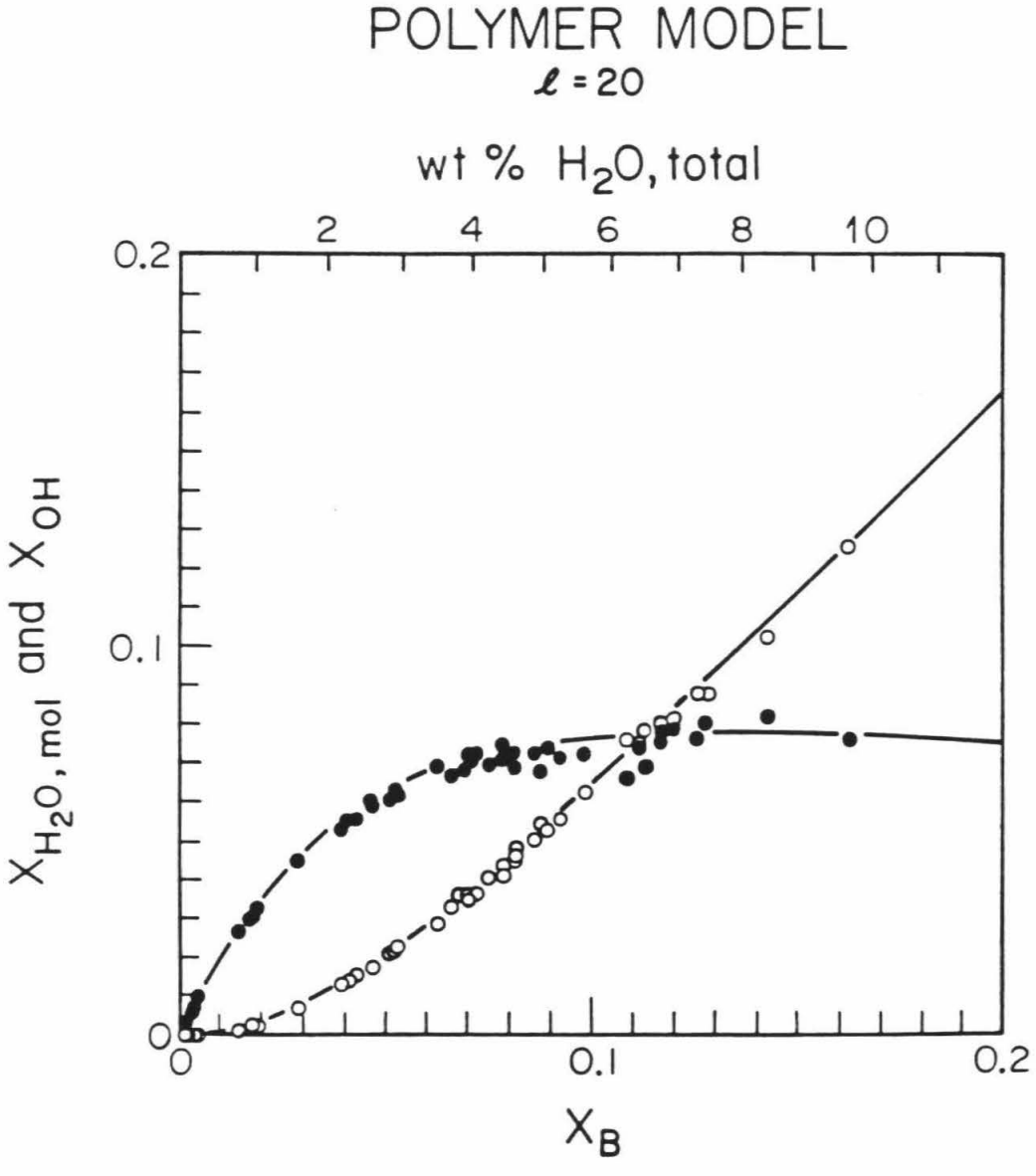
POLYMER MODEL
ℓ = 20
wt % H2O, total
2
4
6
8
10
0.2
0.1
0
0
0.1
0.2
XH2O, mol and XOH
XB

silicate melts and that a more realistic treatment would consider the distribution of these polymers and the possibility that hydroxyl-bearing polymers can have more than one hydroxyl group; such models would be analogous to the silicate polymer models of melts developed by Masson (1965) and Gaskell (1982). I have also explored models involving equilibria between silicate tetrahedra with four bridging oxygens, H_2O molecules and silicate units with one to four OH groups, e.g., $SiO_3(OH)$, $Si(OH)_4$. This type of model also can account for the observed species concentrations as long as the hydrous silicate units do not have too many OH groups, consistent with the results of Farnan et al. (1987) for hydrous silica glass. At this point, however, given the success of the simple model in retrieving the measured species concentrations and the lack of detailed structural information for hydrous melts, the introduction of further complexities seems to be unwarranted.

Mixing Models with Several Types of Distinguishable Oxygens and Hydroxyls

The models discussed thus far include the assumption that all of the anhydrous oxygens are indistinguishable and equally reactive with water molecules to produce hydroxyl groups; i.e., a single reaction such as equation (2) suffices to describe the homogeneous equilibria between water molecules, hydroxyl groups, and oxygens. This is probably unrealistic. It has, for example, long been inferred by glass scientists that in alkali silicate melts, bridging oxygens react with water preferentially over non-bridging oxygens to form hydroxyl groups (Uys & King, 1963). In aluminosilicate compositions such as albite, it

is likely that oxygens bridging two Si-bearing tetrahedra are not as reactive with water molecules as those attached to Al-bearing tetrahedra (McMillan et al., 1983; Remmele et al., 1986) and this may explain the lower solubility of water in silica than in aluminosilicate melts. Phase relations in the system albite-orthoclase-silica-water have been used to infer that Na-bearing units are more reactive than K-bearing units, which are more reactive than alkali-free species (e.g., Pichavant & Ramboz, 1985). The levelling off of hydroxyl group concentrations at high total water contents could indicate that one kind of oxygen species is much more reactive than others and it has been essentially entirely consumed when the hydroxyl concentration saturates.

It is simple in principle to relax the assumption that all of the oxygen atoms are indistinguishable. First, all of the species of interest must be specified and a complete, linearly independent set of reactions such as equation (2) among these species must be written and then the equilibrium constant for each reaction can be formulated. Assuming ideal mixing (or any other mixing law that gives activity expressions that can be substituted into the equilibrium constant expressions) the equilibrium species concentrations for any bulk composition and values of the equilibrium constants can be determined by solving a simultaneous set of equations made up of the independent equilibrium constant expressions plus mass balance constraints. The equilibrium constants can then be adjusted until the molecular water and total hydroxyl contents match the measured values. The difficulty is in deciding on the species to be included in the model. There is always a temptation to include a large number of species, but the problem then

becomes poorly constrained because given enough species, it will almost always be possible to approximate the macroscopic thermodynamic properties of a solution, or in this case, to get a close approximation to the molecular water and hydroxyl group concentrations.

To illustrate how the simple ideal mixing model can be readily extended to include more than one type of oxygen and hydroxyl in the melt, I have used it to approximate the cation exchange model developed by Burnham (1975). Although albitic melts probably contain many types of oxygens (e.g. Si-O-Si, Al-O-Al, Si-O-Al, Si-O-NaAl, and NaAl-O-NaAl), the model proposed by Burnham (1975) considers only Si-O-Si and Si-O-NaAl groups, and assumes there are no Al-O-Al groups. The interaction between the silicate melt and H_2O is illustrated schematically in Fig. 15. These coupled equilibria can be expressed as

$$H_2O,\text{molecules (melt)} + \text{SiOSi (melt)} = 2\text{SiOH (melt)} \qquad (12.1)$$

$$\text{SiOH (melt)} + \text{SiONaAl (melt)} = \text{SiONa (melt)} + \text{SiAlOH (melt)} \qquad (12.2)$$

Reaction (12.2) involves the exchange of Na and H atoms. These equilibria are governed by equilibrium constants:

$$K_1 \equiv \frac{(a^m_{\text{SiOH}})^2}{(a^m_{\text{SiOSi}})(a^m_{H_2O,\text{mol}})} = \frac{(X^m_{\text{SiOH}})^2}{(X^m_{\text{SiOSi}})(X^m_{H_2O,\text{mol}})} \qquad (13.1)$$

$$K_2 \equiv \frac{(a^m_{\text{SiONa}})(a^m_{\text{SiAlOH}})}{(a^m_{\text{SiOH}})(a^m_{\text{SiONaAl}})} = \frac{(X^m_{\text{SiONa}})(X^m_{\text{SiAlOH}})}{(X^m_{\text{SiOH}})(X^m_{\text{SiONaAl}})} \qquad (13.2)$$

assuming ideal mixing of the species. For any bulk composition and values of K_1 and K_2, the species concentrations in the melt can be determined. The magnitudes of K_1 and K_2 define the reactivities of the

Figure 15. Schematic molecular description of the coupled exchange reactions given in equations (12.1) and (12.2), illustrating the interaction of water with an albitic melt. After Burnham (1975, 1979).

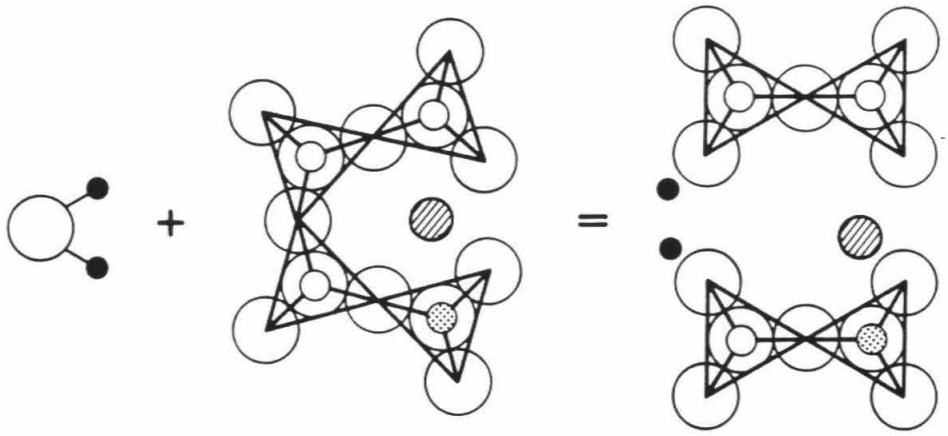

$$H_2O^{melt}_{molecular} + SiOSi^{melt} = 2\ SiOH^{melt} \quad (12.1)$$

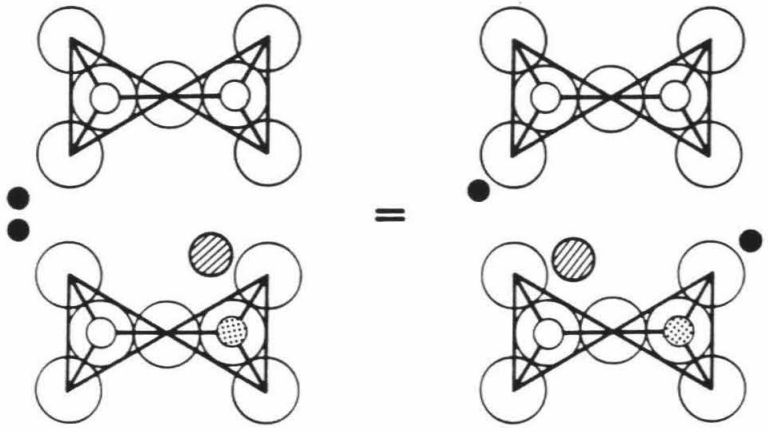

$$SiOH^{melt} + SiONaAl^{melt} = SiONa^{melt} + SiAlOH^{melt} \quad (12.2)$$

oxygen
Si^{4+}
Na^{+}
Al^{3+}
H^{+}

different oxygen units; with appropriate choices of K_1 and K_2, it is possible to reproduce the measured species concentrations. Figure 16 shows the results of the model calculation for K_1=0.003 and K_2=10. The calculated species concentrations are consistent with the spectroscopic measurements and demonstrates that this type of behavior could be important in controlling the dissolution of water in albitic melts. In addition, this model predicts that at a given total water content hydrous silica glass will have a much higher molecular H_2O to OH ratio than albitic glass and that the OH content of silica glass will not level off as sharply with increasing total water content as it does in albitic melt. It will be interesting to compare the speciation of water in silica glass to that of albitic glasses when systematic infrared or NMR spectroscopic data become available.

Summary

1. The simple mixing model developed by Stolper (1982b) and Silver & Stolper (1985) can be used as a starting point for the development of more complex models that can account in detail for the measured concentrations of water molecules and hydroxyl groups in albitic glasses. Individually, inclusion in these models of non-ideal interactions, of the mixing properties of polymeric groups, and of a range of distinguishable types of oxygens in the melt can lead to models that successfully account for the observed species concentrations. Models that combine these three modifications would also be successful.

2. Tests of these models will require more measurements on albitic glass and other compositions. For example, the multiple oxygen species

Figure 16. Calculation of the mole fractions of molecular water and OH groups as functions of the mole fraction of total water, X_B, based on the proton-exchange model (equations 13.1 and 13.2) for K_1=0.003 and K_2=10. Shown for comparison are the mole fractions of hydrous species determined by IR spectroscopy for the samples in Figs. 9 and 10.

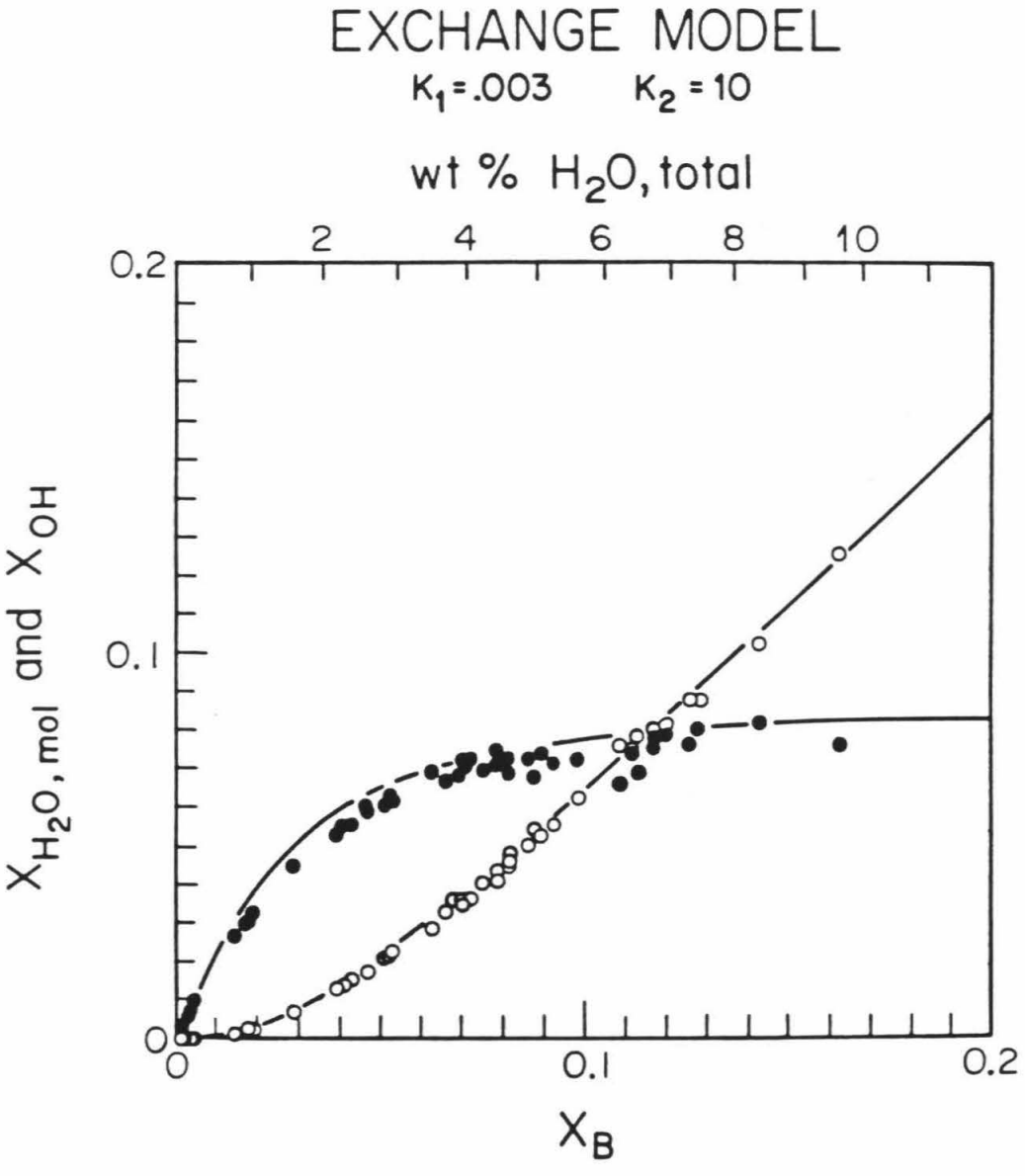
EXCHANGE MODEL
$K_1 = .003$ $K_2 = 10$
wt % H_2O, total
2
4
6
8
10
0.2
0.1
0
0
0.1
0.2
$X_{H_2O, mol}$ and X_{OH}
X_B

model considered above makes specific predictions about the saturation concentration of hydroxyl groups and about the solubility of water along the $NaAlO_2$-SiO_2 join that are grossly consistent with experimental data (i.e., the lower solubility of water in silica glass than in albite) and could be tested in detail by extending these measurements along this join.

3. It will be particularly important to determine if silica glass also shows a saturation in its hydroxyl group concentration that is more abrupt than that predicted by the simple ideal mixing model; if so, it will suggest that this feature is not dependent on the availability of an exchangeable cation that is nearly exhausted at high hydroxyl concentrations. Reliable quantitative measurements of the concentrations of distinguishable hydroxyl units (e.g., SiOH, AlOH, NaOH) and oxygen species (e.g., bridging vs. non-bridging, Al-O-Al, Al-O-Si) would also be useful in developing more accurate models of the dissolution mechanisms of water in silicate melts.

Chapter 3. Phase Equilibria in the Albite–Water System

Thermodynamic models of silicate melts such as those described in the preceding section can be used in conjunction with descriptions of the thermodynamic properties of vapor and crystals to calculate crystal-liquid-vapor phase equilibria (e.g., the pressure and temperature dependence of water solubility, the influence of water pressure on melting). In this section, these types of calculations are illustrated using the assumption that the activity of water in albitic melt is equal to the mole fraction of dissolved molecular water. Though somewhat arbitrary, this relationship will be valid for all ideal mixing models, no matter how many species are involved in the solution, if all species are similar in size. What is most attractive about this approach, if it can be shown to be successful, is that the mole fraction of molecular water and hence the activity of water can be readily determined for any glass by infrared spectroscopy. In addition, to the extent that the activity of water can be approximated by this mole fraction, it suggests that even though we may not have identified all of the species involved, the melt exhibits Henrian behavior over a substantial range of water contents (Darken, 1950; Burnham et al., 1978).

Freezing-Point Depression

I have calculated the position of the albite-saturated liquidus (i.e., the locus of liquid compositions saturated with crystalline albite) in the system albite-H_2O as a function of pressure and temperature using the approach outlined in Silver & Stolper (1985). Using the expressions given in that paper for the entropy of fusion and the dry solidus of crystalline high albite (Table 1 in Silver & Stolper,

1985), their equation (12) can be used to calculate the activity of albite (a^m_{ab}, where the albite component is defined as $Na_{1/8}Al_{1/8}Si_{3/8}O$) in albite-saturated melt as a function of pressure and temperature. The composition of melt in equilibrium with crystalline albite at a given P and T can then be determined given a relationship between melt chemistry and a^m_{ab}. From the assumption that $a^m_{H_2O} = X^m_{H_2O,mol}$, where the mole fraction of molecular water is given by the spectroscopic measurements, the relationship between a^m_{ab} and melt chemistry can be obtained by Gibbs-Duhem integration. The appropriate Gibbs-Duhem relation is

$$(1 - X_B)\, d(\ln a^m_{ab}) = -X_B\, d(\ln X^m_{H_2O,mol}) \qquad (14)$$

where X_B is the mole fraction of total water in the melt where the anhydrous component is taken as having only one oxygen (Wasserburg, 1957; Shaw, 1964; Stolper, 1982b; Silver & Stolper, 1985).[3] Figure 17 shows the resulting a^m_{ab} as a function of X_B; also shown are X^m_O (the mole fraction of unreacted oxygen or albite component, expressed on a single oxygen basis) and $X^m_{H_2O,mol} (\equiv a^m_{H_2O})$ as functions of X_B.

Melt-Vapor Equilibria

The interaction between vapor and water molecules dissolved in the melt can be described by the following reaction:

$$H_2O\ (vapor) = H_2O,molecules\ (melt) \qquad (15)$$

This reaction is governed by an equilibrium constant (Stolper, 1982b; Silver & Stolper, 1985)

---

3. X_B is the mole fraction of total dissolved water, where the anhydrous component is expressed on a one oxygen basis and can be calculated using the expression X_B=(wt% H_2O/18.015)/[wt% H_2O/18.015+(100-wt% H_2O)/32.78].

Figure 17. The activity of the albite (a^m_{ab}) and water ($a^m_{H_2O}$) components as functions of total water content for hydrous albitic melts. These activity-composition relations are based on assuming $a^m_{H_2O} = X^m_{H_2O,mol}$; a^m_{ab} was obtained by a Gibbs-Duhem integration for the binary system albite-H_2O, where the mole fraction of the albite component is based on a single oxygen. The relationship between $X^m_{H_2O,mol}$ and X_B used in the Gibbs-Duhem integration is given by the best fit regular solution model (see Fig. 13). Also shown is the variation in X^m_O (the mole fraction of unreacted oxygen or albite component in the melt; see Silver & Stolper, 1985), where the albite component is taken as having only one oxygen.

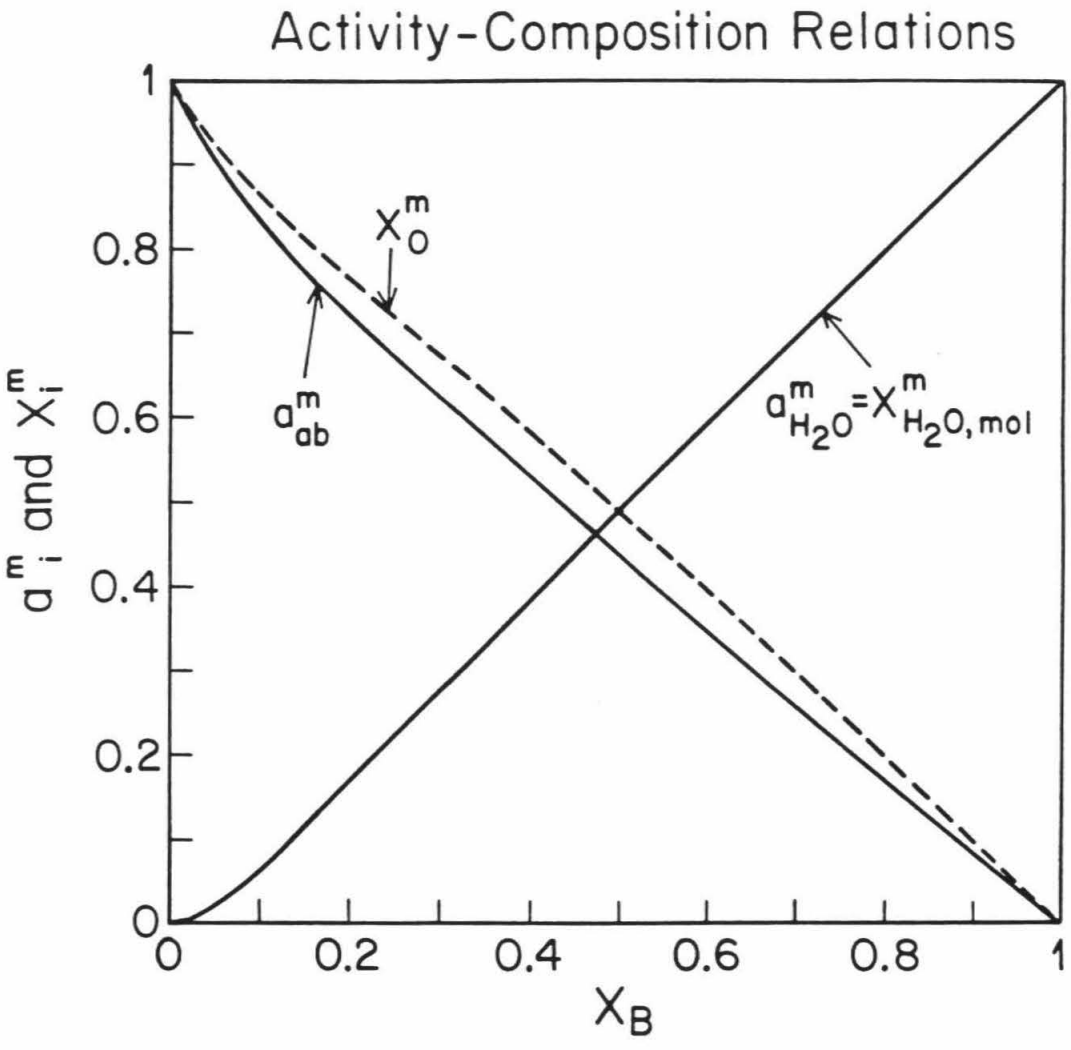
Activity-Composition Relations
1
0.8
0.6
0.4
0.2
0
0
0.2
0.4
0.6
0.8
1
a^m_i and X^m_i
X_B
X^m_O
a^m_{ab}
$a^m_{H_2O}=X^m_{H_2O,mol}$

$$K_2 = \frac{a^m_{H_2O,mol}}{a^v_{H_2O}} = \frac{X^m_{H_2O,mol}}{(f_{H_2O}/f^o_{H_2O})} \qquad (16)$$

The fugacity of water in the vapor in the standard state ($f^o_{H_2O}$) is that of pure water vapor at P and T, and f_{H_2O} is the fugacity of water in the vapor. The activity of water in the vapor is unity if the vapor is pure water and less than unity if the vapor contains other components. As described above, $a^m_{H_2O,mol}$, the activity of water molecules in the melt, defined relative to a standard state of pure water molecules at P and T (Shaw, 1964; Stolper, 1982b; Silver & Stolper, 1985), is assumed to be equal to $X^m_{H_2O,mol}$.

The variation in water solubility with pressure and temperature is then given by

$$X^m_{H_2O,mol}(T,P) = f^o_{H_2O}(T,P)\frac{X^m_{H_2O,mol}(T_r,P_r)}{f^o_{H_2O}(T_r,P_r)}\exp\left(-\int_{P_r}^{P}\frac{\overline{V}^{o,m}_{H_2O}(T,P)}{RT}dP + \int_{T_r}^{T}\frac{\Delta\overline{H}^o_{H_2O}(T,P_r)}{RT^2}dT\right) \qquad (17)$$

where P_r and T_r refer to a reference pressure and temperature, $X^m_{H_2O,mol}(T_r,P_r)$ is the solubility of molecular water in albite melt at T_r and P_r; $f^o_{H_2O}(T,P)$ and $f^o_{H_2O}(T_r,P_r)$ are the fugacities of pure water vapor at T, P and T_r, P_r calculated using the modified Redlich-Kwong equation-of-state for H_2O (Holloway, 1977); $\overline{V}^{o,m}_{H_2O}(T,P)$ is the molar volume of molecular water in the melt in its standard state; $\Delta\overline{H}^o_{H_2O} = \overline{H}^{o,m}_{H_2O} - \overline{H}^{o,v}_{H_2O}$ is the enthalpy change of reaction (15), $\overline{H}^{o,v}_{H_2O}$ is the standard state partial molar enthalpy of water in the vapor at pressures low enough for the vapor phase to be ideal, $\overline{H}^{o,m}_{H_2O}$ is the enthalpy per mole of molecular water in the melt in its standard state at P_r.

Equation (17) is based on the assumption that the vapor in equilibrium with melt is pure water. Given expressions for $\overline{V}^{o,m}_{H_2O}(T,P)$, $\Delta\overline{H}^{o}_{H_2O}(T,P_r)$, and $X^{m}_{H_2O,mol}(T_r,P_r)$, the variation in molecular water solubility as a function of T and P can then be calculated using equation (17). Total water solubility (molecular water plus hydroxyl groups) can then be determined given the relationship between $X^{m}_{H_2O,mol}$ and X_B determined spectroscopically (Fig. 17).

Determination of $\overline{V}^{o,m}_{H_2O}$ and $\Delta\overline{H}^{o}_{H_2O}$

I have used the experimentally determined position of the water-saturated solidus to constrain expressions for the standard state partial molar volume of water in the melt and $\Delta\overline{H}^{o}_{H_2O}(T,P_r)$ in equation (17). At any point on the wet solidus, a^{m}_{ab} can be calculated and hence $X^{m}_{H_2O,mol}$ (as described above) for vapor-saturated melts as a function of P and T along the wet solidus. Assuming that $a^{v}_{H_2O} = 1$ along the wet solidus, a least-squares procedure can then be used to constrain $\overline{V}^{o,m}_{H_2O}(T,P)$, $\Delta\overline{H}^{o}_{H_2O}(T,P_r)$, and $X^{m}_{H_2O,mol}(T_r,P_r)$ in equation (17).[4]

I have taken P_r and T_r to be 5000 bars and 745°C (Silver & Stolper, 1985). The volume of water is approximated by a polynomial of the form

$$\overline{V}^{o,m}_{H_2O}(T,P) = a + b\,(P-P_r) + c\,(P-P_r)^2 + d\,(T-T_r) \qquad (18)$$

where a, b, c and d are constants and $\Delta\overline{H}^{o}_{H_2O}(P_r)$ is assumed to be

---

4. In this treatment, I assume that the activity of water is equal to the mole fraction of molecular water in the melt and then solve for $\overline{V}^{o,m}_{H_2O}$ and the enthalpy difference using the position of the wet solidus (or data on water solubility; see below). Alternatively, if the volume and enthalpy functions were known, data on the P and T dependence of water solubility or the position of the wet solidus could be used to determine the activity of water in the melt as a function of X_B (or $X^{m}_{H_2O,mol}$). This approach was used by Burnham and Davis (1974).

independent of T (i.e., $\Delta c_p(T,P_r) = 0$). Note that in equation (17), only $\Delta\overline{H}^o_{H_2O}(P_r)$ is required; $\Delta\overline{H}^o_{H_2O}$ is, however, a function of P and T. Substituting equation (18) into equation (17), integrating and then taking the logarithm of both sides, gives $\ell n(X^m_{H_2O,mol})$ as a linear function in a, b, c, d, $\Delta\overline{H}^o_{H_2O}$ and $\ell nX^m_{H_2O,mol}(T_r,P_r)$. Values of a, b, c, d, $\Delta\overline{H}^o_{H_2O}$, and $X^m_{H_2O,mol}(T_r,P_r)$ were determined by least squares using points along the wet solidus at 500 bar intervals from 500 to 16000 bars and are listed in Table 6a. The best fit volume function can be approximated by a Murnaghan equation; values of the bulk modulus and the coefficient of thermal expansion are listed in Table 6b.

Burnham & Davis (1971) measured the volumes of albitic melts containing 8.25 and 10.9 wt % H_2O at pressures between 3 and 8.5 kbar and temperatures between 700 and 950°C. Given the fit to $\overline{V}^{o,m}_{H_2O}$ and to the partial molar volume of anhydrous albitic melts based on data in the literature (see Table 6b for parameters), I calculated the volume of albitic melts at the same conditions. Figure 18 compares calculated volumes of albitic melts containing 8.25 and 10.9 wt % H_2O to the measurements of Burnham & Davis (1971) at 750°C. This comparison demonstrates that the best fit $\overline{V}^{o,m}_{H_2O}(T,P)$ function is consistent with the measurements of Burnham & Davis at 750°C. My calculations fit their data equally well at temperatures up to 850°C. At higher temperatures (up to 950°C), the calculations tend to underestimate the volumes, but by no more than 4 percent. Although their parametrization of their results extrapolate to a large partial molar volume of water in the melt at low pressures, this is not required by their data or by my fit to the phase equilibrium data.

Table 6. Parameters for partial molar volume and enthalpy functions

TABLE 6

Parameters for partial molar volume and enthalpy functions[a]

a. Volume and enthalpy functions (best fit to position of the wet solidus):

$$\overline{V}^{o,m}_{H_2O}(T,P) = a + b(P-P_r) + c(P-P_r)^2 + d(T-T_r)$$

P_r=5000 bars, T_r=745°C

$a = 17.9$, $b = -2.6\times10^{-4}$, $c = 9.8\times10^{-9}$, $d = 2.75\times10^{-3}$

$\Delta\overline{H}^{o}_{H_2O}(T,P_r) = -9023$ cal/mol

$X^{m}_{H_2O,mol}(T_r,P_r) = 0.098$

b. Fits to Murnaghan equation:

$$\overline{V}^{o,m}_{i}(T,P) = \overline{V}^{o,m}_{i}(T_r,P_r)\, e^{\{\alpha(T-T_r)\}}\left(1+\frac{K'}{K}(P-P_r)\right)^{-1/K'}$$

i = H_2O[b]:

P_r=5000 bars, T_r=745°C

$\overline{V}^{o,m}(T_r,P_r)$= 17.9 cm^3/mol

K=75000 bars, $\alpha=1.53\times10^{-4}$ deg^{-1}, K'=4

i = albite:

P_r=1 bar, T_r=700°C

$\overline{V}^{o,m}_{ab}(T_r,P_r)$[c] = 13.81 cm^3/mol

K = 130000 bars [d], $\alpha = 4.2\times10^{-5}$ deg^{-1} [d], K' = 4 [e]

Notes:

a. units: a (cm^3/mol), b (cm^3 mol^{-1} bar^{-1}), c (cm^3 mol^{-1} bar^{-2}), d (cm^3 mol^{-1} deg^{-1})
b. Based on best fit to the position of the wet solidus
c. From Arndt & Häberle (1973)
d. From Lange & Carmichael (1987)
e. Assumed

Figure 18. The specific volume (in cm^3/gm) of hydrous albitic melts containing 8.25 and 10.9 wt % H_2O as functions of P at 750°C. The solid lines were calculated by using $\overline{V}^m_{H_2O}(T,P)$ from our model for hydrous albitic melts (parameters are given in Table 6b) and $\overline{V}^m_{ab}(T,P)$ based on data in the literature (see Table 6b for parameters) and then taking $\overline{V}_{total} = X_B\overline{V}^m_{H_2O} + (1-X_B)\,\overline{V}^m_{ab}$. The volumes determined experimentally at the same conditions by Burnham & Davis (1971) are represented by the various symbols.

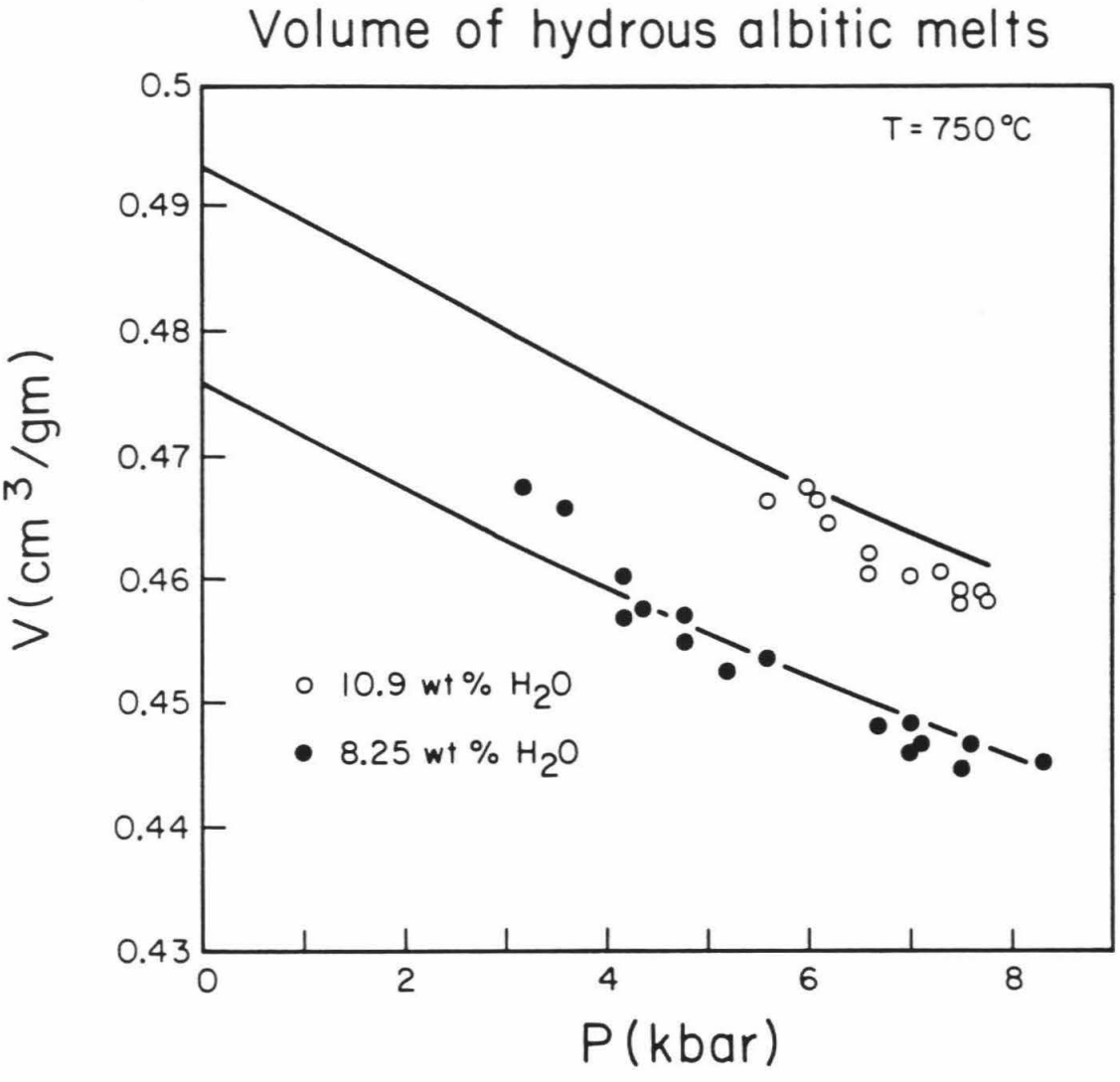
Volume of hydrous albitic melts
T = 750°C
o 10.9 wt % H_2O
● 8.25 wt % H_2O
V (cm^3/gm)
P (kbar)
0.5
0.49
0.48
0.47
0.46
0.45
0.44
0.43
0
2
4
6
8

The value of $\Delta\overline{H}^{o}_{H_2O}(T,P_r)$ from the best fit to the wet solidus is -9 kcal/mol; this is similar to the value of ~ -11 kcal/mol inferred from calorimetric studies (Navrotsky, 1987). This value leads to a negative temperature dependence of water solubility that is similar to that determined by Hamilton & Oxtoby (1986) at low pressures, but is too great at higher pressures. For example, at 1 kbar, the measured temperature dependence of H_2O solubility in albite is ~0.6 wt %/100°C, whereas I calculate a temperature dependence of 0.4 wt %/100°C; at 5 kbar, the measured temperature dependence is ~0.3 wt %/100°C, compared to about 1 wt %/100°C based on the best fit parameters.

Position of the Wet Solidus

Figure 19 compares the experimentally determined position of the water-saturated solidus of albite-H_2O with that calculated using the best fit equation of state for hydrous albitic liquids. The agreement is excellent over the whole range of P and T, but this is not surprising since the volume and enthalpy functions were determined so as to provide a best fit. Nevertheless, the fact that a simple and continuous volume function can account well for the shape of the solidus is encouraging.

The wet solidus for both high and low albite begin to curve downward towards lower temperatures at pressures greater than 14 kbar (Goldsmith & Jenkins, 1985).[5] This feature is also present in the

---

5. At pressures below 4 kbar, the assemblage high albite + water + melt is metastable relative to low albite + water. Above 16 (±1) kbar, the assemblage high albite + water + melt is metastable relative to the jadeite-bearing assemblages (Boettcher & Wyllie, 1969). Thus, the calculated solidus shown in Fig. 19 is metastable at both the high and low pressure ends.

Figure 19. The position of the water vapor-saturated solidus for high albite up to 16 kbar. The symbols with brackets represent experimental determinations for high albite with estimated uncertainties from △ Goranson (1938); ● Tuttle & Bowen (1958); ▲ Luth et al. (1964), corrected by Luth (1976); □ Boettcher & Wyllie (1969); ■ Morse (1970); ○ Bohlen et al. (1982); and | Goldsmith & Jenkins (1985). Arrows are upper temperature limits from Burnham & Jahns (1962). The heavy solid curve is the calculated wet solidus using the a-X relations shown in Fig. 17 and the best-fit parameters given in Table 6. The dry solidus is a best-fit line based on data from Boettcher et al. (1982).

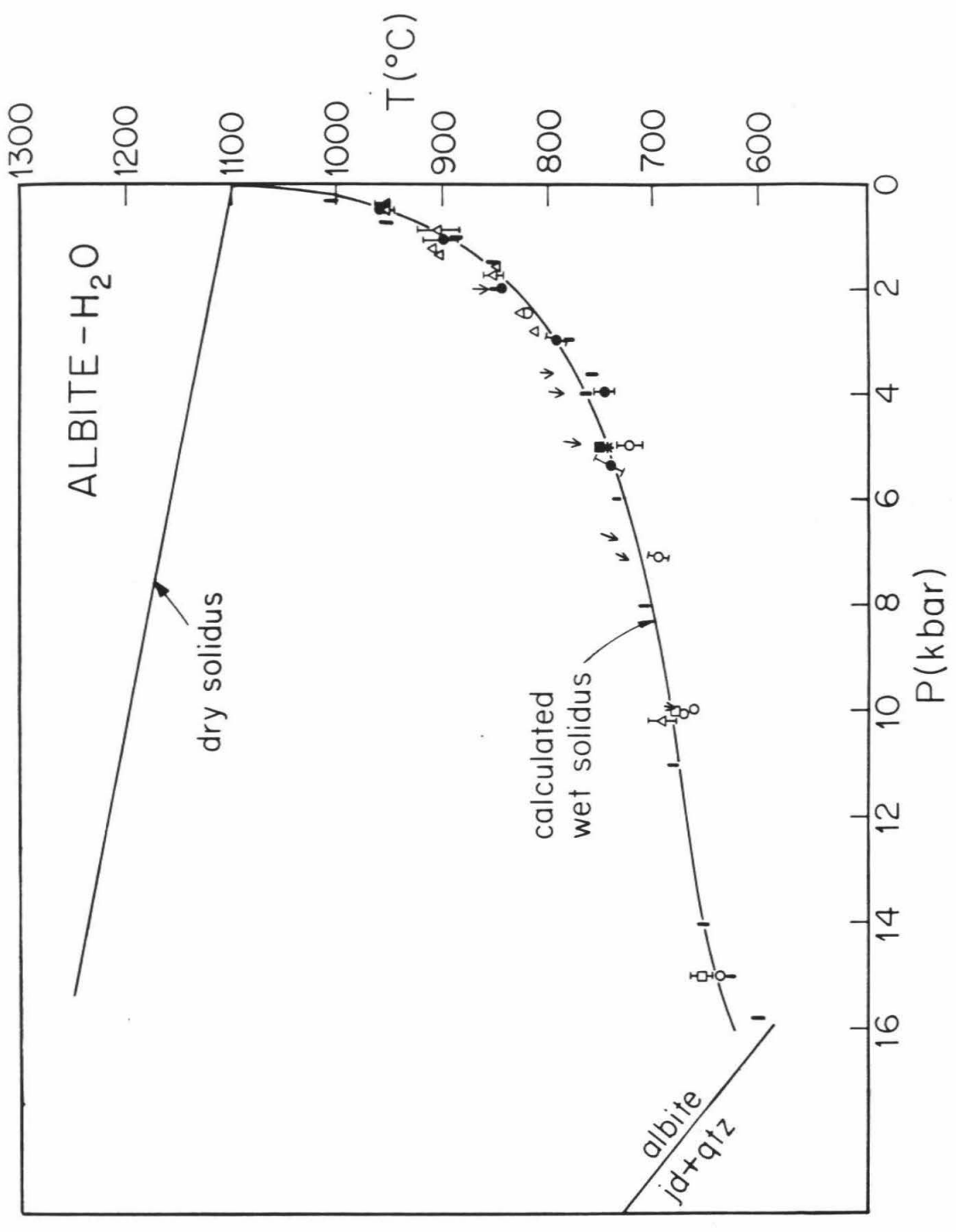
ALBITE-H_2O
dry solidus
calculated
wet solidus
albite
jd+qtz
T(°C)
P(kbar)
1300
1200
1100
1000
900
800
700
600
0
2
4
6
8
10
12
14
16

calculated solidus. It has been suggested that this downturn could reflect structural changes occurring in albitic melts as the albite=jadeite+quartz reaction is approached from the low pressure side (Goldsmith & Jenkins, 1985). Infrared spectra of glasses quenched from melts synthesized at pressures and temperatures near the albite-breakdown curve (samples MAb-10, 16, 34, 105 from Goldsmith & Jenkins, 1985) do not show any systematic changes that indicate a major change in coordination of Al^{3+} (L.A. Silver, unpub. results). Although such a coordination change could contribute to the observed downturn of the solidus, the thermodynamic model described above, with its simple, continuous volume function, a temperature independent enthalpy difference and a pressure independent activity-composition relation for water can account for this feature. Such downturns in temperature with increasing pressure along the water-saturated solidi in silicate systems have long been known (Morey & Fenner, 1917) and they are not always associated with solid-solid phase transformations (Bowen, 1928). Indeed, the wet solidi in many systems actually go through pressure maxima (i.e., $dP/dT = 0$) and these, too, appear unrelated to solid-solid reactions. These phenomena can readily be understood without recourse to changes in melt structure and are more likely related to the high solubility of water and its negative temperature dependence in certain systems (Morey & Fenner, 1917; Morey, 1924, 1957).

Solubility of H_2O in albitic melts

Figure 20 compares experimental determinations of H_2O solubility in albitic melt with that calculated based on equation (17). The H_2O

Figure 20. The pressure dependence of the solubility of H_2O in albite melt up to 16 kbar. The symbols represent experimental data from ● Goranson (1936, 1938), ■ Orlova (1962), ○ Burnham & Jahns (1962), ◆ Khitarov et al. (1963), ◇ Voigt et al. (1981), △ Fenn (1973), from Day & Fenn (1982), □ Blamart et al. (1986), ▷ Richet et al. (1986), and ▲ Hamilton & Oxtoby (1986). The solid curves are the calculated H_2O solubility at 600, 800 and 1000°C based on equation (17), using the best fit parameters given in Table 6b.

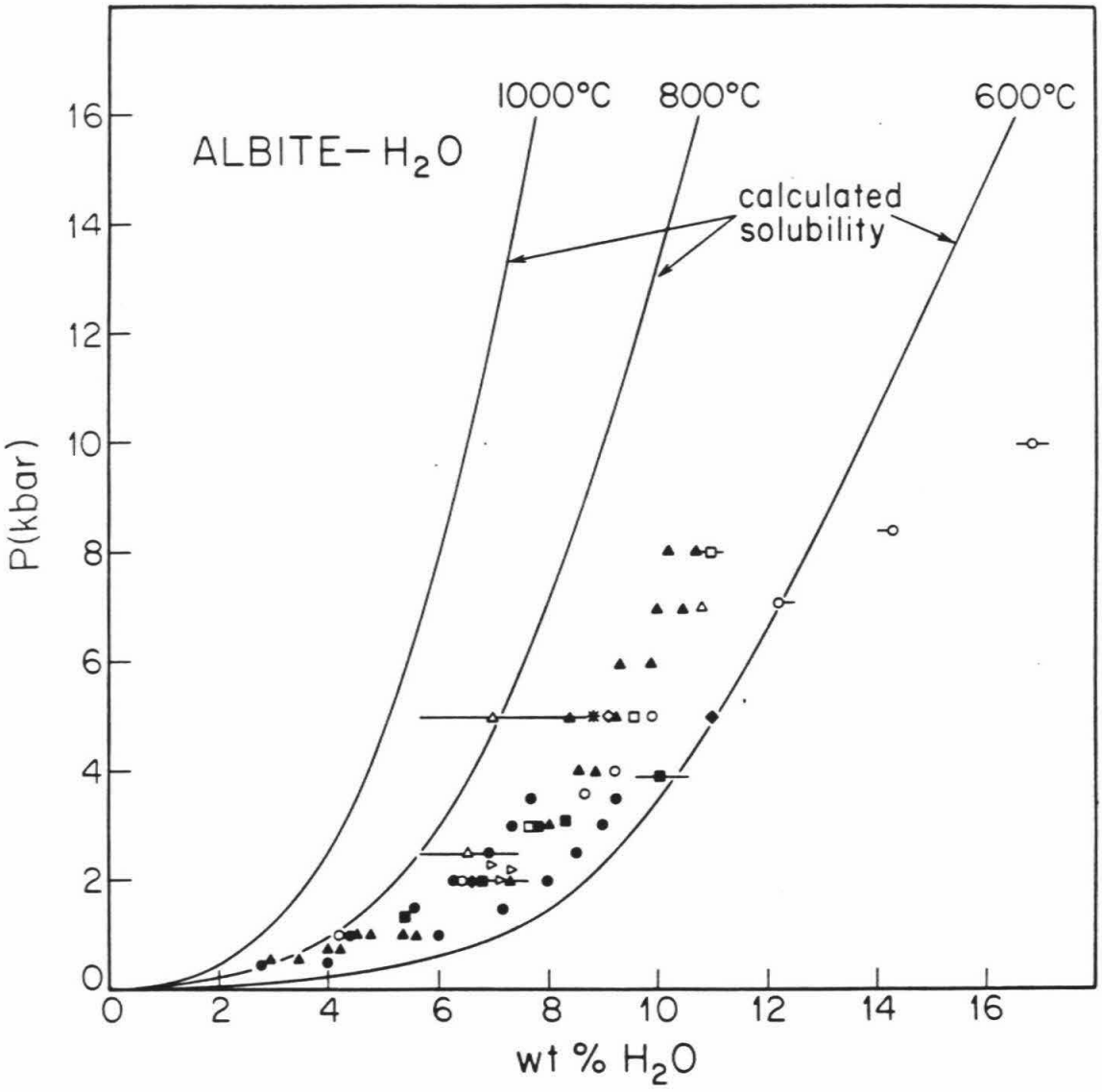
ALBITE– H_2O
1000°C
800°C
600°C
calculated solubility
P(kbar)
wt % H_2O
0
2
4
6
8
10
12
14
16

solubility calculated based on the best fit parameters is typically lower than the experimentally determined values. I could have used the measured water solubility as a function of P and T (rather than the position of the wet solidus) to fit the volume and enthalpy functions in equation (17) and thereby improved the agreement between measured and calculated water solubility. Even though there is considerable uncertainty in the solubility of water in albitic melt, I have explored this alternate approach, using the water solubility data of Hamilton & Oxtoby (1986) to constrain the volume and enthalpy functions (see Table 15 for parameters). When these expressions are used to calculate water solubility and the position of the wet solidus, the calculated water solubility matches their experimental determinations to within 0.5 wt % H_2O. However, the calculated wet solidus does not match the experimental data as well, and is about 30°C too high at 15 kbar, and ~ 60°C too low at 3 kbar. I consider this to be good agreement in view of the uncertainties in determinations of both the wet solidus and water solubility.

Summary

1. The approach to modelling the thermodynamic properties of hydrous albitic melts is based on direct measurements of hydrous species in albitic glasses. The relationship between water content and the activity of water in the melt is defined by assuming $a^m_{H_2O} = X^m_{H_2O,mol}$, where $X^m_{H_2O,mol}$ is measured by infrared spectroscopy.

2. Using this a-X model and phase equilibria in the albite-water system, I constrained expressions for the partial molar volume and

enthalpy of water in hydrous albitic melts. The resulting thermodynamic model can account reasonably well for the volumes of hydrous albitic melts, the pressure and temperature dependence of water solubility, and the position of the water-saturated solidus of crystalline albite.

3. The most important feature of this treatment is the connection between spectroscopic measurements and thermodynamics, though aspects of the model such as the low partial molar volume of water at low pressures and its ability to account for the observed increase in dP/dT along the vapor-saturated solidus at P > 14 kbar without resorting to pressure-induced changes in melt structure are considered to be significant.

Chapter 4. The Speciation of Water in Silicate Glasses

In this chapter, I extend the calibration of the infrared spectroscopic technique for quantitating hydrous species in glasses to a wide range of compositions (orthoclase, albite-orthoclase, jadeite, anorthite-silica-wollastonite). With these calibrations, I used infrared spectroscopy to determine the concentrations of molecular water and OH groups in these glasses for total water contents up to about 10 weight percent. The trends in the speciation of water in these glasses are compared to those observed for albitic glasses, and the generality of the conclusions drawn from the more detailed study of albitic glasses is evaluated.

Experimental Methods

The hydrous glasses described in this study were synthesized by quenching from melts equilibrated at elevated pressures and temperatures. The anhydrous starting materials were prepared in various ways as were the hydrous glasses. Most of the glasses were synthesized at Caltech; the remainder were prepared in other laboratories and made available for this study. Details of sample preparation and synthesis techniques for each composition are described below. Major element compositions of selected glasses were analyzed with the electron microprobe and are listed in Table 7.

Glass synthesis

Anorthite-silica-wollastonite eutectic (CAS) and E2: Starting material of CAS composition was prepared by grinding appropriate amounts of SiO_2, Al_2O_3, and $CaCO_3$ powders (Johnson-Matthey SpecPure reagents)

Table 7. Anhydrous glass compositions

TABLE 7

Anhydrous glass compositions

	CAS	E2	ABOR	ABORFE	ABOR50	KAS	Rhyolite
SiO_2	62.76	63.69	67.80	66.70	66.96	65.17	77.54
Al_2O_3	14.31	14.30	18.13	18.39	18.44	17.84	12.47
CaO	22.88	22.00	0	0	0	0	0.52
FeO	0	0	0	1.40	0.63	0	1.03
Na_2O	0	0	5.65	5.30	5.51	0	3.64
K_2O	0	0	8.42	8.21	8.86	16.96	4.79
Total	100	100	100	100	100	100	100

Notes:
1. Reported analyses are based on an average of 10 individual points per sample and are given in weight percent.

for 5 h in agate under ethanol; this mixture was melted at 1300°C and 1 atm and quenched to a glass; the glass was then finely ground, dried at 800°C for 24 h, and kept stored over dessicant.

Hydrous CAS glasses were synthesized in piston cylinder apparatus. Powdered starting materials with known amounts of triply distilled water were sealed in Pt capsules by arc-welding. These capsules were then held at 15-20 kbar and 1400-1450°C in piston cylinder apparatus for 2-6 h. Many CAS glasses were synthesized at Caltech in a 0.5 inch piston cylinder apparatus, using a talc cell with a pyrex sleeve. Hydrous glasses were also synthesized at the University of California, Los Angeles, in Professor Boettcher's lab, in a one-inch piston cylinder, using a NaCl cell with either a boron nitride (BN) assembly (samples CAS-11, CAS-12, CAS-13, CAS-14) or a fired pyrophyllite assembly (samples CAS-15, CAS-16). Details of the experimental apparatus are described in the Experimental Methods section of Chapter 1; run conditions are listed in Table 8.

A series of hydrous glasses with a bulk composition similar to that of the CAS glasses and with total water contents up to 9.25 wt %, were provided by Professor P. McMillan of Arizona State University. These samples were synthesized in IHPV at pressures between 103 and 5130 bars and temperatures between 1175 and 1191°C; the experimental details for synthesis of these glasses are reported by McMillan et al. (1986) and the run conditions are listed in Table 8.

Orthoclase (KAS): Starting material of orthoclase composition was prepared by grinding appropriate amounts of synthetic oxide-carbonate reagents in agate under ethanol for 5 h; this mixture was dried as

Table 8. Hydrous CAS and E2 glasses: Experimental data

TABLE 8 Hydrous CAS and E2 Glasses: Experimental data[1]

Sample #	starting material	P (kb)	T (C)	Time (min)	amt H2O added	Density[2] (g/l)		H2O,mol wt %	OH wt %	H2O,tot[4] wt %	H2O (total)[3] (wt%)		5,6 REMARKS	mole fractions[7] X(B)	X(H2O)	X(OH)
CAS-2	syn.oxide	15	1450	150	5	2620	e	3.03	2.37	5.40	5.11*(.11)		c,f,p	0.098	0.055	0.086
CAS-3	syn.oxide	15	1450	130	12	2425	h	7.71	2.46	10.17	10.17*(.26)		c,f,p	0.177	0.134	0.086
CAS-4	syn.oxide	15	1450	150	4	2670	e	1.77	2.11	3.89			c,f,p	0.072	0.033	0.078
CAS-6	syn.oxide	20	1450	210	6	2650	e	2.35	2.11	4.46			c,f,p	0.082	0.043	0.077
CAS-7	syn.oxide	20	1450	195	2	2718	e	0.08	0.81	0.89	0.88*(.03)		c,f,p	0.017	0.002	0.031
CAS-8	syn.oxide	20	1450	185	4	2500	e	1.64	2.01	3.66			c,f,p	0.067	0.030	0.074
CAS-11	syn.oxide	15	1450	120	10	2507	d	6.18	2.45	8.63	8.82*(.1),	8.76**(.44)	b,c,f,u,p	0.152	0.109	0.087
CAS-12	syn.oxide	15	1450	120	9	2554	d	4.61	2.46	7.07	7.93*(.11),	7.87**(.39)	b,c,f,u,p	0.127	0.083	0.088
CAS-13	syn.oxide	20	1450	120	2	2700	e	0.30	1.26	1.56	1.76*(.04),	1.73**(.09)	b,c,f,u,p	0.029	0.006	0.047
CAS-14	syn.oxide	20	1450	120	1	2727	d	0.03	0.58	0.61	0.67*(.02),	0.73**(.04)	b,c,f,u,p	0.012	0.001	0.022
CAS-15	syn.oxide	20	1450	90	1	2719	d	0.14	0.95	1.09	0.985*(.02),	1.06**(.05)	c,f,p,u	0.021	0.003	0.036
CAS-16	syn.oxide	20	1450	120	9	2575	e	4.43	2.68	7.11		6.96**(.35)	c,f,p,u	0.127	0.079	0.096
L2-34	syn.oxide	0.103	1180			2535	e	0.07	0.64	0.72	0.93***		f,x,i,s	0.014	0.001	0.024
L2-31	syn.oxide	0.258	1180			2515	g	0.36	1.28	1.64	1.88***		f,i,s	0.031	0.007	0.048
L2-25	syn.oxide	0.445	1170			2505	g	0.87	1.77	2.64	2.57***		f,i,s	0.049	0.016	0.066
L2-26	syn.oxide	0.600	1191			2500	g	1.09	1.89	2.98	2.90***		f,i,s	0.055	0.020	0.070
L2-32	syn.oxide	0.752	1181			2495	e	1.30	2.05	3.35	3.25***		f,i,s	0.062	0.024	0.076
L2-7	syn.oxide	1.004	1175			2485	g	1.64	2.07	3.71			f,i,s	0.068	0.030	0.076
L2-27	syn.oxide	1.025	1179			2485	g	1.70	2.11	3.81	3.89***		f,x,i,s	0.070	0.031	0.078
L2-30	syn.oxide	1.514	1175			2425	g	2.69	2.19	4.88	4.55***		f,i,s	0.089	0.049	0.080
L2-36	syn.oxide	5.130	1177			2405	g	6.56	2.45	9.00	9.25***		f,bb,i,s	0.159	0.116	0.086

Notes: (1) epsilon values: e(5200 cm-1)=1.07, e(4500 cm-1)=0.85 l/mol-cm
(2) Density measured using: d=Berman balance, h=heavy liquids
e= density estimated, g=density calculated from refractive index measured by P. Lambert (P. McMillan, personal comm.)
refractive indices: L2(dry)=1.546, L2-31=1.550, L2-25=1.547, L2-26=1.547, L2-7=1.545, L2-27=1.545, L2-30=1.542, L2-36=1.538
(3) * Total water contents determined by H2 manometry, ( ) indicates estimated error
** Total water contents determined by NMR (error =5%)
*** Total water contents determined by TGA (McMillan et al., 1986)
(4) Total water contents determined from sum of molecular H2O and OH
(5) samples synthesized in: p=piston cylinder apparatus, b=used boron-nitride assemblies
i=samples synthesized in IHPV, u=samples synthesized at UCLA
(6) Infrared spectra taken using: c=Cary 17 spectrometer, f= Nicolet FTIR spectrometer
bb=bubbles, x=crystals, s=saturation experiments
(7) mole fraction calculation, see TABLE 2, footnote 7

described above. Hydrous glasses were synthesized in piston cylinder apparatus by quenching from melts held at 1450°C and 15-20 kbar for 2 h. The syntheses were done either at Caltech, using a talc cell with a pyrex sleeve, or at UCLA, using a NaCl cell with either a BN-bearing assembly (samples KAS-2, KAS-3) or a fired pyrophyllite assembly (samples KAS-5, KAS-6, KAS-7, KAS-8, KAS-9). The run conditions are given in Table 9.

Albite-orthoclase (ABOR): Starting materials of albite-orthoclase (50 mol % albite, 50 mol % orthoclase) and 97.7 wt % albite-orthoclase + 2.3 wt % Fe_2O_3 (ABORFE) compositions were prepared at Corning Glass Works, by grinding production grade oxides and then melting at 1650°C for 6 h. These materials contain a small amount of Sb_2O_3 (0.43 wt%). Another albite-orthoclase mixture (ABOR50) was prepared at Caltech by mixing equal amounts by weight of the ABOR and ABORFE starting materials in agate. One hydrous glass of each composition was synthesized in piston cylinder apparatus, at 1400°C and 15-20 kbar. Samples ABOR and ABORFE were synthesized at UCLA in a one-inch piston cylinder apparatus, using a NaCl cell with a BN assembly. Sample ABOR50 was synthesized at Caltech in a 0.5 inch piston cylinder, using a talc cell with a pyrex sleeve. Run conditions for these samples are given in Table 10.

Jadeite (JD): Starting material of jadeite composition was prepared by grinding Burma jadeite in agate under ethanol for 5 h; the mixture was then dried as described above. Two hydrous JD glasses were synthesized at 1450°C and 15 kbar in a 0.5 inch piston cylinder apparatus, using a talc cell with a pyrex sleeve. Two other JD glasses were synthesized in internally heated pressure vessels (IHPV) at the

Table 9. Hydrous Orthoclase glasses: Experimental data

TABLE 9 Orthoclase glasses: Experimental data [1]

SAMPLE #	starting material	P (kb)	T (C)	Time (min)	Amt H2O added	Density [2] (g/l)		H2O,mol wt %	OH wt %	H2O,tot [4] wt %	H2O (total) (wt%)	REMARKS [6]	mole fractions [7] X(B)	X(H2O)	X(OH)
KAS-2	syn.oxide	15	1450	140	6	2380	e	1.74	1.55	3.29	3.32**(.17)	b,f,u	0.062	0.033	0.058
KAS-3	syn.oxide	15	1400	120	7.5	2335	e	3.46	1.84	5.30	5.95**(.3)	b,f,u	0.098	0.064	0.068
KAS-5	syn.oxide	20	1450	5	1	2438	d	0.39	0.96	1.36	1.5**(.08)	f,u	0.026	0.007	0.037
KAS-6	syn.oxide	20	1450	90	2	2425	d	0.80	1.32	2.12	1.93*(.04), 1.92**(.1)	f,u	0.040	0.015	0.050
KAS-7	syn.oxide	20	1450	90	2	2408	d	1.06	1.38	2.44	2.53*(.03), 2.62**(.13)	f,u	0.046	0.020	0.052
KAS-8	syn.oxide	20	1450	90	4	2487	d	0.13	0.73	0.86	0.963*(.03), 1.01**(.05)	f,u	0.016	0.003	0.028
KAS-9	syn.oxide	20	1450	90	1.5	2425	h	0.71	1.23	1.94	1.87**(.1)	f,u	0.037	0.013	0.047
KAS-10	syn.oxide	20	1450	120	8	2365	h	2.67	1.77	4.44	4.706*(.1), 4.66**(.2)	f	0.082	0.049	0.066
KAS-11	syn.oxide	20	1450	120	12	2290	h	5.07	1.98	7.04	7.09*(.23), 8.42**(.42)	f	0.128	0.092	0.072
KAS-12	syn.oxide	20	1450	120	9	2350	h	4.36	2.13	6.49	6.2*(.1), 6.33**(.32)	f	0.118	0.079	0.078

Notes: (1) epsilon values: e(5200 cm-1)=1.87, e(4500cm-1)=1.43 l/mol-cm
(2) Density measurements: h=made with heavy liquids (error: 25 g/l)
d=density measured with Berman balance (error: 10-20 g/l)
e=density estimated (error: 30 g/l)
(3) * Total H2O content measured by H2 manometry
** Total H2O contents measured by NMR spectroscopy
(4) Total H2O contents determined from sum of molecular H2O and OH, reported total H2O content is average of several analyses
(6) all samples synthesized in piston cylinder apparatus; u=samples synthesized at UCLA
b=used boron-nitride assemblies
Infrared spectra taken with: f=Nicolet FTIR spectrometer
(7) mole fraction calculation, see footnote, TABLE 2

Table 10. Hydrous albite-orthoclase glasses: Experimental Data

TABLE 10 Hydrous albite-orthoclase glasses: Experimental data [1]

SAMPLE #	starting material	P (kb)	T (C)	Time (min)	amt H2O added	Density (g/l) [2]	H2O,mol wt%	OH wt%	H2O,tot [4] wt%	H2O (total) [3] (wt%)	REMARKS [5,6]
ABOR50	syn.oxide	20	1400	120	9	2340 h	4.96	1.91	6.87	7.05*(.11) 6.10**	f
ABORFE	syn.oxide	20	1400	120	9	2325 h	5.44	1.91	7.34	8.113*(.1) 5.9**	b,f,u
ABOR	syn.oxide	15	1400	120	8	2325 h	4.83	1.69	6.52	7.39*(.11) 7.89**	b,f,u

Notes: (1) epsilon values: e(5200 cm-1)=1.77, e(4500 cm-1)=1.28
based on average of albite and orthoclase values
(2) Densities measured with: h=heavy liquids
(3) * Total water contents determined by H2 manometry
** Total water contents determined by NMR spectroscopy
(4) total water content based on sum of molecular H2O and OH
(5) Infrared spectra taken with: f=Nicolet FTIR spectrometer
(6) samples synthesized in piston cylinder apparatus; u= at UCLA
b=used boron nitride assemblies

Johnson Space Center, after sealing powdered starting materials with known amounts of triply-distilled water into Pt capsules by arc-welding. These capsules were held at 1000°C and 5 kbar and 1150°C and 2 kbar for up to 144 h. The details of the experimental apparatus are described in the Experimental Methods section of Chapter 1. One hydrous JD glass (JD+5) was obtained from Dr. B.O. Mysen for which details of the synthesis techniques are reported in Mysen and Virgo (1987b). The run conditions for the JD samples are listed in Table 11.

Anorthite-silica (ANS): A series of hydrous glasses with bulk compositions along the join anorthite-silica (An30Si70 to An51Si49) and total water contents between 8 and 13 wt % were provided by Dr. D. Stewart (sample numbers are the same as reported by Stewart, 1967). These glasses were synthesized in IHPV at 5 to 10 kbar and temperatures between 850 and 1050°C; details of the experimental apparatus are given by Stewart (1967) and the run conditions for these samples are listed in Table 12.

Rhyolites: A naturally-occurring rhyolitic glass (KS) from the ca. 1340 A.D. eruption of the Mono Craters, California was used as a starting material in this study. The rhyolitic glass is bubble-free, with minor amounts of crystallites, and has a water content of 0.78 wt % (Newman et al., 1986). Cores of this rhyolitic glass were drilled with a 3.5 mm diamond drill core, using water as the lubricating liquid. These cores were weighed with known amounts of triply-distilled water into Au capsules that were then sealed by arc-welding. The amount of water loaded into the capsules was enough to ensure that the melt was vapor-saturated at the pressure and temperature of the experiment.

Table 11. Hydrous jadeite glasses: Experimental data

TABLE 11 Hydrous jadeite glasses: Experimental data [1]

Sample #	starting material	P (kb)	T (C)	Time (min)	Amt H2O added	Density [2] (g/l)	H2O, mol wt %	OH wt %	H2O, tot wt %	H2O (total) [3] (wt%)	REMARKS [6]	mole fractions [7] X(D)	X(H2O)	X(OH)
CJD-1	Burma jd	20	1450	360	3.9	2400 e	1.42	1.49	2.91	2.91 (.14)*	f,p	0.053	0.026	0.054
CJD-3	Burma jd	20	1450	330	4.9	2370 e	2.50	1.58	4.08	4.08 (.12)*	f,p	0.074	0.045	0.057
JD+5		15	1550	240	5.0	2367 e	3.22	1.60	4.82	5.0 **	c,p	0.087	0.058	0.057
J1	Burma jd	5	1000	240	1.2	2400 e	1.88	1.59	3.47		c,i	0.063	0.034	0.058
J7	Burma jd	2	1150	8640	10.5	2325 e	5.35	1.62	6.97		c,i	0.123	0.094	0.057

NOTES:

(1) epsilon values: e(5200 cm-1)=1.13, e(4500 cm-1)=1.12 l/mol-cm
(2) e=Densities estimated
(3) * Total water contents determined by H2 manometry
** Total water content based on amount of water weighed into capsule
(4) Total H2O contents determined from sum of molecular H2O and OH, reported H2O content is average of several samples, except JD+5 (one analysis)
(6) Infrared spectra obtained using: c=Cary 17 spectrometer, f=FTIR spectrometer
samples synthesized in: i=IHPV, p=piston cylinder apparatus
(7) mole fraction calculation, see footnote, TABLE 2

Table 12. Hydrous anorthite-silica glasses: Experimental data

TABLE 12 Hydrous Anorthite-Silica glasses: Experimental data [1]

Sample #	Starting Composition	P (kb)	T (C)	Amt H2O added	Density[2] (g/l)	H2O, mol (wt %)	OH (wt %)	H2O, tot[4] (wt %)	H2O (total)[3] (wt%)	REMARKS[5]	mole fractions[6] X(B)	X(H2O)	X(OH)
ANS-162	An30Si70	5.00	1010	15.20	2250	7.69	1.82	9.51	9.90	c,i	0.154	0.125	0.059
ANS-167	An35Si65	5.00	950	16.10	2260	8.88	1.69	10.56	10.60	c,i	0.171	0.144	0.055
ANS-329	An40Si60	10.00	900	17.80	2200	10.73	1.58	12.30	12.30	c,i	0.198	0.173	0.051
ANS-156	An40Si60	5.00	875	16.20	2285	8.61	1.72	10.33		c,i	0.169	0.141	0.056
ANS-161	An45Si55	5.00	1010	15.00	2294	6.98	2.09	9.07	8.80	c,i	0.150	0.116	0.069
ANS-367	An45Si55	10.00	1050	18.00	2224	10.14	1.72	11.86	11.30	c,i	0.193	0.165	0.056
ANS-166	An45Si55	5.00	950	16.20	2286	7.60	1.95	9.54	9.60	c,i	0.158	0.126	0.064
ANS-328	An45Si55	10.00	900	25.30	2207	9.62	1.90	11.52	12.50	c,i	0.188	0.157	0.062
ANS-357	An45Si55	10.00	850	18.10	2232	9.62	1.78	11.40	11.20	c,i	0.186	0.157	0.058
ANS-358	An50Si50	10.00	850	19.60	2245	9.15	1.70	10.86	12.00	c,i	0.179	0.151	0.056
ANS-359	An51Si49	10.00	850	12.10	2232	10.11	1.80	11.91	12.10	c,i	0.195	0.166	0.059

NOTES: (1) epsilon values: An30Si70 to An40Si60 e(5200 cm-1)=1.46 e(4500 cm-1)=1.4
An45Si55 to An51Si49 e(5200 cm-1)=1.54 e(4500 cm-1)=1.24 l/mol-cm

(2) Densities determined by Stewart (1967)

(3) Total water contents determined by TGA (Stewart, 1967)

(4) Total water contents determined from sum of molecular H2O and OH

(5) samples synthesized in: i=IHPV
Infrared spectra taken with: c=Cary 17

(6) mole fraction calculation, see footnote, TABLE 2

Hydrous rhyolitic glasses were synthesized in two types of cold seal pressure vessels: (1) "air-quench" apparatus in which the bombs are removed from the furnace after the power is turned off and quenched in air (cooling rates on the order of 200°C/min), and (2) "rapid-quench" apparatus in which the sample is removed from the furnace after the power is turned off and quenched by a cooling water jacket (cooling rates on the order of 800°C/sec (P. Ihinger, personal comm., see also Ihinger & Stolper, in prep. for details of rapid quench apparatus). The capsules were held at constant temperature (850°C) and pressures between 49 and 1500 bars. The pressure medium was triply-distilled water and the pressure was monitored using Heise Bourdon tube gauges. For the air-quench cold-seal pressure vessels, the temperature was controlled by an internal Chromel-Alumel (Cr-Al) thermocouple and was also verified by an external Cr-Al thermocouple. For the rapid quench apparatus, the temperature was controlled by an external Cr-Al thermocouple. The run times varied but were usually longer than 48 h, which, based on the diffusion coefficients for water in rhyolitic glasses given by Karsten et al. (1982), would be sufficient for the water to be homogeneously distributed in the samples. Some of the experiments in the air-quench cold seal bombs were reversal experiments in which the sample was held at pressure of about 200 bars above the final pressure for about 48 h; the pressure was then dropped to the final pressure and held for another 48 h to allow the melt to reequilibrate. The run conditions of the samples synthesized in air-quench cold seal pressure vessels (samples KS-) and those that were synthesized in the rapid quench bombs (samples PDI-) are listed in Table 13.

Table 13. Hydrous rhyolitic glasses: Experimental data

TABLE 13 Hydrous rhyolitic glasses: Experimental data[1,6]

SAMPLE #	P[7] (bars)	T (C)	Time (hrs.)	Density[2] (g/l)	H2O,mol wt%	OH wt%	H2O,tot[4] wt%	H2O(total)[3] (wt %)	REMARKS[5]	mole fractions[8] X(B)	X(H2O)	X(OH)
KS-100	118	850	20.4	2319	0.36	0.77	1.12		c,f,aq	0.020	0.006	0.027
KS-200	223	850	49.5	2317	0.61	0.95	1.56		c,f,aq	0.028	0.011	0.034
KS-300	357	850	50.5	2325	1.08	1.12	2.20		c,f,aq	0.039	0.019	0.040
KS-400	482	850	52.25	2312	1.31	1.17	2.48		c,f,aq	0.044	0.023	0.041
KS-500	522	846	49.5	2325	1.45	1.20	2.66		c,f,aq	0.047	0.026	0.042
KS-500X	500	850	72	2325	1.48	1.13	2.61		bb,c,f	0.046	0.026	0.040
KS-600	717	850	49.3	2315	1.90	1.28	3.18		c,f,aq	0.056	0.033	0.045
KS-800	793	850	22	2315	1.93	1.31	3.24		c,f,aq	0.057	0.034	0.046
KS-900	1044	850	3.5	2310	1.75	1.26	3.01		c,f,aq	0.053	0.031	0.044
KS-310	370/ 232	850	53.5	2350	0.73	0.98	1.70		c,f,aq	0.030	0.013	0.035
KS-311	310/ 113	850	48	2350	0.36	0.83	1.19		c,aq	0.021	0.006	0.030
KS-530	540/ 366	850	72	2340	1.18	1.14	2.32		c,f,aq	0.041	0.021	0.040
KS-640	625/ 452	850	48	2340	1.44	1.23	2.67		c,f,aq	0.047	0.025	0.043
KS-650	680/ 548	850	114	2340	1.68	1.26	2.95		c,f,aq	0.052	0.030	0.044
KS-800.2	800	850	94	2310	2.26	1.37	3.63		c,f,aq	0.064	0.040	0.048
KSH-800	1000/000	850	116	2310	2.32	1.34	3.67		f,aq	0.064	0.041	0.047
KS-950	945	850	67	2300	2.46	1.35	3.80		c,f,aq	0.067	0.043	0.047
KS-960	960	850	25	2300	2.26	1.34	3.60		c,f,aq	0.063	0.040	0.047
KS-1000	1000	850	29.3	2300	3.07	1.45	4.53		bb,c,aq	0.079	0.053	0.051
UOUS-152	500	850	151	2340	1.70	1.16	2.86	3.08 (.12)	aq,f,**	0.050	0.030	0.041
UOUS-153	1000	850	151	2316	3.02	1.29	4.31	4.15 (.06)	aq,c,f,**	0.075	0.053	0.045
UOUS-154	2000	850	151	2294	3.78	1.3	5.08		aq,c,f,**	0.088	0.065	0.045
POIKS107	49	850	59	2341	0.16	0.61	0.76		rq,f	0.014	0.0028	0.022
POIKS108	156	850	94	2334	0.37	0.96	1.33		rq,f	0.024	0.0066	0.034
POIKS110	190	850	67	2333	0.44	1.02	1.46		rq,f	0.026	0.0078	0.036
POIKS105	299	850	57	2329	0.67	1.16	1.83		rq,f	0.032	0.0119	0.041
POIKS101	500	850	45	2320	1.19	1.38	2.57		rq,f	0.045	0.0210	0.049
POIKS102	500	850	64	2321	1.17	1.34	2.51		rq,f	0.044	0.0206	0.047
POIKS104	699	850	50	2314	1.67	1.48	3.15		rq,f	0.055	0.0294	0.052
POIKS114	799	850	46	2310	1.90	1.59	3.50		rq,f	0.061	0.0334	0.056
POIKS103	917	850	49	2307	2.13	1.62	3.75	3.58 (.1)	rq,f	0.066	0.0373	0.057
POIKS115	980	850	56	2305	2.23	1.70	3.94		rq,f	0.069	0.0391	0.060
POIKS111	1470	850	48	2292	3.29	1.77	5.06		rq,f	0.088	0.0570	0.061
POIKS113	1260	850	96	2299	2.68	1.74	4.43		rq,f	0.077	0.0468	0.061
POIKS109	98	850	47	2342	0.09	0.62	0.71		rq,f	0.013	0.002	0.022
POIKS106	1080	850	49	2300	2.07	1.58	3.65		rq,f	0.064	0.036	0.055

Notes:
(1) epsilon values: e(5200 cm-1)=1.61, e(4500 cm-1)=1.73 l/mol-cm
(2) Densities estimated
(3) * total H2O contents determined H2 manometry, ( ) indicates estimated error
(4) total water contents based on sum of molecular H2O and OH
reported value is average of several analyses
(5) Infrared spectra taken with: c=Cary 17 spectrometer, f=Nicolet FTIR spectrometer
bb=bubbles
samples synthesized cold seal apparatus: rq=rapid quench, aq=air-quench apparatus
** samples from H. Shaw
(6) all experiments were saturation experiments
(7) reversal runs indicated by P(start)/P(final)
(8) mole fraction calculation, see footnote, TABLE 2

Infrared spectroscopy

Doubly-polished discs were made of each of the glasses for the infrared spectroscopic work. The sample thicknesses were measured with a digital dial indicator. The infrared spectra were obtained using a Cary 17 spectrometer or a Nicolet Instruments 60SX Fourier transform infrared spectrometer. Details of the experimental techniques are given in the Experimental Methods section in Chapter 1. Densities of most of the glasses were measured using either a Berman balance, weighing in air and in toluene, or by the float-sink method, using heavy liquids of known densities. For samples that contained bubbles, the densities were estimated by comparison with glasses of similar water contents or calculated from the Gladstone-Dale rule (see Appendix 2).

Water analyses

The total water contents of many of the samples were determined by the hydrogen manometric technique described by Newman et al. (1986). Total water contents were also determined in selected glasses by nuclear magnetic resonance (NMR) spectroscopy, using the method described by Eckert et al. (1987b), given in Tables 8-10.

Infrared Spectra

Figure 21 shows the near-infrared absorption spectra (3600-7600 cm^{-1}) of a hydrous jadeite, orthoclase, albitic and E2 glass, all with similar total water contents (2.5-3.5 wt % H_2O).[6] Figure 22 shows

---

6. The water contents referred to in this section were determined by infrared spectroscopy.

Figure 21. Near-infrared absorption spectra (3660-7600 cm^{-1}) of hydrous jadeite, orthoclase, albitic and E2 glasses with total water contents between 2.5 and 3.5 wt %, scaled to a thickness of 300 microns. Spectra have been offset by 0.05 absorbance units for clarity. Samples shown are KAS-7 (2.5 wt % H_2O), CJD-1 (2.88 wt % H_2O), A1010 (2.97 wt % H_2O) and E2-27 (3.5 wt % H_2O).

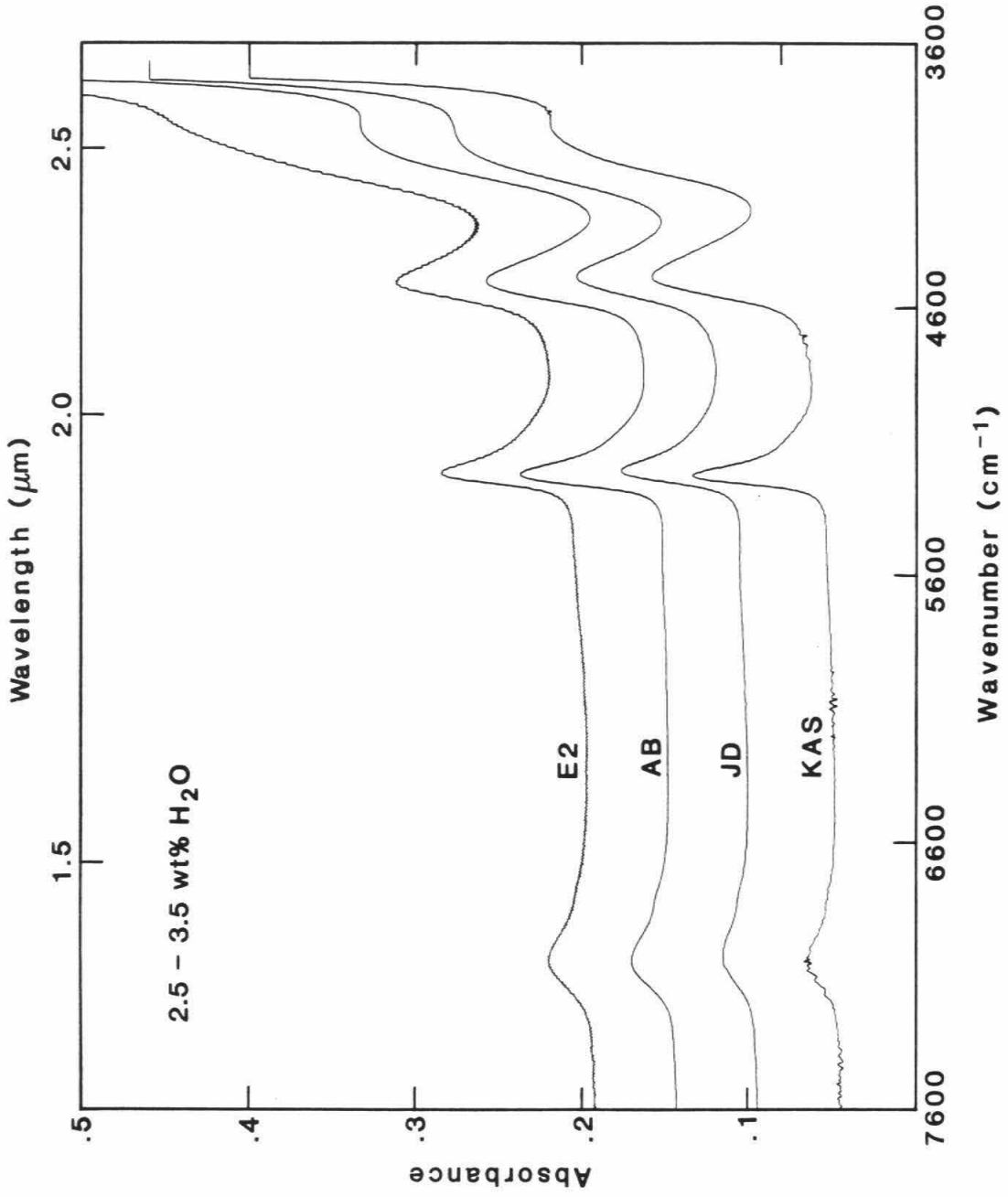
Wavelength (μm)
1.5
2.0
2.5
Wavenumber (cm⁻¹)
7600
6600
5600
4600
3600
Absorbance
.5
.4
.3
.2
.1
2.5 – 3.5 wt% H2O
E2
AB
JD
KAS

Figure 22. Near-infrared absortion spectra (3600-7600 cm^{-1}) of hydrous albite-orthoclase, CAS and anorthite-silica (An30Si70) glasses with total water contents between 7.1 and 9.5 wt %, scaled to a thickness of 300 microns. Spectra have been offset by 0.05 absorbance units for clarity. Sample shown are AB0R50 (7.09 wt % H_2O), CAS-11 (8.61 wt % H_2O) and ANS-162 (9.51 wt % H_2O).

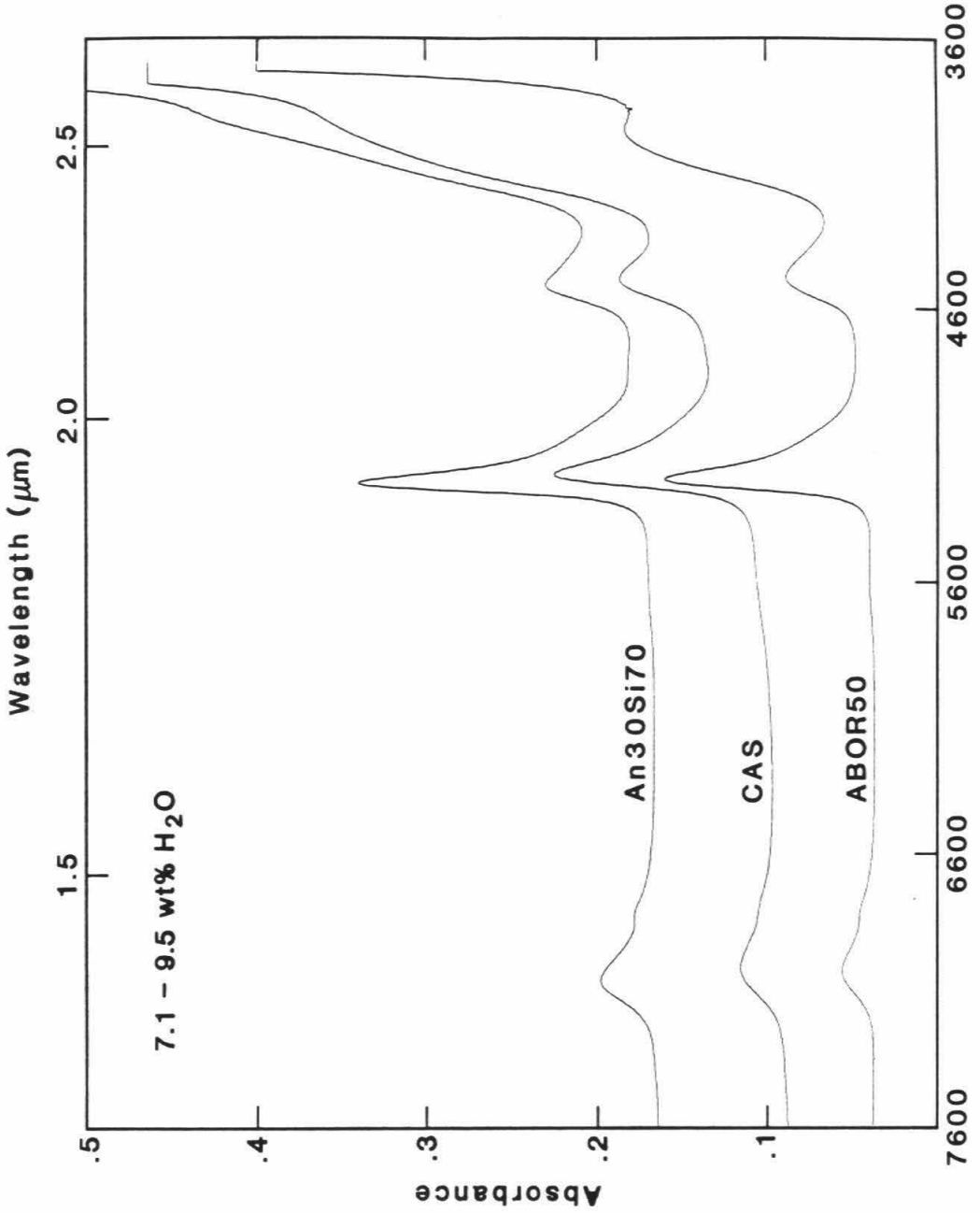
Wavelength (μm)
1.5
2.0
2.5
7.1 – 9.5 wt% H_2O
An30Si70
CAS
ABOR50
Absorbance
.5
.4
.3
.2
.1
7600
6600
5600
4600
3600
Wavenumber (cm^{-1})

the spectra of a hydrous CAS, albite-orthoclase (AB0R50), and anorthite-silica glass, with much higher total water contents (7.1-9.5 wt % H_2O). The exact locations of the bands near 4500, 5200 and 7100 cm^{-1} for each composition are listed in Table 14. As reviewed by Newman et al. (1986), these bands are assigned to combination modes for molecular water (5200 cm^{-1}) and OH groups (4500 cm^{-1}) and combination and overtone modes due to both species (4000 and 7100 cm^{-1}).

For the range of compositions studied, there is a correlation between the frequency of maximum intensity of these bands and the silica content; i.e., the frequency of each band shifts to higher energies with increasing silica content. Despite these small differences in the exact positions of the four bands in this region, the overall lineshapes are similar among these compositions and to those of hydrous albitic glasses. For the An30Si70 glass (Fig. 22), there is an indication of the development of a shoulder near 4400 cm^{-1}, as is observed in the spectrum of hydrous silica glass (L.A. Silver, unpub. results). Figure 22 also shows a well-developed shoulder at 6850 cm^{-1}, similar to the feature seen in the spectra of hydrous albitic glasses with total water contents greater than 3 wt % (Chapter 1); this shoulder may reflect clustering of water molecules by analogy with a similar feature that has been observed in the infrared spectra of opals (Langer & Flörke, 1974).

Determination of Extinction Coefficients

In order to use the intensities of infrared absorption bands to determine species concentrations, the extinction coefficients, ε, for each band for each silicate glass composition must be determined. In

Table 14. Band assignments and extinction coefficients

TABLE 14

Band assignments and extinction coefficients

	molecular water		hydroxyl		OH-overtone
Composition	peak position (cm^{-1})	ε (1/mol-cm)	peak position (cm^{-1})	ε (1/mol-cm)	peak position (cm^{-1})
CAS	5204	1.07	4485	0.85	7028
KAS	5222	1.87	4472	1.43	7030
JD	5207	1.13	4476	1.12	7010
An30Si70	5232	1.47	4503	1.40	7055
An45Si55	5222	1.54	4500	1.27	7030
ABOR	5219	----	4474	----	7022

this chapter, the 5200 and 4500 cm^{-1} bands are used for measuring the concentrations of molecular water and OH groups. The extinction coefficients for these bands were determined following the method of Newman et al. (1986). Briefly, infrared spectra of hydrous glasses spanning a range of total water contents were obtained and the peak heights of the 5200 and 4500 cm^{-1} bands were measured. The total water contents of these same glasses were then determined by hydrogen manometry, using the method described by Newman et al. (1986) and/or NMR spectroscopy, using the method described by Eckert et al. (1987b). The extinction coefficients were determined by a linear regression of an equation of the form

$$\frac{\rho\ d\ conc\ (H_2O,\ total)}{18.015} = \frac{Abs(5200\ cm^{-1})}{(\varepsilon_{5200\ cm^{-1}})} + \frac{Abs(4500\ cm^{-1})}{(\varepsilon_{4500\ cm^{-1}})} \qquad (19)$$

where Abs(i)=absorbance of infrared band i, ρ=sample density (g/l), d=sample thickness (cm), 18.015=molecular weight of H_2O, and ε=molar absorptivity of infrared band i (l/mol-cm). This procedure is based on the assumptions that the extinction coefficients are constant over the range of water contents studied and that there are only two dissolved hydrous species.

Rhyolites: The extinction coefficients for the 5200 and 4500 cm^{-1} bands for the rhyolitic composition have been previously determined by Newman et al. (1986) for rhyolitic glasses with total water contents up to 2.64 wt %. To demonstrate that the extinction coefficients are valid for hydrous rhyolitic glasses with higher water contents, three glasses with up to 5 wt % H_2O were analyzed for total water by hydrogen

manometry. The good agreement between the total water contents determined by infrared spectroscopy based on the best fit extinction coefficients (Table 13) and the water contents determined by manometry demonstrates that the ε values determined by Newman et al. (1986) are valid for hydrous rhyolitic glasses with up to at least 4 wt % H_2O.

CAS and E2 glasses: The compositions of the E2 and CAS glasses are similar and they have been treated as a single data set (Table 8). A total of five glasses of the CAS composition, with water contents between 0.9 and 10.2 wt %, were used in the regression to determine the extinction coefficients. Total water contents for these glasses were determined by H_2 manometry and/or NMR spectroscopy. For the E2 composition, eight glasses with 0.9 to 9.3 wt % H_2O were analyzed for total water contents by a weight loss method (TGA); the results are reported in McMillan et al. (1986), with the exception of E2-31, which has a total water content of 1.88 wt %, not 0.89 wt % as reported (P. McMillan, personal comm.). The best fit ε values for these two bands are given in Table 14. The ε values are similar, within analytical error, if the data on the CAS and E2 glasses are fit separately. Figure 23 demonstrates that the total water contents determined from the sum of the molecular water (from the 5200 cm^{-1} band) and hydroxyl group (from the 4500 cm^{-1} band) contents determined by infrared spectroscopy are similar to the total water contents determined by hydrogen manometry, NMR or TGA. The good agreement between the total water content determined by IR and these other independent methods suggests that the assumption of constant extinction coefficients is valid for total water contents up to 10 wt %.

Figure 23. Total water contents obtained by summing the amounts of molecular water (5200 cm^{-1} band) and OH groups (4500 cm^{-1} band) versus total water contents determined by H_2 manometry, NMR spectroscopy or TGA in CAS (squares) and E2 (triangles) glasses. Filled symbols represent samples synthesized in BN-bearing assemblies. Estimated errors are indicated by error bars. Samples shown are CAS-2, CAS-3, CAS-7, CAS-11, CAS-12, CAS-13, CAS-14, CAS-15, CAS-16, E2-25, E2-26, E2-27, E2-30, E2-31, E2-32, E2-34, and E2-36.

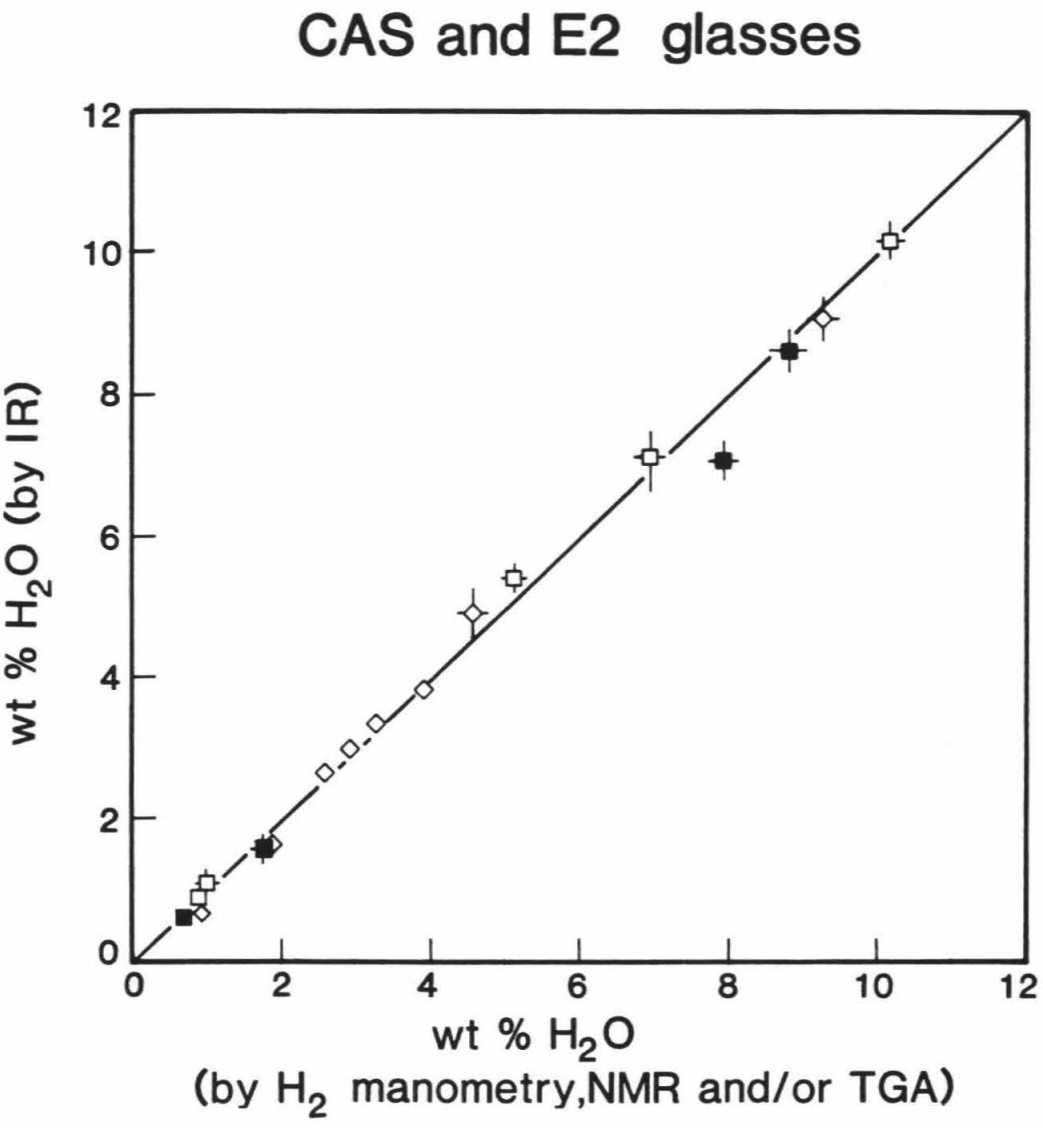
CAS and E2 glasses
wt % H_2O (by IR)
wt % H_2O
(by H_2 manometry,NMR and/or TGA)
0
2
4
6
8
10
12

Four CAS glasses were synthesized in BN assemblies and the infrared spectra of the two low water content samples (CAS-13, CAS-14) show anomalous absorption bands at 4125 and 5030 cm^{-1}. These four samples were not included in the calibration because of the possible existence of additional H-bearing species (see Chapter 1); however, the extinction coefficients are essentially the same whether or not these samples are included in the regression. As shown in Fig. 23, the total water contents determined by infrared spectroscopy for samples synthesized in BN assemblies are typically low, but within 0.3 wt % of the value determined by NMR or manometry (with the exception of CAS-12, for which the IR value is 0.9 wt % less than those determined by manometry and NMR spectroscopy.

Orthoclase glasses: Seven glasses with water contents between 1 and 7 wt % were used in the regression to determine extinction coefficients. Total water contents of these KAS glasses were determined by H_2 manometry and/or NMR spectroscopy. The best fit ε values for the 4500 and 5200 cm^{-1} bands are listed in Table 14. As demonstrated in Fig. 24, the total water contents (molecular water + hydroxyl groups) determined by infrared spectroscopy using the ε values are similar to the total water contents determined by NMR spectroscopy and/or manometry.

Two of the KAS samples were synthesized in BN assemblies and were not included in the regression for reasons discussed above, although the extinction coefficients are essentially identical whether or not these samples are included. As shown in Fig. 24, the water content determined by infrared spectroscopy for sample KAS-2 based on the best fit ε values

Figure 24. Total water contents in orthoclase glasses determined by infrared spectroscopy from the sum of molecular water (5200 cm^{-1} band) and OH groups (4500 cm^{-1} band) versus total water contents determined by H_2 manometry and/or NMR spectroscopy. Open symbols represent samples synthesized in BN-free assemblies; filled symbols represent samples synthesized in BN-bearing assemblies. Estimated errors are indicated by error bars. Samples shown are KAS2, KAS-3, KAS-5, KAS-6, KAS-7, KAS-8, KAS-9, KAS-10, KAS-11, and KAS-12. The water content for KAS-11 as shown was determined by H_2 manometry; the NMR value of 8.4 wt % is not indicated.

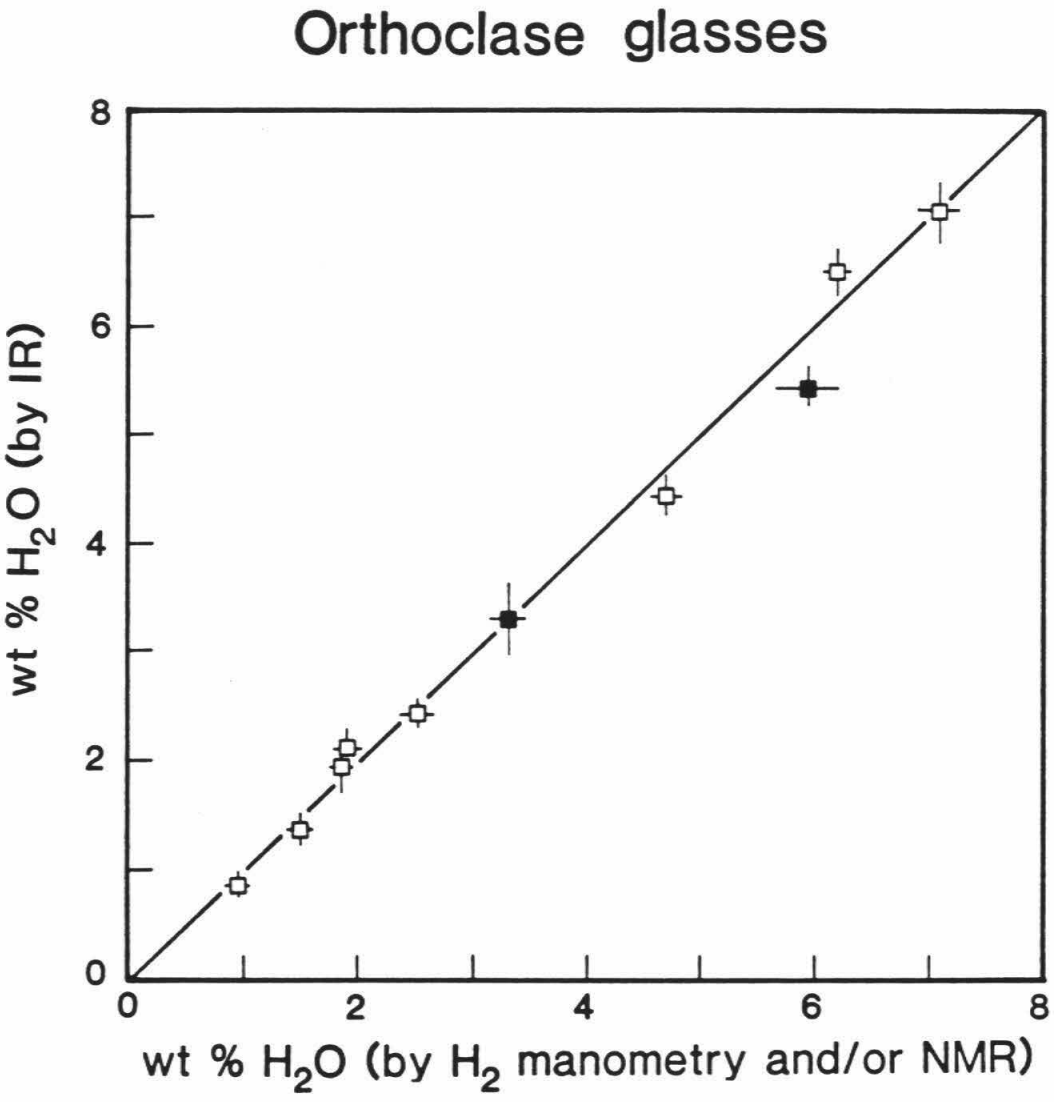
Orthoclase glasses
wt % H_2O (by IR)
wt % H_2O (by H_2 manometry and/or NMR)
0
2
4
6
8

is similar to the amount determined by NMR spectroscopy; however, the water content determined for sample KAS-3 by IR spectroscopy is 0.6 wt % lower than the NMR result.

Albite-orthoclase glasses: Albite-orthoclase glasses with similar total water contents, but with varying total Fe contents, were synthesized to assess the influence of Fe in hydrous glasses on quantitation of water in glasses by NMR spectroscopy (Eckert et al., 1987b). They also offer the opportunity to see if extinction coefficients vary linearly along the albite-orthoclase join and if small amounts of iron influence infrared extinction coefficients.

Total water contents of three glasses (AB0R, AB0RFE, and AB0R50) were determined by manometry; NMR spectra were also obtained, but as discussed by Eckert et al. (1987b), NMR spectroscopy underestimates water contents for Fe-bearing glasses. For the Fe-free glass (AB0R), the water contents determined by the two methods are similar.

It is not possible to solve for the extinction coefficients using the method described above because only one hydrous albite-orthoclase glass was synthesized for each AB0R composition. However, as shown in Fig. 25, using the extinction coefficients for albitic glass for the 4500 and 5200 cm^{-1} bands, the infrared measurements are in good agreement with the manometric results. The orthoclase extinction coefficients and averages of the albite and orthoclase values result in underestimates of the total water contents. The best agreement between the IR measurements and manometry is obtained for sample AB0R50. The AB0R and AB0RFE samples were synthesized in BN-bearing assemblies, and this factor may account for much of the discrepancy between the infrared

Figure 25. Total water contents in albite-orthoclase glasses determined from the sum of molecular water (5200 cm^{-1} band) and OH groups (4500 cm^{-1} band) based on three sets of extinction coefficients versus total water contents determined by manometry. The filled circles represent total water contents based on ε values for orthoclase (Table 14); the crosses represent water contents based on ε values for albite (Table 5); the open circles represent water contents based on an average of albite and orthoclase ε values. Estimated errors are indicated by error bars. Samples shown are ABOR, ABOR50 and ABORFE.

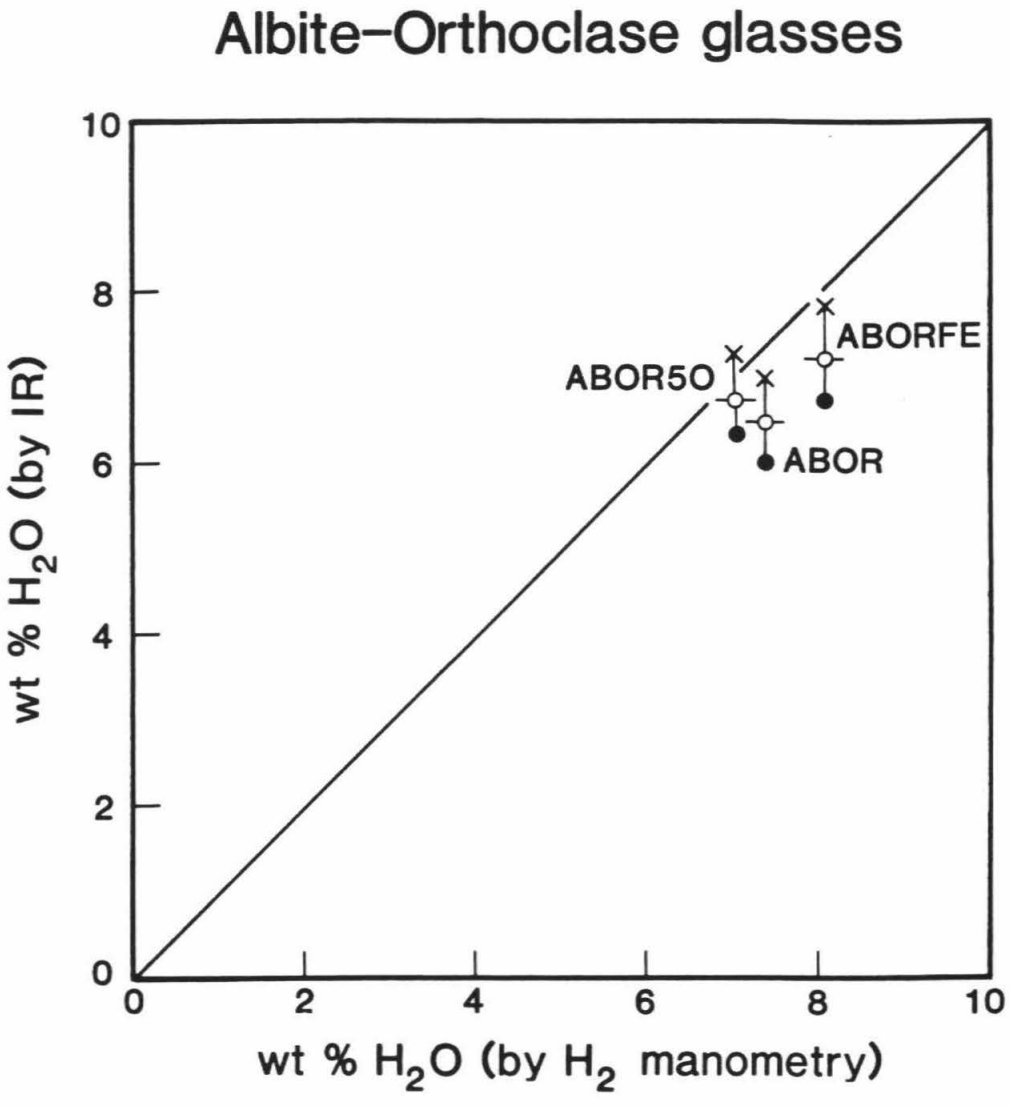
Albite–Orthoclase glasses
wt % H_2O (by IR)
wt % H_2O (by H_2 manometry)
0
2
4
6
8
10
ABORFE
ABOR5O
ABOR

and manometric results. Similar differences are observed in samples CAS-12 and KAS-3, for which the total water contents (based on the best fit ε values) are low relative to the manometric values by as much as 0.9 wt %, however, these large differences are not observed for most other samples synthesized in BN assemblies. Given the uncertainty in the results due to the synthesis conditions, it is not possible to determine if the presence of Fe influences extinction coefficients. Synthesis (in BN-free assemblies) of additional samples, both Fe-free and Fe-bearing, with a greater range in water contents will be necessary to address these issues and to more accurately calibrate the infrared absorbance bands for this composition.

Jadeite glasses: Two jadeite glasses with water contents of 2.9 and 4.1 wt % were used to solve for the extinction coefficients for this composition. Total water contents were measured by hydrogen manometry and the extinction coefficients are listed in Table 14. As a test of these values, the total water content was determined by infrared spectroscopy for a hydrous jadeite glass (JD+5) provided by Dr. B. Mysen, for which Mysen & Virgo (1987b) report a water content of 5 wt % based on the amount of H_2O weighed into the capsule. The total water content based on the best fit ε values (4.8 wt %) is similar to the amount loaded into this sample by Mysen & Virgo (1987b). Despite this good agreement, additional samples with a wider range of water contents, particularly low-water samples, will be needed to confirm this calibration.

Anorthite-silica glasses: The samples provided by Dr. D. Stewart vary in bulk composition (excluding the water content) from An30Si70 to

An51Si49, with total water contents between 8 and 13 wt %. Over this range of silicate composition, it is unlikely that the extinction coefficients are constant and therefore a different set of values should be determined for each individual silicate composition. There are only a few samples of any given composition, so to improve the statistics of the regression, the samples were divided into two groups: three samples with compositions An(30-40)Si(70-60) and six samples with compositions An(45-51)Si(55-49). Total water contents of these glasses were determined by a weight loss method and are reported by Stewart (1967). Using these total water contents, best fit extinction coefficients for the two groups of samples were determined (Table 14). These ε values are at best approximate values. In particular, the ε value for the OH band is poorly constrained because the glasses cover a narrow range in total water contents over which the OH content is approximately constant. Figure 26 compares the calculated total water contents for both groups of samples (based on the best fit ε values) with the total water contents determined by Stewart (1967). The agreement between these two methods is fair, given the uncertainties in the ε values. As discussed above, the calibration could be improved given additional samples of each anorthite-silica composition with a wider range of total water contents.

Summary of calibration

The infrared spectroscopic technique described above has been calibrated against independent techniques for a range of compositions. The extinction coefficients for each composition were determined by

Figure 26. Total water contents in anorthite-silica glasses determined by infrared spectroscopy from the sum of molecular water (5200 cm^{-1} band) and OH groups (4500 cm^{-1} band) versus total water contents determined by TGA. Open squares represent samples with compositions An(45-51)Si(55-49); open circles represent samples with compositions An(30-40)Si(70-60). Estimated errors are indicated by error bars. Samples shown are An(30-40)Si(70-60): ANS-162, ANS-167, ANS-329; An(45-51)Si(55-49): ANS-161, ANS-166, ANS-328, ANS-357, ANS-359.

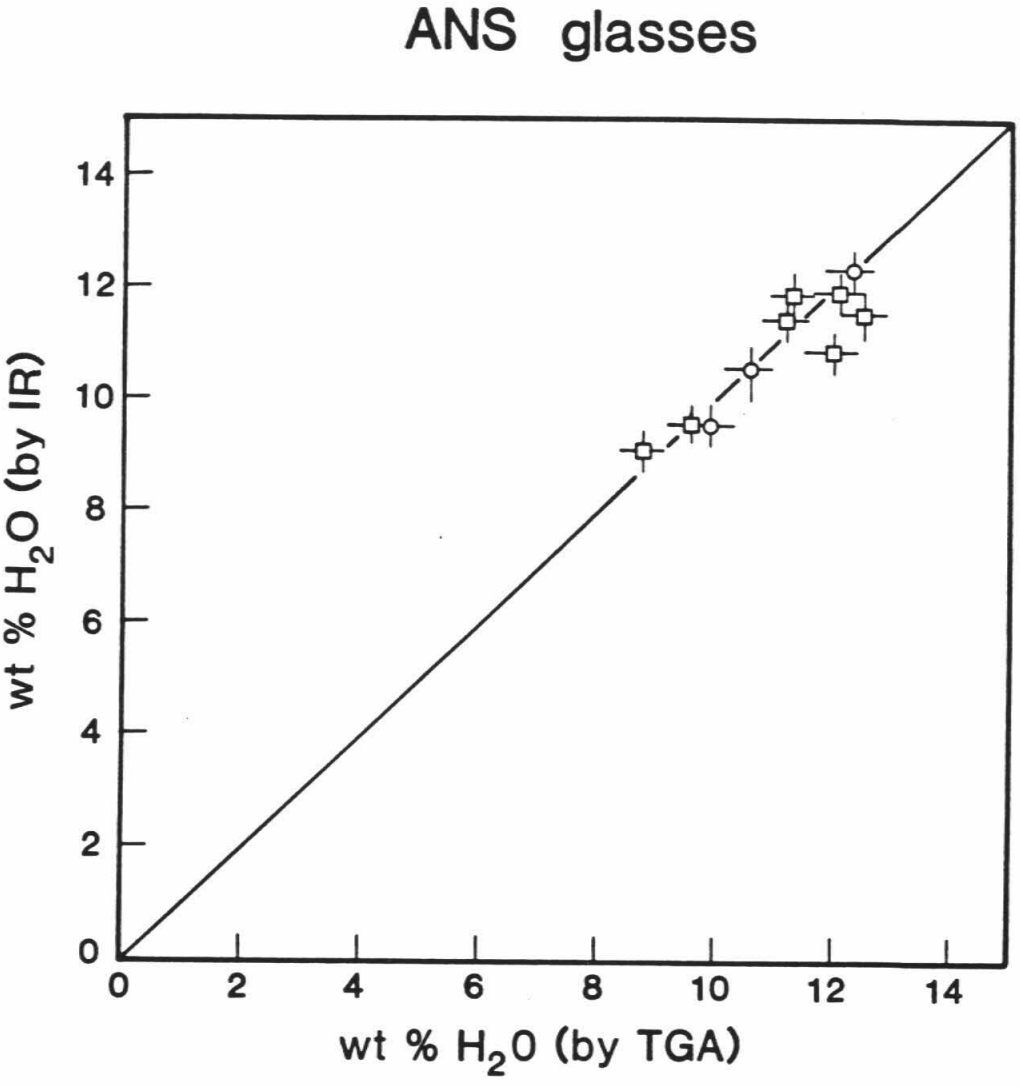
ANS glasses
wt % H_2O (by IR)
wt % H_2O (by TGA)
0
2
4
6
8
10
12
14

linear regression when possible and were successful at retrieving the total water contents determined by manometry, NMR spectroscopy or TGA. The ε values determined in this study vary with silicate composition: 1.1-1.9 l/mol-cm for the 5200 cm^{-1} band and 0.9-1.4 l/mol-cm for the 4500 cm^{-1} band. This variation demonstrates the importance of carrying out a careful calibration for each composition if quantitative results are desired.

To improve the calibrations presented here, additional samples will be required with low total water contents, in the range where nearly all of the water is dissolved as hydroxyl. This is essential to better constrain the ε value for the 4500 cm^{-1} band. This approach was taken by Newman et al. (1986) and the ε values they determined for hydrous rhyolitic glasses based only on glasses with $\leq$3 wt % are still valid when applied to rhyolitic glasses with at least 5 % water. These are probably the best constrained of the extinction coefficients used in this study. They had an advantage in that large quantities of these natural samples could be used for analysis by manometry. For synthetic samples, it is more difficult to synthesize enough homogeneous, low water material for precise, accurate analysis by either manometry or NMR spectroscopy. It is also particularly important that the samples be synthesized in BN-free assemblies, to eliminate the possibility of other H-bearing species. In spite of these difficulties, these results demonstrate that when calibrated properly, infrared spectroscopy provides an accurate and precise method for determining total water contents and species concentrations in hydrous silicate glasses.

The Speciation of Water in Silicate Glasses

Using the calibrations described above, I determined the speciation of water in a variety of synthetic hydrous glasses quenched from melts held at elevated pressures and temperatures. The concentrations of molecular water, hydroxyl groups and total water contents were determined by infrared spectroscopy, based on the best fit values of the extinction coefficients given in Table 14 and in Newman et al. (1986); the hydrous species concentrations are given in Tables 8-12.

CAS-E2 and orthoclase: Figures 27 and 28 show the concentrations of molecular water and hydroxyl groups as functions of total water for the CAS-E2 and orthoclase glasses. Also shown in Figs. 27 and 28 are fits to the measured molecular water and OH group contents (see Appendix 1 for fitting procedure). The general trends in species concentrations are similar to those determined for hydrous albitic glasses (Fig. 9), though the hydroxyl content does not quite level off in the orthoclase glasses for this range of total water contents. At low total water contents, most of the water is dissolved as hydroxyl groups. At a total water content of about 3 (for KAS) and 4 (for CAS) wt %, there are equal amounts of water dissolved as molecular water and OH groups. At higher total water contents, molecular water becomes the dominant species and the OH concentration remains approximately constant or increases very little.

The similarity in the ratio of molecular water to hydroxyl groups at a given total water content for both the CAS and E2 compositions in Fig. 27 demonstrates the lack of pressure and temperature on the speciation of water in these glasses. Although the CAS and E2 glasses

Figure 27. The concentrations of water dissolved as molecules of H_2O (open symbols) and as OH (filled symbols) as functions of total water content in CAS (circles) and E2 (triangles) glasses, together with a best fit to the data (see Appendix 1). The run conditions for all the samples are listed in Table 8.

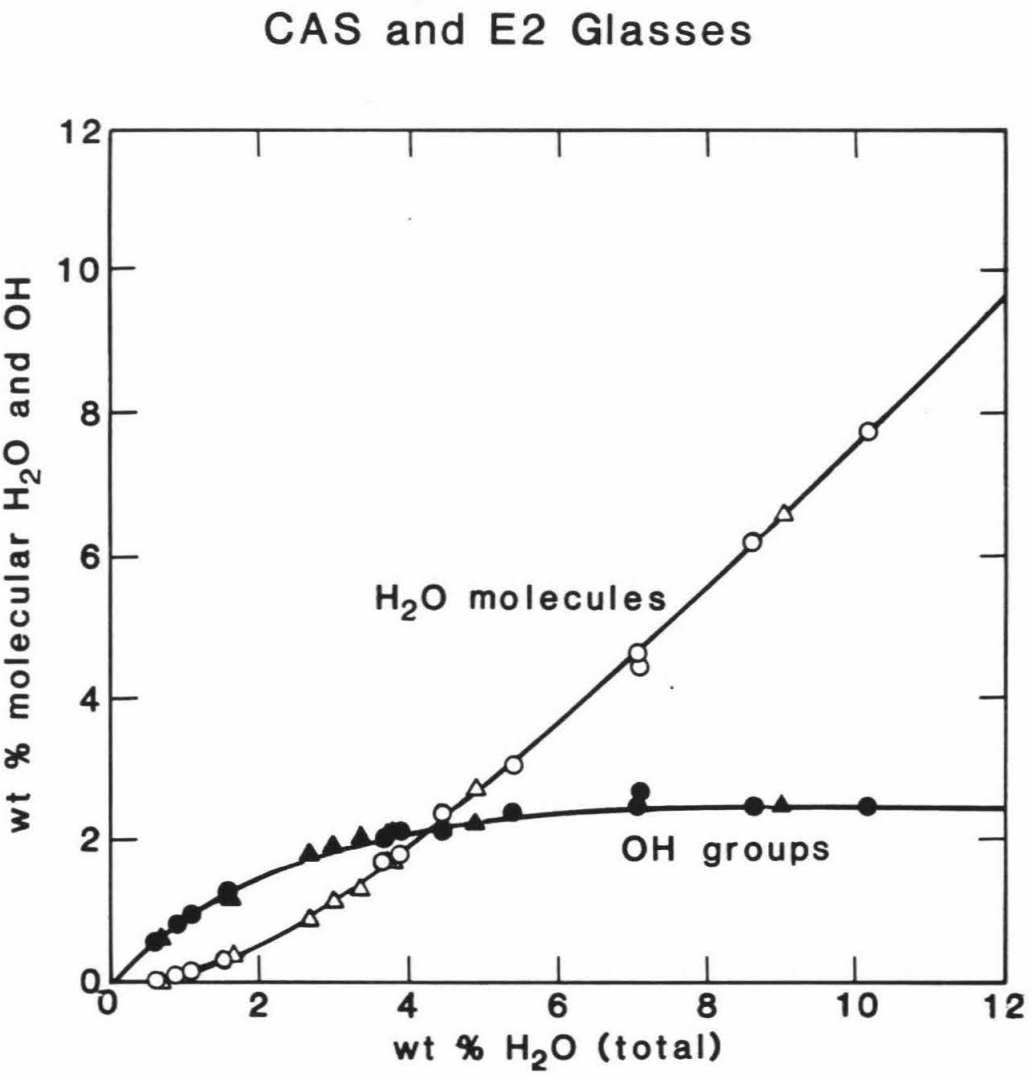
CAS and E2 Glasses
wt % molecular H_2O and OH
wt % H_2O (total)
H_2O molecules
OH groups
0
2
4
6
8
10
12

Figure 28. The concentrations of water dissolved as molecules of H_2O (open symbols) and as OH (filled symbols) as functions of total water content in orthoclase glasses, together with a best fit to the data (see Appendix 1). The run conditions for all the samples are listed in Table 9.

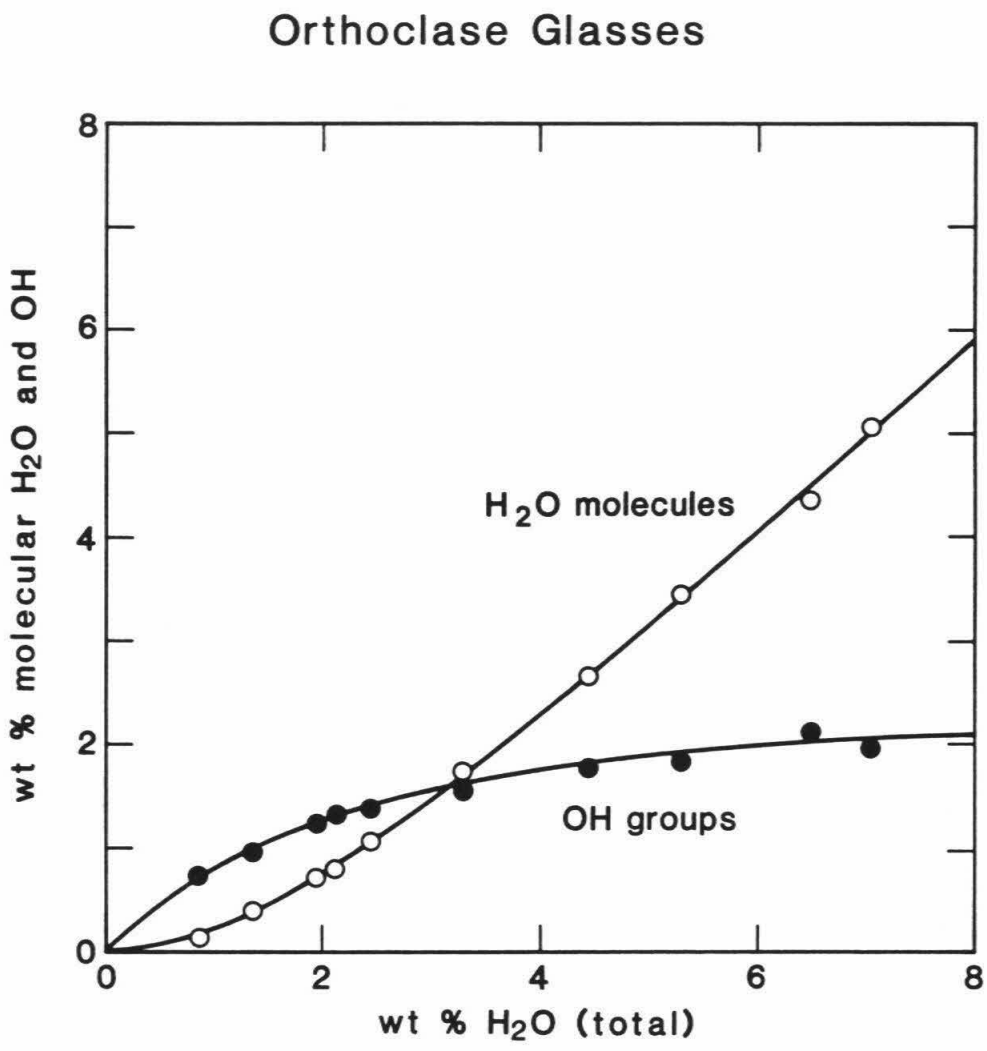
Orthoclase Glasses
wt % molecular H_2O and OH
wt % H_2O (total)
H_2O molecules
OH groups
0
2
4
6
8

were synthesized by different techniques, at different experimental conditions (E2 glasses were synthesized in IHPV, CAS glasses in piston-cylinder apparatus), these results do not indicate any dependence of the speciation of water on quenching rate. This observation contrasts with the results obtained for hydrous albitic glasses (Chapter 1), in which glasses synthesized in IHPV had consistently higher ratios of molecular water to OH groups at a given total water content than those glasses synthesized in piston cylinder apparatus.

Jadeite and anorthite-silica: Figures 29 and 30 show the variation in the concentration of molecular water and hydroxyl groups as a function of total water content for hydrous JD and ANS glasses quenched from melts synthesized over a range of experimental conditions (Tables 11 and 12). Although the extinction coefficients are not well constrained for these compositions, it is clear, regardless of the ε values, that the general trends in the speciation of water for hydrous JD and ANS glasses are the similar to those observed for a variety of other compositions.

The concentration of OH groups in the ANS glasses, shown in Fig. 30, decreases slightly with increasing total water contents at high water contents. Bartholomew et al. (1980) observed a similar trend for OH group contents in a "hydrosilicate" glass at total water contents greater than about 4 wt %. Such a progressive decrease in the OH content at high water contents is consistent with the extrapolated trends of the non-ideal mixing model discussed in Chapter 2. Although this trend may be real, it could also be due to a quenching effect. The ANS samples were synthesized in IHPV and cooled to ambient conditions

Figure 29. The concentrations of water dissolved as molecules of H_2O (open symbols) and as OH (filled symbols) as functions of total water content in jadeite glasses synthesized in piston cylinder apparatus and IHPV over a range of experimental conditions. The open and filled circles represent samples from this study; the open and filled triangle represent the sample from Mysen & Virgo (1986b). The run conditions for all the samples are listed in Table 11.

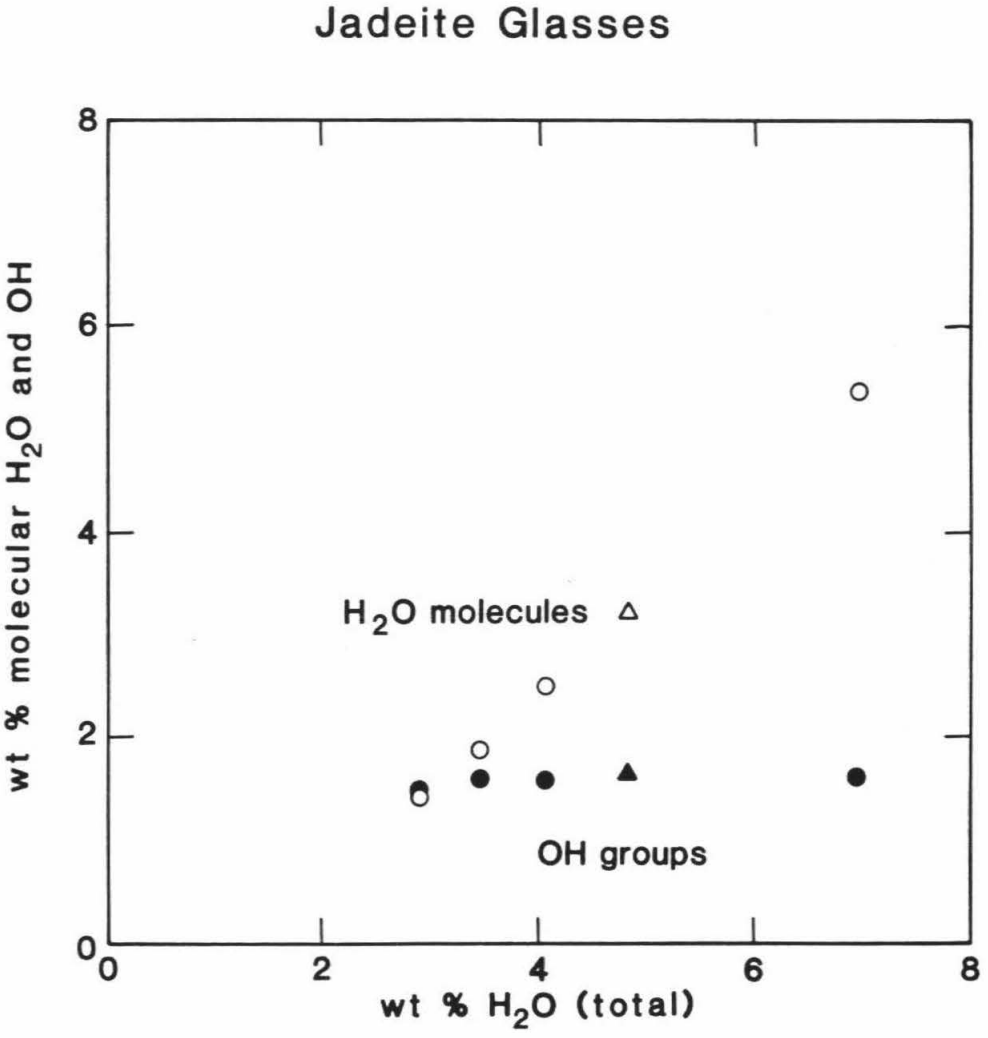
Jadeite Glasses
wt % molecular H_2O and OH
wt % H_2O (total)
H_2O molecules
OH groups
0
2
4
6
8

Figure 30. The concentrations of water dissolved as molecules of H_2O (open symbols) and as OH (filled symbols) as functions of total water content in anorthite-silica glasses. The squares represent samples with bulk compositions An(45-51)Si(55-49); the circles represent samples with bulk compositions An(30-40)Si(70-60). The run conditions for all the samples are listed in Table 12.

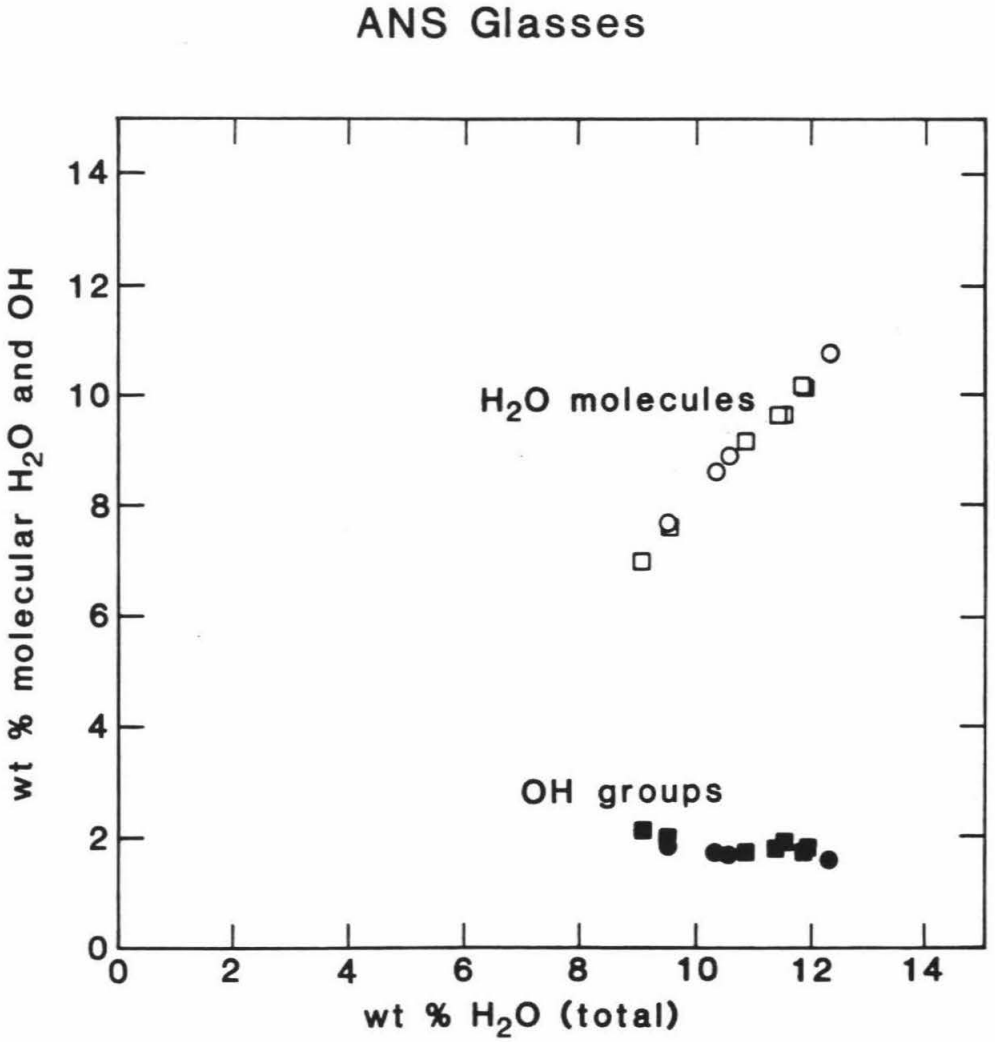
ANS Glasses
wt % molecular H_2O and OH
wt % H_2O (total)
H_2O molecules
OH groups
0
2
4
6
8
10
12
14

over several minutes, during which time the melt may have reequilibrated. As demonstrated in Chapter 1 for albite, and below for rhyolite, the ratio of molecular water to OH groups at a given total water content is higher in hydrous glasses synthesized in IHPV and air-quench cold seal bombs than for samples synthesized at similar conditions in piston cylinder or rapid quench cold seal apparatus, probably due to the slow conversion of hydroxyl to molecular water on slow cooling (though as mentioned above, the CAS/E2 glasses do not appear to show this). Thus, the low hydroxyl contents at the highest total water contents in the ANS glasses may reflect reequilibration of the melt to lower temperatures by conversion of hydroxyl to molecular water, provided that this effect is more extreme for water-rich glasses.

Rhyolitic glasses: Figure 31a shows the concentrations of molecular water and OH groups determined by infrared spectroscopy as functions of total water content for hydrous rhyolitic glasses synthesized in rapid quench cold seal pressure vessels at 850°C and pressures up to 1500 bars, together with fits to the data (see Appendix 1 for fitting procedure). At low total water, most of the water is dissolved as OH groups. At 2.9 weight percent total water, there are equal amounts of molecular water and hydroxyl groups; this cross-over point occurs at the lowest total water content of all the silicate compositions included in this study. At higher total water contents, molecular water is the dominant species and increases rapidly with increasing total water, whereas the OH content increases slightly, but does not completely level off over this range of water contents, in contrast to the behavior observed in albitic and CAS glasses. The

Figure 31a. The concentrations of water dissolved as molecules of H_2O (open symbols) and as OH (filled symbols) as functions of total water content in rhyolitic glasses synthesized in rapid quench cold seal bombs, together with a best fit to the data (see Appendix 1). The run conditions for all the samples are listed in Table 13.

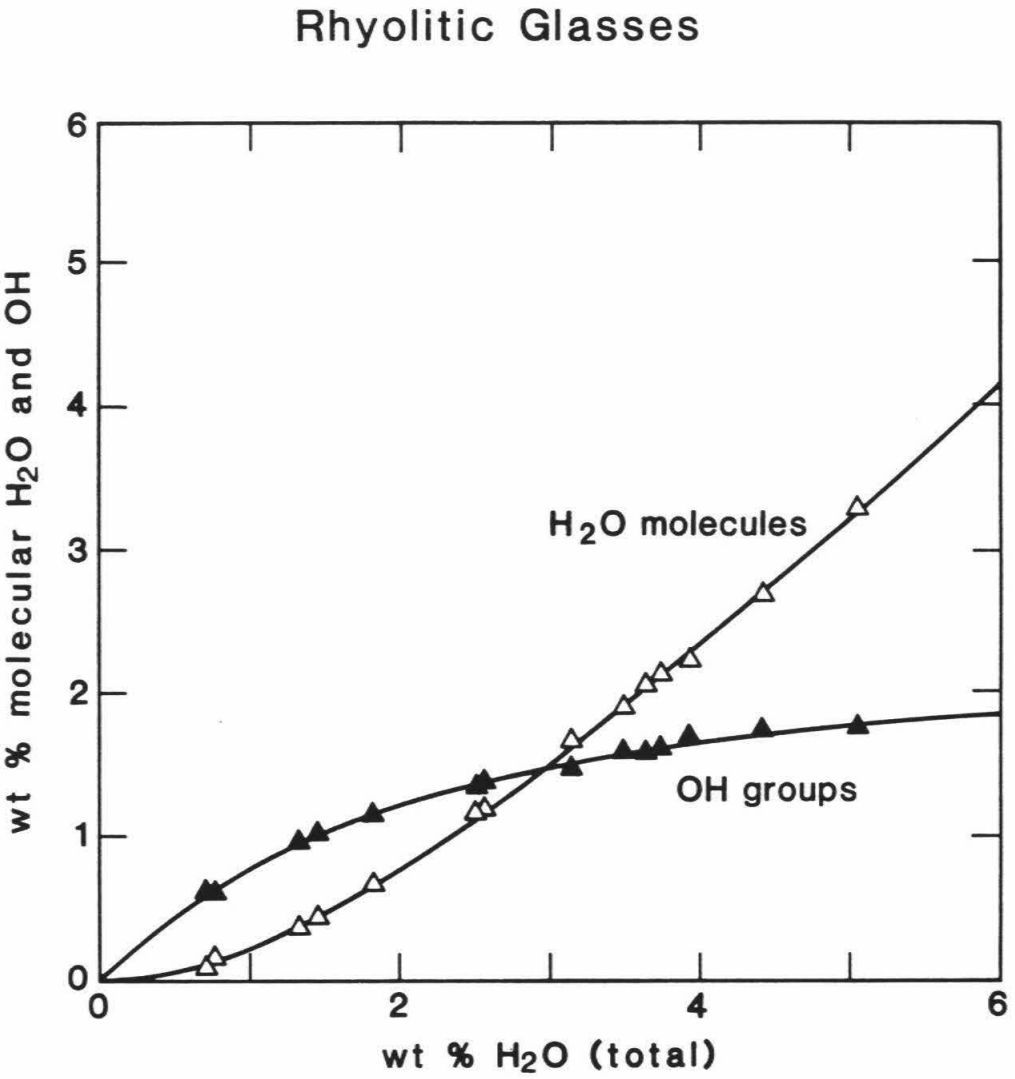
Rhyolitic Glasses
wt % molecular H_2O and OH
wt % H_2O (total)
H_2O molecules
OH groups
0
1
2
3
4
5
6
0
2
4
6

overall trends in the hydrous species concentrations, however, are similar to those observed for all of the simple glasses described above.

Figure 31b compares the concentrations of molecular water and hydroxyl groups as functions of total water content for rhyolitic glasses synthesized in air-quench cold seal pressure vessels at 850°C and pressures up to 1000 bars, represented by the open and filled circles, with the fit to the rapid-quench cold seal data from Fig. 31a. Also shown in Fig. 31b are the concentrations of molecular water and OH groups in a series of naturally-occurring hydrous rhyolitic glasses from the Mono Craters, California (Newman et al., 1987), represented by the open and filled squares. As demonstrated in Fig. 31b, at a given total water content the ratio of molecular water to OH groups for the glasses synthesized in air-quench cold seal apparatus is higher than for the rhyolites synthesized in rapid-quench apparatus (represented by the curves). The difference in the relative proportions of the two hydrous species must be related to the differences in cooling rates because the two sets of experimental glasses were quenched from melts equilibrated at the same temperature and over the same pressure interval. A similar observation has been made for hydrous albitic glasses synthesized in IHPV, where cooling rates are much slower than in piston cylinder apparatus (Chapter 1). As described above, the species concentrations measured in glasses cooled at slow cooling rates, such as in IHPV or air-quench cold seals, probably reflect conversion of OH to molecular water as the melt/glass cooled. The trends illustrated in Fig. 31b demonstrate the necessity for rapid-quench apparatus to preserve the high temperature and pressure characteristics of the melt

Figure 31b. The concentrations of water dissolved as molecules of H_2O (open symbols) and as OH (filled symbols) as functions of total water content in rhyolitic glasses synthesized in air-quench cold seal apparatus (circles) and in rhyolitic glasses from the Mono Craters, California (squares), together with a best fit to the data for the rapid quench rhyolites shown in Fig. 31a. The run conditions for air quench rhyolitic glasses are listed in Table 13; the rhyolitic glasses from the Mono Craters are described by Newman et al. (1987).

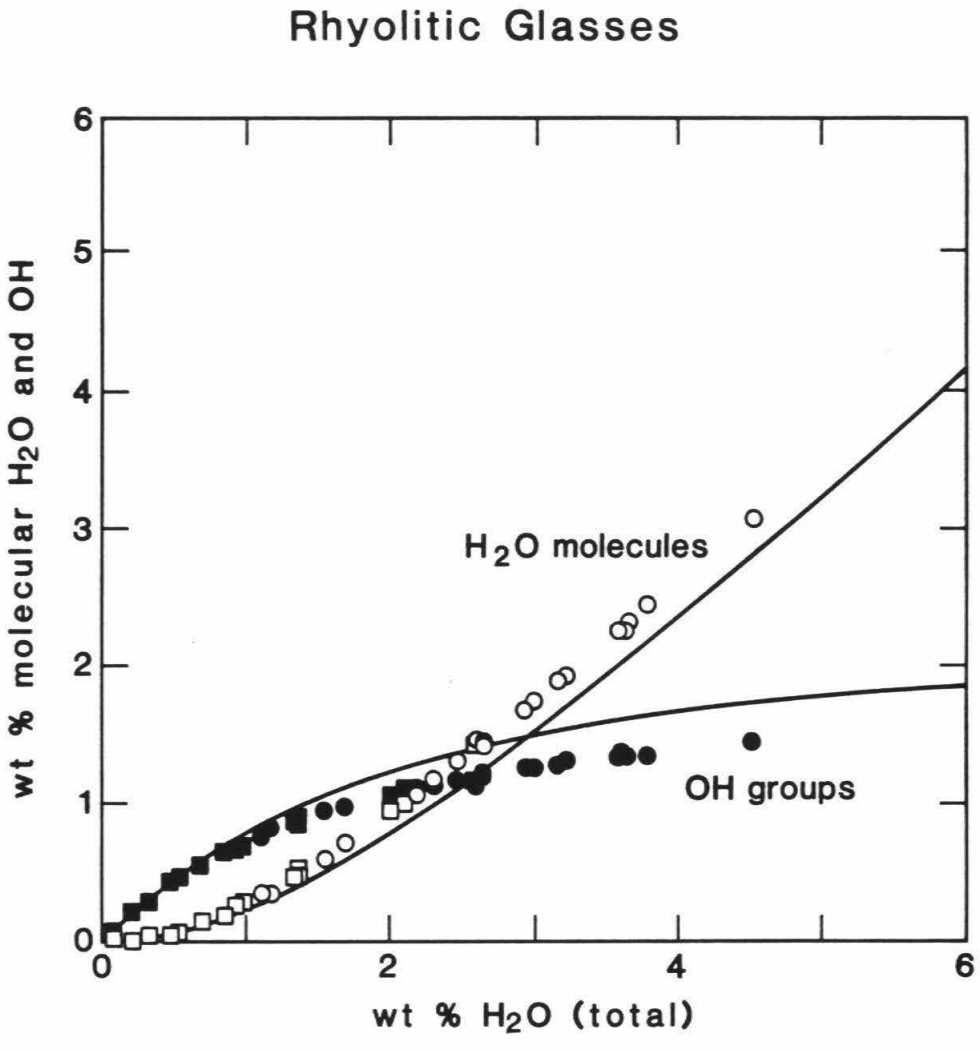
Rhyolitic Glasses
wt % molecular H_2O and OH
wt % H_2O (total)
H_2O molecules
OH groups
0
1
2
3
4
5
6
0
2
4
6

from which the glasses are quenched. There is, however, still the possibility that the hydrous species reequilibrate at rates much faster than those obtainable with rapid-quench apparatus. The only way to test this will be to take in situ infrared spectra on hydrous glasses at elevated temperature and pressure.

The low temperatures recorded in the speciation of water of the natural samples places constraints on eruption temperatures and/or cooling rates for natural volcanic glasses. This has been discussed by Newman et al. (1987); they suggest that these glasses came from glassy margins of the conduit system of the volcano and were held at 500-600°C for a prolonged period and then cooled rapidly on eruption.

Discussion

The influence of bulk composition

Figure 32 summarizes the data for the variation in mole fractions of molecular water and hydroxyl groups as functions of the mole fraction of total water, X_B, for the melt expressed on a single oxygen basis (see footnote, Table 8), for CAS, KAS, rhyolitic (rapid quench) and albitic glasses. The various curves represent fits (see Appendix 1) to the data shown in Figs. 9, 10, 27, 28, and 31a. The JD, ANS and ABOR glasses have been excluded because the extinction coefficients are not well constrained for these compositions; the rhyolitic glasses synthesized in air-quench cold seal bombs have also been excluded because it is unlikely that the species concentrations reflect the conditions of the melt at elevated T and P, as discussed above.

Figure 32. The best fit calculations of the mole fractions of molecular H_2O and OH groups as functions of X_B for CAS-E2, orthoclase, rapid quench rhyolites and albitic glasses represented by the best fits to the data for each composition shown in Figs. 27, 28, 31a, and 13, respectively. See Appendix 1 for best fit parameters.

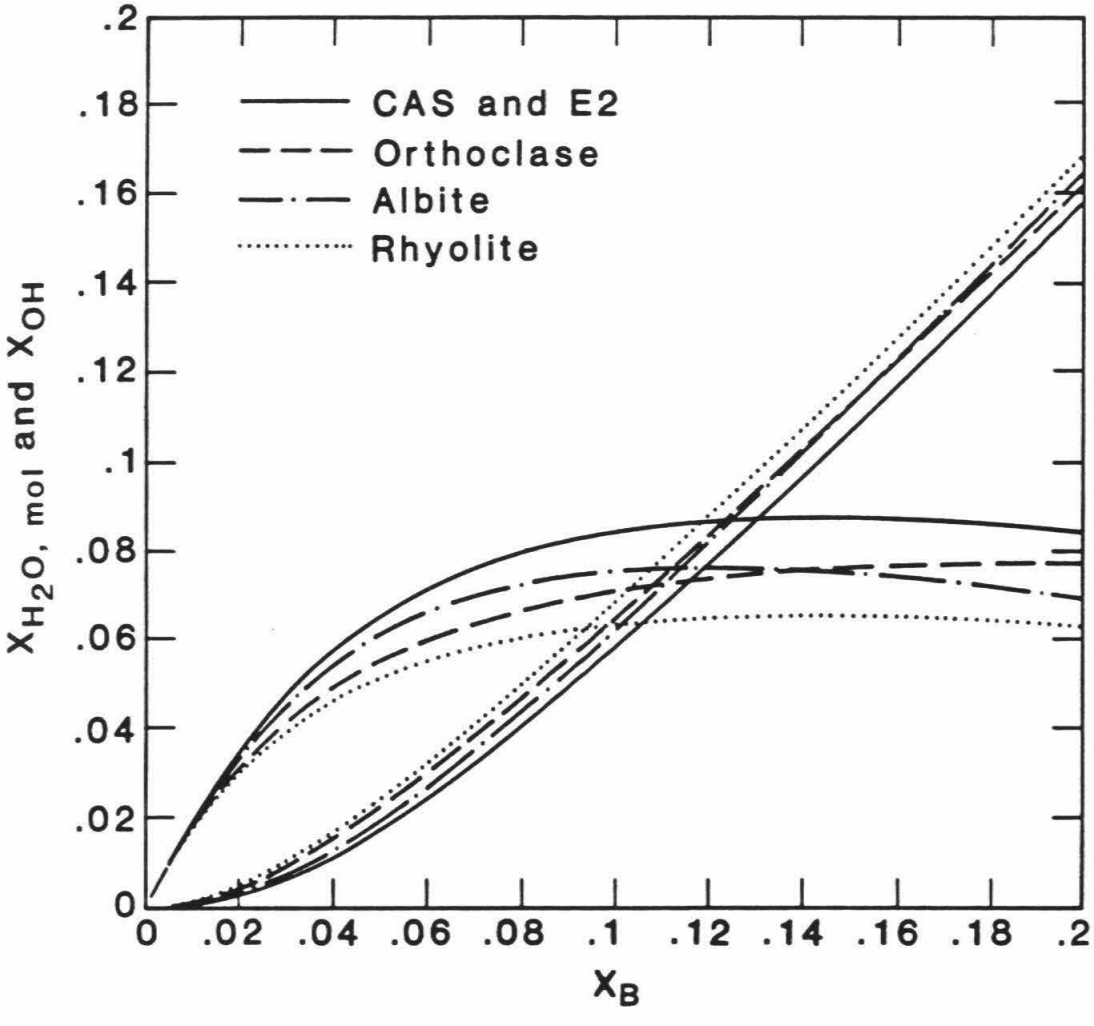
CAS and E2
Orthoclase
Albite
Rhyolite
$X_{H_2O,\ mol}$ and X_{OH}
X_B
0
.02
.04
.06
.08
.1
.12
.14
.16
.18
.2

For all of the compositions studied, the OH content increases rapidly at low total water contents and then its concentration levels off or even begins to decrease at high water contents. The exact concentration at which the OH content begins to level off varies from one composition to another, as does the point at which equal amounts of water are dissolved as molecular water and hydroxyl. At a given total water content, the molecular water to OH ratio increases with increasing silica content from CAS, albite, KAS to rhyolite.

Comparison with other studies

The speciation of water in hydrous silicate glasses determined in this study is similar to that observed in other simple silicate glasses (Bartholomew et al., 1980; Acocella et al., 1984). Although the progressive decline in the hydroxyl group content with increasing total water in hydrosilicate glasses observed by Bartholomew et al. (1980) is more pronounced than for glasses included in this study, the general trends in the speciation are similar.

The concentrations of molecular water and hydroxyl groups as functions of total water content determined in this study by infrared spectroscopy have been verified by NMR spectroscopic studies on many of the same samples (Eckert et al., 1987b). Bartholomew et al. (1980) also used NMR and infrared spectroscopic techniques to determine the speciation of water in hydrosilicate glasses and obtained similar results when both methods were applied to the same samples.

The results presented in Fig. 32 are similar to those obtained for hydrous silica glass by Farnan et al. (1987) using cross-polarization

NMR techniques, and in a preliminary study by me using infrared spectroscopy (L.A. Silver, unpub. results). These results contrast with those presented by Mysen & Virgo (1986a) based on Raman studies of hydrous silica glass. Although further study is necessary to constrain the details for hydrous silica glass, it is unlikely that future work on this composition will confirm the results of Mysen & Virgo (1986a).

The concentrations of molecular water and hydroxyl groups observed in every composition studied to date by either NMR or infrared spectroscopies, exhibit similar trends over a wide range of total water contents. The general similarity in the trends of the molecular water and OH group contents as functions of total water suggests that the dissolution mechanisms for water over the range of silicate glasses (and melts) included in this study are similar and appear to be independent of the number or types of cations. Although the model described in Chapter 2 based on the exchange reaction between H and Na can account for the speciation data, the similarity in the speciation of water over this range of compositions suggests that this is probably not the dominant mechanism. In addition, the similarity of the results for silica with those described for a wide range of compositions suggests that the solution mechanism for water in melts may not be related to the availability of any particular cation and may be correlated with other aspects of the network structure.

My measurements may also be useful for rationalizing certain variations in macroscopic properties of melt-water systems in terms of their molecular level interactions. For example, at a given total water content, there are more OH groups in albitic glasses than in orthoclase

glasses, suggesting that water may be more reactive with Na-bearing units to produce hydroxyls, than with K-bearing ones. Precisely this explanation was offered by Pichavant & Ramboz (1985) to explain phase relations in the system albite-orthoclase-water, in which the phase boundaries move towards more albitic compositions with the addition of water. McMillan & Holloway (1987) also suggest that the preferential reaction of water with certain cations may explain the variations in water solubility as a function of silicate composition. My results offer direct confirmation of these predictions and may ultimately be used to rationalize in a quantitative way the variations in solubility and solid-liquid phase equilibria in this and other systems using the approach outlined above for the albite-H_2O system. Applications of the spectroscopic measurements to understanding this type of macroscopic behavior in melt-water systems are discussed below.

Summary

1. The infrared spectroscopic technique has been calibrated for a range of hydrous compositions. Using these calibrations, I determined the speciation of water in hydrous silicate glasses quenched from melts equilibrated over a range of experimental conditions.

2. For all of the compositions studied, the trends in the concentrations of molecular water and hydroxyl groups as functions of total water content are similar to those observed for albite and for other silicate compositions, using infrared and NMR spectroscopies. The relative proportions of molecular water and hydroxyl groups at a given total water content vary as a function of bulk composition, but for all

the glasses studied, the hydroxyl group content is approximately constant for total water contents greater than 4-5 wt %.

3. The consistently higher ratio of molecular water to OH groups at a given total water content in rhyolitic glassses synthesized in air-quench apparatus compared to those synthesized in rapid-quench apparatus demonstrates the necessity of rapid quenches for preserving the high temperature-pressure characteristics of the melt.

4. The similarity in the speciation of water over a wide range of melt compositions suggests that the dissolution mechanisms for water are similar and are not strongly dependent on the availablity or type of cations in the melt.

Chapter 5. Thermodynamics of Hydrous Silicate Melts

One of the primary goals of this study has been to use the spectroscopic measurements of species concentrations to constrain the thermodynamics of hydrous silicate melts. Though other choices are possible, I have used the approximation that $a^m_{H_2O} = X^m_{H_2O,mol}$ to link my measurements with the thermodynamic properties of silicate liquids. As discussed in detail in Chapter 3, this approximation can account reasonably well for phase equilibrium data in the system albite-H_2O. In this chapter, I use new and previously published data on the solubility of water in silicate melts in conjunction with my measurements of species concentrations to explicitly evaluate the validity of this approximation.

The Solubility of Water in Silicate Melts

The variation in the activity of water in vapor-saturated melt with pressure, at constant temperature, is given by

$$a^m_{H_2O}(T,P) = f_{H_2O}(T,P) \frac{a^m_{H_2O}(T,P_0)}{f_{H_2O}(T,P_0)} \exp\left(- \int_{P_0}^{P} \frac{\overline{V}^{o,m}_{H_2O}(T,P)}{RT} dP \right) \quad (20)$$

where P_0 refers to a reference pressure, $a^m_{H_2O}(T,P)$ and $a^m_{H_2O}(T,P_0)$ are the activities of water in the melt at T and P or P_0, and the other quantities have been defined for equation (17). Equation (20) is the same as equation (17) except that equation (17) includes the temperature dependence. If the activity of water in the melt at single pressure and the pressure dependence of the standard state molar volume of water in the melt are known, then the variation in water activity in vapor-saturated melts with pressure can be calculated from equation (20).

At low pressures, the volume term is negligible and the fugacities can be replaced by pressure. In the low pressure limit the activity of water will be proportional to pressure, and the validity of a particular model for the relationship between activity and composition can be tested by determining whether the water activity in a series of melts equilibrated with water vapor over a range of low total pressures is proportional to pressure (or fugacity).[7] This approach has been taken previously: by noting that there is a linear relationship between the mole fraction of water and the square root of pressure (or fugacity) at very low pressures, glass scientists (Tomlinson et al., 1956; Walsh et al., 1956; Russell, 1957) long ago concluded that the activity of water is equal to the square of the mole fraction of water in the melt and that water dissolves in melts nearly entirely as hydroxyl under these conditions. Thus, if the approximation $a^{m}_{H_2O} = X^{m}_{H_2O,mol}$ is valid, then the mole fraction of molecular water in a series of melts equilibrated with water vapor at low pressure should be linear with fugacity. At higher pressures, the volume term becomes significant and, given the validity of this a-X relation, $\overline{V}^{o,m}_{H_2O}$ can then be determined from the activity-fugacity relationship.

There are four compositions for which both the speciation and solubility measurements are available, though not always on the same samples: rhyolite, CAS-E2, albite and orthoclase. In the following sections, I evaluate the approximation $a^{m}_{H_2O} = X^{m}_{H_2O,mol}$ for each of these

---

7. Note here that the volume term can be completely removed by comparing solubility at constant temperature and pressure with variable f_{H_2O} (P_{H_2O}) by changing the vapor composition.

compositions by comparing $X^{m}_{H_2O,mol}$ vs. f_{H_2O} at low pressures. In each case, the composition of the vapor has been assumed to be pure water vapor, and f_{H_2O} values are based on the modified Redlich-Kwong equation of state (Holloway, 1977). For most of these compositions, data are also available at higher pressure, allowing constraints to be placed on $\overline{V}^{o,m}_{H_2O}$.

Rhyolitic melts

The solubility and speciation of water in hydrous rhyolitic glasses quenched from water-saturated melts held at pressures up to 1500 bars at 850°C have been determined by infrared spectroscopy. Details of the experimental techniques are described in Chapter 4. The concentrations of molecular water and OH groups and total water contents are listed in Table 13. Figure 33 shows the measured mole fraction of molecular water as a function of the fugacity of water for the rhyolitic glasses hydrated in rapid quench apparatus. Shown for comparison are calculated curves based on equation (20) for $\overline{V}^{o,m}_{H_2O}$ = 0 and 10 cc/mol (both are constrained by the 800 bar data point). The linear relationship between $X^{m}_{H_2O,mol}$ and fugacity clearly demonstrates that the activity of water can be described by the mole fraction of molecular water in the melt over this pressure range.

Figure 34 compares the calculated water solubility, assuming a reference at 799 bars and $\overline{V}^{o,m}_{H_2O}$ = 0 cc/mol, with experimental determinations of the solubility of water in rhyolitic melts from this and previous studies, all at 850°C. The right-pointing arrows represent results for glasses that were synthesized in conventional cold seal

Figure 33. The measured values of the mole fraction of molecular water vs. the fugacity of water (from the modified Redlich-Kwong equation of state) for hydrous rhyolitic glasses quenched from water-saturated melts in rapid-quench cold seal apparatus at 850°C. Also shown are the calculated water activities based on equation (20) for $\overline{V}^{o,m}_{H_2O}$ = 0 and 10 cc/mol. At the reference point (799 bars), $X^{m}_{H_2O,mol}$ = 0.033.

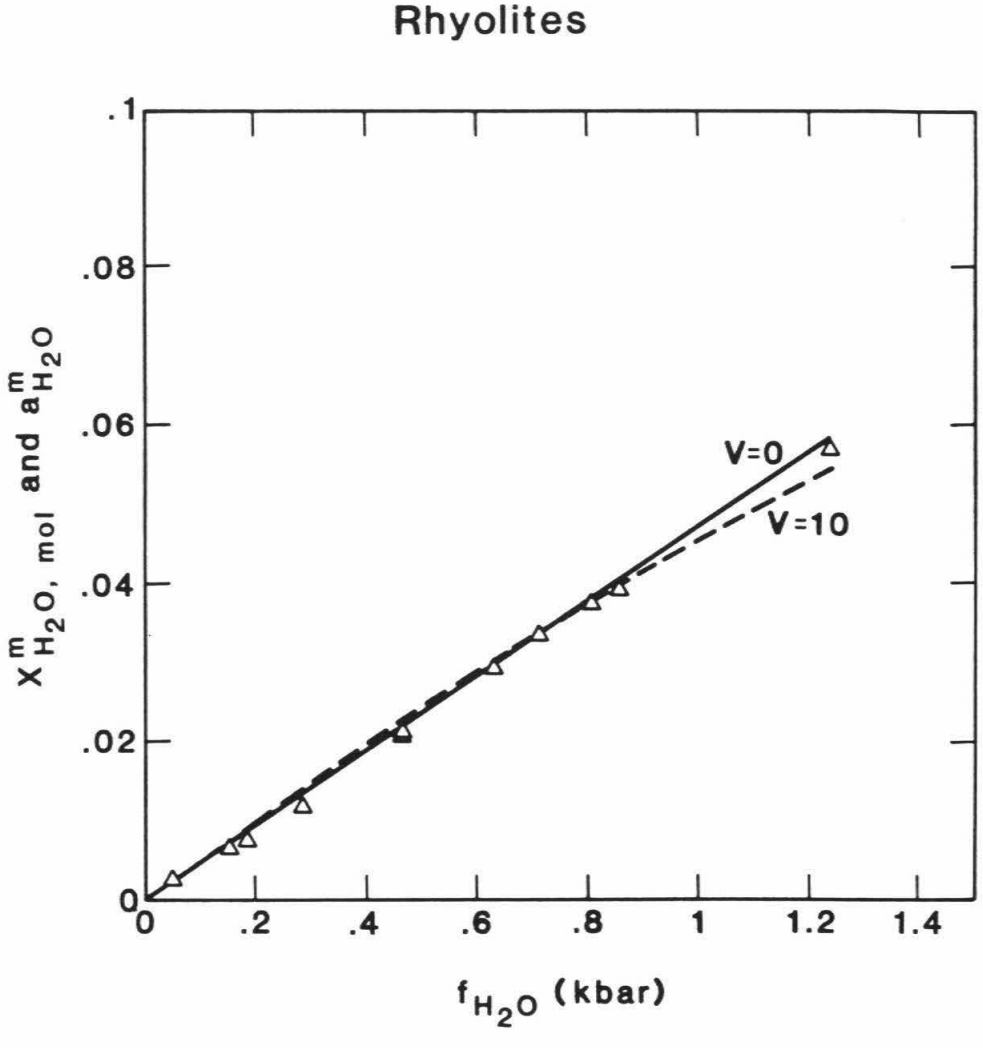
Rhyolites
.1
.08
.06
.04
.02
0
0
.2
.4
.6
.8
1
1.2
1.4
V=0
V=10
$X^m_{H_2O}$, mol and $a^m_{H_2O}$
f_{H_2O} (kbar)

Figure 34. The pressure dependence of water solubility in rhyolitic melts up to 2000 bars at 850°C. The curve represents the calculated water solubility based on equation (20), with a reference point at 799 bars and 850°C, for $\overline{V}^{o,m}_{H_2O}$ = 0 cc/mol. The circles represent water solubility measurements from this study for rhyolitic glasses synthesized in rapid-quench apparatus; the arrows represent reversal runs from this study for rhyolitic glasses synthesized in air-quench cold-seal apparatus; the squares represent experimental data from Karsten et al. (1982); and the diamonds represent data from Shaw (1964). Note that at some pressures two measurements were obtained, one reported in the literature and a second value determined by infrared spectroscopy on the same samples.

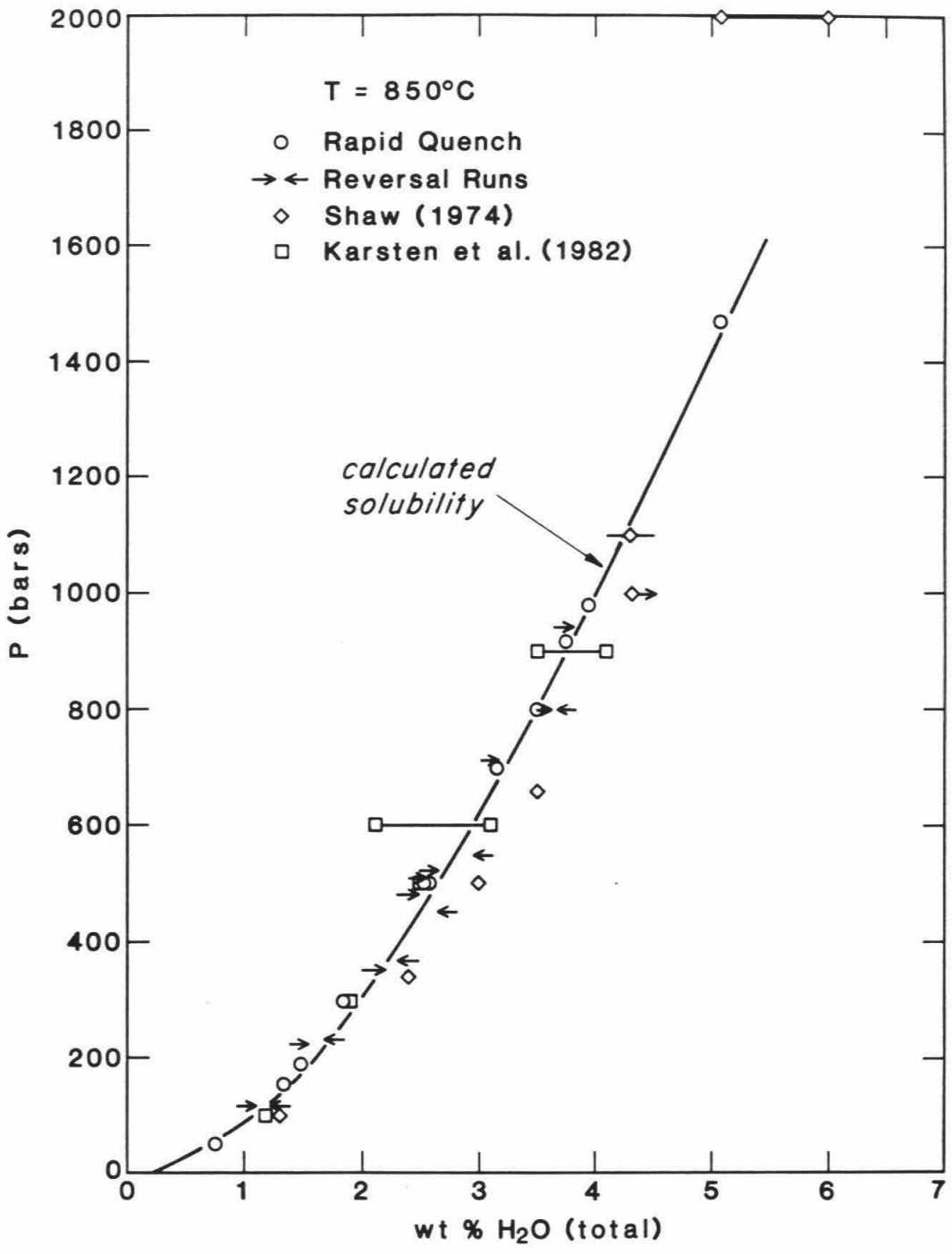
T = 850°C
Rapid Quench
Reversal Runs
Shaw (1974)
Karsten et al. (1982)
calculated solubility
P (bars)
wt % H2O (total)
0
200
400
600
800
1000
1200
1400
1600
1800
2000
1
2
3
4
5
6
7

pressure vessels by equilibrating rhyolitic melts with water vapor at a single pressure and 850°C; the left-pointing arrows represent reversal runs (see Experimental Techniques in Chapter 4). The circles represent results for the rapid quench rhyolites shown in Fig. 33 and the other symbols represent data from Shaw (1964) and Karsten et al. (1982). The curve shown in Fig. 34 was calculated as follows: Equation (20) was used to calculate the variation in $a^m_{H_2O}$ (= $X^m_{H_2O,mol}$) with pressure at a given temperature, assuming a reference point and a value for $\overline{V}^{o,m}_{H_2O}$. Using the relationship between $X^m_{H_2O,mol}$ and X_B from the best fit shown in Fig. 32 (see also Appendix 1), X_B was determined and then converted to weight percent H_2O. As demonstrated in Fig. 34, the agreement between the calculated solubility and the experimental data is excellent. Also noteworthy is the good agreement between the solubility measurements from this study and previous determinations. In addition, Fig. 34 shows that the total water contents determined for both sets of cold seal experiments are essentially identical, even though the relative proportions of molecular water and OH groups at a given total water content are different, due to the differences in cooling rates (Figs. 31a,b). The excellent agreement between the reversed runs demonstrates that equilibrium was achieved in these experiments.

The results presented in Figs. 33 and 34 provide confidence in the approach taken in this study to modelling the thermodynamic properties of hydrous melts and substantiate an activity-composition relation derived from spectroscopic measurements. An alternative and popular approach is the approximation, for total water contents $\lesssim$8 wt %, that $a^m_{H_2O} \propto (X^m_w)^2$, where X^m_w is defined as given by Burnham (1979).

Figure 35 shows $X^m_{H_2O,mol}$ vs. $(X^m_w)^2$ for the rapidly-quenched rhyolitic glasses. The linear relationship between $X^m_{H_2O,mol}$ and $(X^m_w)^2$ demonstrates that the activity of water in the melt according to Burnham's model is basically equivalent to my approximation. However, the validity of Burnham's activity-composition relationship does not imply that his structural model for water dissolution is correct; in fact, my measurements demonstrate that his conclusion that nearly all of the water dissolves as OH groups is incorrect. As discussed by Stolper (1982b), $a^m_{H_2O} = (X^m_w)^2$ is not expected except at very low total water contents if water dissolves exclusively as hydroxyl groups.

Calcium aluminosilicate (E2) melts

The E2 glasses included in this study provide an opportunity to extend this treatment to another hydrous melt composition. These glasses were synthesized in IHPV by quenching from melts equilibrated with water vapor at pressures up to 5130 bars, at about 1180°C. Although experiments of this type should be done in rapid quench apparatus, these glasses do not show any obvious effects due to slow quenching (Fig. 27). The solubility and speciation of water were determined for each glass sample by infrared spectroscopy. Figure 36 shows the spectroscopic measurements of the mole fractions of molecular water as a function of the fugacity of water for the E2 glasses. Shown for comparison are calculated curves based on equation (20) for $\overline{V}^{o,m}_{H_2O}$= 0, 10 and 20 cc/mol (all are constrained to pass through the 1514 bar point). Although the one data point at 5130 bars is best described by $\overline{V}^{o,m}_{H_2O}$ = 15-20 cc/mol, the measured values up to 1500 bars are

Figure 35. The measured values of the mole fractions of molecular water in hydrous rhyolitic glasses synthesized in rapid-quench apparatus as a function of the square of the mole fraction of total water, $(X_w^m)^2$, where X_w^m is given by Burnham (1979). The line represents a best fit to the data, constrained to pass through the origin.

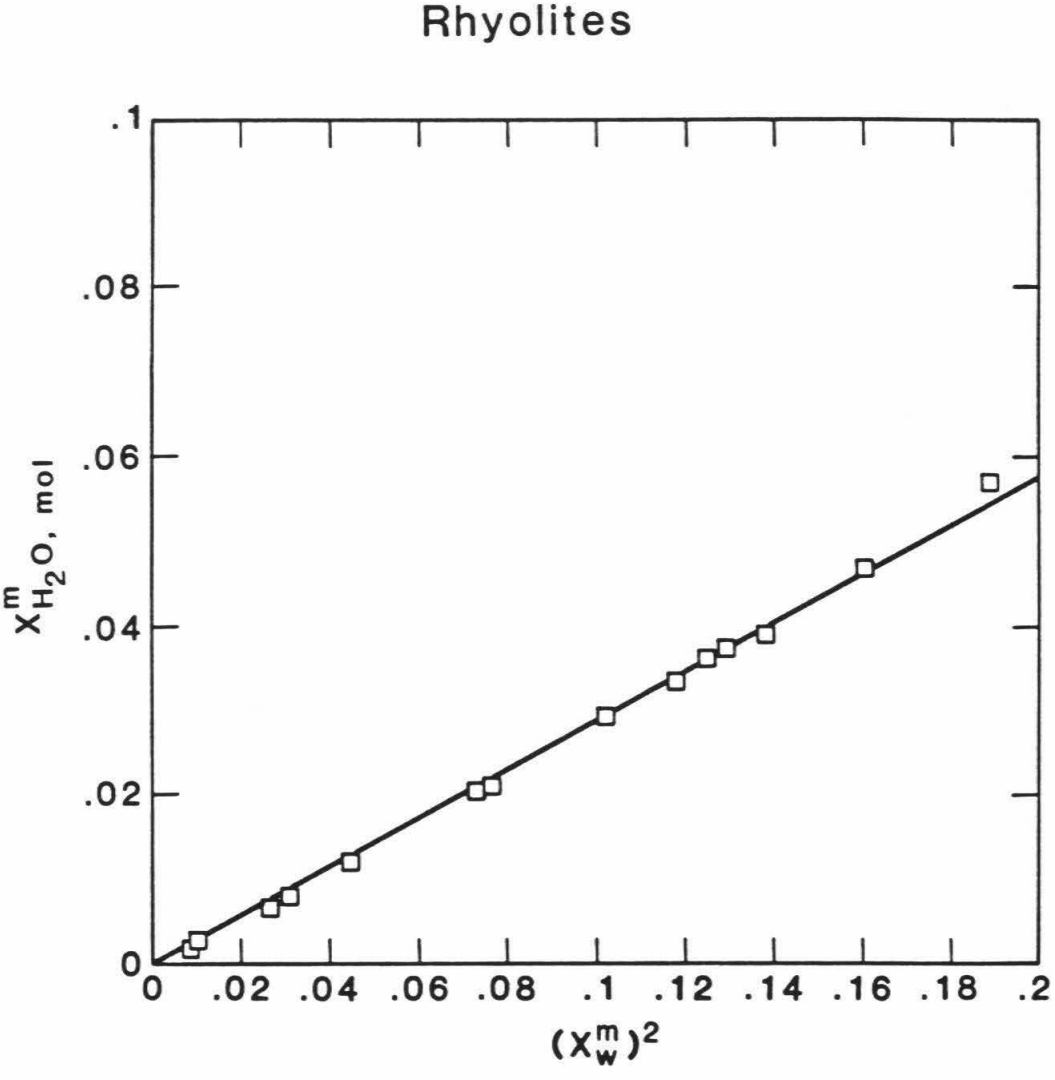
Rhyolites
.1
.08
.06
.04
.02
0
$X^m_{H_2O}$, mol
0
.02
.04
.06
.08
.1
.12
.14
.16
.18
.2
$(X^m_w)^2$

Figure 36. The measured values of the mole fraction of molecular water vs. the fugacity of water (from the modified Redlich-Kwong equation of state) for hydrous E2 glasses quenched from water-saturated melts in IHPV, at ~ 1180°C. Also shown are the calculated water activities based on equation (20) for $\overline{V}^{o,m}_{H_2O}$ = 0, 10, and 20 cc/mol. At the reference point (1514 bars), $X^{m}_{H_2O,mol}$ = .049.

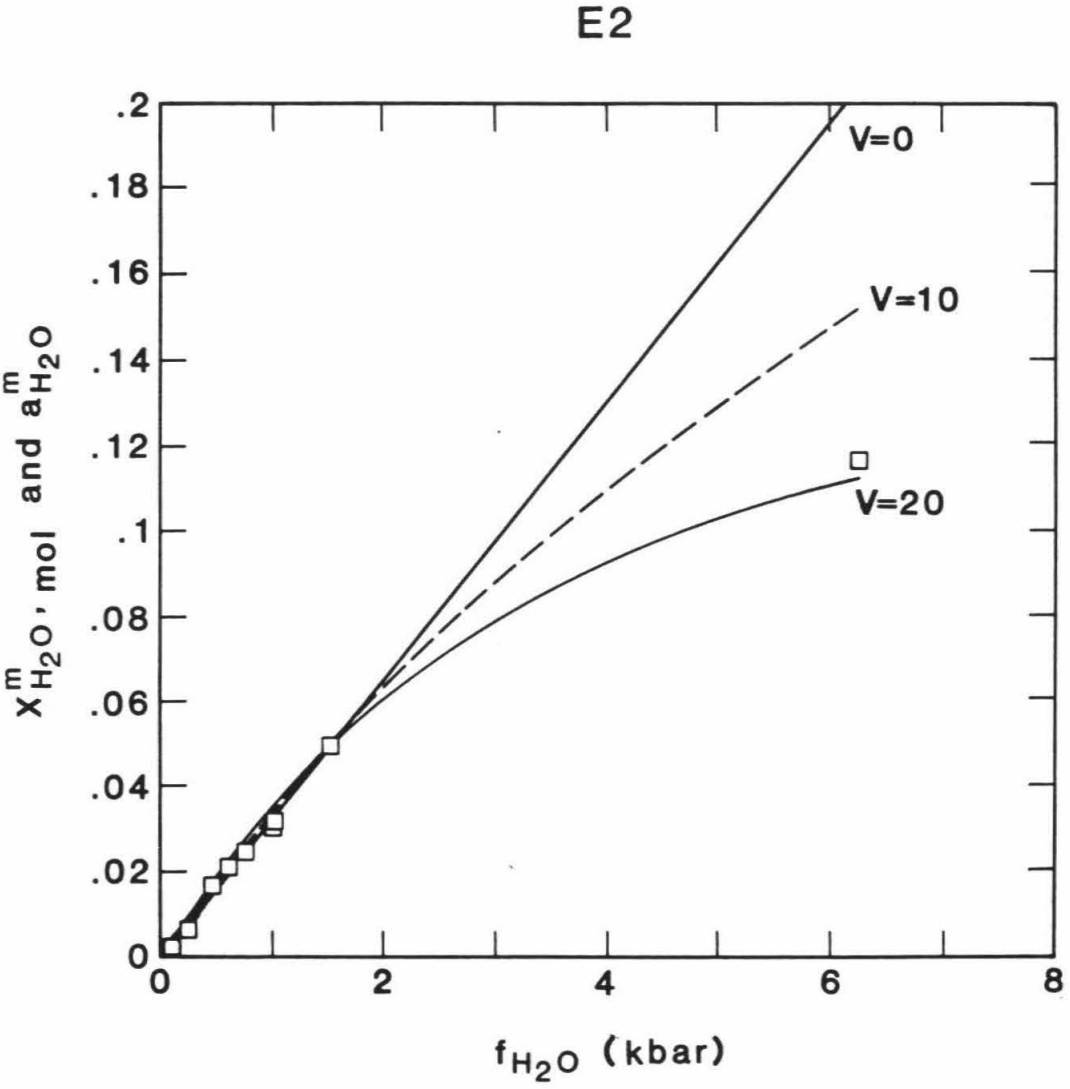
E2
V=0
V=10
V=20
.2
.18
.16
.14
.12
.1
.08
.06
.04
.02
0
0
2
4
6
8
$X^m_{H_2O}$, mol and $a^m_{H_2O}$
f_{H_2O} (kbar)

approximately linear with fugacity, demonstrating the validity of the activity-composition relation.

Albitic melts

Although I do not have measurements of hydrous species concentrations in albitic glasses quenched from melts saturated with water vapor, the speciation of water in undersaturated glasses quenched from albitic melts has been studied in detail (Chapter 1) and varies little with pressure and temperature. Combining these speciation data with the data of Hamilton and Oxtoby (1986) on the solubility of water in albitic melts up to 8 kbar at temperatures between 750 and 1400°C, I can compare $X^m_{H_2O,mol}$ and f_{H_2O} for albitic melts as done for rhyolite and E2. Each total water content reported by Hamilton & Oxtoby (1986) was converted to a value of X_B; the relation between X_B and $X^m_{H_2O,mol}$ shown in Fig. 17 for albitic glasses was then used to obtain a value for $X^m_{H_2O,mol}$. Figure 37 compares the mole fraction of molecular water, determined in this way with the fugacity of water for the experiments of Hamilton & Oxtoby (1986) for pressures between 560 and 7000 bars at 1000°C. Shown for comparison are calculated curves based on equation (20) for $\overline{V}^{o,m}_{H_2O}$ = 0, 20, and 25 cc/mol (all are constrained to pass through the 2000 bar point). Although for P> 2000 bars, the solubility measurements are best described by $\overline{V}^{o,m}_{H_2O} \sim 25$ cc/mol, at low pressures $X^m_{H_2O,mol}$ is approximately proportional to f_{H_2O}, validating the approximation that $a^m_{H_2O} = X^m_{H_2O,mol}$.

Hamilton & Oxtoby (1986) present solubility data over a large enough range of experimental conditions to constrain the $\overline{V}^{o,m}_{H_2O}$ function

Figure 37. The calculated values of the mole fraction of molecular water vs. the fugacity of water (from the modified Redlich-Kwong equation of state) for hydrous albitic based on the water solubility data from Hamilton & Oxtoby (1986) at 1000°C and the spectroscopically determined relationship between total water (X_B) and the mole fraction of water in under-saturated albitic glasses given in Fig. 17. Also shown are the calculated water activities based on equation (20) for $\overline{V}^{o,m}_{H_2O}$ = 0, 20 and 25 cc/mol. At the reference (2000 bars), $X^{m}_{H_2O,mol}$ = 0.081.

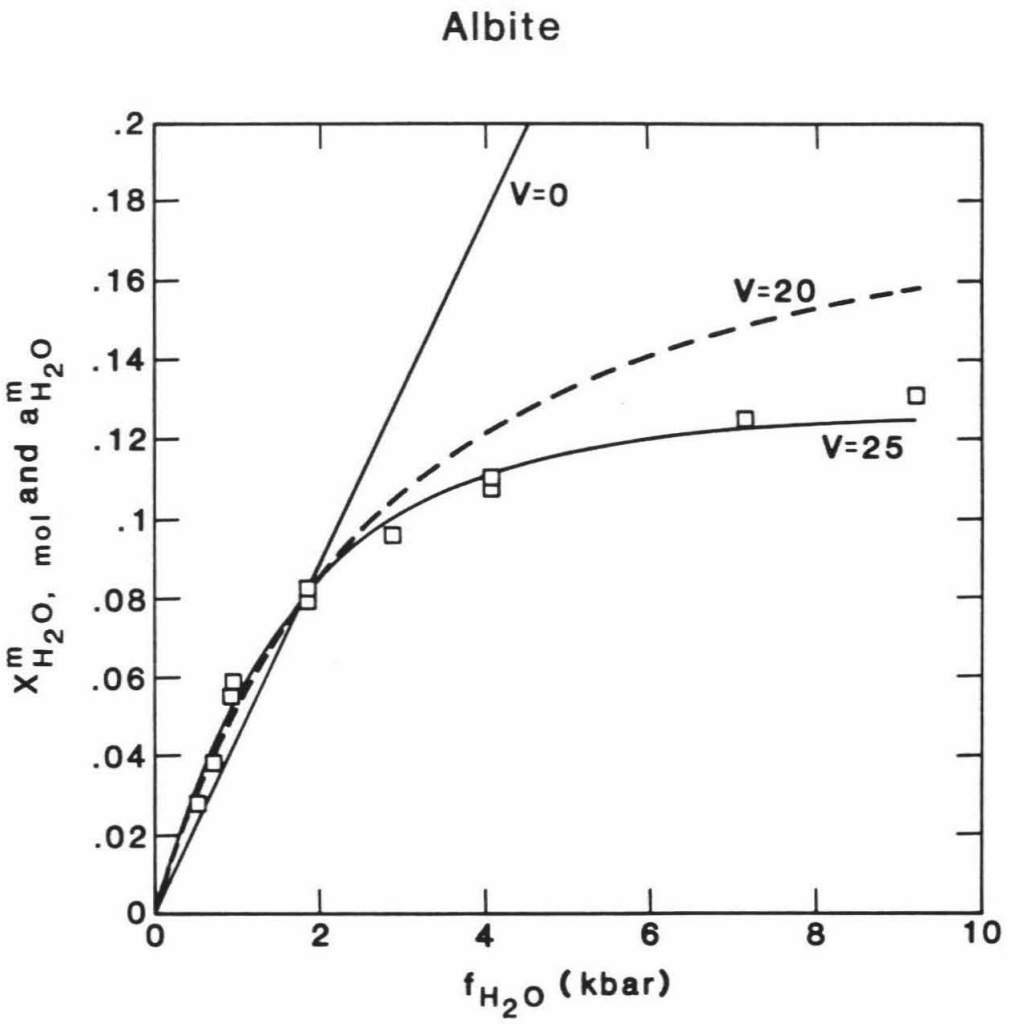
Albite
.2
.18
.16
.14
.12
.1
.08
.06
.04
.02
0
0
2
4
6
8
10
V=0
V=20
V=25
$X^m_{H_2O,\ mol}$ and $a^m_{H_2O}$
f_{H_2O} (kbar)

in equation (2) and $\Delta\overline{H}^{o}_{H_2O}$ using the approximation that the activity of water is given by the mole fraction of molecular water. As described above, each of their solubility measurements was converted to a value of $X^{m}_{H_2O,mol}$ and a least squares fit to $\overline{V}^{o,m}_{H_2O}(T,P)$and $\Delta\overline{H}^{o}_{H_2O}(T,P_r)$ in equation (17) was carried out as described in Chapter 3, where the volume function was taken to be a polynomial of the form given by equation (18). When all of their data is used in the fit, the partial molar volume of water in the melt required by their data at low pressures (560-1000 bars) is about 6 cc/mol, but the function seems unrealistic in that it has a maximum at 4.5 kbar. A second fit, excluding the 560 and 760 bar data, was tried and the best fit parameters are given in Table 15. This volume function was then used to calculate water solubility, volumes of hydrous albitic melts and the position of the wet solidus as described in Chapter 3. For calculating water solubility, this volume function leads to calculated values that are similar to their measured values to within 0.5 wt % at pressures less than 1 kbar and the agreement is even better at higher pressures. The volumes of hydrous albitic melts calculated based on their volume function are similar to but slightly larger (by up to 5 %) than those measured by Burnham & Davis (1971). When used to calculate the position of the water-saturated solidus, the volume function underestimates the temperature at pressures less than 5 kbar by as much as 60°C. However, given the substantial variability in reported water solubility data for albitic melts, it is not clear if these details are significant or meaningful; further progress will only come from measurements of both the solubility and speciation of water by infrared spectroscopy on

Table 15. Parameters for partial molar volume function

TABLE 15

Parameters for partial molar volume function[1]

(Best fit to H_2O solubility data of Hamilton & Oxtoby, 1986)

$$\overline{V}^{o,m}_{H_2O}(T,P) = a + b\,(P-P_0) + c\,(P-P_0)^2 + d\,(T-T_0)$$

T_0=745°C, P_0=5000 bars

a=20.3, b=-1.15×10^{-3}, c=1.08×10^{-7}, d=9.689×10^{-3}

$$\Delta\overline{H}^{o}_{H_2O}(T,P_r) = -3196 \text{ cal/mol}$$

$$X^{m}_{H_2O,mol}(T_r,P_r) = 0.122$$

Notes:

1. units: a (cm^3/mol), b (cm^3 mol^{-1} bar^{-1}), c (cm^3 mol^{-1} bar^{-2}), d (cm^3 mol^{-1} deg^{-1})

glasses quenched from albitic melts over a range of conditions in rapid quench apparatus, as demonstrated above for the rhyolitic glasses.

Orthoclase melts

The solubility of water in orthoclase melts has been experimentally determined at 1000°C by Oxtoby & Hamilton (1978). The speciation of water in orthoclase glasses has been determined in this study (Chapter 4) and the two data sets can be combined as described above for albitic melts to provide useful insights into the thermodynamic properties in this system. Each of the total water contents were converted to a value of X_B; the relationship between X_B and $X^m_{H_2O,mol}$ for hydrous orthoclase glasses (Fig. 32) was used to determine the variation in $X^m_{H_2O,mol}$ for pressures up to 8 kbar. Figure 38 compares the mole fraction of molecular water in orthoclase melts determined in this way with water fugacity. Shown for comparison are calculated curves based on equation (20) for $\overline{V}^{o,m}_{H_2O}$ = 0, 25, and 28 cc/mol (all are constrained to pass through the 2000 bar point). At pressures up to 2000 bars, $X^m_{H_2O,mol}$ is approximately linear with fugacity, illustrating again the success of the $a^m_{H_2O} = X^m_{H_2O,mol}$ approximation. At higher pressures, the data suggest a value of $\overline{V}^{o,m}_{H_2O}$ = 28 cc/mol. This high value of $\overline{V}^{o,m}_{H_2O}$ reflects the fact that according to Oxtoby & Hamilton (1978), water solubility becomes approximately constant at P > 3000 bars.

Discussion

The measurements of hydrous species concentrations in glasses quenched from melts equilibrated with water vapor provide important

Figure 38. The calculated values of the mole fraction of molecular water vs. the fugacity of water (from the modified Redlich-Kwong equation of state) for hydrous orthoclase glasses based on the water solubility data from Oxtoby & Hamilton (1978) at 1000°C and the spectroscopically determined relationship between total water (X_B) and $X^m_{H_2O,mol}$ shown in Fig. 32. Also shown are the calculated water activities based on equation (20) for $\overline{V}^{o,m}_{H_2O}$ = 0,25 and 28 cc/mol. At the reference (2000 bars), $X^m_{H_2O,mol}$ = 0.05.

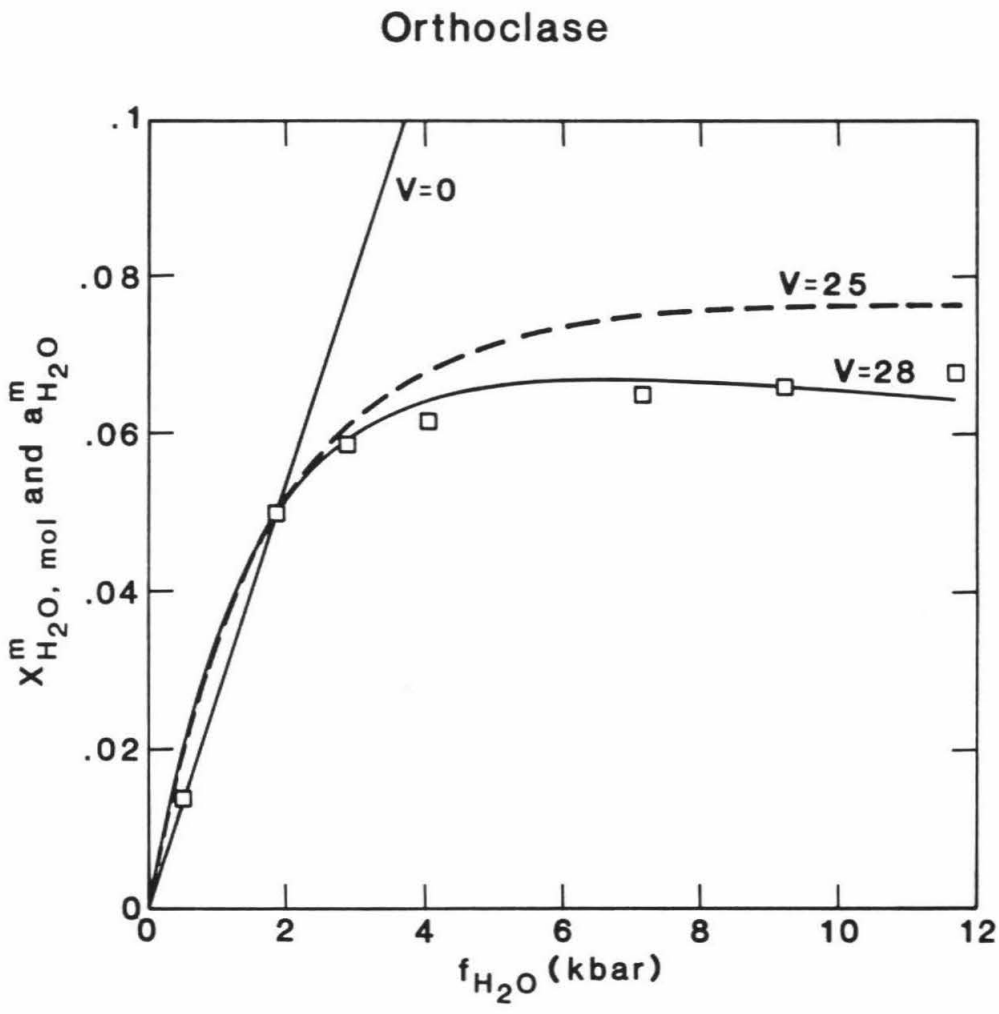
Orthoclase
.1
.08
.06
.04
.02
0
0
2
4
6
8
10
12
V=0
V=25
V=28
$X^m_{H_2O,\ mol}$ and $a^m_{H_2O}$
f_{H_2O} (kbar)

constraints on the thermodynamic properties in these melt-water systems. The treatment described in the preceding section is based on the assumption that the activity of water in the melt can be approximated by the mole fraction of molecular water, measured spectroscopically. The low pressure data for all four compositions considered are similar and the approximately linear relationship between fugacity and the mole fraction of molecular water in these glasses further validate this assumption.

The results presented above are consistent with the suggestion that at low pressures, the partial molar volume of water in these hydrous melts is small or even equal to zero and at higher pressures, the solubility mechanism for water may be different than at low pressures. A small partial molar volume of water would be consistent with a dissolution mechanism for water in which the water enters the melt by filling holes. This observation is consistent with density measurements on hydrous glasses with low total water contents reported by McMillan and Chlebik (1980) for a sodium silicate glass. They found that the density of these glasses increased with the initial incorporation of water (all as hydroxyl) into the glass structure. Analysis of their data suggests that the partial molar volume of water at low total water contents is close to zero, or even negative. In addition, Boulos & Kreidl (1972) postulated that the dissolution of water as OH in glasses may result in an increase in density as a result of the collapse of the network structure, due to local hydrogen bonding. Although the data presented for rhyolitic glasses indicate that the partial molar volume of water could be small at low pressures, the precision of the

measurements may not warrant such a conclusion; i.e., at low pressures the effects of volume are small and therefore hard to discern without accurate measurements. For all four compositions studied, a small partial molar volume of water is consistent with the low pressure data, but a larger value is indicated at higher pressures. Although the measurements from Burnham & Davis (1971) on the volumes of hydrous albitic melts also yield large values for the partial molar volume of water, their data was obtained at pressures > 3 kbar and total water contents > 8 wt % H_2O and do not provide constraints for the low pressure partial molar volume of H_2O. Further work involving high precision measurements of species concentrations and/or density will be essential at low pressures to differentiate between the partial molar volumes suggested by the data.

Summary

1. For hydrous rhyolitic glasses, the linear relationship between $X^m_{H_2O,mol}$ and f_{H_2O} demonstrates that the assumption $a^m_{H_2O} = X^m_{H_2O,mol}$ is valid for total water contents up to at least 5 wt % and pressures up to 1500 bars. The approximately linear relationship between the measured values of $X^m_{H_2O,mol}$ and the water fugacity at pressures less than 2000 bars for the E2, albite and orthoclase glasses validates this assumption for these systems as well.

2. The relationship between the activity of water (i.e. the mole fraction of molecular water) in glasses quenched from melt saturated with water based on the infrared measurements and the fugacity of water provides constraints on the partial molar volume of water. Although a

small partial molar volume of water is consistent with the data presented for rhyolitic, albitic, E2, and orthoclase glasses at low pressures, no firm conclusions can be made from these results. Further study of species concentrations in glasses quenched from water-saturated melts at low pressure will be needed to constrain $\overline{V}^{o,m}_{H_2O}$.

3. The approach taken in this study can readily be applied to any silicate system for which spectroscopic measurements of the hydrous species are available. Although the results presented here relied on the calibration of the infrared spectroscopic technique for measuring the absolute concentrations of molecular water and hydroxyl groups in hydrous glasses, this is not absolutely critical. It is also possible to obtain information on the relative amounts of molecular water without knowing the extinction coefficients by comparing measurements of absorbance/thickness between samples. With this information, an approach similar to the one described here could be used to qualitatively constrain thermodynamic properties in a variety of other silicate systems.

Conclusions

1. H_2 manometry and NMR spectroscopy have been used to calibrate an infrared spectroscopic method for measuring the concentrations of molecular H_2O and hydroxyl in hydrous silicate glasses. This technique offers a precise, accurate, and non-destructive method for measuring species concentrations and total water contents in hydrous glasses.

2. Infrared spectroscopy has been used to determine the speciation of water in hydrous glasses covering a range of compositions with total water contents up to about 11 wt %. At low total water contents, hydroxyl groups are the dominant form of dissolved water; at total water contents greater than 4 wt %, molecular water becomes the dominant hydrous species and the hydroxyl group concentration levels off. These results are in agreement with the species concentrations determined for many of the glasses included in this study using NMR spectroscopy. The similarity in the speciation of water for the glasses studied here and with those observed in other silicate glass compositions, including silica, suggests that the dissolution mechanisms for water in silicate liquids are not related to the availablity of any particular cation-oxygen unit.

3. The proportions of molecular H_2O and OH in glasses quenched from albitic melts equilibrated at temperatures in the range 1000-1600°C and pressures between 8 and 25 kbar in piston cylinder apparatus are independent of the P and T of equilibration. This suggests that ΔV^o and ΔH^o for the reaction $H_2O + O = 2OH$ are small. The speciation of water measured in hydrous albitic and rhyolitic glasses synthesized in rapid-quench apparatus is different from that observed in hydrous albitic and rhyolitic glasses synthesized in IHPV or air-quench

cold seal apparatus and demonstrates the necessity for rapid quench techniques.

4. Several mixing models of the homogeneous equilibria between melt species in albitic melts have been explored. All are based on simple equilibria of the form $H_2O + O = 2OH$. Although simple ideal mixing of these three species cannot account for the saturation of the hydroxyl group concentration for total water contents greater than about 4 wt %, this feature can be reproduced if the effects of non-ideal mixing of melt species, of polymerization, or of several distinguishable types of anhydrous melt species are considered. Further tests of these models may come from extension of these measurements to other compositions on the SiO_2-$NaAlO_2$-H_2O join and in other systems, as well.

5. I have developed a model of the thermodynamics of hydrous silicate melts based on the assumption that the activity of water is equal to the mole fraction of molecular water measured spectroscopically. This model can account reasonably well for the measured volumes of hydrous albitic melts, the pressure and temperature dependence of water solubility in albitic melt and the position of the water-saturated solidus of crystalline albite.

6. Spectroscopic measurements of H-bearing species in other hydrous glasses synthesized from melts equilibrated with water vapor at low pressures validate the approach used in modelling the thermodynamics of hydrous albitic melts and provide important constraints on the thermodynamic properties of these melt-water systems. These results demonstrate the generality of the conclusions presented in this study.

7. The primary goal of this study was to demonstrate the potential

of spectroscopic measurements of species concentrations for modelling the thermodynamic properties of silicate melts. Although the choice of $a^m_{H_2O} = X^m_{H_2O}$ was arbitrary, it is clearly an excellent approximation. Stolper et al. (1987) had similar success in modelling the thermodynamics of CO_2-bearing albitic melt using the assumption that $a^m_{CO_2} = X^m_{CO_2,mol}$. Further development of this kind of model requires two kinds of experiments: First, the speciation of water in glasses quenched from melts saturated with pure water vapor as a function of P and T must be measured using rapid quench apparatus, as demonstrated for the rhyolitic glasses. These measurements can be used to directly constrain the thermodynamic properties such as the partial molar volume and enthalpy of water in hydrous silicate liquids. Second, experiments could be done at constant pressure and temperature, but with variable vapor composition. If the assumption that $a^m_{H_2O} = X^m_{H_2O,mol}$ is valid, $X^m_{H_2O,mol}$ will be proportional to f_{H_2O}. This approach does not depend on knowledge of $V^{o,m}_{H_2O}(T,P)$ and $\Delta H^o_{H_2O}$, and the experiments can probably be carried out easily at low pressures by equilibrating melts with H_2O-CO_2 gas mixtures. With these data, a complete description of the thermodynamics of hydrous silicate melts can then be developed and applied to understanding the macroscopic behavior in these systems.

References

Acocella, J., Tomozawa, M., & Watson, E.B., 1984. The nature of dissolved water in sodium silicate glasses and its effect on various properties. J. Non-Crystalline Solids **65**, 175-183.

Adams, R.V., & Douglas, R.W., 1959. Infra-red studies of various samples of fused silica with special reference to the bands due to water. J. Soc. Glass Technol. **43**, 147-158 T.

Aines, R.D., Silver, L.A., Rossman, G.R., Stolper, E.M., & Holloway, J.R., 1983. Direct observation of water speciation in rhyolite at temperatures up to 850°C. Geol. Soc. Am. Abstr. Prog. **15**, 512.

Arndt, J., & Häberle, F., 1973. Thermal expansion and glass transition temperatures of synthetic glasses of plagioclase-like compositions. Contr. Miner. Petrol. **39**, 175-183.

Bartholomew, R.F., & Schreurs, J.W.H., 1980. Wide-line NMR study of protons in hydrosilicate glasses of different water content. J. Non-Crystalline Solids **38/39**, 679-684.

Bartholomew, R.F., Butler, B.L., Hoover, H.L., & Wu, C.K., 1980. Infrared spectra of a water-containing glass. J. Am. ceram. Soc. **63**, 481-485.

Blamart, D., Graham, C.M., & Sheppard, S.M.F., 1986. The system $NaAlSi_3O_8$(melt)-H_2O-sea water: Solubility of water and hydrogen isotope fractionation factor at 3, 5 and 8 kb. Intl. Symp. Exp. Miner. Geochem. Abstr., 23-24.

Boettcher, A.L., & Wyllie, P.J., 1969. Phase relationships in the system $NaAlSiO_4$-SiO_2-H_2O to 35 kilobars pressure. Am. J. Sci. **267**, 875-909.

Boettcher, A.L., Burnham, C.W., Windom, K.E., & Bohlen, S.R., 1982. Liquids, glasses, and the melting of silicates to high pressures. J. Geol. **90**, p. 127-138.

Bohlen, S.R., Boettcher, A.L., & Wall, V.J., 1982. The system albite-H_2O-CO_2: A model for melting and activities of water at high pressures. Am. Miner. **67**, 451-462.

Bottinga, Y., Weill, D., & Richet, P, 1982. Density calculation for silicate liquids: I. Revised method for aluminosilicate compositions. Geochim. cosmochim. Acta **46**, 909-919.

Boulos, E.N., & Kreidl, N.J., 1972. Water in glass: A review. J. Canad. ceram. Soc. **41**, 83-90.

Bowen, N.L., 1928. The Evolution of the Igneous Rocks. New York: Princeton Univ. Press, 334 pp.

Burnham, C.W., 1975. Water and magmas: A mixing model. Geochim. cosmochim. Acta **39**, 1077-1084.

_____ 1979. The importance of volatile constituents. In: Yoder, H.S. Jr. (ed.) The Evolution of the Igneous Rocks. Princeton Univ. Press, 439-482.

_____ Davis, N.F., 1971. The role of H_2O in silicate melts: I. P-V-T relations in the system $NaAlSi_3O_8$-H_2O to 1 kilobars and 1000°C. Am. J. Sci. **270**, 54-79.

_____ _____ 1974. The role of H_2O in silicate melts: II. Thermodynamic and phase relations in the system $NaAlSi_3O_8$-H_2O to 10 kilobars, 700° to 1100°C. Am. J. Sci. **274**, 902-940.

_____ Jahns, R.H., 1962. A method for determining the solubility of water in silicate melts. Am. J. Sci. **260**, 721-745.

_____ Darken, L.S., & Lasaga, A.C., 1978. Water and magmas: Application of the Gibbs-Duhem equation: A response. Geochim. cosmochim. Acta **42**, 277-280.

Church, B.N., & Johnson, W.M., 1980. Calculation of the refractive index of silicate glasses from chemical composition. G.S.A. Bull. **91**, 619-625.

Darken, L.S., 1950. Application of the Gibbs-Duhem equation to ternary and multicomponent systems. J. Am. Chem. Soc. **72**, 2909-2914.

Day, H.W., & Fenn, P.M., 1982. Estimating the P-T-X_{H_2O} conditions during crystallization of low-calcium granites. J. Geol. **90**, 485-507.

Eckert, H., Yesinowski, J.P., Stolper, E.M., Stanton, T.R., & Holloway, J., 1987a. The state of water in rhyolitic glasses: A deuterium NMR study. J. Non-Crystalline Solids (in press).

_____ _____ Silver, L.A., & Stolper, E.M., 1987b. Water in silicate glasses: Quantitation and structural studies by ^1H solid echo and MAS-NMR methods. J. Chem. Phys. (submitted).

Ernsberger, F.M., 1977. Molecular water in glass. J. Am. ceram. Soc. **60**, 91-92.

Farnan, I., Kohn, S.C., & Dupree, R., 1987. A study of the structural role of water in hydrous silica glass using cross-polarization magic angle spinning NMR. Geochim. cosmochim. Acta (submitted).

Fenn, P.M., 1973. Nucleation and growth of alkali feldspars from melts in the system $NaAlSi_3O_8$-$KAlSi_3O_8$-H_2O. Ph.D. thesis, Stanford University.

Fine, G., & Stolper, E., 1985. The speciation of carbon dioxide in sodium aluminosilicate glasses. Contr. Miner. Petrol. **91**, 105-121.

Flory, P.J., 1953. Principles of Polymer Chemistry. New York: Cornell University Press, 672 pp.

Gaskell, P.H., 1982. A structural interpretation of the density of alkali silicate glasses. J. Physique Collique C9, suppl. to no. 12, **43**, 101-105.

Gladstone, J.H., & Dale, T.P., 1864. Researches on the refraction, dispersion, and sensitiveness of liquids. Philos. Trans. Roy. Soc. London **153**, 317-343.

Goldsmith, J.R., & Jenkins, D.M., 1985. The hydrothermal melting and low and high albite. Am. Miner. **70**, 924-933.

Goranson, R.W., 1931. The solubility of water in granite magmas. Am. J. Sci. **22**, 481-502.

_____ 1936. Silicate-water systems: The solubility of water in albite-melt. Trans. Am. Geophys. Union **17**, 257-259.

_____ 1938. Silicate-water systems: Phase equilibria in the $NaAlSi_3O_8$-H_2O and $KAlSi_3O_8$-H_2O systems at high temperatures and pressures. Am. J. Sci. **35A**, 71-91.

Guggenheim, E.A., 1952. Mixtures. Oxford University Press, 270 pp.

Hamilton, D.L., & Oxtoby, S., 1986. Solubility of water in albite-melt determined by the weight-loss method. J. Geol. **94**, 626-630.

Holloway, J.R., 1971. Internally-heated pressure vessels. In: Ulmer, G.C. (ed.) Research Techniques for High Pressure and High Temperature, New York: Springer-Verlag, 217-258.

_____ 1977. Fugacity and activity of molecular species in supercritical fluids. In: Fraser, D. (ed.) Thermodynamics in Geology. Boston, D. Reidel, 161-181.

Ihinger, P. & Stolper E. Water solubility in rhyolitic melts: The effects of temperature and pressure. (in prep).

Karsten, J.L., Holloway, J.R., & Delaney, J.R., 1982. Ion microprobe studies of water in silicate melts: Temperature-dependent water diffusion in obsidian. Earth planet. Sci. Lett. **59**, 420-428.

Khitarov, N.I., Kadik, A.S., & Lebedev, E.B., 1963. Estimate of the thermal effect of the separation of water from felsic melts based on data for the system albite-water. Geokhimiya **7**, 637-649.

Kushiro, I., 1978. Viscosity and structural changes of albite ($NaAlSi_3O_8$) melt at high pressures. Earth planet. Sci. Lett. **41**, 87-90.

Lange, R., & Carmichael, I.S.E., 1987. Densities of Na_2O-K_2O-CaO-MgO-FeO-Fe_2O_3-Al_2O_3-TiO_2-SiO_2 liquids: New measurements and derived partial molar properties. Geochim. cosmochim. Acta (submitted).

Langer, K., and Flörke, O.W., 1974. Near infrared absorption spectra (4000-9000 cm^{-1}) of opals and the role of "water" in these $SiO_2 \cdot nH_2O$ minerals. Fortsch. Miner. **52**, 17-51.

Larsen, E.S., 1909. The relationship between refractive index and density of some crystallized silicates and their glasses. Am. J. Sci. **28**, 263-274.

Luth, W.C., 1976. Experimental petrology: Igneous rocks. In: Bailey, D.K., & MacDonald, R. (eds.) The Evolution of the Crystalline Rocks, New York: Academic Press, 333-417.

_____ Jahns, R.H., & Tuttle, O.F., 1964. The granite system at pressures of 4 to 10 kb. J. geophys. Res. **69**, 759-773.

_____ Mysen, B.O., & Virgo, D., 1987. Hydrogen in silicate liquids: Solution mechanisms of hydrogen in liquids in the system Na_2O-Al_2O_3-SiO_2-H_2. Am. Miner. **72**, 481-486.

Mandarino, J.A., 1976. The Gladstone-Dale relationship: Part I. Derivation of new constants. Can. Miner. **14**, 498-502.

Masson, C.R., 1965. An approach to the problem of ionic distribution in liquid silicates. Proc. Roy. Soc. (London) **287A**, 201-221.

McMillan, P.F., & Chlebik, A., 1980. The effect of hydroxyl ion content on the mechanical and other properties of soda-lime-silica glass. J. Non-cryst. Solids **38/39**, 509-514.

_____ Holloway, J.R., 1987. Water solubility in aluminosilicate melts. Contr. Miner. Petrol. (submitted).

_____ Remmele, R.R., Jr., 1986. Hydroxyl sites in SiO_2 glass: A note on infrared and Raman spectra. Am. Miner. **71**, 772-778.

_____ Piriou, B., & Navrotsky, A., 1982. A Raman spectroscopic study of glasses along the joins silica-calcium aluminate, silica-sodium aluminate, and silica-potassium aluminate. Geochim. cosmochim. Acta **46**, 2021-2038.

_____ Jakobsson, S., Holloway, J.R., & Silver, L.A., 1983. A note on the Raman spectra of water-bearing albite glasses. Geochim. cosmochim. Acta **47**, 1937-1943.

_____ Peraudeau, G., Holloway, J., & Coutures, J.-P., 1986. Water solubility in a calcium aluminosilicate melt. Contr. Miner. Petrol. **94**, 178-182.

Morey, G.W., 1924. Relation of crystallization to thw water content and vapor pressure of water in a cooling magma. J. Geology **32**, 291-295.

_____ 1954. The Properties of Glass (2nd ed.). A.C.S. Monograph 124, New York: Reinhold, p591.

_____ 1957. The solubility of solids in gases. Econ. Geol. **52**, 225-251.

_____ Fenner, C.N., 1917. The ternary system H_2O-K_2SiO_3-SiO_2. J. Am. chem. Soc. **39**, 1173-1229.

Morse, S.A., 1970. Alkali feldspars with water at 5 kb pressure. J. Petrology **11**, 221-251.

Mysen, B.O., & Virgo, D., 1980. Solubility mechanisms of water in basalt melt at high pressures and temperatures: $NaCaAlSi_2O_7$-H_2O as a model. Am. Miner. **65**, 1176-1184.

_____ _____ 1986a. Volatiles in silicate melts at high pressure and temperature. 1. Interaction between OH groups and Si^{4+}, Al^{3+}, Ca^{2+}, Na^{+} and H^{+}. Chem. Geol. **57**, 303-331.

_____ _____ 1986b. Volatiles in silicate melts at high pressure and temperature. 2. Water in melts along the join $NaAlO_2$-SiO_2 and a comparison of solubility mechanisms of water and fluorine. Chem. Geol. **57**, 333-358.

_____ _____ Harrison, W.J., & Scarfe, C.M., 1980. Solubility mechanisms of H_2O in silicate melts at high pressures and temperatures: A Raman spectroscopic study. Am. Miner. **65**, 900-914.

_____ Finger, L.W., Seifert, F.A., & Virgo, D., 1982. Curve-fitting of Raman spectra of amorphous materials. Am. Miner. **67**, 686-696.

Navrotsky, A., 1987. Calorimetric studies of melts, crystals, and glasses, especially in hydrous systems. In: Mysen, B.O. (ed) Magmatic Processes: Physicochemical Principles. Geochemical Society, Spec. Pub. No. 1, 411-422.

Nelson, S.A., & Carmichael, I.S.E., 1979. Partial molar volumes of oxide components in silicate liquids. Contr. Miner. Petrol. **71**, 117-124.

Newman, S., Stolper, E.M., & Epstein, S., 1986. Measurement of water in thyolitic glasses: Calibration of an infrared spectroscopic technique. Am. Miner. **71**, 1527-1541.

_____ Epstein, S., & Stolper, E.M., 1987. Water, carbon dioxide, and hydrogen isotopes in glasses from the ca. 1340 A.D. eruption of the Mono Craters, California: Constraints on degassing phenomena and initial volatile content. J. Volcanol. geotherm. Res. (submitted).

Orlova, G.P., 1962. The solubility of water in albite melts. Int. Geol. Rev. **6**, 254-258.

Oxtoby, S., & Hamilton, D.L., 1978. Solubility of water in melts of the Na_2O-Al_2O_3-SiO_2 and K_2O-Al_2O_3-SiO_2 systems. In: Mackenzie, W.S. (ed), Progress in Experimental Petrology, Natl. Environ. Res.

Council Pub., Ser. D, No. 11, Dept. Geology, Manchester Univ.

Paterson, M.S., 1982. The determination of hydroxyl by infrared absorption in quartz, silicate glasses and similar materials. Bull. Mineral. **105**, 20-29.

Pichavant, M., & Ramboz, C., 1985. Premiere détermination experimentale des relations de phases dans le systeme haplogranitique en conditions de sous-saturation en H_2O. C.R. Acad. Sci. Paris **301**, Sér. II, 607-610.

Prigogine, I., & Defay, R., 1954. Chemical Thermodynamics, Everett, D.H. (trans.), New York: Longmans Green and Co., 543 pp.

Remmele, R., Stanton, T., McMillan, P., & Holloway, J., 1986. Raman spectra of hydrous glasses along the quartz-albite join. EOS **67**, 1274.

Richet, P., Roux, J., & Pineau, F., 1986. Hydrogen isotope fractionation in the system H_2O-liquid $NaAlSi_3O_8$: New data and comments on D/H fractionation in hydrothermal experiments. Earth planet. Sci. Lett. **78**, 115-120.

Russell, L.E., 1957. Solubility of water in molten glass. J. Soc. Glass Technol. **41**, 304-317T.

Scholze, H., 1959. Der Einbau des Wassers in Gläsern. Glastech. Ber. **32**, 81-88, 142-145, 278-281.

Seifert, F., Mysen, B.O., & Virgo, D., 1981. Quantitative determination of proportions of anionic units in silicate melts. Carnegie Inst. Wash. Yrb. **80**, 301-302.

Shaw, H.R., 1964. Theoretical solubility of H_2O in silicate melts: Quasi-crystalline models. J. Geol. **72**, 601-617.

Silver, L.A., & Stolper, E., 1985. A thermodynamic model for hydrous silicate melts. J. Geol. **93**, 161-178.

Stewart, D.B., 1967. Four-phase curve in the system $CaAl_2Si_2O_8$-SiO_2-H_2O between 1 and 10 kilobars. Schweiz Mineralogische Petrographische Mitteilungen **47/1**, 35-59.

Stolen, R.H., & Walrafen, G.E., 1976. Water and its relation to broken bond defects in fused silica. J. Chem. Phys. **64**, 2623-2631.

Stolper, E.M., 1982a. Water in silicate glasses: An infrared spectroscopic study. Contr. Miner. Petrol. **81**, 1-17.

_____ 1982b. The speciation of water in silicate melts. Geochim. cosmochim. Acta **46**, 2609-2620.

_____ Silver, L.A., 1985. The speciation of water in silicate glasses: The influence of bulk composition. EOS **66**, 1140.

_____ _____ Aines, R.D., 1983. The effects of quenching rate and temperature on the speciation of water in silicate glasses. EOS **64**, 339.

_____ Fine, G., Johnson, T., & Newman, S., 1987. The solubility of carbon dioxide in albitic melt. Am. Miner. (in press).

Takata, M., Acocella, J., Tomozawa, M., & Watson, E.B., 1981. Effect of water content on the electrical conductivity of $Na_2O{\cdot}3SiO_2$ glass. J. Am. ceram. Soc. **64**, 719-724.

Tomlinson, J.W., 1956. A note on the solubility of water in molten sodium silicate. J. Soc. Glass Technol. **40**, 25-31.

Tuttle, O.F., & Bowen, N.L., 1958. Origin of granite in light of experimental studies in the system $KAlSi_3O_8$-$NaAlSi_3O_8$-SiO_2-H_2O. Geol. Soc. Amer. Mem. **74**, 153 pp.

Uys, J.M., & King, T.B., 1963. The effect of basicity on the solubility of water in silicate melts. Trans. met. Soc. AIME **227**, 492-500.

Voigt, D.E., Bodnar, R.J., & Blencoe, J.G., 1981. Water solubility in melts of alkali feldspar composition at 5 kb, 950°C. EOS **62**, 428.

Walsh, J.H., Chipman, J., T.B. King, & N.T. Grant, 1956. Hydrogen in steelmaking slags. Trans. met. Soc. AIME **206**, 1568-1576.

Wasserburg, G.J., 1957. The effect of H_2O in silicate systems. J. Geol. **65**, 15-23.

Watson, E.B., 1981. Diffusion in magmas of depth in the earth: The effects of pressure and dissolved H_2O. Earth planet. Sci. Lett. **52**, 291-301.

Wu, C., 1980. Nature of incorporated water in hydrated silicate glasses. J. Am. ceram. Soc. **63**, 453-457.

Appendix 1. Best Fit Parameters to Speciation Measurements

The spectroscopic measurements of species concentrations provide the basis for a useful activity-composition relation for hydrous melts. In order to use the spectroscopic data for calculating phase equilibria or for other applications, the relationship between the measurements of species concentrations and total water must be described in a usable mathematical form. As demonstrated for hydrous albitic glasses in Chapter 2, a best fit was determined to the speciation measurements based on a regular solution model involving Margules parameters for the binary interaction energies. This same procedure has been applied to the CAS, orthoclase and rhyolitic speciation data and the method is outlined below.

The non-ideal model described in Chapter 2 is based on the equilibrium between water molecules, hydroxyl groups and anhydrous oxygens in silicate melt. The non-idealities arise from the three binary interaction terms given by the Margules parameters. The best fits to the data for each composition are based on an equation of the form

$$-\ell n\left(\frac{(X_{OH}^{m})^{2}}{(X_{H_2O,mol}^{m})(X_{O}^{m})}\right) = A' + B'\ X_{OH}^{m} + C'\ X_{H_2O,mol}^{m} \qquad (21.1)$$

where A', B' and C' are functions of the binary interaction parameters, and $X_{H_2O,mol}^{m}$, X_{OH}^{m} and X_{O}^{m} $(=1-X_{H_2O,mol}^{m}-X_{OH}^{m})$, the mole fractions of the three species, are obtained from the spectroscopic measurements. Using the infrared measurements of the concentrations of molecular water and hydroxyl groups in a series of glasses (of a given bulk composition) covering a range of total water contents, A', B' and C' were determined

by least squares for the CAS, KAS, rhyolitic and albitic glasses included in this study. These parameters are given in Table 16.

Equation (21.1) can be rewritten in terms of the bulk composition of the system (given by N_O and N_{H_2O}, where N_O = the number of oxygens contributed by the anhydrous silicate component expressed on a single oxygen basis and N_{H_2O} = the number of water molecules) and X_{OH}:

$$-\ell n\left(\frac{(X^m_{OH})^2}{(N_{H_2O}-0.5X^m_{OH})(N_O-0.5X^m_{OH})}\right)=A+B(X^m_{OH}-1)+2C(N_O-X^m_{OH})+2D(N_{H_2O}-X^m_{OH}) \quad (21.2)$$

where $A = -\ell n(K_1)^o$, $B = W_{H_2O,mol-O}/RT$, $C = W_{O-OH}/RT$, and $D = W_{H_2O,mol-OH}/RT$; they are defined in terms of A', B' and C' as follows: $A = C' + A'/3 + B'/3$; $B = C'/6 - B'/3$; $C = -C'/12 - B'/3$; and $D = 5C'/12 - B'/3$. The interaction parameters and $\ell n(K_1)^o$ determined from the constants derived in the least squares regression are given in Table 16 for each composition. With these constants, equation (21.2) provides an empirical relationship between the concentrations of the various species. Equation (21.2) can be solved for X_{OH} at a given bulk composition (i.e., values of N_O and N_{H_2O}, where $N_O + N_{H_2O} = 1$, for convenience) by an iterative method. From X_{OH}, N_O, and N_{H_2O}, the mole fraction of molecular water can be obtained as follows:

$$X^m_{H_2O,mol} = 1 - N_O - 0.5X^m_{OH} \quad (22.1)$$

$$X^m_O = N_O - 0.5X^m_{OH} \quad (22.2)$$

and the mole fraction of total water, X_B, is then given by

$$X_B = 0.5X^m_{OH} + X^m_{H_2O,mol} \quad (22.3)$$

These mole fractions can then be recast in terms of weight percent water as follows:

Table 16. Interaction parameters

TABLE 16

Interaction parameters

Composition	A'	B'	C'
CAS	0.215	14.662	8.753
KAS	0.878	16.72	5.395
Rhyolites	1.093	16.858	7.892
Albite	0.403	15.333	10.894

Composition	A $(\ln(K_1)^o)$	B $(W_{H_2O,mol-O}/RT)$	C (W_{O-OH}/RT)	D $(W_{H_2O,mol-OH}/RT)$
CAS	-8.451	-4.099	-6.279	-1.918
KAS	-8.25	-4.674	-6.024	-3.326
Rhyolites	-9.345	-4.304	-6.277	-2.328
Albite	-9.143	-3.295	-6.019	-0.572

$$\text{wt \% } H_2O,\text{mol} = \frac{18.015 \; X^{m}_{H_2O,\text{mol}}}{18.015 \; X_B + (1-X_B) \; M_O} \times 100 \qquad (23.1)$$

$$\text{wt \% } H_2O,\text{total} = \frac{18.015 \; X_B}{18.015 \; X_B + (1-X_B) \; M_O} \times 100 \qquad (23.2)$$

$$\text{wt \% OH (as } H_2O) = \text{wt \% } H_2O,\text{ total} - \text{wt \% } H_2O,\text{mol} \qquad (23.3)$$

In practice, I tabulated values of X_B, the mole fractions of molecular water and hydroxyl groups and the weight fractions in narrow intervals so the calculations would not have to be done more than once and for the detailed calculations, the values could be read directly from the tables.

Appendix 2. Densities of Hydrous Silicate Glasses

Densities of hydrous glasses quenched from melts equilibrated over a range of experimental conditions have been measured. For samples in which individual pieces on the order of 10-40 mg by weight could be obtained, densities were measured using a Berman balance, by weighing in air and in toluene at a known temperature. The density of a quartz standard was measured each time density measurements were made to ensure reliability in the results. The quartz standard has a density of 2.659 ± 0.0048 gm/cc (1σ) based on 45 repeated analyses using the same technique. The density measurements made with a Berman balance typically have errors of about 1.8 %, for samples that are about 20-40 mg by weight. For samples that weighed less than 10-15 mg, the densities were determined using heavy liquids of known densities in the range 2.2 to 2.5 gm/cc, with tolerances of ±.005 gm/cc. The densities of these liquids were checked using sink-float standards (with tolerances of ±0.0005 gm/cc) each time the liquids were used to assess any changes in density due to evaporation or other aging effects. The density measurements made by this technique are considered to be less accurate and typically have errors of 0.013 to 0.025 gm/cc, or about 2-3 %.

Figure 39a shows the variations in density with total water content for a series of bubble-free albitic, orthoclase, and CAS glasses quenched from melts equilibrated at 1200-1450°C and 15-20 kbar. The densities of these glasses were determined either by a Berman balance or heavy liquids, with estimated errors as indicated. Also shown in Fig. 39a is the variation in density with total water content for a series of rhyolitic glasses quenched from melts equilibrated at 1-7 kbar and 800-

Figure 39a. The variation in measured densities with total water content for glasses included in this study. The CAS, albite and KAS samples were synthesized at 15-20 kbar and 1200-1450°C. The rhyolitic glasses were synthesized at 1-7 kbar and 600-1150°C (unpub. results). The density measurements were made with using a Berman balance (open symbols) or a float-sink method, using heavy-liquids of known densities (filled symbols). The diamonds represent CAS glasses; the inverted triangles represent albite glasses; the squares represent orthoclase (KAS) glasses; and the triangles represent rhyolitic glasses. Typical errors for the Berman balance measurements are $\leq$ the size of the symbols; for heavy liquids measurements, typical errors are 0.02 gm/cc.

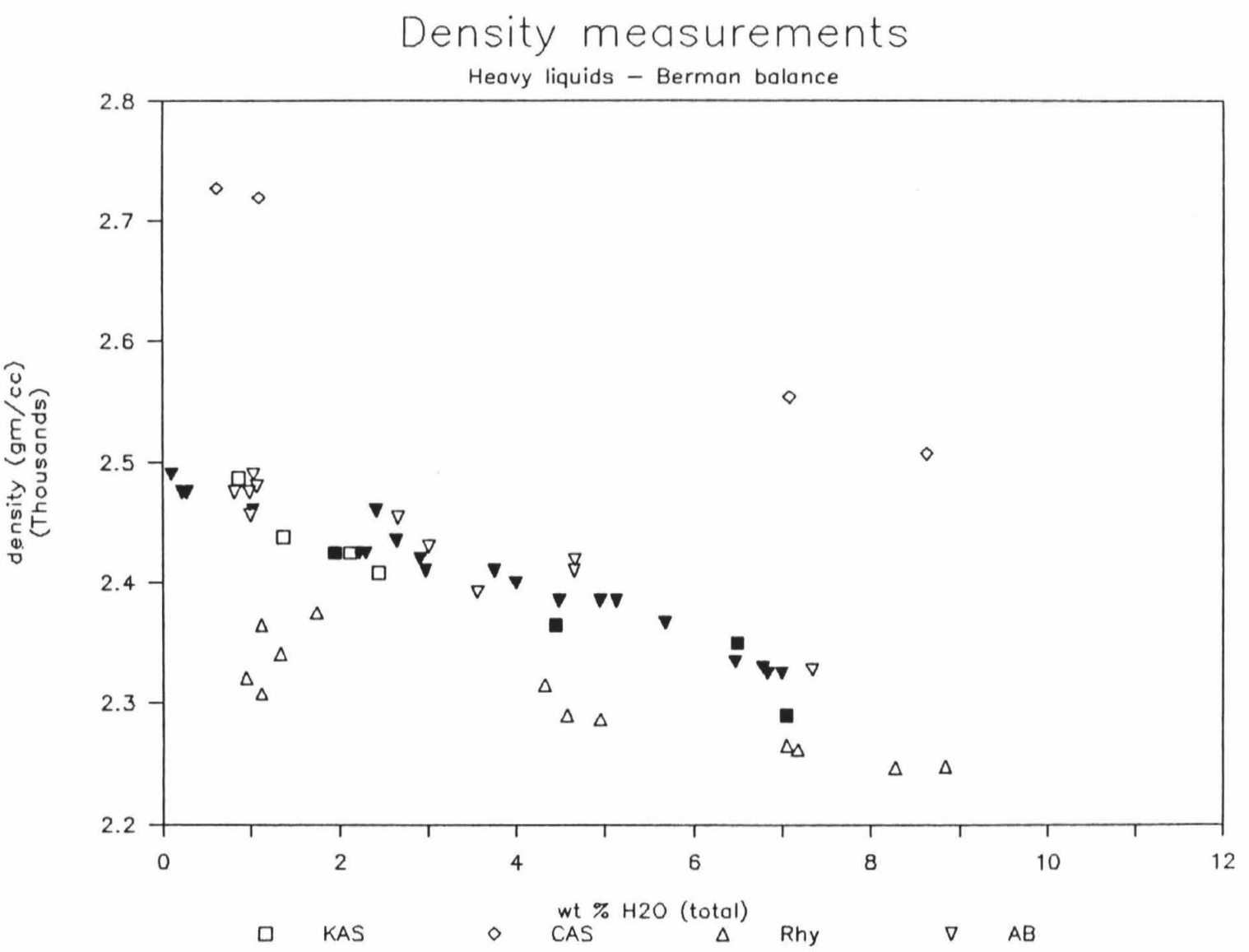
Density measurements
Heavy liquids – Berman balance
density (gm/cc)
(Thousands)
2.8
2.7
2.6
2.5
2.4
2.3
2.2
0
2
4
6
8
10
12
wt % H2O (total)
KAS
CAS
Rhy
AB

1150°C in IHPV or cold-seal pressure vessels (L.A. Silver, unpub. results). For all of the glasses studied, there is a roughly linear relationship between density and water content, such that the density decreases with increasing water content. Figure 39b shows the relationship between density and total water content determined for hydrous glasses of other compositions, including a "hydrosilicate" (Bartholomew et al., 1980), $Na_2Si_3O_7$ (Acocella et al., 1984) and albitic glasses (Orlova, 1962); these results are similar to the results shown in Fig. 39a.

Density measurements can be used to calculate the molar volume of glass (on a single oxygen basis) from the following equation

$$\overline{V}_0(tot) = \frac{100}{\rho\ (wt\%\ H_2O/18.015 + (100-wt\%\ H_2O)/M_0)} \qquad (24)$$

where $\overline{V}_0(tot)$ is the molar volume of the glass, ρ is the density in gm/cc, 18.015 is the molecular weight of water, and M_0 is the molecular weight of the anhydrous silicate based on a single oxygen as follows: for albite, M_0=32.78 gm/mol; for CAS, M_0=34.32 gm/mol; for KAS, M_0=34.79 gm/mol; for rhyolite, M_0=32.49 gm/mol; for $Na_2Si_3O_7$, M_0=34.57; for hydrosilicate, M_0=35.36 gm/mol. For each of the samples shown in Figs. 39a and 39b the molar volume per oxygen was determined from equation (24). Figure 40a shows $\overline{V}_0(tot)$ as a function of the mole fraction of total water, X_B, for albite, KAS and CAS glasses synthesized at high P and T in this study. Figure 40b shows the volumes derived from the density measurements reported by Orlova (1962) for albitic glasses, Bartholomew et al. (1980) for hydrosilicate glasses, Acocella et al.

Figure 39b. The variation in measured densities with total water content for synthetic silicate glasses reported in the literature. These glasses were all synthesized at pressures < 4 kbar. The diamonds represent "hydrosilicate glasses from Bartholomew et al. (1980); the triangles represent $Na_2Si_3O_7$ glasses from Acocella et al. (1984); and the squares represent albitic glasses from Orlova (1962). The estimated errors (as reported by the authors) are ≤ the size of the symbols.

Density measurements

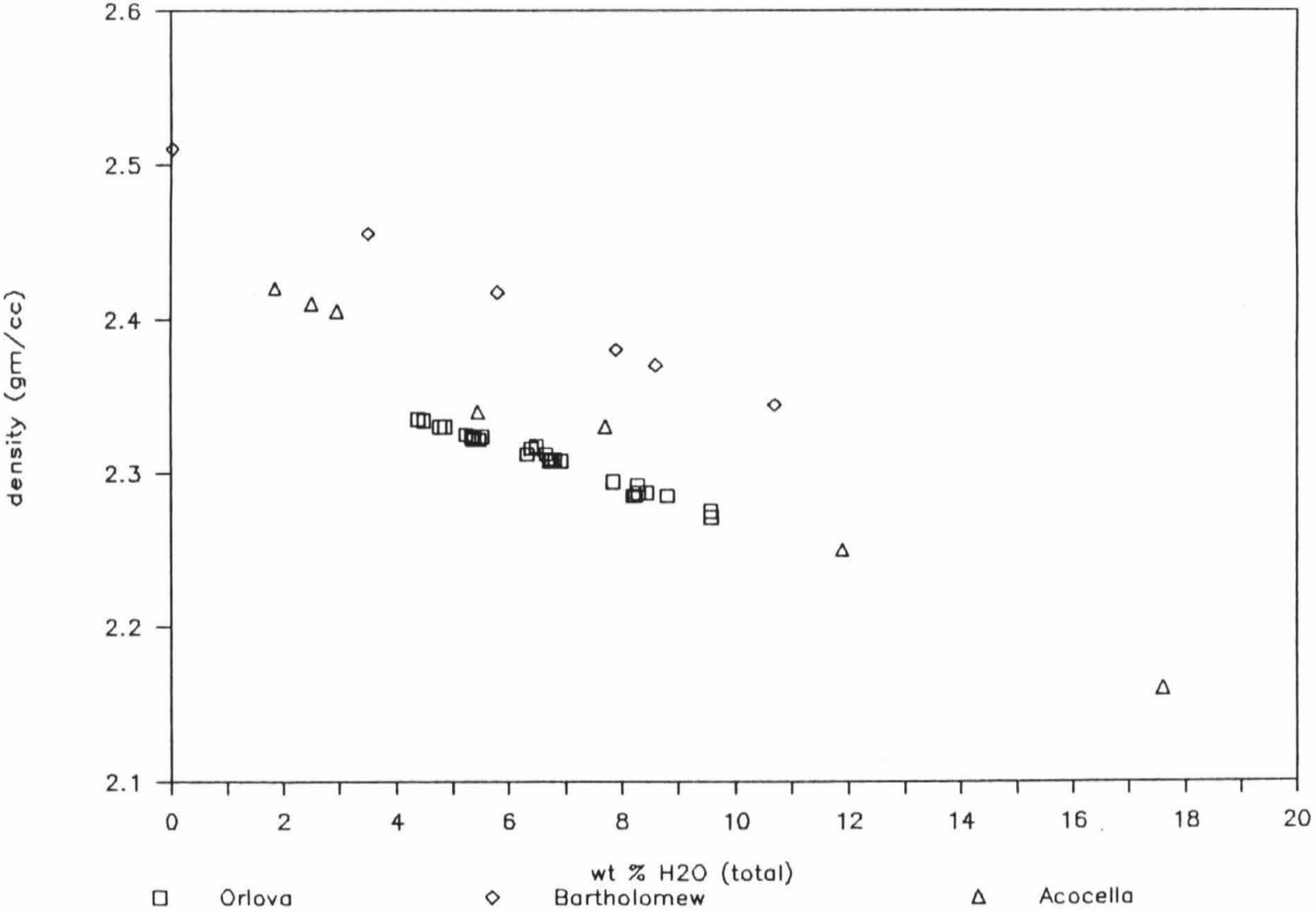

Figure 40a. The variation in the volumes of hydrous glasses (per mole of oxygen) with total water content expressed as the mole fraction of total water, X_B, for the CAS, KAS and albite glasses included in this study, all synthesized at 15-20 kbar and 1200-1450°C. The volumes were calculated from the measured densities using equation (24). The diamonds represent CAS glasses; the inverted triangles represent albite glasses; and the squares represent KAS glasses. The best fit lines were calculated from equation (25) and the partial molar volumes of water for each composition are indicated by the best fit lines at $X_B = 1$.

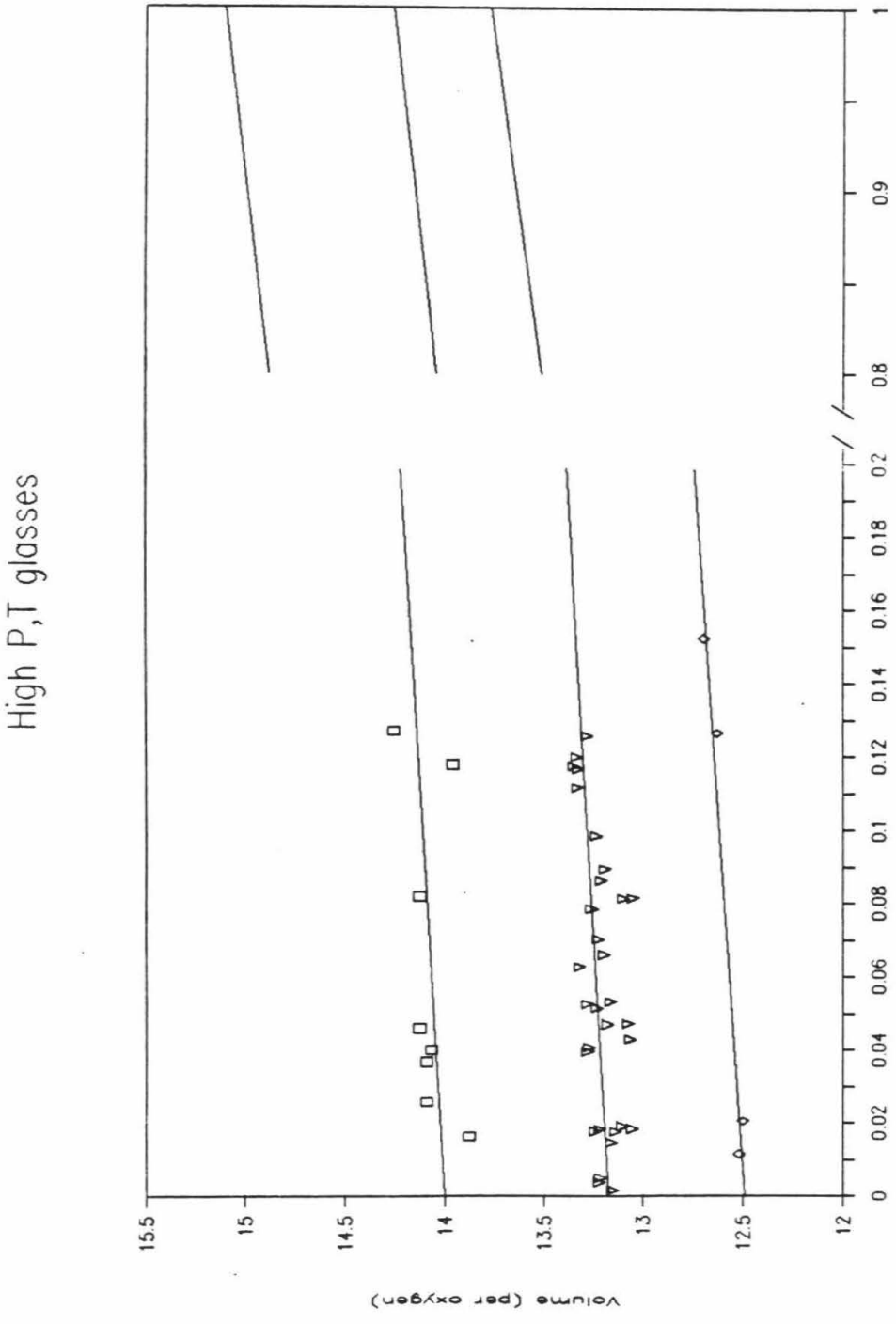
High P,T glasses
Volume (per oxygen)
15.5
15
14.5
14
13.5
13
12.5
12
0
0.02
0.04
0.06
0.08
0.1
0.12
0.14
0.16
0.18
0.2
0.8
0.9
1
X(B)
KAS
CAS
AB

Figure 40b. The variations in the molar volumes (on a single oxygen basis) of hydrous glasses with total water, expressed as the mole fraction, X_B, for glasses synthesized at P<7 kbar. The volumes were calculated from the measured densities using equation (24). The diamonds represent hydrosilicate glasses from Bartholomew et al. (1980); the inverted triangles represent rhyolitic glasses (L.A. Silver, unpub. results); the squares represent albitic glasses from Orlova (1962); and the triangles represent $Na_2Si_3O_7$ glasses from Acocella et al. (1984). The best fit lines were calculated from equation (25) and the partial molar volumes of water for each composition are indicated by the best fit lines at $X_B = 1$.

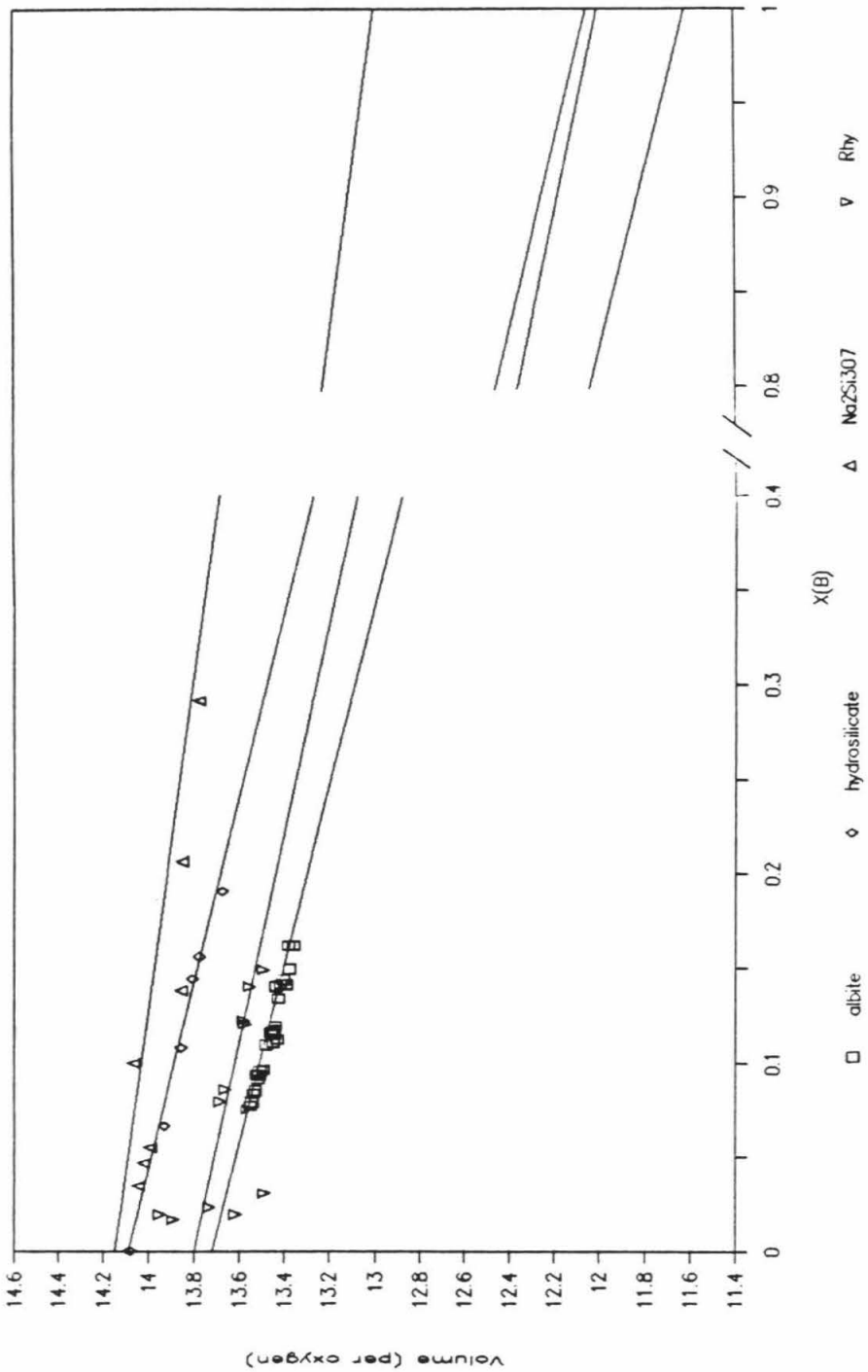
Low P (< 7 kbar) glasses
Volume (per oxygen)
14.6
14.4
14.2
14
13.8
13.6
13.4
13.2
13
12.8
12.6
12.4
12.2
12
11.8
11.6
11.4
0
0.1
0.2
0.3
0.4
0.8
0.9
1
X(B)
albite
hydrosilicate
Na2Si3O7
Rhy

(1984) for $Na_2Si_3O_7$ glasses and rhyolitic glasses (L.A. Silver, unpub. results) at lower pressure as functions of X_B.

For the albite (this study), CAS, and KAS glasses, the molar volume (per oxygen) increases slightly with increasing total water content, whereas the molar volume (per oxygen) decreases with increasing total water content for the rhyolitic, $Na_2Si_3O_7$, albite (from Orlova, 1962) and hydrosilicate glasses even though for all the glasses the density decreases with increasing total water content. The difference between the two groups of samples is probably due to the effects of different pressure. The former three sets of glasses were synthesized at high pressures (15-20 kbar) and the latter four were synthesized at low pressures (< 7 kbar). Kushiro (1978) demonstrated that the densities of silicate glasses quenched from melts synthesized at elevated pressure were higher than those in glasses quenched from melts equilibrated at lower pressure, and the most dramatic increase took place at pressures between 15 and 20 kbar. The effect of synthesis conditions on the densities of glasses can be seen in Figs. 39a and 39b, where for the albitic glasses in this study, my measured densities are about 0.05 gm/cc higher than the values reported in Orlova (1962) at similar total water contents.

It should be possible to use the variation in the molar volumes with total water content to determine the partial molar volumes of molecular water, OH groups and the anhydrous oxygen component in a series of glasses with a range of total water contents. This requires density measurements on anhydrous glasses, to constrain the anhydrous volume component, $\overline{V}_0$ and glasses with a range of total water contents,

particularly with low total water contents, where almost all of the water is dissolved as OH groups, to constrain $\overline{V}_{OH}$, and with higher total water contents, to constrain $\overline{V}_{H_2O,mol}$, quenched from melts equilibrated at the same pressure and temperature. The density measurements in this study are not extensive enough to use this approach.

The data shown in Fig. 40 have been used to constrain the partial molar volumes of the water and silicate components in these glasses, using the relation

$$\overline{V}_O(tot) = X_B\overline{V}_{H_2O} + (1-X_B)\,\overline{V}_O \qquad (25)$$

assuming ideal mixing of the water and silicate components. Figs. 40a and 40b show the partial molar volumes of the anhydrous and water components (indicated by the best fit lines at $X_B = 0$ and 1, respectively) derived from a least squares regression of equation (25) based on the density measurements and the known total water contents for each composition. The values of $\overline{V}_{H_2O}$ and $\overline{V}_O$ vary with both bulk composition and with the pressure from which the glasses were quenched. For albitic glasses, the value for $\overline{V}_O$ of 13.8 cc/mol from Orlova (1962) is similar to the values determined by Arndt & Häberle (1973) and Kushiro (1978) at 1 atm and 25°C; my data on albitic glasses synthesized at high P indicates a value for $\overline{V}_O$ of about 13.2 cc/mol, similar to the value based on density measurements from Kushiro (1978) at similar pressures. The partial molar volume of water for the albitic glasses in this study and the value derived from Orlova's data on the same composition are also different and either reflect real differences in the partial molar volumes of water or the effects of quenching. In

either case, these data provide a method for estimating the densities of hydrous glasses and the partial molar volumes of water in hydrous glasses with known total water contents.

There have been many other methods proposed for calculating the densities of silicate glasses and liquids based on the bulk composition of the system (Bottinga & Weill, 1982; Nelson & Carmichael, 1979; Lange & Carmichael, 1987) These methods have been proposed for anhydrous liquid compositions. An alternate method, first proposed by Gladstone & Dale (1864) and later applied to the Earth sciences by Larsen (1909) is the Gladstone-Dale rule. This is an empirical relationship between the specific refractive energy K and the mean refractive index $\bar{n}$ and the density given by

$$K = \frac{\bar{n} - 1}{D} = \Sigma\, k_i w_i \qquad (26)$$

where w_i are the weight fractions and k_i are the specific refractive energies of the oxide components in the glass. Using the data given by Morey (1954) on the densities and refractive indices of over 400 simple oxide glasses at 1 atm and using my own and other hydrous samples that were available to me, I solved for values for k_i for 7 oxide components, including H_2O by a multiple least squares regression of equation (26). The coefficients are given in Table 17; also included are coefficients for FeO and TiO_2 from Mandarino (1976).

This method provides a straightforward way to calculate densities of glasses for which the refractive indices have been measured. Comparison of the measured densities with those calculated using equation (26) indicates that this method can retrieve the measured

Table 17. Coefficients for Gladstone-Dale rule and Church-Johnson equation

TABLE 17

Coefficients for the Gladstone-Dale rule and Church-Johnson equation

Oxide	k_i (a)	n_i (b)
SiO_2	0.208	0.46
TiO_2	0.115	1.158
Al_2O_3	0.2249	0.581
FeO	0.188	0.897
MgO	0.215	0.767
CaO	0.2269	0.795
Na_2O	0.1941	0.505
K_2O	0.2035	0.495
H_2O	0.3128	0.442

Notes:

a. This study, except FeO and TiO_2 from Mandarino (1976).

b. Church & Johnson (1980), except H_2O from this study.

values to within 0.050 gm/cc, but the agreement is generally much better for glasses that do not contain FeO or MgO (typically within 0.01 gm/cc of the measured values).

The application of this method depends on a refractive index measurement. If the refractive index is not known, it can be calculated from the equation given by Church & Johnson (1980) which provides an empirical relationship between the mean refractive index (for glassy materials) and bulk composition given by

$$n = \Sigma\, n_i w_i + 1 \qquad (27)$$

Using the values of n_i given by Church & Johnson (1980) for eight oxides, I solved for the coefficient for H_2O in this equation by a least squares method; all of the n_i are given in Table 17. Thus, using equations (26) and (27), the density of a hydrous glass can be calculated if the bulk composition is known.

This method was used to calculate the densities for the E2 glasses from McMillan et al. (1986) for which the refractive indices had been determined by P. Lambert (P. McMillan, personal comm.). The calculated densities are given in Table 8 and are approximately 0.05 gm/cc lower than those measured for the CAS glasses using a Berman balance. This difference is not unexpected given the fact that the E2 glasses were synthesized at pressures less than 5200 bars and the CAS glasses were quenched from melts equilibrated at pressures greater than 15 kbar. As demonstrated above for albitic glasses in Figs. 39a and 39b, the effect of pressure could easily account for the difference.

Appendix 3. A Thermodynamic Model for Hydrous Silicate Melts

A THERMODYNAMIC MODEL FOR HYDROUS SILICATE MELTS[1]

LYNN SILVER AND EDWARD STOLPER
Division of Geological and Planetary Sciences, California Institute of Technology, Pasadena, CA 91125

ABSTRACT

A simple thermodynamic model describing hydrous silicate melts has been applied to the systems albite-, diopside-, and silica-H_2O. The model is based on the assumption of ideal mixing of hydroxyl groups, H_2O molecules, and oxygens in the melt. Calculated and experimentally determined freezing-point depressions and H_2O solubilities for these systems are in agreement over substantial pressure and temperature intervals. The success of this model in accounting for observed phase equilibria of hydrous systems and its consistency with spectroscopic measurements of the concentrations of H-bearing species in glasses suggests that it accurately represents the interaction between H_2O and silicate melts at a molecular level.

INTRODUCTION

Thermodynamic models of water-bearing silicate melts have been widely applied both to provide a framework for understanding the observed variations in chemical and physical properties of melts with varying water content and to provide a way to quantitatively model phase equilibria relevant to petrological systems. Thus Burnham (1975), for example, attempted to infer the solubility mechanism of water in silicate melts from an equation of state for hydrous albitic melts and related this to observed variations in physical properties with water content. Spera (1974) applied another model of the mixing properties of hydrous silicate melts to predict water solubilities in melts in the upper mantle and tried to explain the stabilization of the low velocity zone. Thermodynamic models provide powerful tools for addressing these and other petrologically important issues.

Thermodynamic models of hydrous silicate melts fall into two broad categories. The first approach is largely macroscopic and empirical. For example, Burnham and Davis (1971) fitted data on the partial molar volumes of water and albite components in hydrous albitic melt to third-order polynomials in P and T with 10 constants. By appropriate manipulations of this expression, in which phase equilibrium data were used as reference points, Burnham and Davis (1974) developed an activity-composition relationship for this system. This expression, in somewhat modified form, was applied to hydrous diopside melts by Eggler and Burnham (1984). Spera (1974) used solubility data to constrain activity-composition relations for water-bearing silicate melts using the standard formulae for asymmetric regular solutions. Nicholls (1980) followed a similar approach using a symmetric regular solution formulation. These formulations are extremely valuable for predicting phase equilibria in hydrous systems and have been successfully applied to a wide range of interesting geological problems. The expressions for activity versus composition in these cases, however, have no microscopic significance. They are empirical, in some cases arbitrary, and they contain no explicit information on the molecular level interactions leading to the observed activity-composition relations. There is no inherent problem with this, because thermodynamics need not consider the nature of molecular interactions within the substance of interest; it suffices to have accurate empirical information on the substance's equation of state. However, information about molecular level processes and equilibria can be obtained only with difficulty, if at all, from such descriptions of the properties of systems as complex as liquid silicates.

The second approach to the thermodynamics of hydrous silicate melts is better suited to constraining the nature of their molecular level structures and homogeneous equilibria. In this treatment, first applied to hydrous silicate melts by Wasserburg (1957) and further developed by Shaw (1964, 1968) and Stolper (1982*a*), statistical thermodynamics is used,

[1] Manuscript received July 9, 1984; revised December 11, 1984.

[JOURNAL OF GEOLOGY, 1985, vol. 93, p. 161–178]

0022-1376/85/9302-008$1.00

given certain assumptions about species and their interactions on a molecular level, to generate expressions for the thermodynamic properties of silicate melts. Although these models are simple, they provide a basis for understanding the thermodynamic properties of silicate melts and solubility mechanisms of water on a molecular level. These models specify the functional form of the activity-composition relationship based on the assumed molecular level interactions. To the extent that these thermodynamic functions can explain macroscopic phenomena (e.g., solubility relations, freezing-point depressions), these models may be judged acceptable and hence represent possible descriptions of melt structure.

In this paper, we apply the model of Stolper (1982*a*) to calculating phase equilibria in the systems albite-, diopside-, and silica-H_2O. We show that the activity-composition relations that arise from our simple model of interactions between molecules of water, hydroxyl groups, and oxygen atoms in melts in these systems are consistent with available experimentally determined phase equilibria. When coupled with the fact that this model also predicts concentrations of each of these species that are broadly consistent with a growing body of spectroscopic data, we conclude that this model provides a useful tool both for understanding the species level properties of hydrous silicate melts and for modelling their macroscopic phase equilibria.

THE MODEL

We model hydrous silicate melts as ideal mixtures of water molecules, hydroxyl groups, and oxygen atoms. These species interact through the following homogeneous equilibrium:

$$\begin{matrix} H_2O,\text{molecular (melt)} \\ + \text{ O (melt)} = 2\text{OH (melt)} \end{matrix} \qquad (1)$$

where O = an oxygen atom, OH = a hydroxyl group, and H_2O,molecular = a water molecule in the melt. Associated with this reaction is an equilibrium constant,

$$K_1 = \frac{(a^m_{OH})^2}{(a^m_O)(a^m_{H_2O,mol})} \qquad (2)$$

where a^m_{OH}, $a^m_{H_2O,mol}$, and a^m_O refer to the activities of hydroxyl groups, molecular water and "free" oxygens (in the sense that they are not associated with hydrogens) in the melt. The melt is modeled as a mixture of n_O "free" oxygens, n_{OH} hydroxyl groups and $n_{H_2O,mol}$ water molecules over $\Sigma n = n_O + n_{OH} + n_{H_2O,mol}$ sites. Because the mixture is ideal and all "free" oxygens are taken to be energetically equivalent and indistinguishable, the activity of each species is equal to its mole fraction:

$$a^m_{H_2O,mol} = X^m_{H_2O,mol} = \frac{n_{H_2O,mol}}{\Sigma n} \qquad (3.1)$$

$$a^m_{OH} = X^m_{OH} = \frac{n_{OH}}{\Sigma n} \qquad (3.2)$$

$$a^m_O = X^m_O = \frac{n_O}{\Sigma n} \qquad (3.3).$$

When N_1 moles of H_2O are mixed with N_2 moles of anhydrous silicate that contributes r oxygens per mole of silicate (e.g., r = 2 for SiO_2, r = 8 for $NaAlSi_3O_8$), they react until equilibrium as given by reaction (1) is achieved. The relationship between the reactants and products is described by:

$$n_O = rN_2 - \frac{1}{2}n_{OH} \qquad (4.1)$$

$$n_{H_2O,mol} = N_1 - \frac{1}{2}n_{OH} \qquad (4.2).$$

Substituting these expressions into (2) and (3), we obtain the following equations for the mole fractions of each species, given values for the bulk composition of the system (i.e., N_1, rN_2) and K_1:

$$X^m_{OH} = \left\{\frac{1}{2} - \left[\frac{1}{4} - \left(\frac{K_1 - 4}{K_1}\right)(X_B - X_B^2)\right]^{1/2}\right\} \Big/ \left(\frac{K_1 - 4}{2K_1}\right) \qquad (5.1)$$

$$X^m_{H_2O,mol} = X_B - \frac{1}{2}X^m_{OH}$$

$$= X_B - \left\{\frac{1}{2} - \left[\frac{1}{4} - \left(\frac{K_1 - 4}{K_1}\right)(X_B - X_B^2)\right]^{1/2}\right\} \Big/ \left(\frac{K_1 - 4}{K_1}\right) \qquad (5.2)$$

$$X_O^m = 1 - 2X_B + X_{H_2O,mol}^m$$

$$= 1 - X_B - \left\{\frac{1}{2} - \left[\frac{1}{4} - \left(\frac{K_1 - 4}{K_1}\right)(X_B - X_B^2)\right]^{1/2}\right\} \Big/ \left(\frac{K_1 - 4}{K_1}\right) \quad (5.3)$$

where $X_B = N_1/(N_1 + rN_2)$.

X_B is the variable that we use to express the bulk composition of the system; it is the mole fraction of total water in the melt where the anhydrous component is taken as having only one oxygen. In other words, X_B = ⅓ when the melt consists of one mole of H_2O and one mole of $NaAlSi_3O_8$. X_B can be calculated for a complex melt composition with a known water content using the following equation:

$$X_B = \frac{\text{wt \% } H_2O/18.015}{(\text{wt \% } H_2O/18.015) + (100 - \text{wt \% } H_2O)/(\text{molecular weight of anhydrous silicate per oxygen})} \quad (6).$$

The molecular weight of the silicate per oxygen refers to the molecular weight of anhydrous melt on a single oxygen basis and would, for example, be 32.78 for albite. Equations (5.1–5.3) constitute the activity-composition relationships for hydrous silicate melts given by our model of molecular level interactions. Note again that these equations are based on the approximation that all free oxygens are equivalent and equally reactive.

K_1 can be determined directly from infrared spectroscopic measurements on hydrous silicate glasses (Stolper, 1982*b*) by which the concentrations of hydroxyl groups and molecules of water can be precisely determined (assuming that the speciation in a glass reflects that of the melt from which it was quenched). However, for the purposes of applying this model without bias, we will determine the value of K_1 for each system that best fits the phase equilibrium data without reference to K_1 values determined by spectroscopic methods. The degree to which these two means of determining K_1 produce similar values provides an independent check of the validity of our model. In our treatment, K_1 is assumed to be independent of T, P, and total water content, but is allowed to vary with the anhydrous melt composition. Based on spectroscopic measurements, this appears to be valid to first order, although K_1 does appear to be weakly dependent on total water content (Stolper 1982*a*, 1982*b*), temperature (Stolper et al. 1983), and perhaps pressure (Nogami and Tomozawa 1984).

The solubility of water in silicate melts, i.e., the concentration of water dissolved in the melt when it is in equilibrium with water vapor, is readily modeled given the activity-composition relations of equations (5.1–5.3). The equilibrium between the vapor and the dissolved H_2O in the melt is described by:

$$H_2O \text{ (vapor)} = H_2O,\text{molecular (melt)} \quad (7).$$

This reaction has an equilibrium constant,

$$K_2 = \frac{a_{H_2O,mol}^m}{a_{H_2O}^v} = \frac{X_{H_2O,mol}^m}{f_{H_2O}/f_{H_2O}^o} \quad (8).$$

The standard state fugacity for the vapor ($f_{H_2O}^o$) is defined as that of pure water at P and T; f_{H_2O} is the fugacity of water in the vapor. The activity of water in the vapor at any P and T, $a_{H_2O}^v$, is thus equal to one if the vapor is pure water and less than one if the vapor has other constituents in addition to water. Equation (5.2) can be rearranged to give total water content in terms of $X_{H_2O,mol}^m$:

$$X_B = X_{H_2O,mol} + \frac{1}{4}\{-K_1X_{H_2O,mol} + [(K_1X_{H_2O,mol})^2 - 4K_1X_{H_2O,mol}^2 + 4K_1X_{H_2O,mol}]^{1/2}\} \quad (9).$$

If K_1, K_2, and f_{H_2O} are known, we can calculate total solubility:

$$X_B = K_2a_{H_2O}^v + \frac{1}{4}\{-K_1K_2a_{H_2O}^v + [(K_1K_2a_{H_2O}^v)^2 - 4K_1(K_2a_{H_2O}^v)^2 + 4K_1K_2a_{H_2O}^v]^{1/2}\} \quad (10).$$

X_B can be converted to weight percent H_2O by the following relation:

$$\text{wt \% } H_2O = \frac{(X_B)(18.015)}{(X_B)(18.015) + (1 - X_B)(\text{molecular weight of anhydrous silicate per oxygen})} \quad (11).$$

As demonstrated by Stolper (1982*a*), this model successfully predicts the observed linear relationship between f_{H_2O} and $(X_B)^2$ for melts at low total water contents, provided that K_1 has a value similar to the ~0.2 derived spectroscopically. We will now show that our model can also adequately reproduce the experimentally determined hydrous melting relations and water solubilities as functions of P for three silicate-H_2O systems.

FREEZING POINT DEPRESSION

Our first goal is to calculate the depression of the liquidus of a silicate with the addition of water (e.g., curve A-B in fig. 1). At any P and T, the activity of the anhydrous component in a binary silicate-H_2O liquid in equilibrium with a crystalline silicate with the composition of the anhydrous component (e.g., the activity of albite in a hydrous albite melt in equilibrium with crystalline albite) is given by:

$$a^m_{\text{silicate}} = \exp\left[\frac{1}{RT}\int_{T^P_m}^{T} \Delta\bar{S}_f(T,P)dT\right] \quad (12).$$

$\Delta\bar{S}_f(T,P)$ is the molar entropy of fusion of the anhydrous crystalline silicate. T^P_m is the anhydrous melting temperature of the crystalline silicate at P (e.g., point A in fig. 1). The standard states of the anhydrous crystal and liquid components are taken to be anhydrous crystal and liquid at P and T (e.g., the activities of albite in pure crystalline and liquid albite are unity at all T and P).

For our model, $a^m_{\text{silicate}} = (a^m_O)^r = (X^m_O)^r$ where, as described earlier, r is equal to the number of oxygen atoms per gram-formula-unit of anhydrous silicate. Therefore, equation (12) becomes:

$$X_O = \exp\left[\frac{1}{rRT}\int_{T^P_m}^{T} \Delta\bar{S}_f(T,P)dT\right] \quad (13).$$

This factor of r can be avoided if the anhydrous silicate component is always given by a formula unit with only one oxygen. Equation (5.3) can be rearranged to give:

$$X_B = 1 - X_O + \frac{1}{4}\{K_1X_O - [(K_1X_O)^2 + 4K_1X_O - 4K_1X_O^2]^{1/2}\} \quad (14).$$

By substituting equation (13) into equation (14), we obtain an equation for the liquidus in a binary silicate-H_2O system; i.e., the amount of water dissolved in a silicate melt in equilibrium with anhydrous silicate crystals as a function of temperature. This calculation requires expressions for $\Delta\bar{S}_f(T,P)$, $T^P_m(P)$ and for K_1. The entropies of fusion and the expressions for the dry solidus are available from thermochemical measurements and phase equilibria. The expressions that we used and the sources of the data are given in table 1. K_1 can be determined spectroscopically or can be calculated from phase equilibria data as explained below.

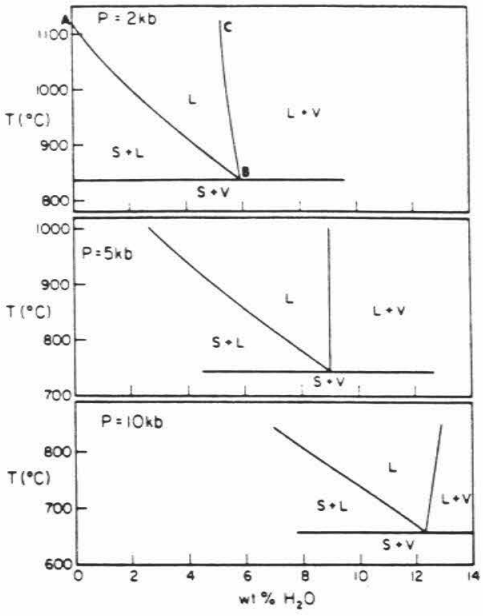

FIG. 1.—Calculated isobaric T-X sections for the water-poor region of the albite-H_2O system at P = 2, 5, and 10 kb. Point A is the anhydrous melting temperature of albite at P = 2 kb. Curve A-B is the liquidus calculated for P = 2 kb and K_1 = 0.17. Curve B-C is the vapor-saturation boundary calculated using equations (24) and (10). See text for details.

THERMODYNAMIC MODEL FOR MELTS

MELT-VAPOR EQUILIBRIUM

Each liquidus curve shown in figure 1 ultimately intersects the wet solidus, i.e., a temperature is reached at which anhydrous crystal, hydrous liquid and vapor coexist. We will next show how to calculate the *variations* in temperature and water content of the hydrous melt at the wet solidus with pressure given the activity-composition relationships of our model.

Notice that we write that we can calculate the *variations* in temperature and water content of the melt at the wet solidus as functions of pressure. Our formulation of the thermodynamics of hydrous silicate melts involves two equilibrium constants, K_1 and K_2. Values of these must somehow be determined at a reference point before we can carry out the phase equilibrium calculations that are of interest. The most direct way would be to measure the concentrations of the hydroxyl groups and molecular water in a glass quenched rapidly from a melt saturated with vapor at some P and T. K_1 and K_2 values could be determined from these measurements and then used to carry out the desired calculations. An alternate approach, and the one we have chosen here, is to take a single point on the wet solidus and the solubility of water in the melt at this point as given; this fixes K_1 and K_2 at the reference temperature (T_r) and pressure (P_r) and allows calculations of the remainder of the phase diagram. As explained earlier, our reason for choosing this second approach is that K_1 and K_2 determined in this way are independent of any spectroscopic measurements. To the extent that the values determined in this way agree with the spectroscopic measurements, they demonstrate the internal consistency of our model of the thermodynamics of hydrous melts.

The value of K_1 is calculated in the following way. A point on the wet solidus is taken as known, with values for temperature, pressure and total water solubility given by T_r, P_r and X_B^r. Solving equation (13) at $T = T_r$ and $P = P_r$ provides a value for X_O^r at the reference point. This value and X_B can then be substituted into the following expression to obtain K_1 at the reference point (and at all other T and P, given our assumption of constant K_1):

$$K_1 = 4(1 - X_B - X_O)^2/X_O(X_O - 1 + 2X_B) \quad (15).$$

Assuming that the vapor is pure water (i.e., $a^v_{H_2O} = 1$), we can substitute equation (5.2) into equation (8) to obtain the following equation for K_2, at the reference point in terms of X_B^r and K_1:

$$K_2(T_r,P_r) = X^r_{H_2O.mol} = X^r_B - \left\{\frac{1}{2} - \left[\frac{1}{4} - \left(\frac{K_1 - 4}{K_1}\right)(X^r_B - (X^r_B)^2)^{1/2}\right]\right\}\Big/\left(\frac{K_1 - 4}{K_1}\right) \quad (16).$$

The reference point in each system was chosen to be midway along the solidus at a point where the solidus and solubility are well constrained. Choosing other points along the solidus and solubility curves as the reference does result in different values for K_1 and K_2. Uncertainties in K_1 and K_2 that result from different choices of reference points do not lead to significant uncertainties in our calculations of phase equilibria.

The variation in K_2, and thus water solubility, with pressure and temperature can now be calculated. For all melts saturated with vapor,

$$\mu^v_{H_2O} = \mu^m_{H_2O.mol} \quad (17)$$

where μ = chemical potential, m = melt phase and v = vapor phase. Expressing the chemical potentials in terms of activities,

$$\mu^{o,v}_{H_2O}(P,T) + RT \ln a^v_{H_2O} = \mu^{o,m}_{H_2O.mol}(P,T) + RT \ln a^m_{H_2O.mol} \quad (18).$$

The standard state for the vapor phase is pure water vapor at P and T. For molecular water in the melt, the standard state refers to a fictive material at T and P with the composition of pure molecular water but with an arrangement of these water molecules similar to that of oxygens in the anhydrous silicate melt (Stolper 1982*a*). Recalling that K_2 is equal to $(a^m_{H_2O.mol}/a^v_{H_2O})$, we obtain that at $T = T_r$ and $P = P_r$:

TABLE 1

$\Delta\bar{S}_f(T,P)$ and $\int_{T_m^P}^{T} \Delta\bar{S}_f(T,P)dT$

Diopside ($Ca_{1.11}Mg_{1.11}Si_{2.67}O_6$):

$$\Delta\bar{S}_f(T,P)^a = \Delta\bar{S}_f^o(T_m^o,1) - 28.163 \ln (T_m^o) + 3.018(10^{-4})(T_m^o) + 2.0645(10^6)/(T_m^o)^2 - 4.635(10^{-6})(P-1) + 28.163 \ln (T) - 3.018(10^{-4})T - 2.0645(10^6)/T^2$$

$\Delta\bar{S}_f^o(T_m^o,1) = 19.82$ cal/K mole where $T_m^o = 1664$ K at 1 bar.

$$\int_{T_m^P}^{T} \Delta\bar{S}_f(T,P)dT = [\Delta\bar{S}_f^o(T_m^o,1) - 28.163 \ln (T_m^o) + 3.018(10^{-4})(T_m^o) + 2.0645(10^6)/(T_m^o)^2 - 4.635(10^{-6})(P-1)](T - T_m^P) + 28.163\{[T \ln (T) - T] - [T_m^P \ln (T_m^P) - T_m^P]\} - 1.509(10^{-4})[T^2 - (T_m^P)^2] + 2.0645(10^6)\left(\frac{1}{T} - \frac{1}{T_m^P}\right)$$

The dry solidus[b]: $T_m^P(K) = 1664 + .0126\,P - 4.93(10^{-8})\,P^2$

Albite ($NaAlSi_3O_8$):

$$\Delta\bar{S}_f(T,P)^c = \Delta\bar{S}_f^o(T_m^o,1) + 72.27 \ln (T_m^o) - 3.506(10^{-2})(T_m^o) - 3.793(10^5)(T_m^o)^{-2} + 3.812(10^3)(T_m^o)^{-1/2} + 4.3725(10^{-6})(T_m^o)^2 - 6.93(10^{-6})(P-1) - 72.27 \ln (T) + 3.506(10^{-2})(T) + 3.793(10^5)(T^{-2}) - 3.812(10^3)T^{-1/2} - 4.3725(10^{-6})T^2$$

$\Delta\bar{S}_f^o(T_m^o,1) = 10.90$ cal/K mole where $T_m^o = 1373$ K at 1 bar.

$$\int_{T_m^P}^{T} \Delta\bar{S}_f(T,P)dT = [\Delta\bar{S}_f^o(T_m^o,1) + 72.27 \ln (T_m^o) - 3.506(10^{-2})(T_m^o) - 3.793(10^5)(T_m^o)^{-2} + 3.812(10^3)(T_m^o)^{-1/2} + 4.3725(10^{-6})(T_m^o)^2 - 6.93(10^{-6})(P-1)](T - T_m^P) - 72.27\{[T \ln (T) - T] - [T_m^P \ln (T_m^P) - T_m^P]\} + 1.753(10^{-2})[T^2 - (T_m^P)^2] - 3.793(10^5)\left(\frac{1}{T} - \frac{1}{T_m^P}\right) - 7.624(10^3)[T - (T_m^P)^{1/2}] - 1.4575(10^{-6})[T^3 - (T_m^P)^3]$$

The dry solidus[d]: $T_m^P(K) = 1373 + .0095\,P$

Silica (β-SiO_2):

$$\Delta\bar{S}_f(T,P)^e = \Delta S_f^o(T_m^o,1) - 1.2089(10^{-6})(P-1) - 3.847 \ln (T_m^o) + 1.321(10^{-3})(T_m^o) + 2.2064(10^5)/(T_m^o)^2 + 3.847 \ln (T) - 1.321(10^{-3})T - 2.2064(10^5)/T^2$$

$\Delta\bar{S}_f^o(T_m^o,1) = 1.32$ cal/K mole where $T_m^o = 1700$ K at 1 bar.

$$\int_{T_m^P}^{T} \Delta\bar{S}_f(T,P)dT = [\Delta\bar{S}_f^o(T_m^o,1) - 1.2089(10^{-6})(P-1) - 3.847 \ln (T_m^o) + 1.321(10^{-3})(T_m^o) + 2.2064(10^5)/(T_m^o)^2](T - T_m^P) + 3.847\{[T \ln (T) - T] - [T_m^P \ln (T_m^P) - T_m^P]\} - 6.607(10^{-4})[T^2 - (T_m^P)^2] + 2.2064(10^5)\left(\frac{1}{T} - \frac{1}{T_m^P}\right)$$

The dry solidus[f]: $T_m^P(K) = 1700 + .0469\,P - 5.89 \times 10^{-7}\,P^2$

NOTES.—Units in above equations: T in Kelvin, P in bars. $\Delta\bar{V}$ enters into the calculation for $\Delta\bar{S}_f$ as follows: $\Delta\bar{S}_f(T,P) = \Delta\bar{S}_f(T_m^o,1) + \int_{T_m^o}^{T} \frac{\Delta c_P}{T}\,dT - \int_1^P \alpha\Delta\bar{V}\,dP$.

[a] ΔH_f, $\Delta\bar{C}_p$: Stebbins et al. (1983), α: Skinner (1966), $\Delta\bar{V}$: Ghiorso and Carmichael (1980).
[b] Best-fit curve to Boettcher et al. (1982).
[c] ΔH_f, $\Delta\bar{C}_p$: Stebbins et al. (1983), α: Skinner (1966), $\Delta\bar{V}$: Ghiorso and Carmichael (1980).
[d] Best-fit curve to Boettcher et al. (1982).
[e] ΔH_f, $\Delta\bar{C}_p$: Richet et al. (1982), α: Bottinga and Weill (1970). ΔV: Ghiorso and Carmichael (1970), Richet et al. (1982).
[f] Best-fit curve to Jackson (1976).

$$\ln K_2(P_r,T_r) = [\mu^{o,v}_{H_2O}(P_r,T_r) - \mu^{o,m}_{H_2O,mol}(P_r,T_r)]/RT_r = \Delta\mu^o(P_r,T_r)/RT_r \quad (19).$$

We assume that solubility is independent of temperature at the reference pressure, i.e., $(\partial\Delta\mu^o/\partial T)_{P_r} = 0$. This is valid as a first approximation because the temperature dependence of solubility is small (Burnham and Jahns 1962; Karsten et al. 1981). This assumption does, however, lead to a small variation in solubility with temperature at $P \neq P_r$, as explained below. Since $(\partial\mu/\partial P)_T = \bar{V}$, we obtain:

$$\Delta\mu^o(P,T) = \Delta\mu^o(P_r,T_r) + \int_{P_r}^{P} \bar{V}^v_{H_2O}(P,T)dP - \int_{P_r}^{P} \bar{V}^m_{H_2O,mol}(P,T)dP \quad (20)$$

where $\bar{V}^v_{H_2O}(P,T)$ and $\bar{V}^m_{H_2O,mol}(P,T)$ are the partial molar volumes of water in the vapor and of molecular water in the melt.
For water in the vapor,

$$\int_{P_r}^{P} \bar{V}^v_{H_2O}(P,T)dP = RT \ln [f^o_{H_2O}(P,T)/f^o_{H_2O}(P_r,T)] \quad (21).$$

We have calculated $f^o_{H_2O}(P,T)$, the fugacity of pure H_2O at T and P, from the modified Redlich-Kwong equation of state for H_2O (Holloway 1977; Flowers 1979).

To use equation (20), we must estimate the partial molar volume of molecular water in the melt. Instead of using a constant value for $\bar{V}^m_{H_2O,mol}$ in evaluating equation (20), we have allowed it to decrease with increasing pressure as a result of compression. We have assumed that $\bar{V}^m_{H_2O,mol}$ is independent of temperature. This approximation is based on the fact that for reasonable values of α, the coefficient of thermal expansion, $\bar{V}^m_{H_2O,mol}$ would vary only by a percent or two over the temperature range of interest. We have modeled the pressure dependence using the Murnaghan equation:

$$\bar{V}^m_{H_2O,mol}(P) = \bar{V}^m_{H_2O,mol}(1)\left[1 + \frac{B'}{B_o}(P - P_o)\right]^{-1/B'} \quad (22.1).$$

In this equation, B_o is the isothermal bulk modulus at 1 bar, B' is the pressure derivative of B, $\bar{V}^m_{H_2O,mol}(1)$ is the partial molar volume of dissolved molecular water at 1 bar. We have chosen B_o = 200 kbar and B' = 4, typical values for oxygens in silicate melts (Stolper et al. 1981). $\bar{V}^m_{H_2O,mol}(P)$ is then given by,

$$\bar{V}^m_{H_2O,mol}(P) = \bar{V}^m_{H_2O,mol}(1)[1 + 2(10^{-5})P]^{-1/4} \quad (22.2).$$

Then,

$$\int_{P_r}^{P} \bar{V}^m_{H_2O,mol}(P)dP = \frac{2}{3}(10^5)\bar{V}^m_{H_2O,mol}(1) \{[1 + 2(10^{-5})P]^{1/4} - [1 + 2(10^{-5})P_r]^{1/4}\} \quad (23).$$

Substituting eqs. (20), (21) and (23) into eq. (19) leads to the following expression for the variation of K_2 with pressure and temperature:

$$\ln K_2(P,T) = \ln (a^m_{H_2O,mol}/a^v_{H_2O}) = \ln K_2(T_r,P_r) + \ln [f^v_{H_2O}(P,T)/f^o_{H_2O}(P_r,T)] - \frac{2}{3}(10^5)\bar{V}^m_{H_2O,mol}(1)\{[1 + 2(10^{-5})P]^{1/4} - [1 + 2(10^{-5})P_r]^{1/4}\}/RT \quad (24).$$

What values should we use for $\bar{V}^m_{H_2O,mol}(1)$ in equation (24)? Our assumption of ideal mixing implies that the volumes of the molecular species should be similar to each other. According to Guggenheim (1952) they should differ by less than about 30% if ideal mixing is to hold. The molar volume of oxygen atoms in albite melt at 1100°C is about 14 cm^3 (Arndt and Häberle 1973). If anything, we would expect $\bar{V}^m_{H_2O,mol}$ to be somewhat greater than $\bar{V}^m_O$. Thus we can expect that if the assumptions of our model are to hold, $\bar{V}^m_{H_2O,mol}$(1 bar, 1100°C) should be between 14 and 18.5 cm^3/mole. At high water contents where most of the water would be present in the melt as molecular water for the K_1 values that we have determined both spectroscopically (Stolper 1982) and using equation (15), the partial molar volume of water determined experimentally would be similar to $\bar{V}^m_{H_2O,mol}$. Based on the data of Burnham and Davis (1971), in which the densities of albitic melt

with 8.25 and 10.9 wt % dissolved water are reported over a range of pressures and temperatures, $\bar{V}^m_{H_2O} \cong \bar{V}^m_{H_2O,mol}$ is in the range of 15–17 cc/mole, similar to that estimated above. Hodges (1974) calculated a similar value of 16.5 cc/mole for $\bar{V}^m_{H_2O}$ in diopside melt at 20 kb. While all values of $\bar{V}^m_{H_2O,mol}(1)$ in the range of 15–18 cc/mole result in solution models consistent with available phase equilibrium data, we have chosen values in the range of 16.4–17.8 cc/mole since these result in the best matches between our model phase equilibria and experimental data.

Our approach has been to assume a value for $\bar{V}^m_{H_2O,mol}(1)$ and a variation of this partial molar volume with pressure according to the Murnaghan equation and then to use these values to calculate the wet solidus. This calculated solidus is then compared to the actual solidus based on experiment. Alternatively, we could have solved for the $\bar{V}^m_{H_2O,mol}$ as a function of pressure that precisely matched the best fit solidus. The volumes determined in this alternate way are essentially similar to those that we have derived from the Murnaghan equation.

Given a choice of a reference point on the wet solidus, which allows us to fix K_1 and K_2 at this reference point (equations 15 and 16), equation (24) can be used to calculate K_2 at any other pressure and temperature. The solubility of water in a silicate melt for any value of $a^v_{H_2O}$ at any T and P can then be calculated by substitution of $K_2(P,T)$ from equation (24) and $a^v_{H_2O}$ into equation (10) to give X_B. The temperature of the wet solidus can then be calculated by equating equation (10) and solving for T. In practice, we did not determine an analytic expression for T but instead for each P calculated X_B as a function of T for the undersaturated liquidus and X_B for $a^v_{H_2O} = 1$ as a function of T from equations (24) and (10) and took their intersection as the wet solidus.

RESULTS

As discussed above, the goal of this paper is to see whether the thermodynamic formulation for hydrous silicate melts that we have developed based on our molecular model is consistent with available phase equilibrium data. In the paragraphs that follow, we discuss the application of this model to the systems albite-H_2O, diopside-H_2O, and silica-H_2O.

1. Albite-H_2O.—The reference point is P_r = 5000 bars, T_r = 745°C, with a total water solubility at T_r, P_r of 9 wt % H_2O. $\Delta\bar{S}_f(P,T)$ is based on Stebbins et al. (1983) and is given in table 1. We have chosen $\bar{V}^m_{H_2O,mol}(1)$ to be 16.4 cc/mole. The dry solidus is from Boettcher et al. (1982). The calculated value of K_1 is 0.17. This is similar to K_1 values determined by infrared spectroscopic measurements on hydrous albite and rhyolitic glasses (Stolper, 1982*a*, 1982*b*).

Calculated isobaric sections for albite-H_2O are shown in figure 1 for P = 2000, 5000 and 10,000 bars. In principle, the positions of these liquidus boundaries could be determined experimentally and used to test our calculated liquidus boundaries; however, there are few available data points of this type.

The results of the calculation of the wet solidus for albite-H_2O are shown in figure 2. Shown for comparison are experimental determinations of the wet solidus reported in the literature. The agreement between our calculated solidus and the experimental data is excellent over the entire pressure range.

Figure 3 shows the variation in solubility of H_2O in albite melt as a function of P calculated using our model. Shown for comparison is a collection of experimental solubility determinations from the literature. The calculated solubility curve falls within the range of the experimental data for P up to 8 kbar; at higher P, our model solubility and the experimental determinations diverge.

2. Diopside-H_2O.—The reference point was chosen as P_r = 6000 bars, T_r = 1265°C, with a total water solubility at T_r, P_r of 8.0 wt % H_2O (Eggler and Burnham, 1984). The $\Delta\bar{S}_f(P,T)$ is based on Stebbins et al. (1983) and is given in table 1. $\bar{V}^m_{H_2O,mol}(1)$ was taken to be 17.8 cc/mole. The dry solidus is from Boettcher et al. (1982). The calculated K_1 value is 0.085. This lower value for diopside than for albite may indicate that more water dissolves as molecular water in diopside than in albite melt for a given total water content. As mentioned earlier, choosing other points along the solidus and solubility curves as references does result in different values for K_1 (e.g., for diopside, a 30 kbar point yields K_1 = 0.07, a 20 kbar point yields K_1 = 0.04 and a 2 kbar point gives K_1 = 0.02), but these differences do not critically affect the results of the calculation.

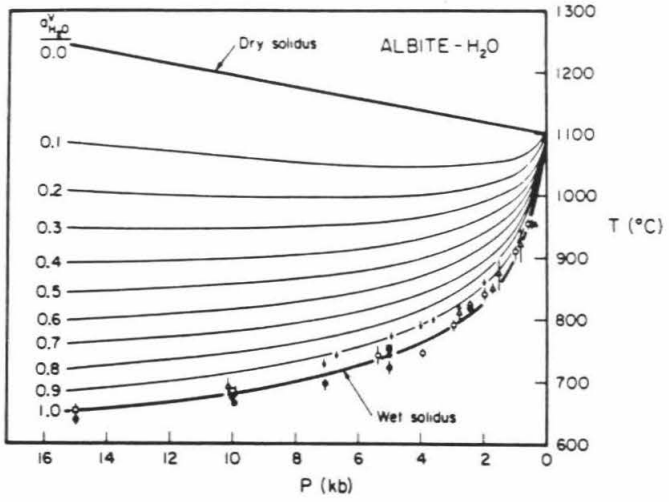

FIG. 2.—The wet solidus for albite up to 15 kb. Symbols with brackets represent experimental data with estimated uncertainties from: white triangles—Goranson (1938); white circles—Tuttle and Bowen (1959); black triangles—Luth et al. (1964) corrected by Luth (1976); white squares—Boettcher and Wyllie (1969); black squares—Morse (1970); and black circles—Bohlen et al. (1982). Arrows represent upper temperature limits from Burnham and Jahns (1962). The heavy solid line represents our calculated wet solidus for $\bar{V}^m_{H_2O,mol}(1)$ = 16.4 cc/mole, K_1 = 0.174. The lighter lines represent contours for $a^v_{H_2O}$ from 0.1 to 0.9. The dry solidus is a best-fit curve based on data from Boettcher et al. (1982). The reference point is an average value based on data from Burnham and Jahns (1962), Morse (1970) and Bohlen et al. (1982) and is shown by an asterisk. See text for details.

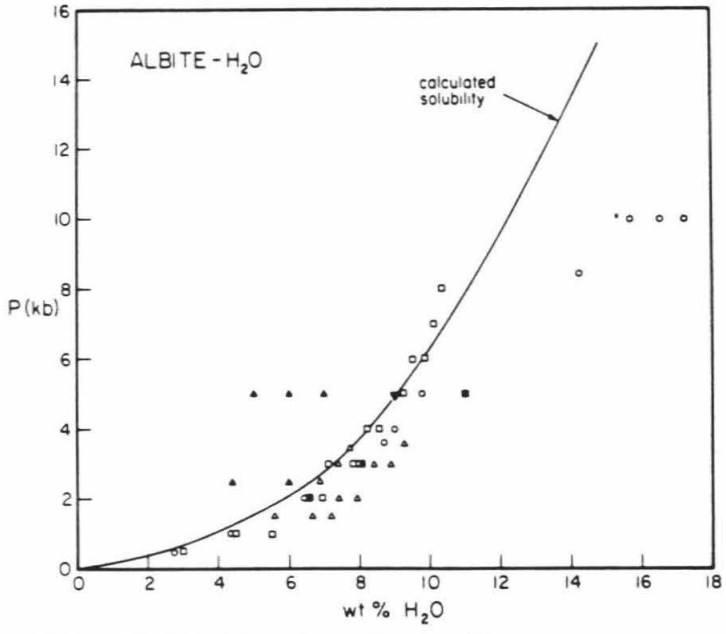

FIG. 3.—The solubility of H_2O in albite melt as a function of P at temperatures near the wet solidus. Symbols represent experimental data from: white triangles—Goranson (1938); white circles—Burnham and Jahns (1962); black squares—Khitarov et al. (1963); white squares—Oxtoby and Hamilton (1978); white triangles—Voigt et al. (1981) and black triangles—Day and Fenn (1982). Most of the data were derived from compilations by Bottinga et al. (1981) and Day and Fenn (1982). The solid curve represents solubility calculated with our model. The reference point was taken from Voigt et al. (1981) and is shown by an asterisk.

The results of our model calculations for the wet solidus for diopside are shown in figure 4 along with available experimental data. Again, the agreement between our calculated solidus and the experimental data up to 30 kbar is excellent.

Figure 5 compares the calculated solubility of H_2O in diopside melt as a function of P with values from the literature. Our model is consistent with the experimental data up to 20 kbar. Owing to a large discrepancy in the solubility determinations at 30 kbar, it is difficult to judge our model curve against actual data. However, our calculated values compare well with Hodges' (1974) determination of 21.5 wt % H_2O at 30 kbar.

3. Silica-H_2O.—The reference point was chosen as P_r = 6000 bars, T_r = 1070°C and water solubility at P_r, T_r of 6.0 wt % H_2O (Kennedy et al., 1962). The $\Delta\bar{S}_f(P,T)$ is based on Richet et al. (1982) and is given in table 1. $\bar{V}^m_{H_2O,mol}(1)$ was taken as 17 cc/mole. The dry solidus was taken from Jackson (1976). The model calculation yields a K_1 value of 0.11.

The results of our model calculation of the stable and metastable regions of the wet solidus for β-quartz are compared with experimental determinations in figure 6. There is good agreement between the model calculation and the experimental data.

Calculated and measured water solubility as function of P are presented in figure 7. The agreement between the model and experimental data is good up to ~7 kbar. For P >7 kbar, the calculated solubility diverges from measured values. This reflects the fact that there is a critical end point at 9–10 kbar (Kennedy et al. 1962; Boettcher 1984). Our model, with its ideal mixing law, cannot account for critical phenomena and thus would not be expected to work well as the critical end point is approached.

DISCUSSION

The success of the activity-composition relationships for hydrous silicate melts that we have adopted is manifest in figures 2–7. The shape of the wet solidus and the solubility of water are well accounted for by our model in the systems albite-water, diopside-water, and silica-water over most of the pressure range for which experimental constraints are available. We may thus conclude that the ideal mixing law and the molecular level interactions that we assumed in formulating our

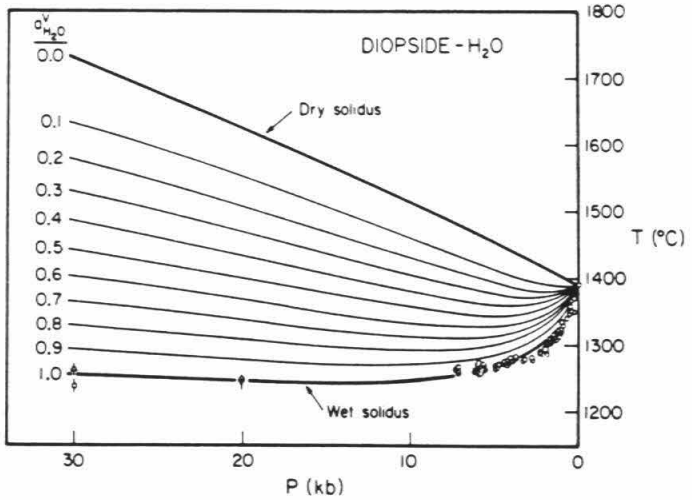

FIG. 4.—The wet solidus for diopside up to 30 kb. Symbols and brackets represent experimental data and estimated uncertainties from: up-pointed triangles—Eggler (1973); down-pointed triangles—Hodges (1974); white circles—Eggler and Rosenhauer (1978); and white squares—Eggler and Burnham (1984). The heavy solid curve represents our model calculation, with $\bar{V}^m_{H_2O,mol}(1)$ = 17.8 cc/mole, K_1 = .085. The lighter lines are contours of $a^{v}_{H_2O}$ from 0.1 to 0.9. The dry solidus is a best-fit curve based on data from Boettcher et al. (1982). The reference point was taken from Eggler and Burnham (1984) and is shown by an asterisk. See text for details.

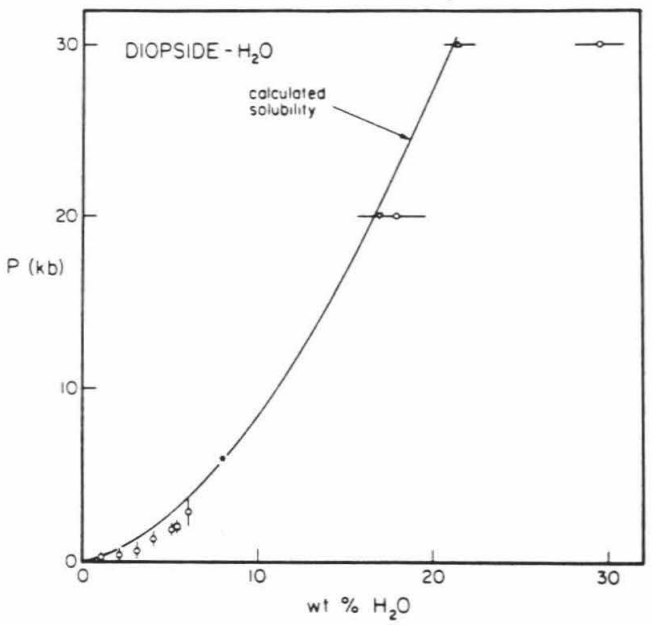

FIG. 5.—The solubility of H_2O in diopside melt as a function of P along the solidus. Symbols with brackets represent experimental data from same sources as in figure 4. Solid curve represents H_2O solubility calculated with our model. The reference point was taken from Eggler and Burnham (1984) and is shown by an asterisk.

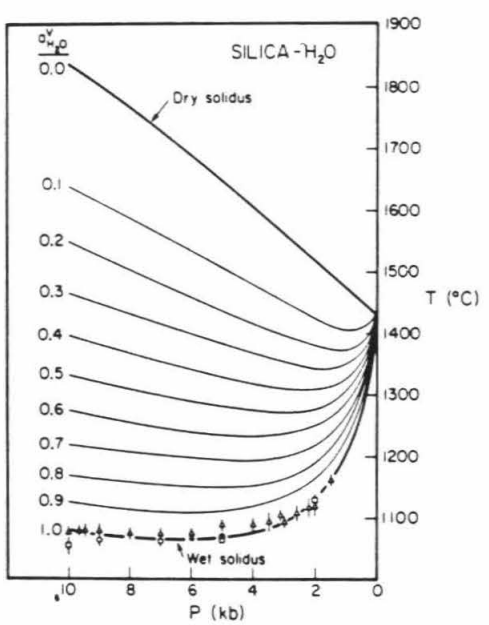

FIG. 6.—The wet solidus for β-qtz. Symbols with brackets represent experimental data with estimated uncertainties from: black circles—Ostrovskii et al. (1959); white triangles—Kennedy et al. (1962); white squares—Stewart (1967); and white circles—Boettcher (1984). The critical end point is at ≈10 kb. The heavy solid curve is our calculated wet solidus, with $\bar{V}^m_{H_2O,mol}(1)$ = 17 cc/mole, K_1 = 0.11. The lighter curves are contours of $a^v_{H_2O}$ = 0.1 to 0.9. The dry solidus is a best-fit curve from Jackson (1976) for P >6 kb and the 1 bar metastable melting temperature from Richet et al. (1982). The reference point was based on data from Kennedy et al. (1962) and is shown by an asterisk.

activity-composition relations are at least permissible descriptions of the solubility mechanisms of water in melts and the species level interactions of hydrous silicate melts. In other words, the concept that molecular water and hydroxyl groups are dissolved in silicate melts and that their relative proportions are controlled through homogeneous equilibria such as that described by equation (1) are consistent with phase equilibrium data.

If all that were available to constrain our thinking on solubility mechanisms and speciation in hydrous silicate melts were experimental data of the sort we have fit in figures 2–7, we could go no further than the permissive statement made above. Undoubtedly, other formulations of molecular level interactions involving different species and solubility mechanisms could also yield activity-

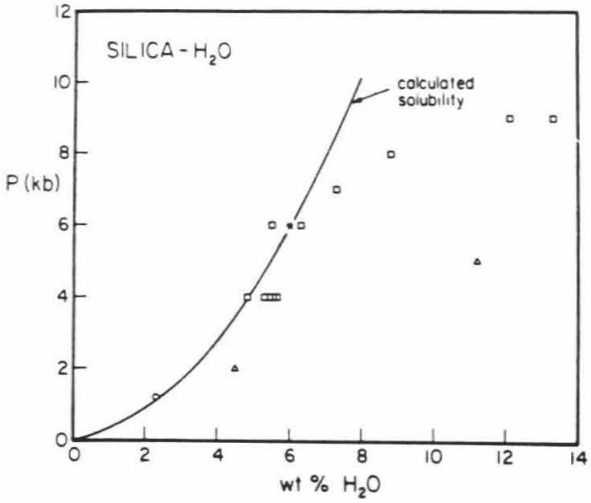

FIG. 7.—The solubility of H_2O in β-quartz melt as a function of P and T at and above the solidus. Symbols represent experimental data from: circles—Tuttle and England (1955); squares—Kennedy et al. (1962); and triangles—Stewart (1967). The solid curve is our model H_2O solubility. The reference point is from Stewart (1967) and is shown by an asterisk.

composition relations capable of accounting for the phase equilibrium data. We feel, however, that a much stronger statement about the significance of our results can be made, because our modelling predicts concentrations of molecular water and hydroxyl groups in silicate melts that are similar to the concentrations measured in hydrous silicate glasses using infrared spectroscopy (Stolper 1982*a*). Spectroscopically determined values of K_1 for albitic and rhyolitic glasses of 0.1–0.3 (Stolper 1982*a*) compare favorably to the values of 0.1–0.2 determined independently in this paper. Finally, the values of K_1 consistent with our modelling and the spectroscopic measurements are precisely those that best account for the proportionality between f_{H_2O} and the square of the mole fraction of the dissolved water at low water contents (Stolper 1982*a*). Thus, not only does our thermodynamic formulation provide a basis for modelling the macroscopic properties of hydrous silicate melts (e.g., phase equilibria), it also embodies a description of the molecular level structures and interactions of H-bearing species in silicate melts that is, to first order, acceptable.

Further development of this type of model of hydrous silicate melts will, we believe, depend on systematic measurements of the concentrations of molecular water and hydroxyl groups in glasses quenched from melts. The pressure and temperature dependences of K_1 that have been neglected in our treatment could then be determined and incorporated into more refined treatments. Stolper et al. (1983) have detected a variation in K_1 with temperature in hydrous rhyolitic glasses. Nogami and Tomozawa (1984) interpret some of their results on hydrous silica glass in terms of a pressure dependence of K_1 (i.e., ΔV° for reaction (1) was suggested to be negative).

A second refinement would consider that most melts contain several different kinds of "free" oxygens that are undoubtedly energetically distinguishable. Thus, for example, in nearly fully polymerized aluminosilicate melts (e.g., albite) there are bridging oxygens between two Si tetrahedra, two Al tetrahedra, and between one Al and one Si tetrahedron. Recent Raman spectroscopic studies of hydrous glasses in such systems (Mysen et al. 1980; Mysen and Virgo 1980; McMillan et al. 1983) suggest that these oxygens are not equally reactive with water molecules. Our model could easily be extended to include several different types of oxygens each obeying an equilibrium such as that given in equation (1), but with different K_1 values. We have not done this because it would introduce two additional constants and

we do not believe that available experimental data are adequate to constrain them. Likewise for diopsidic melts where bridging, nonbridging and free oxygens (in the sense of Toop and Samis 1962) should probably be distinguished in our treatment, but again data necessary to constrain their individual K_1 values are not available.

Our treatment implies a slight dependence of solubility on temperature at most pressures. This effect is illustrated in figures 1 and 8. At $P = P_r$, the vapor-saturation boundary is assumed to be vertical, i.e., water solubility is assumed to be independent of temperature at the reference pressure. At P = 2000 and 10,000 bars in figure 1, there are slight slopes to the vapor-saturation boundary (e.g., curve B-C at 2000 bars). This small dependence of solubility on temperature is the result of our assumptions that $\bar{V}^m_{H_2O,mol}$ and K_1 are independent of temperature and that $(\partial \Delta\mu^\circ_{H_2O}/\partial T)_{P_r} = 0$. There, however, several sets of experimental data on the temperature dependence of solubility available for comparison with the temperature dependence of solubility implied by our model. Karsten et al. (1982) determined the temperature dependence of water solubility in rhyolitic melt at 700 bars between 650°C and 950°C. Burnham and Jahns (1962) determined solubility for the Harding pegmatite at 1000 bars. These two data sets are shown in figure 8, along with our calculated solubility for albitic melt at 1000 bars. Although not negligible, the effect of temperature on solubility is small, and more importantly, the magnitude of the temperature dependence that is implicit in our approach is, fortuitously, comparable to available experimental data.

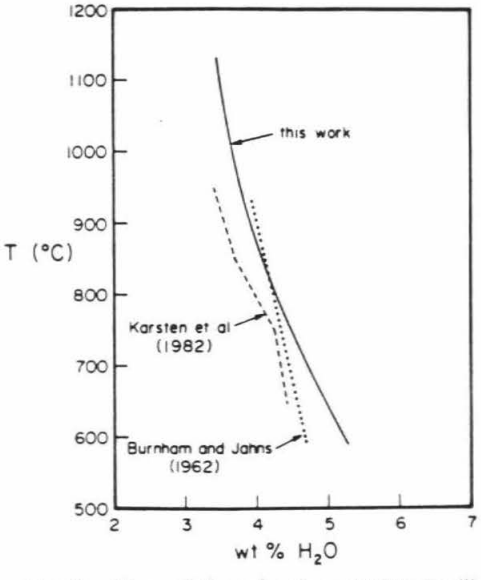

FIG. 8.—The variation of water solubility in silicate melts with temperature. The solid curve represents our calculated solubility for albite at P = 1000 bars; below T = 906°C, this curve is metastable. The dotted curve represents data from Burnham and Jahns (1962) for H_2O solubility in the Harding pegmatite at P = 1000 bars. The dashed curve represents data from Karsten et al. (1982) for the measured H_2O solubility in rhyolite at P = 700 bars.

Our approach to the thermodynamics of silicate melts provides an indirect way to determine the partial molar volume of molecular water in silicate melts. Figure 9 shows the calculated solubility of molecular water as $\ln(K_2)$ at 1000°C in diopside, albite and silica as functions of pressure. Because K_2 is a function of the partial molar volume of water, it is possible to extract the values that we used for the volume of molecular water in the melt from figure 9. Rearrangement and differentiation of equation (24) yields the following:

$$\left\{\frac{\partial[\ln (K_2/f^\circ_{H_2O}(P,T))]}{\partial P}\right\}_T = \frac{-\bar{V}^m_{H_2O,mol}(P,T)}{RT} \qquad (25).$$

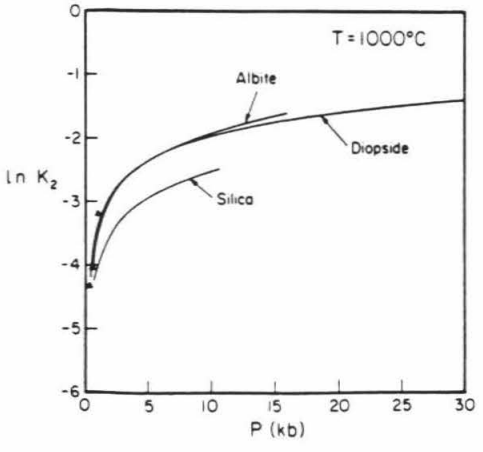

FIG. 9.—H_2O solubility plotted as $\ln(K_2) = \ln(X^m_{H_2O,mol})$ as a function of P for hydrous diopside, albite and silica melts. All three curves are at T = 1000°C. Black triangles represent measured $X^m_{H_2O,mol}$ for three rhyolites from Karsten et al. (1982) and Stolper (1982*b*). The rhyolites were equilibrated with vapor at T = 950°C.

Thus, when $\ln[K_2(P,T)/f^{\circ}_{H_2O}(P,T)]$ is plotted versus P, as we have done in figure 10, the slope of the curve for each composition can be used to compute the partial molar volume of molecular water in the melt. The slopes of the albite, diopside and silica curves in figure 10 simply reflect the values of $\bar{V}^{m}_{H_2O,mol}$ chosen for our modelling as described previously. However, by using infrared spectroscopy to determine $X^{m}_{H_2O,mol}$ (= K_2) in glasses quenched from vapor-saturated melts from different pressures, one could independently determine both K_2 and through its pressure dependence, $\bar{V}^{m}_{H_2O,mol}$.

Stolper (1982*a*, 1982*b*) suggested that K_2 would probably not be strongly dependent on melt composition. Figures 9 and 10 show that this is indeed the case. The values for albite, diopside and rhyolite (from obsidian samples from Karsten et al. 1982, with K_2 values measured spectroscopically by Stolper 1982*b*), are essentially identical while that for silica is only slightly different. We thus propose that the K_2 values shown in figures 9 and 10 can be used, along with K_1 values of 0.1–0.2, and the equations given in this paper, to calculate phase equilibria and water solubility as functions of pressure and temperature for a wide range of melt compositions with a reliability at least comparable to that achieved with empirical treatments (e.g., Burnham 1975, 1979; Eggler and Burnham 1984).

What are the relative merits of our approach to the thermodynamics of hydrous silicate melts versus the largely macroscopic and empirical approaches of Burnham and Davis (1974), Burnham (1979), and Eggler and Burnham (1984) or the regular solution approximations employed by Spera (1974) or Nicholls (1980)? Our feeling is that unless one is interested in modelling systems in the vicinity of critical phenomena, in which case only the approach of Spera (1974) of those that have yet been employed would be applicable, empirical fits of essentially arbitrary activity-composition relationships are less useful than the formulation we have adopted. Granted, these formulations are capable, given sufficient variable parameters, of retrieving the data used to constrain them. However, they have no basis for use in extrapolation, nor do they give any direct insights into melt structures or speciation, nor do they appear to do any better in matching

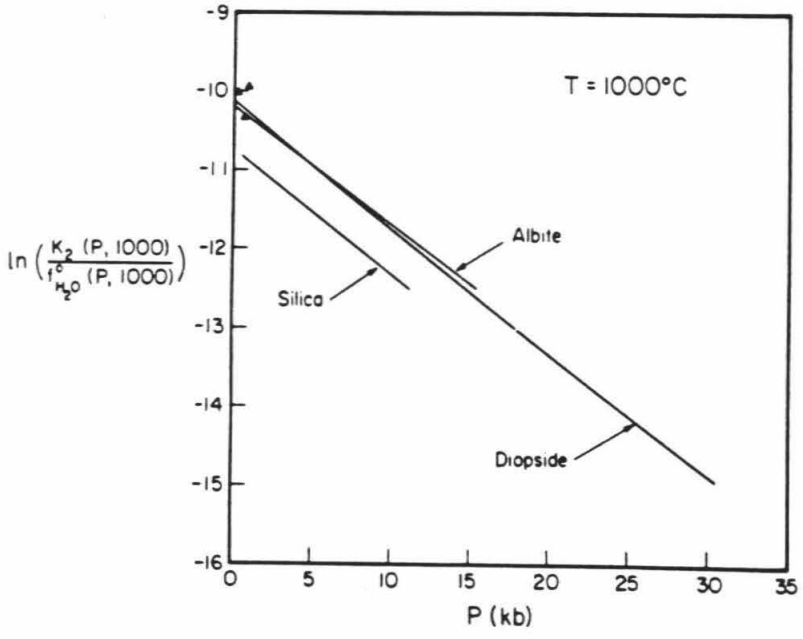

FIG. 10.—H_2O solubility as $\ln [K_2/f^{\circ}_{H_2O}(P,T)]$ as a function of P. All three curves are referenced to T = 1000°C. The slope of each curve at any point is: $-[\bar{V}^{m}_{H_2O,mol}(P,T)]/RT$. The closed triangles represent the measured $X^{m}_{H_2O,mol}$ for three rhyolites (OBS E, OBS G, and OBS I), equilibrated with vapor at 950°C, from Karsten et al. (1982) and Stolper (1982*b*).

phase equilibrium data than do our formulations. In short, the success of our model and its consistency with independent measures of species concentrations makes it more fundamental and more testable, and thus, in the long run, we hope more useful.

CONCLUSIONS

Thermodynamic modelling of hydrous silicate melts can be approached either by macroscopic, empirical treatments or by modelling species interactions at a molecular level. We have chosen the second approach and have demonstrated that despite its simplicity, our model is successful in accounting for the phase equilibria (i.e., solubility, freezing point depression) of the albite-water, diopside-water and silica-water systems. It has the additional important feature that it is independently testable by and consistent with the available body of spectroscopic measurements of species concentrations of hydrous silicate glasses and melts. It is thus possible to use statistical thermodynamics to produce a viable working model for the macroscopic thermodynamic properties of silicate-H_2O systems and in the process get testable insights into molecular level phenomena.

ACKNOWLEDGMENTS.—We have benefited from discussions with A. L. Boettcher, T. S. Bowers, and I. S. E. Carmichael and from reviews by M. S. Ghiorso and A. Navrotsky. Supported by NSF Grant EAR-8212765. Division of Geological and Planetary Sciences Contribution #4124.

REFERENCES CITED

ARNDT, J., and HÄBERLE, F., 1973, Thermal expansion and glass transition temperatures of synthetic glasses of plagioclase-like compositions: Contrib. Mineral. Petrol., v. 39, p. 175–183.

BOETTCHER, A. L., 1984, The system SiO_2-H_2O-CO_2: melting, solubility mechanisms of carbon, and liquid structure to high pressures: Am. Mineral., v. 69, p. 823–833.

———; BURNHAM, C. W.; WINDOM, K. E.; and BOHLEN, S. R., 1982, Liquids, glasses, and the melting of silicates to high pressures: Jour. Geology, v. 90, p. 127–138.

———, and WYLLIE, P. J., 1969, Phase relationships in the system $NaAlSiO_4$-SiO_2-H_2O to 35 kilobars pressure: Am. Jour. Sci., v. 267, p. 875–909.

BOHLEN, S. R.; BOETTCHER, A. L.; and WALL, V. J., 1982, The system albite-H_2O-CO_2: a model for melting and activities of water at high pressures: Am. Mineral., v. 67, p. 451–462.

BOTTINGA, Y., and WEILL, D. F., 1970, Densities of liquid silicate systems calculated from partial molar volumes of oxide components: Am. Jour. Sci., v. 269, p. 169–182.

———; ———; and RICHET, P., 1981, Thermodynamic modelling of silicate melts, *in* NEWTON, R. D.; NAVROTSKY, A.; and WOOD, B. J., eds., Thermodynamics of Minerals and Melts: New York, Springer-Verlag, p. 207–245.

BURNHAM, C. W., 1975, Water and magmas: a mixing model: Geochim. Cosmochim. Acta, v. 39, p. 1077–1084.

——— 1979, The importance of volatile constituents, *in* YODER, H. S., JR., ed., The Evolution of the Igneous Rocks: Princeton, Princeton Univ. Press, p. 439–482.

———, and DAVIS, N. F., 1971, The role of H_2O in silicate melts: I. P-V-T relations in the system $NaAlSi_3O_8$-H_2O to 10 kilobars and 1000°C: Am. Jour. Sci., v. 270, p. 54–79.

———, and ———, 1974, The role of H_2O in silicate melts: II. thermodynamic and phase relations in the system $NaAlSi_3O_8$-H_2O to 10 kilobars, 700° to 1100°C: Am. Jour. Sci., v. 274, p. 902–940.

———, and JAHNS, R. H., 1962, A method for determining the solubility of water in silicate melts: Am. Jour. Sci., v. 260, p. 721–745.

DAY, H. W., and FENN, P. M., 1982, Estimating the P-T-X_{H_2O} conditions during crystallization of low-calcium granites: Jour. Geology, v. 90, p. 485–507.

EGGLER, D. H., 1973, Role of CO_2 in melting processes in the mantle: Carnegie Inst. Washington Yearbook, v. 72, p. 457–467.

———, and BURNHAM, C. W., 1984, Solution of H_2O in diopside melts: a thermodynamic model: Contrib. Mineral. Petrol., v. 85, p. 58–66.

———, and ROSENHAUER, M., 1978, Carbon dioxide in silicate melts: II. solubilities of CO_2 and H_2O in $CaMgSi_2O_6$ (diopside) liquids and vapors at pressures to 40 kb: Am. Jour. Sci., v. 287, p. 64–91.

FLOWERS, G. C., 1979, Correction of Holloway's (1977) adaptation of the modified Redlich-Kwong equation of state for calculation of the fugacities of molecular species in supercritical fluids of geologic interest: Contrib. Mineral. Petrol., v. 69, p. 315–318.

GHIORSO, M. S., and CARMICHAEL, I. S. E., 1980, A regular solution model for met-aluminous silicate liquids: applications to geothermometry, immiscibility, and the source regions of basic magmas: Contrib. Mineral. Petrol., v. 71, p. 323–342.

GORANSON, R. W., 1938, Silicate water systems: phase equilibria in the $NaAlSi_3O_8$-H_2O and $KAlSi_3O_8$-H_2O systems at high temperatures and pressures: Am. Jour. Sci., v. 35A, p. 71–91.

GUGGENHEIM, E. A., 1952, Mixtures: Oxford, Oxford University Press, 270 p.

HODGES, F. W., 1974, The solubility of H_2O in silicate melts: Carnegie Inst. Washington Yearbook, v. 73, p. 251–255.

HOLLOWAY, J. R., 1977, Fugacity and activity of molecular species in supercritical fluids, *in* FRASER, D., ed., Thermodynamics in Geology: Boston, D. Reidel, p. 161–181.

JACKSON, I., 1976, Melting of the silica isotypes SiO_2, BeF_2, and GeO_2 at elevated temperatures: Physics Earth Planet. Interiors, v. 13, p. 218–231.

KARSTEN, J. L.; HOLLOWAY, J. R.; and DELANEY, J. R., 1982, Ion microprobe studies of water in silicate melts: temperature-dependent water diffusion in obsidian: Earth Planet. Sci. Letters, v. 59, p. 420–428.

KENNEDY, G. C.; WASSERBURG, G. J.; HEARD, H. L.; and NEWTON, R. C., 1962, The upper three-phase region in the system SiO_2-H_2O: Am. Jour. Sci., v. 260, p. 501–521.

KHITAROV, N. I.; KADIK, A. S.; and LEBEDEV, E. B., 1963, Estimate of the thermal effect of the separation of water from felsic melts based on data for the system albite-water: Geochemistry, v. 7, p. 637–649.

LUTH, W. C., 1976, Experimental petrology: igneous rocks, *in* BAILEY, D. K., and MACDONALD, R., eds., The Evolution of the Crystalline Rocks: New York, Academic Press, p. 333–417.

———; JAHNS, R. H.; and TUTTLE, O. F., 1964, The granite system at pressures of 4 to 10 kb: Jour. Geophys. Res., v. 69, p. 759–773.

MCMILLAN, P. F.; JAKOBSSON, S.; HOLLOWAY, J. R.; and SILVER, L. A., 1983, A note on the Raman spectroscopy of water-bearing albite glasses: Geochim. Cosmochim. Acta, v. 47, p. 1937–1943.

MORSE, S. A., 1970, Alkali feldspars with water at 5 kb pressure: Jour. Petrol., v. 11, p. 221–251.

MYSEN, B. O., and VIRGO, D., 1980, Solubility mechanisms of water in basalt melt at high pressures and temperatures: $NaCaAlSi_2O_7$-H_2O as a model: Am. Mineral., v. 65, p. 1176–1184.

———; ———; HARRISON, W. J.; and SCARFE, C. M., 1980, Solubility mechanisms of H_2O in silicate melts at high pressures and temperatures: a Raman spectroscopic study: Am. Mineral., v. 65, p. 900–914.

NICHOLLS, J., 1980, A simple thermodynamic model for estimating the solubility of H_2O in magmas: Contrib. Mineral. Petrol., v. 74, p. 211–220.

NOGAMI, M., and TOMOZAWA, M., 1984, Effect of stress on water diffusion in silica glass: Jour. Am. Ceram. Soc., v. 67, p. 151–154.

OSTROVSKII, I. A.; MISHINA, G. P.; and POVILAITIS, V. M., 1959, Pressure-temperature projection of the system silica-water: Doklady Akademii Nauk SSSR (Doklady Academy of Sciences USSR), v. 126, p. 587–588.

OXTOBY, W., and HAMILTON, D. L., 1978, The discrete association of water with Na_2O and SiO_2 in NaAl silicate melts: Contrib. Mineral. Petrol., v. 66, p. 185–188.

RICHET, P.; BOTTINGA, Y.; DENIELOU, L.; PETITET, J. P.; and TEQUI, C., 1982, Thermodynamic properties of quartz, cristobalite and amorphous SiO_2: drop calorimetry measurements between 1000 and 1800 K and a review from 0 to 2000 K: Geochim. Cosmochim. Acta, v. 46, p. 2619–2658.

SHAW, H. R., 1964, Theoretical solubility of H_2O in silicate melts: quasi-crystalline models: Jour. Geology, v. 72, p. 601–617.

——— 1968, Chemical states of H_2O and reaction in silicate-H_2O liquids and glasses: Geol. Soc. America Special Paper, v. 121, 274 p.

SKINNER, B. J., 1966, Thermal expansion, *in* CLARK, S. P., JR., ed., Handbook of Physical Constants: New York, Geol. Soc. America, p. 75–96.

SPERA, F. J., 1974, A thermodynamic basis for predicting water solubilities in silicate melts and implications for the low velocity zone: Contrib. Mineral. Petrol., v. 45, p. 175–186.

STEBBINS, J. F.; CARMICHAEL, I. S. E.; and WEILL, D. E., 1983, The high temperature liquid and glass heat contents and the heats of fusion of diopside, albite, sanidine, and nepheline: Am. Mineral., v. 68, p. 717–730.

STEWART, D. B., 1967, Four-phase curve in the system $CaAl_2Si_2O_8$-SiO_2-H_2O between 1 and 10 kilobars: Schweiz Mineralogische und Petrographische Mitteilungen, v. 47, pt. 1, p. 35–59.

STOLPER, E. M., 1982*a*, The speciation of water in silicate melts: Geochim. Cosmochim. Acta, v. 46, p. 2609–2620.

——— 1982*b*, Water in silicate glasses: an infrared spectroscopic study: Contrib. Mineral. Petrol., v. 81, p. 1–17.

———; SILVER, L. A.; and AINES, R. D., 1983, The effects of quenching rate and temperature on the speciation of water in silicate glasses (Abs.): EOS, v. 65, p. 339.

———; WALKER, D.; HAGER, B. H.; and HAYS, J. F., 1981, Melt segregation from partially molten source regions: the importance of melt density and source region size: Jour. Geophys. Res., v. 86, p. 6261–6271.

TOOP, G. W., and SAMIS, C. S., 1962, Activities of ions in silicate melts: Trans. Metallurgical Soc. America, v. 224, p. 878–887.

TUTTLE, O. F., and BOWEN, N. L., 1958, Origin of granite in light of experimental studies in the system $KAlSi_3O_8$-$NaAlSi_3O_8$-SiO_2-H_2O: Geol. Soc. America Mem. 74, 153 p.

———, and ENGLAND, J. L., 1955, Preliminary report on the system SiO_2-H_2O: Geol. Soc. America Bull., v. 66, p. 149–152.

VOIGT, D. E.; BODNAR, R. J.; and BLENCOE, J. G., 1981, Water solubility in melts of alkali feldspar composition at 5 kb, 950°C (Abs.): EOS, v. 62, p. 428.

WASSERBURG, G. J., 1957, The effect of H_2O in silicate systems: Jour. Geology, v. 65, p. 15–23.

Appendix 4. A Note on the Raman Spectra of Water-Bearing Albite Glasses

Geochimica et Cosmochimica Acta Vol. 47, pp. 1937–1943

0016-7037/83/111937-07$03.00/0

A note on the Raman spectra of water-bearing albite glasses

PAUL F. MCMILLAN,[a] SIGURDUR JAKOBSSON,[a] JOHN R. HOLLOWAY[a] and LYNN A. SILVER[b]
[a] Department of Chemistry, Arizona State University, Tempe, Arizona 85287
[b] Division of Geological and Planetary Sciences, California Institute of Technology, Pasadena, California 91125

(*Received January* 3, 1983; *accepted in revised form August* 8, 1983)

Abstract—The Raman spectra of albite glasses with 4.5 and 6.6 weight percent water have been obtained, and are compared with that of a dry sample. The hydrous glasses show bands near 3600 cm^{-1} due to O-H stretching, and a previously unreported weak band near 1600 cm^{-1} due to bending of molecular H_2O. Other weak spectral features are discussed, and the effect of dissolved water on the aluminosilicate framework vibrations is considered.

INTRODUCTION

THE IMPORTANCE of water as a magmatic volatile has been discussed by a number of authors (*e.g.*, BURNHAM, 1967, 1979; MYSEN, 1977; HOLLOWAY, 1981), and there have been several attempts to model its solubility behaviour in aluminosilicate melts. Thermodynamic relations in the system $NaAlSi_3O_8$-H_2O have been the subject of a number of experimental studies (e.g., BURNHAM and JAHNS, 1962; ORLOVA, 1962; BURNHAM and DAVIS, 1971, 1974; KADIK and EGGLER, 1974; OXTOBY and HAMILTON, 1978). Such results led to the melt-water mixing model of BURNHAM (1975), which has been reasonably successful in predicting water solubilities in a variety of melts. However, the model is critically dependent on the choice of hydrous species present in the melt, which BURNHAM (*e.g.*, 1975) assumed to be hydroxyl (OH^-). STOLPER (1982a,b) has recently suggested that realistic models should include both dissolved molecular H_2O and hydroxyl species, on the basis of infra-red measurements.

Vibrational spectroscopy, especially infra-red absorption, has been used by workers in the glass sciences for many years to characterize the hydroxylated species present in hydrous silicate glasses (*e.g.*, ADAMS, 1961; SCHOLZE, 1966). These studies have generally been of glasses prepared near atmospheric pressure with relatively low water contents. A few infra-red and Raman studies of more petrologic interest have been carried out on hydrous aluminosilicate glasses quenched from several kilobars pressure in an attempt to understand the dissolution mechanism of H_2O in corresponding melts (*e.g.*, ORLOVA, 1962; MYSEN *et al.*, 1980a; MYSEN and VIRGO, 1980; STOLPER, 1982a). All of the studies on hydrous silicate glasses have shown a band near 3500–3600 cm^{-1}, or some multiple (overtone) of this. This band is characteristic of O-H stretching (NAKAMOTO, 1970, pp. 79, 88–91), but does not distinguish between hydroxyl or H_2O species (*e.g.*, SCHOLZE, 1960). However, a number of studies (*e.g.*, ORLOVA, 1962; ERNSBERGER, 1977) of glasses with a wide range in water content have also observed a band near 1600 cm^{-1}, due to the ν_2 bending vibration of the H_2O molecule (NAKAMOTO, 1970, pp. 18, 83), and which is characteristic of molecular H_2O dissolved in the glass. This is supported by recent proton nuclear magnetic resonance studies of hydrous glasses (BARTHOLOMEW and SCHREURS, 1980). ORLOVA (1962) also observed a band near 4500 cm^{-1} in hydrous albite glasses, due to the combination of O-H stretching at 3500 cm^{-1} and Si-O stretching near 1000 cm^{-1}, which she assigned to Si-OH groups in the glass. BURNHAM (1975) used this assignment as support for his dissolution model *via* hydroxyl groups, but ignored ORLOVA's (1962) band at 1600 cm^{-1} indicative of molecular H_2O. STOLPER (1982a,b) has re-examined the near-infrared spectra of water-bearing albite glasses. Apart from the fundamental O-H stretching near 3500 cm^{-1} and its overtone near 7000 cm^{-1}, he observed a band near 5200 cm^{-1} which may be assigned to a combination of H-O-H bending near 1600 cm^{-1} with the O-H fundamental (STOLPER, 1982a). A band near 4500 cm^{-1} was attributed to Si-O-H groups, similar to ORLOVA (1962). These assignments then indicated that both hydroxyl and molecular H_2O groups were dissolved in the glasses, and STOLPER (1982b) used the variation of their relative concentration with total water content to construct an alternative quantitative model for melt-water interactions.

However, MYSEN *et al.* (1980a) measured Raman spectra of albite glasses with 1.2, 2.5 and 4.2 wt% water, quenched from hydrous liquids held at 20 kbars and 1500°C. They found no evidence for a band near 1600 cm^{-1}, and concluded that molecular H_2O was not present in these glasses. (MYSEN *et al.* (1980a) do suggest (p. 905) that a weak band near 1380 cm^{-1} on their Fig. 2 is due to H-O-H bending. The band in fact appears on their Fig. 1, occurs near 1280 cm^{-1} on that figure and is almost certainly not that due to H-O-H bending, although it could be due to Si-O-H bending (RYSKIN, 1974). The present study was undertaken to resolve the apparent conflict between the above infra-red and Raman studies.

EXPERIMENTAL METHODS

The reference dry albite for Raman work was a bubble-free sample prepared from a gel mix by vacuum melting (sample CG-Ab in MCMILLAN *et al.*, 1982) while that for infra-red was obtained from Corning Glass Works. The hydrous samples were also prepared from a gel mix, using analytical grade reagents. The gel was fired at 1000°C for 24 hours, ground under acetone, dried at 125°C for 6 hours, then loaded into Pt capsules (0.2" OD, 0.2" long) with appropriate amounts of doubly-distilled deionized water. The capsules were run for 4 hours at 1200°C and 10 kbars in a piston cylinder apparatus (BOYD and ENGLAND, 1960; PATERA and HOLLOWAY, 1978) using the piston-out technique. The pressure medium was a 0.5" talc-pyrex-graphite assembly with alumina spacers which was predried at 125°C. In order to deter diffusion of H_2 through the capsule walls, the capsules were embedded in powdered pyrex. Temperatures were measured with a Pt-Pt 90 Rh 10 thermocouple separated from the capsule-pyrex powder assembly by an alumina disc, and are believed accurate to within ±5°C for the temperature at the capsule centre. No corrections have been applied to the pressure readings.

Unpolarized Raman spectra were obtained from small chips (~1–2 mm across) using the 4880 Å line of a Spectra-Physics 171 argon laser, a Spex 1402 double monochromator, and an RCA photomultiplier with photon-counting electronics.

Quantitative infrared transmission spectra were obtained for doubly-polished thin sections of the hydrous samples with Cary 17 and Perkin-Elmer 180 spectrophotometers, following the technique used by STOLPER (1982a). Some powder KBr disc spectra were also run on the Perkin-Elmer instrument. From the molar absorptivities given by STOLPER (1982a) for the bands near 5200 and 4500 cm^{-1}, the amounts of water dissolved as molecular H_2O and hydroxyl species were calculated. These were summed to give total water contents of 4.5 and 6.6 wt% for the hydrous albite samples.

EXPERIMENTAL RESULTS

The Raman spectra of the dry and hydrous albite glass samples are shown in Figs. 1 and 2. A weak feature is present at 1635 cm^{-1} in both the 4.5 and 6.6 wt% samples, which is more clearly observed in the spectra of Fig. 2, run at higher gain. Overtone and combination bands from aluminosilicate network vibrations might be expected to appear in this region (WALRAFEN and STONE, 1975; GALEENER and LUCOVSKY, 1976), however the reference dry albite sample shows no analogous band (see inset to Fig. 1). The frequency of this band agrees well with that of the ν_2 vibration of molecular H_2O (NAKAMOTO, 1970). Further, the 4000–1500 cm^{-1} region of the infra-red spectrum of the 4.5 wt% glass (Fig. 3a), shows a sharp peak near 1630 cm^{-1} along with the O-H stretching fundamental near 3500 cm^{-1}. We suggest that the band appearing near 1630 cm^{-1} in the Raman and infra-red spectra of these hydrous albite glasses is due to the fundamental bending vibration of H_2O, and is indicative of molecular H_2O dissolved in the glasses. This band is extremely weak in the Raman spectrum of even the 6.6 wt% glass, suggesting why the band may have been overlooked by MYSEN *et al.* (1980a).

Figure 3b shows the near infra-red spectra of the 4.5 and 6.6 wt% samples, which show the bands near 5200 and 4500 cm^{-1} respectively assigned by previous workers to combination vibrations of molecular H_2O and SiOH (and/or AlOH) groups (see STOLPER, 1982a). Following STOLPER (1982a), their intensities were used to calculate the amounts of water dissolved as hydroxyl and molecular H_2O in the glasses. Figure 4 shows the H_2O/OH ratios for the present albite glasses *versus* total water content, compared with values obtained by STOLPER (1982a, Fig. 12) for other hydrous albite, rhyolitic and basaltic glasses.

It may be argued that the molecular H_2O observed in these glasses is present as fluid inclusions, perhaps exsolved from the melt during quenching. This question has been addressed in some detail by STOLPER (1982a,b), who presents a reasonable case for molecular H_2O as a dissolving species in the melt. No bubbles were observed optically (×1000) or by scanning electron microscopy (×50000) in the present samples. Further, STOLPER *et al.* (1983) have shown that molecular H_2O persists in hydrous glasses to at least 500°C at atmospheric pressure. However, it remains possible that other hydroxylated species are present in hydrous aluminosilicate melts at high pressure and temperature, which may react to give molecular water or hydroxyl during even the fastest quench currently attainable.

Two weak peaks are observed in the Raman spectra of the hydrous albite glasses at 2327 and 1554 cm^{-1} (Figs. 1 and 2). These correspond to the stretching vibrations of molecular N_2 and O_2 (NAKAMOTO, 1970, p. 78; MYSEN *et al.*, 1980a). These may have been incorporated as air in the gel mix during capsule loading or could be due to nitrate compounds incompletely removed during firing, and may be physically dissolved in the glasses. A peak near 2175 cm^{-1} was assigned by MYSEN *et al.* (1980a) to N_2^+ species. The peak observed here at 2177 cm^{-1} (Figs. 1 and 2) is quite intense for the spectra of the dry and 4.5 wt% H_2O samples, collected when the fluorescent lights in the room adjoining the Raman laboratory were on. This peak is practically absent from the spectrum of the 6.6 wt% sample when these lights were switched off. The frequency 2177 cm^{-1} relative to the 4880 Å laser line corresponds to 5461 Å, which agrees well with an intense emission line of Hg vapour (CRC Handbook of Chemistry and Physics, 60th edition 1980, p. E-277; 5460.74 Å). It is likely that the observed 2177 cm^{-1} peak is due to emission from mercury vapour in the laboratory fluorescent lights. A weak peak remains in the spectrum of the 6.6 wt% sample (Fig. 2), which may arise from the corridor lighting adjacent to the laboratory. A final weak peak is observed in this region at 1378 cm^{-1} for the 4.5 wt% sample, which is not present for the dry or 6.6 wt% samples (Figs. 1 and 2). No such band is observed in the powder infrared spectrum of the 4.5 wt% sample (Fig. 3c). Its frequency could correspond to the deformation vibration of strongly hydrogen-bonded silanol groups (RYSKIN, 1974), but such a

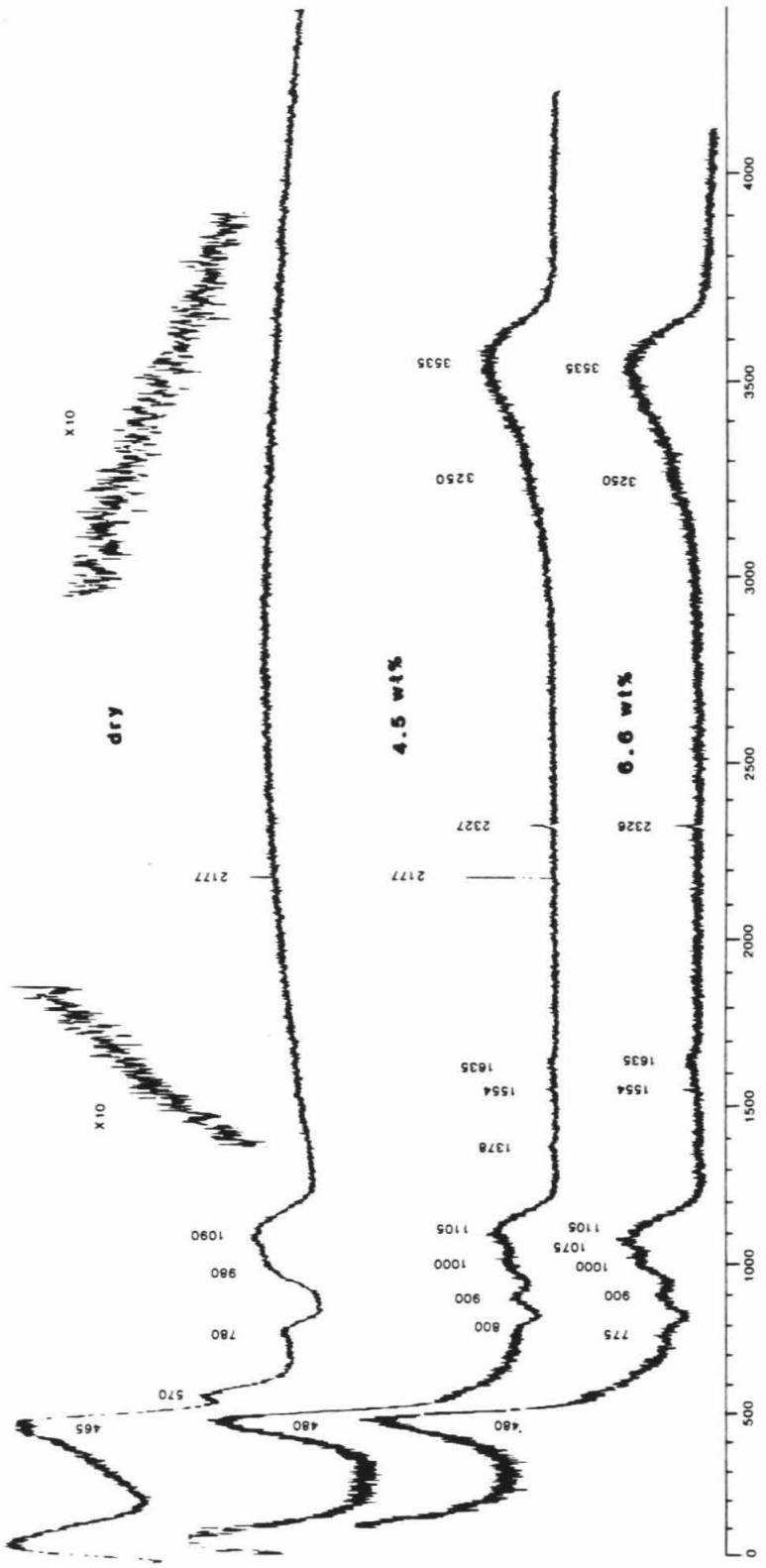

FIG. 1. Unpolarized Raman spectra of dry, (1 atm) albite glass (CG-Ab) and 4.5 wt% and 6.6 wt% water-bearing (10 kbar) albite glasses. The two insets above the dry glass spectrum show the regions near 1600 cm^{-1} and 3500 cm^{-1} amplified ×10. Slit width 150 $\mu \approx 4$ cm^{-1}.

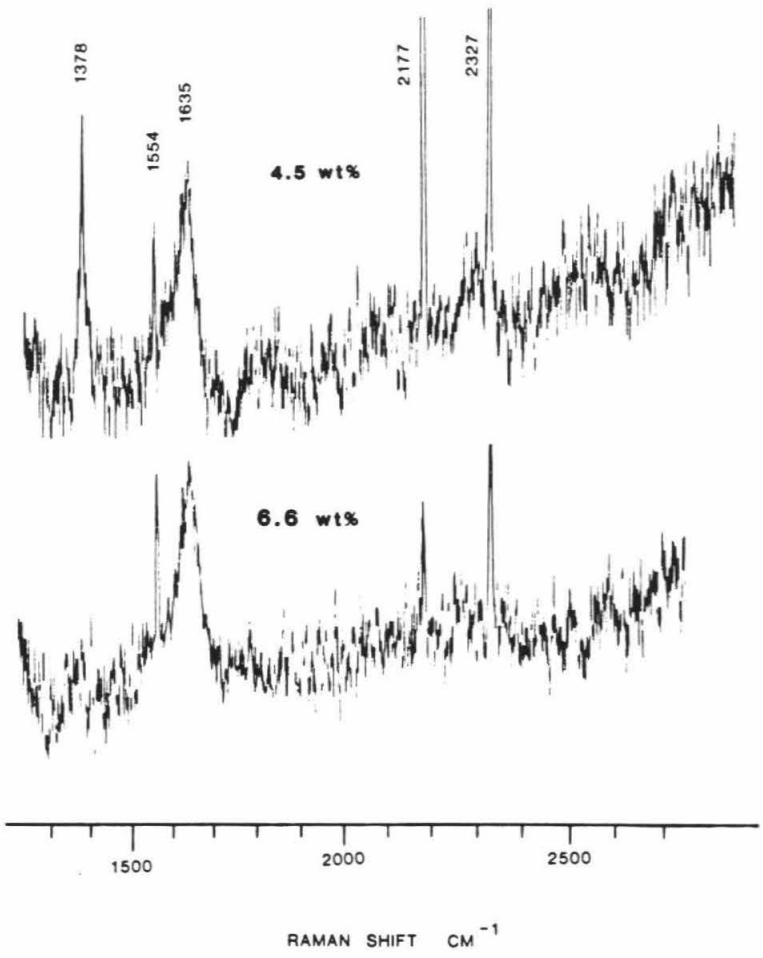

FIG. 2. The 1400–2400 cm^{-1} region of the Raman spectra of 4.5 wt% and 6.6 wt% water-bearing albite glasses, run at higher gain ($\approx \times 10$).

band would likely be broader, occur also for the 6.6 wt% sample, and appear in the infra-red spectrum. The 1378 cm^{-1} peak observed here could also correspond to a vibration of a small molecular species accidentally incorporated in the glass. MYSEN *et al.* (1980a) observed weak peaks near 1280 cm^{-1} (or 1380 cm^{-1}?; see above) for both H_2O- and D_2O-bearing albite glasses which are likewise difficult to interpret.

A band occurs near 900 cm^{-1} in the Raman spectra of H_2O-bearing albite glass (Fig. 1). A similar band was observed at 870–883 cm^{-1} by MYSEN *et al.* (1980a), which increased in intensity with increasing water content. The same band appeared at 886 cm^{-1} for a D_2O-bearing albite glass (MYSEN *et al.*, 1980a). Based on the apparent absence of an isotope shift for this band, (but see FREUND, 1982; MYSEN and VIRGO, 1982), these authors concluded that the band did not involve Si-OH or Al-OH groups, and assigned it to a vibration of the aluminosilicate network. They attributed the Si-OH stretching vibration to a component near 980 cm^{-1} deconvoluted from their high-frequency band group.

A weak Raman band has been observed at 970 cm^{-1} in vitreous SiO_2 containing trace quantities of water, which was assigned to an Si-OH stretching vibration (*e.g.*, STOLEN and WALRAFEN, 1976). VAN DER STEEN and VAN DEN BOOM (1977) diffused H_2 and D_2 into vitreous silica and observed the appearance of bands at 2254 (1629) and 3685 (2720) cm^{-1}, respectively assigned to Si-H (Si-D) and SiO-H (SiO-D) stretching vibrations. The same experiment was carried out by HARTWIG and RAHN (1977), who observed a band at 969 (941) cm^{-1} which they assigned to Si-OH (Si-OD) stretching, giving an isotope effect $\nu_{SiOH}/\nu_{SiOD} = 1.030$. It is of interest that the reduced mass ratio of the silanol group with motion of both Si and OH (OD) relative to their centre of mass is $\mu_{SiOD}/\mu_{SiOH} = 1.018$ (FREUND, 1982), while the assumption of motion of OH(OD) against a silicate

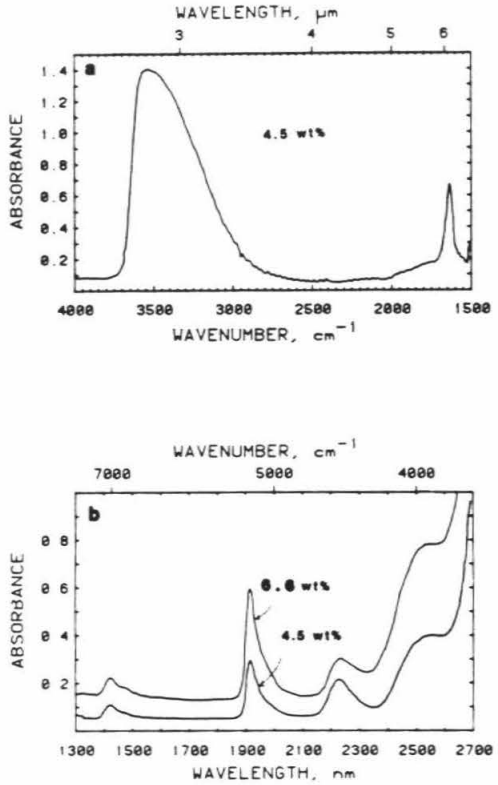

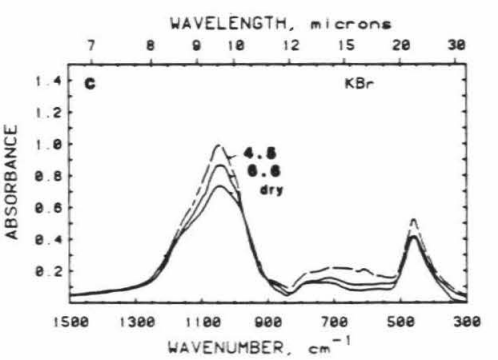

FIG. 3. (a) Infrared absorption spectrum from 4000–1500 cm^{-1} of a doubly-polished thin section of 4.5 wt% albite glass. A background spectrum due to epoxy used for mounting sample has been subtracted.

(b) Infrared absorption spectra in 7700–3700 cm^{-1} region of thin sections of 4.5 and 6.6 wt% albite glasses.

(c) Powder infrared absorption spectra in 1500–300 cm^{-1} region of dry (Corning), 4.5 wt% and 6.6 wt% albite samples run in KBr discs. Spectra are scaled to 0.5 mg glass in disc.

network of infinite mass gives $\sqrt{m_{OD}/m_{OH}}$ = 1.029, close to the experimental value. This may suggest that the 969 cm^{-1} band in fused silica containing silanol groups corresponds to movement of a hydroxyl group against stationary silicon held in a semi-rigid framework. This would be consistent with the isotope shift of near 1.35 (ν_{SiOH}/ν_{SiOD}) observed by VAN DER STEEN and VAN DEN BOOM (1977) for the O-H (O-D) stretching vibration, near the value of 1.37 expected for free hydroxyl.

MYSEN *et al.* (1980a) also observed a band near 860–870 cm^{-1} appearing for hydrous $NaAlSi_2O_6$ glasses, and perhaps a weak shoulder near 900 cm^{-1} for $Na_2Si_3O_7$ glass with high water contents. MYSEN and VIRGO (1980) also observed a shoulder appearing near 850–870 cm^{-1} for hydrous $NaCaAlSi_2O_7$ glass. We suggest that the Raman band in the 850–900 cm^{-1} region which appears on addition of H_2O to these various silicate and aluminosilicate glasses may be an Si-OH and/or Al-OH stretching vibration, possibly analogous to that observed in hydroxylated vitreous silica. It is likely that Al-OH stretching vibrations also occur in the region 700–900 cm^{-1} (*e.g.*, KOLESOVA and RYSKIN, 1959; RYSKIN, 1974). Such vibrations could contribute to the band near 900 cm^{-1} in the present glasses. However changes are also observed in the profile of the unresolved band group near 800 cm^{-1} with increasing water content (Fig. 1), which could be due to bands associated with Al-OH vibrations. Deformation vibrations of Al-O-H and Si-O-H groups are commonly found near 1000–1100 cm^{-1} (KOLESOVA and RYSKIN, 1959; RYSKIN, 1974), which overlaps with the stretching vibrations of the aluminosilicate network (MYSEN *et al.*, 1980a,b; MCMILLAN *et al.*, 1982). Some modifications are

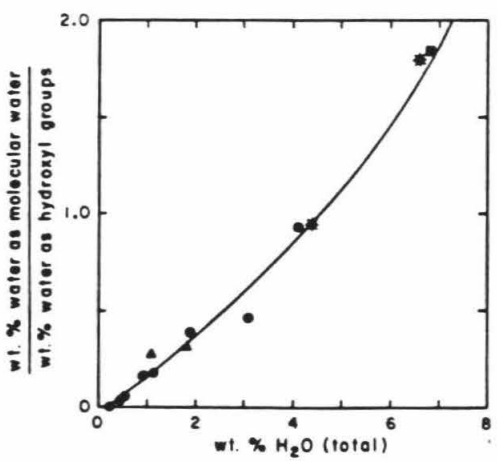

FIG. 4. Ratio of wt% water as molecular H_2O to wt% water as hydroxyl *versus* total water content calculated from intensities of infrared bands in Fig. 3 and molar absorptivities of STOLPER (1982a): ϵ (5200 cm^{-1}) = 1.78; ϵ (4500 cm^{-1}) = 0.98. The 4.5 wt% sample had density = 2.371 g cm^{-3}, thickness = 0.047 cm and absorbances of 0.241 (5200 cm^{-1}) and 0.136 (4500 cm^{-1}). The 6.6 wt% sample had density ~ 2.300 g cm^{-3}, thickness = 0.0142 cm and absorbances of 0.137 (5200 cm^{-1}) and 0.42 (4500 cm^{-1}). *, Albite glasses: this study. Other symbols are from Fig. 12 of STOLPER (1982a). ●, rhyolitic glasses; ▲, basaltic glasses; ■, albite glass

observed in the unresolved 1000–1100 cm^{-1} band group of hydrous albite samples, with the possible appearance of a band near 1075 cm^{-1} (Fig. 1). These could be related to the presence of bands associated with Al-O-H and/or Si-O-H deformation in the hydrous glasses. It is of interest that MYSEN *et al.* (1980a) observed a shoulder appearing near 1060–1080 cm^{-1} for hydrous $Na_2Si_2O_5$ glasses, which could correspond to Si-O-H deformations. The powder infra-red spectra of the present hydrous albite samples (Fig. 3c) do show some changes in this region, but are not easily described or interpreted. However, the presence of the combination band near 4500 cm^{-1} (Fig. 3b) reflects the presence of Si-O-H and/or Al-O-H deformation and/or stretching modes near 1000 ($\pm$100) cm^{-1}, coupling with the O-H stretch. We conclude that detailed interpretation of bands in this region must await more systematic studies of hydrous silicate glasses.

Finally, dry albite glass has a major Raman band near 465 cm^{-1} with a pronounced shoulder at lower frequency, and a weak band resolved at 570 cm^{-1} (Fig. 1). MCMILLAN *et al.* (1982) have assigned the 570 cm^{-1} band to a vibration associated with Al-O-Al linkages within the glass, and the low-frequency shoulder to modes predominantly characteristic of Si-O-Si linkages. These assignments are retained here, although other interpretations have been proposed (*e.g.*, MYSEN *et al.*, 1980a,b; 1982). Both the 570 cm^{-1} band and the low-frequency shoulder are markedly reduced in relative intensity on addition of water to the glass (Fig. 1; MYSEN *et al.*, 1980a). The major band maximum apparently increases to 480 cm^{-1}, but this is probably in part due to removal of the lower frequency component from its shoulder. This may suggest that Al-O-Al and Si-O-Si linkages are suppressed relative to Al-O-Si (responsible for the 480 cm^{-1} band) by preferential reaction with H_2O in the hydrous glasses. It is known that the 400–500 cm^{-1} Raman bands of dry albite glass do show similar changes with increasing pressure due to intertetrahedral angle changes (*e.g.*, MYSEN *et al.*, 1980b; MCMILLAN and GRAHAM, 1981). However, effects analogous to the present 10 kbar hydrous glasses are not observed at pressures below 20 kbar in dry albite glass.

SUMMARY

We conclude that the Raman spectroscopic experiments on hydrous albite glasses are in accord with the infra-red measurements (and with nuclear magnetic resonance spectra for other hydrous glasses), and that molecular H_2O is present in these glasses. Previous Raman studies may have overlooked its characteristic band near 1630 cm^{-1} due to its low intensity. Due to this low Raman cross section, and the weakness or absence of higher order Raman transitions (*e.g.*, STONE and WALRAFEN, 1982), Raman spectroscopy is probably a less useful tool for quantitative studies of water speciation in silicate glasses than is infra-red spectroscopy. In contrast, Raman studies have been much more powerful than infra-red spectroscopy in structural studies of the aluminosilicate glass network, with vibrations below 1200 cm^{-1}, and are sensitive to changes introduced by dissolution of water. It remains only to re-state one of the principles of vibrational spectroscopy, that infra-red and Raman experiments are necessary and complementary ingredients in a given vibrational study.

Acknowledgements—This work was funded by N.S.F. grant EAR-8108748 and N.A.S.A. grant NAGW 182 (J. Holloway) and N.S.F. grants EAR-8212765 and EAR-8009798 (E. Stolper). We thank the Center for Solid State Science at A.S.U. for use of the Raman facility and Nita Dagon and Mike Palitz for typing. Infrared and near-infrared spectra were obtained in the laboratory of Dr. G. R. Rossman at Caltech, and we thank him for making these facilities available. We are grateful to Drs. J. E. Dickinson and E. Stolper for careful reviews of the manuscript.

REFERENCES

ADAMS R. V. (1961) Infra-red absorption due to water in glasses. *Phys. Chem. Glasses* **2**, 39–49.

BARTHOLOMEW R. F. and SCHREURS J. W. H. (1980) Wide-line NMR study of protons in hydrosilicate glasses of different water contents. *J. Non-Crystalline Solids* **38/39**, 679–684.

BOYD F. R. and ENGLAND J. L. (1960) Apparatus for phase-equilibrium measurements at pressure up to 50 kilobars and temperatures up to 1750°C. *J. Geophys. Res.* **65**, 749–756.

BURNHAM C. W. (1967) Hydrothermal fluids at the magmatic stage. In *Geochemistry of Hydrothermal Ore Deposits* (ed. H. L. BARNES) pp. 34–76. Holt, Rinehart and Winston, Inc.

BURNHAM C. W. (1975) Water and magmas; a mixing model. *Geochim. Cosmochim. Acta* **39**, 1077–1084.

BURNHAM, C. W. (1979) The importance of volatile constituents. In *The Evolution of the Igneous Rocks: Fiftieth Anniversary Perspectives* (ed. H. S. YODER) pp. 439–479. Princeton University Press.

BURNHAM C. W. and DAVIS N. R. (1971) The role of H_2O in silicate melts: I. P-V-T relations in the system $NaAlSi_3O_8$-H_2O to 10 kilobars and 1000°C. *Amer. J. Sci.* **270**, 54–79.

BURNHAM, C. W. and DAVIS, N. F. (1974) The role of H_2O in silicate melts: II. Thermodynamic and phase relations in the system $NaAlSi_3O_8$-H_2O to 10 kilobars, 700° to 1100°C. *Amer. J. Sci.* **274**, 902–940.

BURNHAM C. W. and JAHNS R. H. (1962) A method for determining the solubility of water in silicate melts. *Amer. J. Sci.* **260**, 721–745.

ERNSBERGER, F. M. (1977) Molecular water in glass. *J. Amer. Ceram. Soc.* **60**, 91–92.

FREUND F. (1982) Solubility mechanisms of H_2O in silicate melts at high pressures and temperatures: a Raman spectroscopic study: discussion. *Amer. Mineral.* **67**, 153–154.

GALEENER F. L. and LUCOVSKY G. (1976) Second order vibrational spectra of vitreous silica. In *Light Scattering in Solids* (ed. M. BALKANSKI, R. C. LEITE, S. P. S. PORTO) pp. 641–645. Flammarion Sciences, Paris.

HARTWIG C. M. and RAHN L. A. (1977) Bound hydroxyl in vitreous silica. *J. Chem. Phys.* **67**, 4260–4261.

HOLLOWAY J. R. (1981) Volatile interactions in magmas. In *Thermodynamics of Minerals and Melts*. Advances in Physical Geochemistry, Vol. I (ed. R. C. NEWTON, A.

NAVROTSKY and B. J. WOOD), pp. 273–293. Springer-Verlag.

KADIK A. A. and EGGLER D. H. (1975) Melt vapor relations on the join $NaAlSi_3O_8$-H_2O-CO_2. *Carnegie Inst. Wash. Yearb.* **74**, 479–484.

KOLESOVA V. A. and RYSKIN YA. I. (1959) Infrared absorption spectrum of hydrargillite $Al(OH)_3$. *Optics and Spectroscopy* **7**, 165–167.

MCMILLAN P. F. and GRAHAM C. M. (1981) The Raman spectra of quenched albite and orthoclase glasses from 1 atm. to 40 kb. In *Progress in Experimental Petrology*, Fifth Progress Report of Research Supported by N.E.R.C. (ed. C. E. FORD), pp. 112–115. Natural Environment Research Council Publications Series D No. 18, Eaton Press, Wallasey, England.

MCMILLAN P., PIRIOU B. and NAVROTSKY A. (1982) A Raman spectroscopic study of glasses along the joins silica-calcium aluminate, silica-sodium aluminate, and silica-potassium aluminate. *Geochim. Cosmochim. Acta* **46**, 2021–2038.

MYSEN B. O. (1977) The solubility of H_2O and CO_2 under predicted magma genesis conditions and some petrological and geophysical implications. *Rev. Geophys. Space Physics* **15**, 351–361.

MYSEN B. O. and VIRGO D. (1980) Solubility mechanisms of water in basalt melt at high pressures and temperatures: $NaCaAlSi_2O_7$-H_2O as a model. *Amer. Mineral.* **65**, 1176–1184.

MYSEN B. O. and VIRGO D. (1982) Solubility mechanisms of H_2O in silicate melts at high pressures and temperatures: a Raman spectroscopic study: reply. *Amer. Mineral.* **67**, 155.

MYSEN B. O., VIRGO D., HARRISON W. J. and SCARFE C. M. (1980a) Solubility mechanisms of H_2O in silicate melts at high pressures and temperatures: a Raman spectroscopic study. *Amer. Mineral.* **65**, 900–914.

MYSEN B. O., VIRGO D. and SCARFE C. M. (1980b) Relations between the anionic structure and viscosity of silicate melts—a Raman spectroscopic study. *Amer. Mineral.* **65**, 690–710.

MYSEN B. O., VIRGO D. and SEIFERT F. A. (1982) The structure of silicate melts: Implications for chemical and physical properties of natural magma. *Rev. Geophys. Space Phys.* **20**, 353–383.

NAKAMOTO K. (1970) *Infrared Spectra of Inorganic and Coordination Compounds*, second edition. Wiley-Interscience.

ORLOVA G. P. (1962) The solubility of water in albite melts. *Int. Geol. Rev.* **6** (1964), 254–258.

OXTOBY S. and HAMILTON D. L. (1978) The discrete association of water with Na_2O and SiO_2 in NaAl silicate melts. *Contrib. Mineral. Petrol.* **66**, 185–188.

PATERA E. S. and HOLLOWAY J. R. (1978) A non-end-loaded piston cylinder design for use to forty kilobars (abstr.). *EOS* **59**, 1217–1218.

RYSKIN YA. I. (1974) The vibrations of protons in minerals: hydroxyl, water and ammonium. In *The Infrared Spectra of Minerals* (ed. V. C. FARMER), pp. 137–181. Mineralogical Society, London.

SCHOLZE H. (1960) Zur Frage der Unterscheidung zwischen H_2O-Moleceln und OH-Gruppen in Gläsern und Mineralen. *Naturwiss.* **47**, 226–227.

SCHOLZE H. (1966) Gases and water in glass. *The Glass Industry*, 546–551, 622–628 and 670–675.

STOLEN R. H. and WALRAFEN G. E. (1976) Water and its relation to broken bond defects in fused silica. *J. Chem. Phys.* **64**, 2623–2631.

STOLPER E. (1982a) Water in silicate glasses: an infrared spectroscopic study. *Contrib. Mineral. Petrol.* **81**, 1–17.

STOLPER E. (1982b) On the speciation of water in silicate melts. *Geochim. Cosmochim. Acta* **46**, 2609–2620.

STOLPER E., SILVER L. A. and AINES R. D. (1983) The effects of quenching rate and temperature on the speciation of water in silicate glasses (abstr.). *EOS* **64**, 339.

STONE J. and WALRAFEN G. E. (1982) Overtone vibrations of OH groups in fused silica optical fibers. *J. Chem. Phys.* **76**, 1712–1722.

VAN DER STEEN G. H. A. M. and VAN DEN BOOM H. (1977) Raman spectroscopic study of hydrogen-containing vitreous silica. *J. Non-Crystalline Solids* **23**, 279–286.

WALRAFEN G. E. and STONE J. (1975) Raman spectral characterization of pure and doped fused silica optical fibers. *Appl. Spectroscopy* **29**, 337–344.

Appendix 5. Water in Silicate Glasses: Quantitation and Structural Studies by ^{1}H Solid Echo and MAS-NMR Methods

Water in Silicate Glasses: Quantitation and Structural Studies by ^{1}H Solid Echo and MAS-NMR Methods

Hellmut Eckert and James P. Yesinowski
Division of Chemistry and Chemical Engineering
California Institute of Technology

Lynn A. Silver and Edward M. Stolper
Division of Geological and Planetary Sciences
California Institute of Technology

ABSTRACT

^{1}H wideline and magic angle spinning (MAS) NMR results are reported for water in a series of synthetic glasses and naturally-occurring silicate glasses containing from 0.04 to 9.4 wt.% H_2O. For glasses free of paramagnetic metal ions, the absolute water contents can be accurately determined by a solid echo ^{1}H NMR technique with pyrophyllite, $Al_2Si_4O_{10}(OH)_2$, as an intensity reference. The MAS-NMR spectra can be interpreted as superpositions of the individual spectra of OH and anisotropically constrained H_2O groups, the latter giving rise to spinning sidebands extending over ca. 100 kHz. Two methods are described to obtain percentages of OH and H_2O groups from the relative intensities of the centerband and the spinning sidebands in these glasses. The MAS-NMR results are consistent with previous IR analyses indicating that low levels of water (< 2-4 wt. percent) are mainly present as OH groups whereas at higher concentrations molecular H_2O species dominate. Simulations of the MAS-NMR spectra based on the individual spectra of compounds in which the hydrogen-bearing species are structurally isolated (OH in tremolite and H_2O in analcite) accurately reproduce the experimental spectra, indicating that the OH or H_2O groups in the glasses are not preferentially clustered. The MAS-NMR centerband lineshapes are dominated by a distribution of isotropic chemical shifts. The well-established linear dependence of ^{1}H chemical shifts on the O-H···O distance (a measure of the hydrogen bonding strength) leads to average distances of 290 $\pm$ 1.5 pm in all synthetic glasses except silica, 293 $\pm$ 1.5 pm in the volcanic rhyolite glasses, and 298 pm in silica glass. This value does not depend on the total water contents, indicating that the hydrogen bonding characteristics of OH and H_2O species in the glasses are similar.

The ^{1}H wideline NMR procedure above yields underestimates of the total water content for synthetic and volcanic glasses containing ca. 1 wt.% iron, presumably due to extreme signal broadening by the strong dipolar fields from the electron spins of the paramagnetic ions. These dipolar couplings also affect the lineshape of the observable portion of the hydrogen resonance and produce intense spinning sidebands in the MAS-NMR spectra which invalidate determinations of OH/H_2O

ratios in this case.

INTRODUCTION

The state of water in oxide glasses has received considerable attention both in geology and in materials science.[1] Water plays a crucial role in modifying the phase equilibria and physical properties of magmas; hence much effort has been devoted to determining the concentration and speciation of water in volcanic glasses[2] and in synthetic analogues of magmas.[3] From a materials research standpoint, the presence of even minor amounts of water in silicate glass has been shown to alter drastically the physicochemical properties and possible ranges of technological applications.[4] While the influence of water upon the macroscopic properties of silicate melts has been studied extensively,[5,6] *direct* structural information about the nature of the hydrogen-bearing species and their bonding environments cannot be obtained readily from such measurements. Investigation of glasses quenched from melts is a frequent approach to answering these questions.[7] Recent studies of infrared overtone and combination bands[1−3,7] demonstrate that water in silicate glasses is present as OH and molecular H_2O groups. These studies suggest that low contents of water disrupt the glass network, transforming (Al,Si)-O-(Al,Si) linkages into (Al,Si)-OH bonds. Above ca. 2-4 wt.% H_2O (depending on the glass composition) the number of hydroxyl groups thereby created levels off, and water enters the glass structure predominantly in the form of molecular species. The concentrations of these species as well as the absolute proton content of glasses determined by infrared spectroscopy have been shown to be compatible with a thermodynamic analysis of phase equilibrium data for hydrous silicate melts.[3,7,8] In spite of this agreement, confirmation of these results by an independent method would be highly desirable. In addition, there are many questions into which vibrational spectroscopy offers little insight: for instance, the bonding site of the hydroxyl groups, the occurrence of isolated or clustered water molecules, the spatial relationship between OH and H_2O species, and the motional state of H_2O.

Solid state NMR spectroscopy is a powerful technique for the investigation of

glassy systems since it provides selective information about the immediate environment of the nucleus being observed. Several proton NMR studies of water in glasses have appeared.[9-12] In the first detailed application of wideline NMR to this problem, Müller-Warmuth et al.[9] established a close proximity between protons and alkali metal cations in alkali silicate glasses by analyzing the compositional dependence of the second moment. Direct NMR evidence for the presence of molecular H_2O in addition to Si-OH groups was presented in a study by Bartholomew and Schreurs on hydrosilicate glasses.[10] The possibility of distinguishing between H_2O and OH groups in glasses by a mathematical analysis of the free induction decay was proposed,[11] and recently results on naturally occurring glasses with very low proton contents have been reported.[12]

Early wideline NMR studies of water in glasses utilized the linebroadening arising from internuclear dipolar interactions as the major diagnostic tool. In contrast, recently developed high-resolution techniques increase the spectral resolution by removing these interactions, and place emphasis upon the chemical shift as the major source of information. Although high-resolution conditions are especially difficult to achieve in proton NMR studies, where large homonuclear dipolar couplings predominate and chemical shift effects are small, the pioneering work of Haeberlen[13] and Vaughan and coworkers[14], using multiple-pulse methods on single crystals have provided a valuable database of proton chemical shifts. A linear dependence of the isotropic chemical shift on the O-H···O bonding distance was noted for a wide range of crystalline compounds.[14] More accurate chemical shift measurements have been carried out using multiple-pulse methods in combination with MAS.[15] However, little work has been reported using high-speed ^{1}H MAS-NMR without multiple-pulse methods, a technique that preserves valuable information about homonuclear dipolar couplings.[16] Also, the application of high resolution proton NMR to amorphous systems has, to date, been limited to a brief report on results obtained on dried silica gels.[17]

We present here the first systematic high resolution ^{1}H MAS-NMR study of glassy systems. A major focus is the effect of water content in a series of closely

related synthetic and natural silicate glasses upon the hydrous species present. In addition to the structural information provided by NMR methods, the proportionality of the signal intensity to the number of contributing nuclei enables NMR to be used as a non-destructive means of determining absolute water contents and the concentrations of individual H-bearing species in glasses without paramagnetic ions. In the present study, we have addressed these quantitative aspects of ^1H wideline and magic-angle spinning NMR in detail and developed optimized conditions under which satisfactory results can be obtained both in naturally-occurring and in synthetic samples.[18]

EXPERIMENTAL

Preparation of the synthetic glasses: Samples with several different anhydrous glass compositions were studied: albite (A); orthoclase (O); albite-orthoclase (AO), with and without FeO; and the anorthite-silica-wollastonite eutectic (ASW). Table I lists the nominal compositions of these glass systems. Anhydrous AO glasses were prepared at Corning Glass Works from production grade oxides by melting at 1650 °C for 16 h. The other starting materials were crystalline Amelia albite (A) or mixtures of Johnson-Matthey SpecPure oxides (O,ASW), which were finely ground in ethanol, dried for 24 h at 800 °C, and stored over a desiccant. In the case of the albite and ASW glasses, the oxides were pre-melted at 1 atm and 1300 °C, quenched to glass, re-ground and dried at 800 °CH_2O were loaded into Pt capsules which were then sealed by arc-welding. Capsules were run at 1400-1450°C, 15-20 kbar in a 1.0 inch solid-media piston cylinder apparatus, containing a NaCl cell with a pyrex sleeve and either boron nitride or fired pyrophyllite as the inner sleeve material, or in a 0.5 in piston cylinder apparatus, using a talc cell with a pyrex sleeve.[3,19] All of the samples were liquid under run conditions; they were quenched to glasses at ca. 150-200 °C/s by turning off the graphite furnace.

A sample of vitreous silica was prepared at Corning glass by flame hydrolysis of $SiCl_4$ at 1000 °C and 1 atm and subsequent sintering. The water content of this sample was determined by infrared spectroscopy to be 0.04 wt.%, using an

extinction coefficient of 181 $[H_2O]\cdot l/mol\cdot cm$.[20]

Origin of the volcanic glasses. The volcanic glasses under study originate from the ca. 1340 A.D. eruption of the Mono Craters (Central California) and are of rhyolitic composition. They form a complete series of different water contents ranging from 0.1 to 2.6 weight percent H_2O, depending on their time-sequence in the original eruption.[2] A volcanic glass sample containing several weight percent water isotopically diluted with D_2O was made by hydration of Los Posos rhyolite with $(H_{0.1-0.15}D_{0.9-0.85})_2O$ at 700 bars and 850 °C for several days in a rapid quench vessel.[21]

Analytical characterization of the glass samples. Selected samples of each glass composition were analyzed with an automated JEOL 733 Superprobe electron microprobe to verify glass composition and homogeneity, to assess possible Na and K loss during the synthesis of the anhydrous starting materials, and to determine Fe contents. These analyses were carried out with a 15 kV accelerating voltage, a sample current of 5 nA and a 20-25 μ spot size. These data, reported in Table II, represent the averages of 5-10 measurements on different sampling points. Total water contents were determined by a manometric technique described earlier,[22] and infrared spectra were obtained on ca. 5-10 doubly polished thin sections of each glass sample using a Nicolet 60SX FTIR spectrometer. The details and results of the infrared spectroscopic work will be reported elsewhere.[3,23] Synthesis conditions and analytical data for the glasses under study are listed in Table II. *The concentrations of both OH and H_2O species are reported as the amount of water that would be released on heating if all species were released as H_2O.*

Reference NMR data were obtained on powdered samples prepared from single crystals of the minerals tremolite, $Ca_2Mg_5Si_8O_{22}(OH)_2$; pyrophyllite, $Al_2Si_4O_{10}(OH)_2$; analcite, $NaAlSi_2O_6 \cdot H_2O$; and gypsum, $CaSO_4 \cdot 2H_2O$. The water content of the pyrophyllite sample (from Mariposa Co., California) used for absolute quantitation purposes was determined to be 4.98 $\pm$ 0.06 wt.%. by manometry.[22] The tremolite and analcite samples used in fitting the MAS-NMR spectra of the hydrous glasses were high quality single-crystalline materials from

the mineral collection of the California Institute of Technology. Electron microprobe analysis confirmed that the tremolite sample was close to the theoretical stoichiometry and contained very little iron (0.1 wt.%). The identity of the analcite sample was confirmed by x-ray powder diffraction.

NMR Experiments: Room temperature nuclear magnetic resonance spectra were recorded at 200.27 MHz on a homebuilt spectrometer system interfaced with a Nicolet 293B pulse programmer, Explorer fast digitizer, and Nicolet 1280 computer system. Details of the spectrometer have been described elsewhere.[21] Wideline NMR spectra were obtained on 100-300 mg samples of coarsely ground powders (> 44-300 μm) or glass chunks in a homebuilt probe with a 5mm diameter solenoidal coil. A solid echo pulse sequence[24] (90°_x - τ - 90°_y - τ - acquire) was used to circumvent the spectrometer "dead time" after an rf pulse. The 90° pulse length was 1.8 to 2 μs; typically, a refocusing delay τ of 8 μs was used. Spin lattice relaxation times were measured using the inversion recovery sequence. The recycle delay times were always chosen to be at least five times as long as the experimentally measured spin lattice relaxation times T_1, which were found to be ca. 0.05 and 1-10 seconds in the volcanic and the synthetic glass samples, respectively. (No systematic trends of T_1 with glass composition or absolute water content were observed). Typically, 64 scans were acquired and processed with an exponential linebroadening function of 100 Hz.

^{1}H magic angle spinning spectra were obtained at 200.27 MHz and at 500.13 MHz (the latter using a Bruker WM 500 spectrometer). Finely ground powders (44-150 μm) were packed into 5 mm o.d. sapphire rotors which were spun in high-speed magic angle spinning probes from Doty Scientific. Both probes were specially designed to yield as low a proton background as possible. At 200 MHz, spectra were acquired with 45° pulses (1.0 μs); 10-30° pulses were used at 500.13 MHz, in order to improve the uniformity of excitation across the spectrum excitation due to the lower pulse power available (90° pulse length at 500 MHz = 8 μs). For each sample, spectra were obtained at a series of different spinning speeds, ranging from 2.0 to 8.0 kHz. Typically, 64 free induction decays were acquired and then

processed with an exponential linebroadening function of 50 Hz. Chemical shifts were determined using the hydroxyl resonance of a hydroxyapatite sample (δ_{iso} = 0.2 ppm with respect to TMS) as a secondary reference.[16]

RESULTS

Figure 1 shows typical ^1H wideline NMR spectra of some synthetic orthoclase and albite glasses. These spectra are characteristic of solid state NMR powder patterns, and show that the hydrogen-bearing species do not exhibit isotropic mobility at room temperature. Thus, water is present not in the form of liquid like "pools" or inclusions in any detectable amounts, but rather in the form of anisotropically constrained OH and H_2O species.

In this section, we describe the NMR methodology used in the present study to

- measure absolute H_2O contents, and
- determine the concentrations of distinguishable H-bearing species (i.e. H_2O and OH)

in these synthetic glass systems. The extension of these analytical approaches to the study of naturally-occurring glasses, and the structural inferences to be drawn from the MAS-NMR spectra, will be discussed in the next section.

Methodology of H_2O Quantitation. The direct proportionality of the area under an NMR peak to the number of nuclear spins contributing to that peak is the basis of quantitative NMR applications. As detailed below, this approach to measuring the water content of glasses by wideline NMR encounters several complications. The finite spectrometer deadtime necessitates a certain delay (ca. 10 μs in the present study) before useful data acquisition can begin after a pulse. A substantial irreversible magnetization decay occurs during this deadtime for the present samples, resulting in signal loss and lineshape distortions. The solid echo pulse sequence circumvents the dead-time problem by refocusing the homonuclear dipolar couplings to produce an echo signal some time τ after the second pulse.

However, the refocussing effect strictly applies only to an isolated pair of spins with I $= 1/2$.[24] In the presence of multiple homonuclear dipolar interactions, an irreversible magnetization decay (with a time constant T_2^*) occurs during the evolution period τ, resulting in an incomplete echo formation. Thus, serious quantitation errors can be introduced if the T_2^* values differ greatly among the samples studied and the standards used. To address this question, we monitored this magnetization decay by measuring the integrated signal intensity as a function of τ for different glass samples and several crystalline model compounds (tremolite, $Ca_2Mg_5Si_8O_{22}(OH)_2$, and pyrophyllite, $Al_2Si_4O_{10}(OH)_2$, for OH groups; gypsum, $CaSO_4 \cdot 2H_2O$, and analcite, $NaAlSi_2O_6 \cdot H_2O$, for H_2O groups). Figure 2 shows a representative decay curve observed for an orthoclase glass containing 2.6 wt.% H_2O. For all of the glasses investigated, one can obtain an approximate T_2^* decay constant by fitting the data for $8\mu s < \tau < 100\ \mu s$ to a single exponential decay. The estimates of T_2^* thus obtained are listed in Table III. (No obvious dependence of these T_2^* values on the basic glass composition or the absolute water content could be found.) The T_2^* decay curve of pyrophyllite was found to be very similar to those of the glasses, yielding a much better agreement with the latter than any of the decay curves observed for the other crystalline reference compounds. Hence, pyrophyllite was used as the standard for all of the glasses studied. The water contents measured by this NMR method (accuracy ca. $\pm$ 5%) are listed in Table II and compared in Figure 3 to analytical data obtained by manometry.

Methodology of determining H_2O and OH Species concentrations. In addition to the total water content, the relative amounts of hydroxyl groups and molecular water groups are also of interest. It is clearly seen in Figure 1 that the spectra of all of the glasses contain two distinct components: a broad line suggestive of the "Pake doublet"[25] observed for molecular water units in crystalline hydrates such as analcite and gypsum, and a sharper component that has been assigned to hydroxyl groups.[9,10] Figure 1 shows that, with increasing H_2O content, the signal contribution due to the broader component increases, reflecting an increasing fraction of molecular H_2O species.

Earlier results by Bartholomew and Schreurs[10] indicated that it might be possible to analyze these trends in some fashion to obtain the respective OH and H_2O contents of these glasses. Such a quantitative lineshape decomposition is, however, very difficult in practice, since the individual lineshapes of these species are unknown and difficult to predict because of the additional broadening effects often observed in glasses arising from distributions of isotropic and anisotropic chemical shifts. Also, discrimination of both spectral components on the basis of different spin-lattice relaxation times (used in a previous ^2H NMR study of water in glasses[21]) is rendered impossible by fast spin diffusion.

Figure 4 shows that high-speed magic angle spinning dramatically improves the resolution of the ^1H spectra of glasses. The spectra consist of a relatively sharp, intense centerband at the isotropic chemical shift position and a set of associated spinning sidebands spaced at integer multiples of the spinning speed ν_r. At a constant resonance frequency (200.27 MHz) and spinning speed (8.0 kHz) increasing relative intensity is distributed into the spinning sidebands as the total water content of the glasses is increased. In the following, we outline how the percentages of OH and molecular H_2O can be obtained.

As theoretically predicted[26] and experimentally observed,[16,27] the sideband intensity patterns observed in ^1H MAS-NMR spectra are significantly different for OH and H_2O groups in crystalline compounds. For rigid OH groups the spinning sideband intensities are governed by the ^1H chemical shift anisotropy as well as homonuclear and heteronuclear dipole-dipole interactions (e.g. with ^{23}Na and ^{27}Al). Under the experimental conditions used, the hydroxyl groups exhibit only one or two pairs of spinning sidebands with rapidly diminishing intensities. For example, the 200.27 MHz ^1H MAS-NMR spectrum (Figure 5, top) of the structurally isolated OH groups in the mineral tremolite demonstrates that the dominant contribution to the spectral area (86 percent at $\nu_r = 8$ kHz) arises from the centerband.

In contrast, structural H_2O in crystal hydrates gives rise to much wider spinning sideband patterns, extending over ca. 100 kHz. This characteristic intensity pattern, the envelope of which resembles that of a Pake doublet in the slow-spinning

limit, arises mainly from the strong homonuclear dipole-dipole interaction which is inhomogeneous in character for an isolated pair of nuclear spins.[26] As an example, Figure 5 (bottom) shows the ^1H MAS-NMR spectrum of analcite, a compound with structurally isolated H_2O groups. Only a minor fraction of the total signal area (18 percent) is contained in the MAS centerband.

The substantial differences between the spinning sideband patterns observed for the model compounds tremolite (OH) and analcite (H_2O) suggest that in samples containing both H_2O and OH, the intensity profile of the spinning sideband pattern could serve as a measure of their relative percentages. The simplest approach is to consider the spectrum of the glasses as the sum of the weighted individual MAS-NMR peak patterns of OH and H_2O in the model compounds, ignoring the small chemical shift difference, and assuming that these peak patterns are not modified by dipolar interactions between these species.

To test the validity of the latter assumption, we compared the MAS-NMR center and sideband intensities (as measured by peak heights) observed in the synthetic glasses with those obtained by adding properly weighted individual spectra of tremolite and analcite. Best fit simulated spectra were obtained by constraining both the centerband peak heights as well as the sums of the centerband and all sideband intensities to be equal for experimental and simulated spectra. The percentages of water present as molecular H_2O based on this procedure at a spinning speed of 8 kHz are listed in Table III. Figures 6a-c compare these simulations with the experimental spectra (the constrained centerbands are omitted). The agreement between individual sideband intensities, especially at the highest spinning speed (8 kHz), supports the hypothesis that, at such speeds, the OH and H_2O species in these glasses can be treated as non-interacting species. While at 8 kHz the impact of the dipolar interactions between OH and H_2O species on the spinning sideband patterns is inferred to be minimal, more pronounced differences between experimental and simulated spectra occur at lower spinning speeds. This is especially apparent for the first spinning sideband pair at 5 kHz, shown in Figure 6c. Thus, the highest possible spinning speeds (> 8 kHz) are desirable in this analysis.

Since the linewidths of the sidebands may differ among each other and from that of the centerband for several reasons, it is generally preferable to use integrated areas rather than peak heights for quantitative studies. Consequently, we developed an alternate procedure for determining the H_2O and OH percentages by using the area ratio

$$P = \frac{area(centerband)}{area(centerband + sidebands)}$$

At a spinning speed of 8 kHz, P = 0.855 for tremolite (100% OH) and P = 0.183 % for analcite (100% H_2O). Linear interpolation between these values yields the percentages of water present as OH and H_2O from the values for P measured for the glasses. Following this procedure, we found these results to be independent of the spinning speed above 6 kHz. Below this limit, the H_2O/OH ratios obtained from this analysis tend to increase, presumably reflecting a breakdown of the assumption that OH and H_2O are non-interacting species. Table III lists the results of this procedure and shows that the percentages of water present as molecular H_2O species obtained by the two different methods discussed above are generally in good agreement.

DISCUSSION

Quantitative analysis by ^1H wideline NMR. The hydrogen contents of the synthetic iron-free glasses obtained from the ^1H solid echo NMR quantitation agree very well with those obtained by hydrogen manometry (Figure 3). In contrast, for volcanic glasses the NMR quantitation values are only ca. 70 % of the manometric values. We attribute the signal loss observed in the volcanic glasses to the presence of paramagnetic constituents (all volcanic glass samples contain ca. 1 wt.% FeO, see Table II), because we observe similar effects in iron-containing synthetic glasses: In two albite/orthoclase samples containing ca. 8 wt.% H_2O and 0.58 and 1.27 wt.% FeO, respectively, the observable fractions of water were determined to be 87.4 % and 73.2 %, respectively. These results show that the numerical value of the scaling factor describing this signal loss is roughly proportional to the level of iron in the glass. The linearity of the NMR quantitation in Figure 3 for all of the volcanic

glasses studied indicates that the scaling factors are essentially identical, consistent with microprobe analyses, which indicate that variations in iron contents among these glasses are small. The present results suggest that NMR can be calibrated to obtain absolute water contents in naturally-occurring as well as synthetic glasses if the concentration of paramagnetic constituents is known.

The experimentally observed signal loss in Fe-bearing glasses is attributed to extreme broadening caused by the strong dipolar interactions between the hydrogen nuclei and nearby unpaired electron spins on the paramagnetic ion. The NMR results show that neither water molecules nor OH groups are associated preferentially with the iron ions, since such behavior would not lead to the dependence observed in Figure 3 (i.e. a straight line through the origin).

Our results demonstrate that ^{1}H NMR is a quantitative, non-destructive method for determining water contents in glasses that requires virtually no sample preparation. Based on the favorable sensitivity of high-field proton NMR, quantitation at levels as low as 0.001 wt.% H_2O should be possible. Because the background signal from the probe itself dominates at such low concentrations, we estimate that in the present study the lowest water content measurable with reliable accuracy ($\pm$ 5 %) was ca. 0.05 wt.% in a 200 mg sample.

^{1}H MAS-NMR determination of H_2O and OH species concentrations. Figure 7 compares determinations of the speciation of water in glasses obtained from ^{1}H MAS-NMR integrations of center- and sidebands with results obtained from infrared spectroscopy. The percentage of water occurring in the form of molecular H_2O determined by NMR is plotted against the corresponding values from IR results. The agreement between these independent methods is very good. One advantage of the MAS-NMR speciation is its generality. While determination of the speciation of water in glasses by infrared spectroscopy requires that the extinction coefficients for OH and H_2O species be determined by laborious calibration experiments,[3,22,23] the NMR analysis can be performed on any glass as long as the level of paramagnetic constituents is low. On the other hand, the MAS-NMR speciation procedure requires more material and is model dependent; it assumes that

the ratio of the centerband area to the total signal area in tremolite is the same as that of the OH species in the glasses, and that the corresponding ratio in analcite is identical to that of the H_2O species in the glasses. The good agreement between the calculated and experimental spinning sideband intensities (especially Figure 6a), the weak dependence of the results upon spinning speeds (between 5 and 8 kHz), as well as the compatibility of these analyses with the infrared results indicate that this assumption is justified at sufficiently high spinning speeds. Further support is provided by the ^1H MAS NMR spectrum (Figure 8) of a vitreous silica sample containing ca. 0.04 wt.% water, which is known from infrared spectroscopy to contain only OH groups. Even at a significantly lower spinning speed (3.3 kHz), the spinning sidebands in this silicate glass are extremely weak, and hardly detectable above the noise level. This is similar to the observed weak spinning sidebands in the spectrum of tremolite. The suitability of tremolite and analcite to represent OH and H_2O groups in glasses leads to interesting conclusions concerning the proximity of the hydrous species, as discussed in the next section.

For glasses containing significant levels of paramagnetic ions, the MAS-NMR sideband pattern analysis described in the Results section cannot be used to obtain the percentages of H_2O and OH species. Figure 9a shows ^1H MAS NMR spectra for two albite-orthoclase glasses containing zero and 1.27 wt.% FeO and comparable levels of H_2O. This comparison illustrates that the presence of paramagnetic iron in glasses results in more intense spinning sidebands. This sideband enhancement is also seen in the volcanic glasses of the present study (data not shown), where the experimentally observed spinning sideband intensities are much higher than expected from the spectra observed for synthetic glasses with similar water contents. A similar effect has been noted by Murdoch et al. on the ^{29}Si spectra of albitic glasses.[28] The origin of this behavior lies with the dipolar interactions between protons and unpaired electron spins, which affect the ^1H NMR lineshapes as illustrated in spectra of non-spinning samples (Figures 9b and c). The signals reveal a characteristically broadened "tent shape" in which the distinction between OH and H_2O signal components is gradually lost. Theoretical calculations reveal

that these dipolar interactions, which are inhomogeneous in character, contribute substantially to MAS-NMR spinning sideband intensities.[29]

Spatial relationships OH and H_2O species. At high spinning speeds the experimental ^1H MAS-NMR spectra of the glasses agree very well with simulated spectra obtained by adding the individual spectra of analcite and tremolite in the appropriate proportions (Figure 6a). In contrast, Figure 10 shows that no such agreement can be obtained when pyrophyllite is used instead of tremolite as the standard OH compound. (Also, an analysis of the fractional centerband areas results in much higher OH contents than indicated by the infrared results.) This comparison provides information about the spatial relationships of the OH and H_2O groups.

Studies of hydrogen-containing minerals have shown that homonuclear proton-proton interactions contribute substantially to spinning sideband intensities, if the spinning speeds are comparable to the magnitude of the interactions.[27] In tremolite the OH groups are structurally very isolated from each other (the hydrogen atoms are separated by more than 500 pm)[30], resulting in weak dipolar interactions and low spinning sideband intensities. In contrast, the closest distances between the OH groups in pyrophyllite are significantly shorter (249 pm) [31], resulting in stronger homonuclear dipolar interactions and more intense spinning sidebands.

Thus, the comparison of the experimental spectra with both simulations (Figure 10) strongly suggests that in the glasses the OH groups are structurally very distant from each other and have only weak dipolar couplings. Similarly, there is no evidence for proximity or clustering of OH and H_2O or of two or more H_2O groups. We note, however, that the question of clusters involving H_2O groups may be complicated by the fact that the dipolar interactions between these species are reduced by two-fold rotations ("flips") around the bisector axis of the water molecule, such as have been shown to occur in rhyolitic glasses.[21] This behavior might contribute to the observation that even at very high water contents (7.9 wt.% H_2O), where stronger ^1H-^1H dipolar interactions are expected purely on statistical grounds, the treatment in terms of non-interacting OH and H_2O species still appears to be valid.

Chemical Shifts and Hydrogen Bonding Strengths. Figure 11 and Table III indicate that magic angle-spinning results in substantial line-narrowing, the residual linewidths amounting to 250 Hz for vitreous silica and 800 to 1600 Hz for all the other glasses. The question of whether these linewidths arise predominantly from insufficient spinning speeds or from a distribution of isotropic chemical shifts can be addressed by measuring the residual centerband linewidths as a function of:

(a) magnetic field strength: the chemical shift (in Hz) is linearly dependent on the strength of the external magnetic field, whereas dipolar couplings are field-independent;

(b) spinning speeds: the residual linewidth of a sample generally decreases at higher spinning speeds, reaching a plateau value at a spinning speed that depends on the strength of the homonuclear dipolar couplings;

(c) isotopic dilution[32]: isotopic dilution with deuterium greatly reduces the homonuclear H-H dipolar interactions generally responsible for broadening at lower spinning speeds.

Our experimental results indicate unambiguously that the predominant source of the residual ^{1}H MAS NMR linewidths is a distribution of chemical shifts: a) on increasing the magnetic field strength from 4.7 to 11.7 T the centerband linewidth (at 8 kHz spinning speed) for both the synthetic and volcanic glasses increases in roughly the same ratio (other linebroadening factors such as field inhomogeneity and angle missetting are small and comparable for both probes); b) the linewidth of the centerband is largely independent of the spinning speed within the range 5 kHz $< \nu_{rot} <$ 8 kHz in both volcanic and synthetic glasses, suggesting that a spinning rate of 5 kHz is sufficiently rapid; c) the ^{1}H MAS NMR centerband linewidth of the residual protons in the hydrated rhyolitic glass in which 85-90 % of the dissolved water is D_2O (data not shown) is identical to that observed in corresponding non-deuterated samples.

Having demonstrated that the ^{1}H MAS NMR linewidths of these glasses are due primarily to a distribution of chemical shifts, we next consider the significance of this distribution. Experimental results[14] and theoretical calculations[33] indicate that

the ^1H chemical shifts of oxygen-bound hydrogen depend linearly on the O-H···O distance, an index of the hydrogen bond strength. Figure 12 shows this correlation using all of the available experimental data[14,15,34,35], with the exception of older data obtained by less-accurate multiple pulse methods[14]. The data are well-fitted by the equation:

$$\frac{\delta_{iso}}{ppm} = 79.05 - 0.255\frac{d(O-H\cdots O)}{pm}$$

From this function we can determine the average O-H···O distance corresponding to the chemical shift of the peak maximum, as well as the shape and width of the O-H···O distance distribution. A slightly discontinuous character in this distribution for most of the synthetic glasses with lower water contents is suggested by the observation of a distinct upfield shoulder in the spectra (see for instance Figure 11a). Similar effects have been observed in the ^1H MAS-NMR spectra of dried silica gel.[17] The fractional area of this shoulder does not appear to depend on the total water content in any systematic fashion and does not offer any means of discriminating between OH and H_2O species. We cannot exclude the possibility that this shoulder is due to surface-adsorbed water. In synthetic glasses with water contents above ca. 5 wt.% the linewidths tend to increase, possibly reflecting a contribution of homonuclear dipolar interactions. Figure 9a shows that line-broadening effects also result from the presence of iron in the glasses. Although these effects may reflect T_2 or susceptibility broadening, it is also possible that iron may influence the hydrogen bonding characteristics of water in glasses.

The average O-H···O distance, as determined from the measured isotropic chemical shifts (determined at peak maximum) in conjunction with Figure 12, amounts to 288.5-291.5 pm in the synthetic glasses, 291.5-294.5 pm in the rhyolite glasses, and 297.5 pm in silica glass. These relatively long distances are consistent with weak hydrogen bonding and are in excellent agreement with previous ^2H NMR data obtained on rhyolite glasses[21], as well as infrared measurements.[36] The isotropic chemical shifts listed in Table III show that the average O-H···O distances are essentially independent of the overall glass composition over the range we have studied as well

as the total water content. Since the percentage of molecular H_2O increases with increasing total water content, the hydrogen bonding strengths of the OH and H_2O species must be very similar, a conclusion also supported by ^2H NMR results.[21] The half-height widths of the O-H···O distance distributions, calculated from eq. [1] using the full linewidths at half height $\Delta\nu_{1/2}$ of the ^1H MAS NMR centerbands, are listed in Table III. These values contrast with those of ca. ± 20 pm obtained from infrared studies[36] and ^2H NMR.[21] We believe that this discrepancy may result from the inadequacy of eq. [1] in predicting the dependence of chemical shift on hydrogen bonding length for O-H···O distances greater than 290 pm. By analogy with the results on ^2H nuclear electric quadrupole coupling constants,[21] the chemical shifts at longer O-H···O distances may depend less strongly on this parameter. However, very few ^1H NMR chemical shift data have been reported in this range of weak hydrogen bonding strengths; such a database is needed to determine accurate and reliable distribution functions of hydrogen bonding strengths in water-containing glasses by NMR methods.

CONCLUSIONS

The present study shows that high-power ^1H solid-echo and magic angle spinning (MAS) NMR techniques can provide new insights into the bonding state of the hydrous species in glasses. The most important results are:

1. With pyrophyllite or other suitable standards, ^1H solid echo NMR provides a non-destructive, sensitive method for obtaining absolute water contents in glasses. The quantitation results agree well with those obtained by manometric methods down to a level of ca. 0.1 wt.% H_2O; analysis for lower concentrations would require further reduction of the background signal from the probe. In the presence of paramagnetic constituents, ^1H NMR underestimates the water content to an extent that depends on the iron concentration. It should be possible to use appropriate NMR calibration curves to obtain accurate values from samples with known concentrations of paramagnetic species.

2. High-speed magic angle spinning (at 5-8 kHz) results in substantial line-

narrowing and characteristic spinning sideband intensity patterns. For water-containing glasses with low levels of paramagnetic ions, the ^1H MAS-NMR spectra can be simulated as the sum of the individual MAS-NMR spectra of the model compounds tremolite (OH) and analcite (H_2O). Such simulations, as well as analyses of the fractional centerband areas in the experimental spectra can be used to obtain the percentages of OH and H_2O in hydrous glasses. The species concentrations measured by NMR and infrared methods are in good agreement.

3. The agreement of the experimental MAS-NMR spectra with simulations based on the individual spectra of compounds in which the hydrogen-bearing species are structurally isolated (OH in tremolite and H_2O in analcite), indicates that OH or H_2O groups in the glasses are not preferentially clustered.

4. The lineshape of the ^1H MAS-NMR centerbands in these glasses is governed by a continuous distribution of isotropic chemical shifts; since these shifts are correlated with the O-H···O distance, the centerband lineshape reflects the distribution function of this distance.

5. The average O-H···O distances in the glasses studied (290-293 pm) depend very little on the glass composition or the absolute water contents, implying that the hydrogen bonding characteristics of H_2O and OH species are very similar.

ACKNOWLEDGMENTS

The NMR experiments were carried out at the Southern California Regional NMR Facility at the California Institute of Technology, supported by NSF grant no. CHE 84-40137. E.M.S. acknowledges additional support by NSF grants EAR 84-17434 and EAR 86-18229. We also thank the donors of The Petroleum Research Fund, administered by the American Chemical Society, for partial support of this research (grant number 17737-AC2). We thank Professor A. L. Boettcher (University of California, Los Angeles) for assistance with preparation of some of the glasses and Drs. P. Dobson and S. Newman (Division of Geological and Planetary Sciences, California Institute of Technology) for help with the manometric analyses, which were carried out in the laboratory of Prof. S. Epstein. Thanks are also due to Prof.

David Live (Chemistry, Emory University) for stimulating discussions, to Dr. G. J. Fine and the Corning Glass Works for providing the anhydrous starting materials for several of the samples investigated and to Prof. J. R. Holloway (Chemistry, Arizona State University) for providing a water-containing rhyolite glass isotopically diluted with D_2O. Caltech Division of Geological and Planetary Sciences contribution number 4507.

REFERENCES

1. R. F. Bartholomew, *Treatise on Materials Science and Technology 22*, 75 (1982).
2. S. Newman, S. Epstein, and E. M. Stolper, *J. Volc. Geotherm. Res.*, submitted.
3. L. A. Silver and E. M. Stolper, *J. Petrol.*, submitted.
4. M. Tomozawa, *J. Noncryst. Solids 73*, 197 (1985).
5. C. W. Burnham, *Geochim. Cosmochim. Acta 31*, 1077 (1975).
6. E. B. Watson, *Earth Planet. Sci. Lett. 52*, 291 (1981).
7. E. M. Stolper, *Contrib. Miner. Petrol. 81*, 1 (1982).
8. E. M. Stolper, *Geochim. Cosmochim. Acta 46*, 209 (1982).
9. W. Müller-Warmuth, G. W. Schulz, N. Neuroth, F. Meyer, and N. Deeg, *Z. Naturforsch. 20a*, 902 (1965).
10. R. F. Bartholomew and J. W. H. Schreurs, *J. Noncryst. Solids 38/39*, 679 (1980).
11. P. S. Belton, *J. Chem. Techn. Biotechnol. 29*, 19 (1979).
12. P. J. Bray and R. Holupka, *J. Noncryst. Solids 67*, 119 (1984).
13. U. Haeberlen, *High Resolution NMR in Solids*, Academic Press New York, San Francisco, London **1976**, p. 149.
14. B. Berglund and R. W. Vaughan, *J. Chem. Phys. 73*, 2037 (1980) and references therein.
15. G. Scheler, U. Haubenreisser, and H. Rosenberger, *J. Magn. Reson. 44*, 134 (1981).
16. J. P. Yesinowski and H. Eckert, *J. Am. Chem. Soc.*, in press.

17. H. Rosenberger, G. Scheler, H. Bürger, and M. Jakob, *Colloids and Surfaces 12*, 53 (1984).

18. Preliminary results have been presented: H. Eckert, J. P. Yesinowski, and E. M. Stolper, *Eos Trans., American Geophysical Union 66*, 1139 (1985); J. P. Yesinowski and H. Eckert, poster presented at the 26th Experimental NMR Conference, Baltimore 1986.

19. G. Fine and E. M. Stolper, *Contrib. Mineral. Petrol. 91*, 105 (1985).

20. J. E. Shelby, J. Vitko, Jr., and R. E. Benner, Commun. Am. Ceram. Soc. C59 (1982).

21. H. Eckert, J. P. Yesinowski, E. M. Stolper, T. R. Stanton, and J. R. Holloway, *J. Noncryst. Solids*, in press.

22. S. Newman, E. M. Stolper, and S. Epstein, *Am. Mineral. 71*, 1527 (1986).

23. L. A. Silver, P. D. Ihinger, and E. M. Stolper, in preparation.

24. J. G. Powles and J. H. Strange, *Proc. Phys. Soc. 82*, 6 (1963)

25. G. E. Pake, *J. Chem. Phys. 16*, 327 (1948).

26. M. M. Maricq and J. S. Waugh, *J. Chem. Phys. 70*, 3300 (1979).

27. J. P. Yesinowski, H. Eckert, and G. R. Rossman, in preparation.

28. J. B. Murdoch, J. F. Stebbins, and I. S. E. Carmichael, *Am. Mineral. 70*, 332 (1985).

29. A. Nayeem and J. P. Yesinowski, in preparation.

30. F. C. Hawthorne and H. D. Grundy, *Can. Mineral. 14*, 334 (1976).

31. R. Wardle and G. W. Brindley, *Am. Mineral. 57*, 732 (1972).

32. R. Eckman, *J. Chem. Phys. 76*, 2767 (1982).

33. C. M. Rohlfing, L. C. Allen, and R. Ditchfield, *J. Chem. Phys. 79*, 4958 (1983).

34. H. Rosenberger and A. R. Grimmer, *Z. Anorg. Allg. Chem. 448*, 11 (1979).

35. C. I. Ratcliffe, J. A. Ripmeester, and J. S. Tse, *Chem. Phys. Lett. 120*, 427 (1985).

36. E. M. Stolper, R. D. Aines, and G. R. Rossman, in preparation.

Glass	SiO_2	Al_2O_3	Na_2O	K_2O	CaO	FeO
A	68.74	19.44	11.82			
	(68.04)	(19.97)	(11.60)	(0.18)	(0.17)	(0.03)
O	64.76	18.32	16.92			
	(65.19)	(17.84)	(16.97)	(0.01)	(0.00)	(0.01)
AO	66.41	18.76	5.70	8.67		
	(67.77)	(18.11)	(5.65)	(8.42)	(0.00)	(0.01)
AO	65.64	18.55	5.64	8.57		1.04
	(67.01)	(18.45)	(5.52)	(8.46)	(0.01)	(0.63)
AO	64.86	18.34	5.57	8.47		2.08
	(66.68)	(18.38)	(5.30)	(8.21)	(0.01)	(1.41)
ASW	62.35	14.40			23.25	
	(63.02)	(13.92)	(0.33)	(0.02)	(22.66)	(0.03)
R	(77.50)	(12.50)	(3.90)	(4.80)	(0.53)	(1.00)

Table I. Nominal compositions of the glass systems under study. Numbers in parentheses denote compositions determined by electron probe microanalysis. A = albite, O = orthoclase, AO = albite-orthoclase, ASW = anorthite-silica-wollastonite eutectic, R = rhyolite.

Glass	Pressure (kbar)	Temp. (°C)	Time (min)	% H_2O manom.	% H_2O NMR
A	20	1400	140	0.96	1.05
	20	1400	140	1.04	0.99
	20	1400	140		2.22
	15	1225	120	2.97	2.97
	15	1100	120	4.76	4.60
	20	1400	140	5.59	5.82
O	20	1450	90	0.96	1.01
	20	1400	05		1.50
	20	1450	90		1.87
	20	1450	90	1.93	1.92
	20	1450	90	2.53	2.62
	15	1450	110		3.32
	20	1450	120	4.72	4.66
	15	1400	150		5.95
	20	1450	120		6.33
	20	1450	120	7.10	8.42
AO	15	1400	120	7.39	7.89
	20	1400	120	7.05	6.16[a]
	20	1400	120	8.11	5.90[b]
ASW	20	1450	120	0.67	0.73
	20	1450	120	0.99	1.06
	20	1450	120	1.76	1.73
	20	1450	120		6.96
	15	1400	120	7.93	7.87
	15	1400	120	8.82	8.76
R[c]				0.12	0.08
				0.41	0.27
				0.55	0.35
				0.69	0.45
				0.78	0.49
				1.52	0.90
				1.72	1.19
				2.02	1.33
				2.26	1.33
				2.56	1.65

[a] 0.58 wt.% FeO
[b] 1.27 wt.% FeO
[c] all rhyolites contain 0.96 to 1.04 wt.% FeO.

Table II. Synthesis conditions and water contents of the glasses under study.

Table III.

200.27 MHz ^{1}H NMR results for the glasses studied by both solid echo and MAS-NMR. T_2^* is the deay time of the solid echo, δ_{iso} is the chemical shift with respect to TMS determined by MAS-NMR, $\Delta\nu_{1/2}$ is the full width at half height of the MAS-NMR centerband, which was used to calculate Δd(O-H···O), the distribution of O-H···O distances about the mean value (see text). H_2O/OH ratios determined by infrared spectroscopy and two MAS-NMR procedures are given in terms of weight percent H_2O for both species (see text). A = albite, O = orthoclase, AO = albite-orthoclase, ASW = anorthite-silica-wollastonite eutectic, R = (volcanic) rhyolite.

TABLE III

Sample	Total Water Content % H_2O[a]	T_2^* / s	δ_{iso} / ppm (± 0.2 ppm)	$\Delta\nu_{\frac{1}{2}}$ / Hz (± 20 Hz)	Δd(O-H···O) / pm	Ratio H_2O/OH		
						NMR Sideband Intensities	NMR Integration	IR
SiO_2	c.a. 0.04		3.2	250	± 2.5	0/100	0/100	0/100
A	2.22[b]		4.8	950	± 9.3	37.1/62.9	40.4/59.6	33.8/66.2
	2.97	52.0 ± 0.6						
	4.76	42.0 ± 0.8	5.1	1280[c]	± 12.6		57.1/42.9[c]	55.6/44.4
	5.59[d]	39.9 ± 0.5	5.3	1140	± 11.2	46.1/53.9	54.9/45.1	61.5/38.5
O	0.96	43.1 ± 0.4	4.8	900[c]	± 8.8		23.1/76.9[c]	20.0/80.0
	1.50[b]		4.6	840	± 8.2	34.3/65.7	32.8/67.2	30.0/70.0
	1.87[b]		4.7	900	± 8.8	32.4/67.6	36.7/63.3	35.3/64.7
	1.96		4.7	920	± 9.0	32.9/67.1	41.2/58.8	35.8/64.2
	2.53	50.4 ± 0.5	4.7	920	± 9.0	45.0/55.0	48.1/51.9	42.6/57.4
	3.32[b]	55.1 ± 0.6	5.1	1100	± 10.8	45.3/54.7	48.4/51.6	51.2/48.8
	5.95[b,d]	44.3 ± 0.6	4.8	1200	± 11.8	46.1/53.9	54.1/45.9	67.2/32.8
AO	7.39	35.6 ± 0.3	5.0	1630	± 16.0[e]	56.7/43.3	59.1/40.9	71.9/28.1
	8.11	22.4 ± 0.3	5.6	2200	[f]	[f]	[f]	[f]
ASW	0.99						18.9/81.1[c]	11.7/88.3
	7.93	32.5 ± 0.3	5.2	1050[c]	± 10.3	63.5/36.5	67.3/32.7	69.6/30.4
	8.82	40.1 ± 0.9	4.8	1660	± 16.3[e]			
R	0.69	49.0 ± 2.0	4.3	1610	[f]	[f]	[f]	
	0.78		4.2	1410	[f]	[f]	[f]	
	1.25		4.3	1680	[f]	[f]	[f]	
	2.26	36.8 ± 1.0	4.3	1550	[f]	[f]	[f]	
Pyrophyllite	4.98	46.8 ± 0.6	2.3	850	[e]			
Tremolite		53.8 ± 1.8	0.7	320	[e]			
Analcite		46.2 ± 1.3	3.1	1270	[e]			
Gypsum		21.7 ± 0.2	5.3	3200	[e]			

Notes: a. By H_2 manometry, error ± 3 %
b. By NMR, error ± 5 %
c. determined at spinning speeds less than 5k Hz
d. samples with inhomogeneous distribution of water
e. linewidth partly determined by homonuclear dipole coupling
f. determination precluded by effects of paramagnetic Fe(II) and Fe(III)

Figure Captions:

Figure 1a

Solid echo ^{1}H NMR spectra at 200.27 MHz of orthoclase glasses with different water contents determined by H_2 manometry. Refocusing delay 8 μs, recycle delay 60 s, 64 scans; Lorentzian linebroadening 100 Hz.

Figure 1b

Solid echo ^{1}H NMR spectra at 200.27 MHz of albite glasses with different water contents determined by H_2 manometry. Refocusing delay 8 μs, 64 scans, recycle delay 60 s; Lorentzian linebroadening 100 Hz.

Figure 2

T_2^* decay curve (^{1}H NMR at 200.27 MHz) of an orthoclase glass containing 2.6 wt.% H_2O, recycle delay 60 s. The integrated area (arbitrary units) of the echo signal is plotted against the refocusing delay of the solid-echo pulse sequence. The data are fitted by a Lorentzian decay curve with $T_2^* = 50.4 \pm 0.5$ μs.

Figure 3

Water content determined by solid echo ^{1}H NMR at 200.27 MHz versus water content determined by manometric analysis (see text). The solid line represents the identity. The dashed line is a guide to the eye for the natural rhyolitic glasses.

Albite composition

Orthoclase composition

Albite-orthoclase composition

0.01 wt.% FeO

0.58 wt.% FeO

1.27 wt.% FeO

ASW composition

Volcanic rhyolite glasses

Pyrophyllite (standard)

Figure 4

^{1}H MAS-NMR spectra at 200.27 MHz of water-containing glasses. Spinning speed 8.0 kHz. 45° pulse, recycle delay 10 s, 64 scans, linebroadening 50 Hz.

a) Orthoclase glass containing 1.50 wt.% H_2O

b) Orthoclase glass containing 2.53 wt.% H_2O

c) Anorthite-silica-wollastonite glass containing 7.93 wt.% H_2O

Figure 5

^{1}H MAS-NMR spectra at 200.27 MHz of model compounds. Spinning speed 8.0 kHz. 45° pulse, recycle delay 10 s, 32 scans; linebroadening 50 Hz.

top: Tremolite, $Ca_2Mg_5Si_8O_{22}(OH)_2$,

bottom: Analcite, $NaAlSi_2O_6 \cdot H_2O$.

Figure 6

^{1}H MAS-NMR (200.27 MHz) spinning sideband peak heights (in arbitrary intensity units) for the three glasses of Figure 4. Solid lines represent experimental results, crosses are heights predicted by additive superposition of the experimental spectra of analcite and tremolite. The centerbands (not shown) have been scaled to identical heights for all figures.

a) spinning speed 8.0 kHz

b) spinning speed 7.0 kHz

c) spinning speed 5.0 kHz.

Figure 7

Percentage of water present as molecular H_2O determined by analyzing the fractional ^{1}H MAS-NMR (200.27 MHz) centerband area versus percentage of water present as molecular H_2O determined by infrared methods (see text). Symbols as in Figure 3.

Figure 8

200.27 MHz ^{1}H MAS-NMR spectrum of vitreous silica containing 0.04 wt.% H_2O. Inversion recovery experiments were used to separate the signal of the sample from probe background absorption. The negative excursion in the baseline arises from

the probe background, which remains unaffected by the inversion recovery sequence. Recycle delay 600 s, 32 scans. Spinning speed 3.3 kHz.

Figure 9

Influence of iron content upon the 200.27 MHz ^{1}H NMR spectra of water-containing glasses.

a) ^{1}H MAS-NMR spectra of synthetic albite-orthoclase glasses, 45° pulse, recycle delay 10 s (5 s for iron-containing glass), 64 scans.

top: 8.10 wt.% H_2O, 1.27 wt.% FeO;

bottom: 7.39 wt.% H_2O, 0.01 wt.% FeO.

b) ^{1}H solid echo NMR spectra of synthetic albite-orthoclase glasses. 90° pulse length 1.9 μs, refocusing delay 8 μs, recycle delay 60 s, 64 scans, line-broadening 50 Hz.

From top to bottom: 8.10 wt.% H_2O, 1.27 wt.% FeO; 7.05 wt.% H_2O, 0.58 wt.% FeO; 7.39 wt.% H_2O, 0.01 wt.% FeO.

c) ^{1}H solid echo NMR spectra of volcanic rhyolite glasses. 90° pulse length 2.0 μs, refocusing delay 8 μs, recycle delay 1 s, 64 scans.

Figure 10

^{1}H MAS-NMR (200.27 MHz) spinning sideband peak heights for an orthoclase glass containing 1.5 wt.% H_2O at 8.0 kHz spinning speed. Solid lines represent experimental results, crosses and circles are heights experimentally and predicted by additive superposition of the experimental spectra of analcite and

tremolite,

pyrophyllite.

The centerbands (not shown) have been scaled to the same heights in all three cases. Note the significantly better fit to the data when the tremolite spectrum is used to simulate the spectrum.

Figure 11

200.27 MHz ^{1}H MAS-NMR centerband lineshapes for three water containing glasses:

(a) orthoclase glass, containing 1.50 wt% H_2O

(b) orthoclase glass, containing 2.53 wt.% H_2O

(c) anorthite-silica-wollastonite glass, containing 7.93 wt.% H_2O

Figure 12

^1H NMR isotropic chemical shifts vs. O-H···O distance, using literature data for crystalline compounds.[15,34,35] The solid line represents the least squares fit to the data.

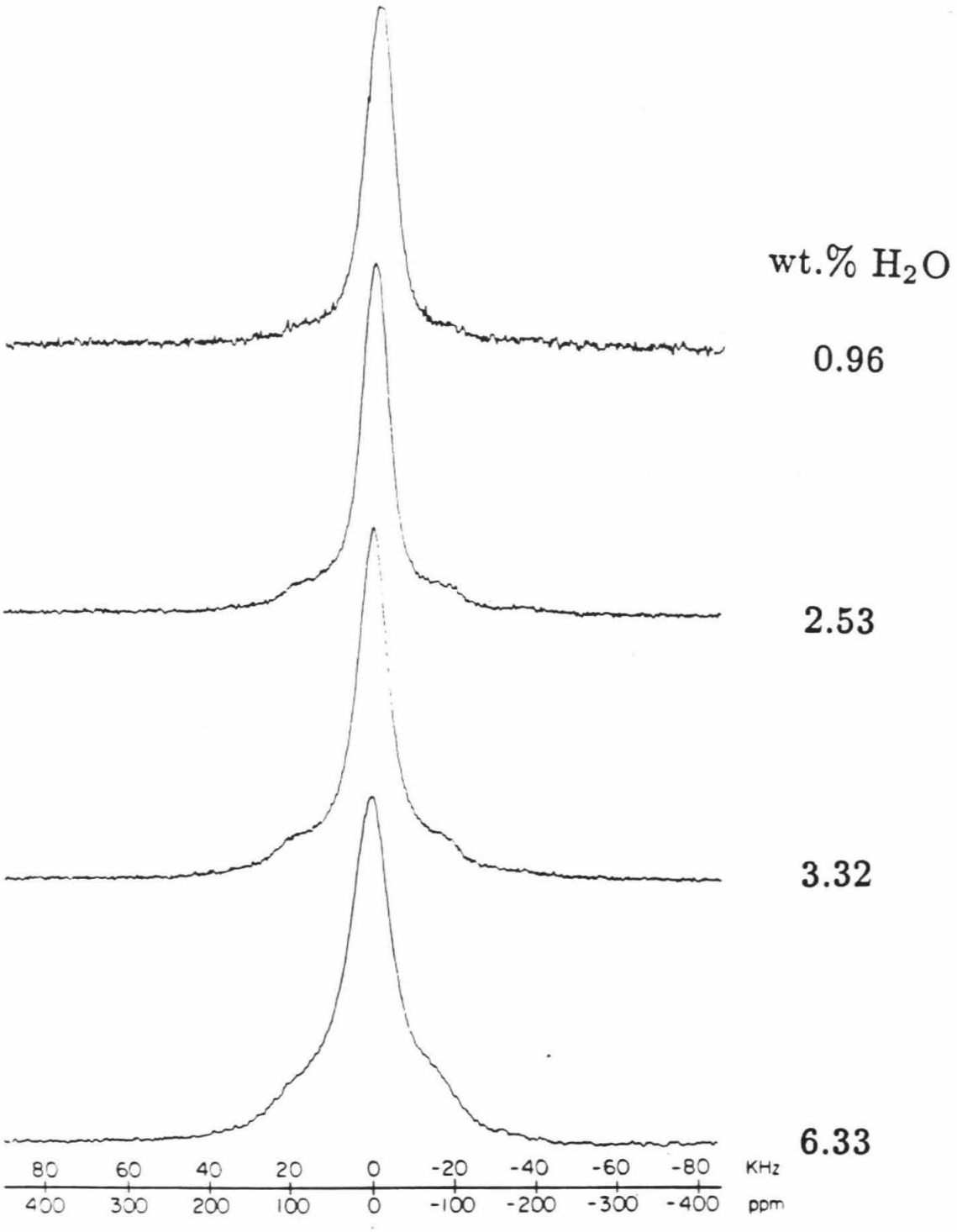
wt.% H_2O
0.96
2.53
3.32
6.33
80 60 40 20 0 -20 -40 -60 -80 KHz
400 300 200 100 0 -100 -200 -300 -400 ppm

Figure 1a

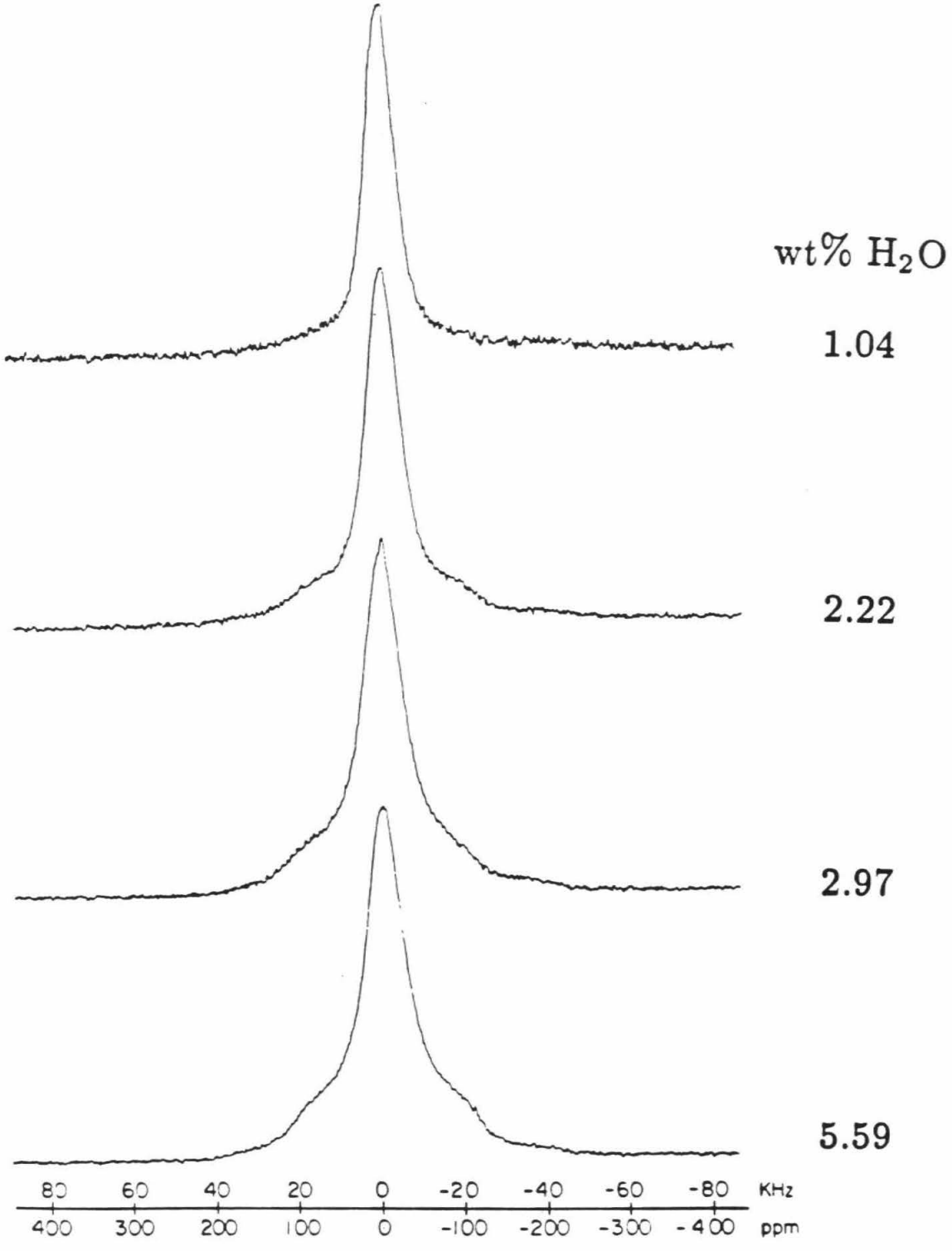
wt% H_2O
1.04
2.22
2.97
5.59
80 60 40 20 0 -20 -40 -60 -80 KHz
400 300 200 100 0 -100 -200 -300 -400 ppm

Figure 1b

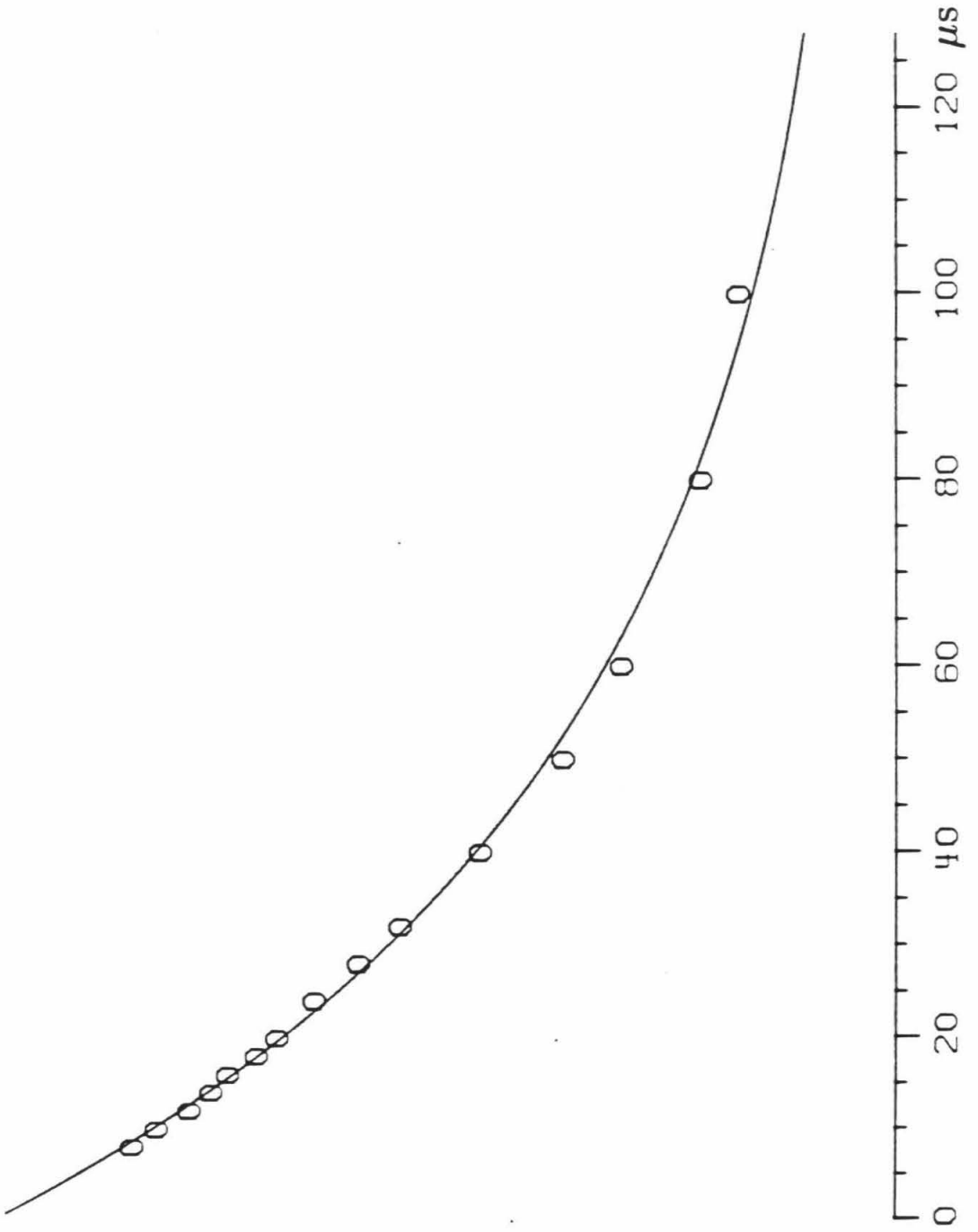

Figure 2

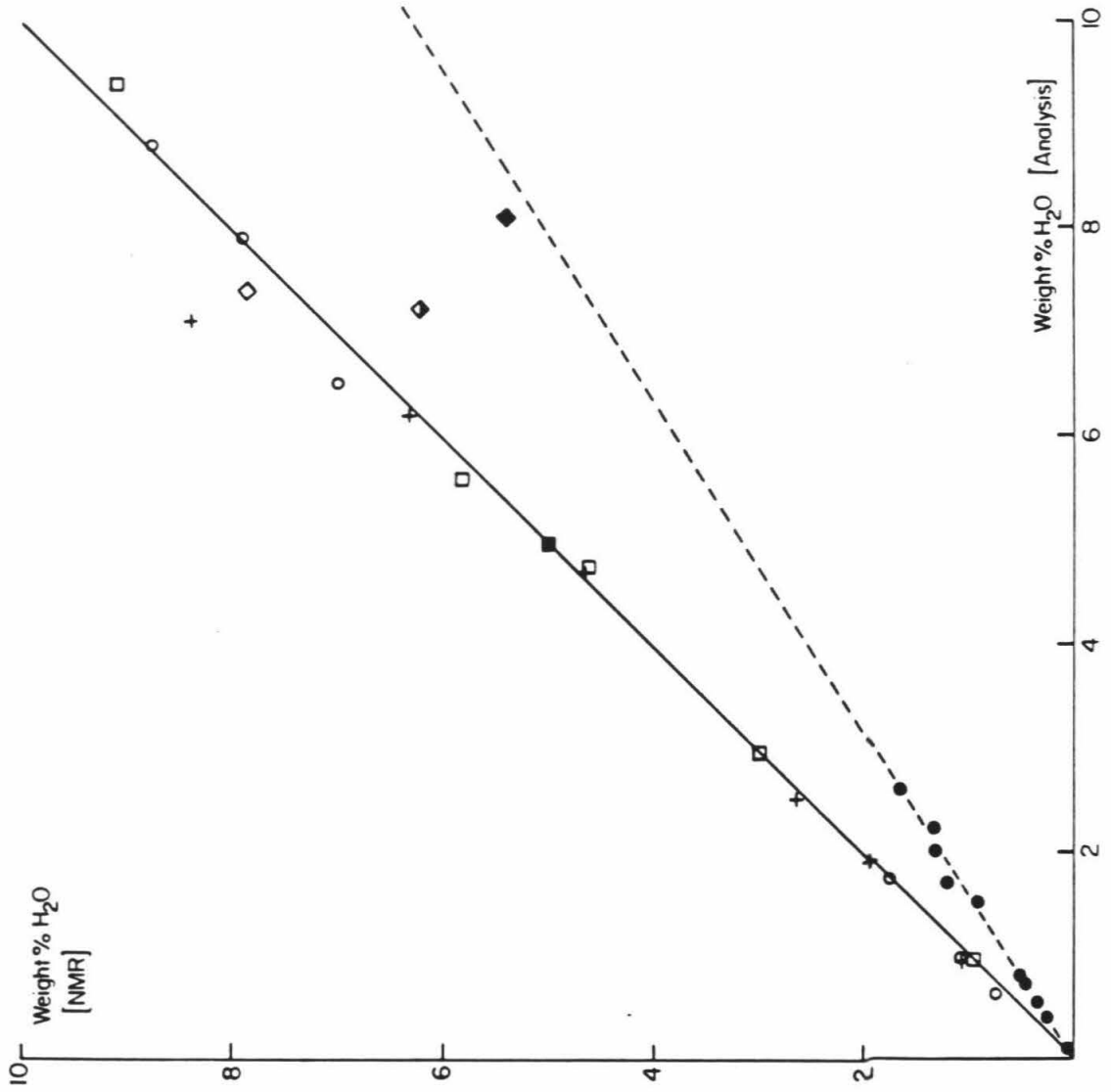

Figure 3

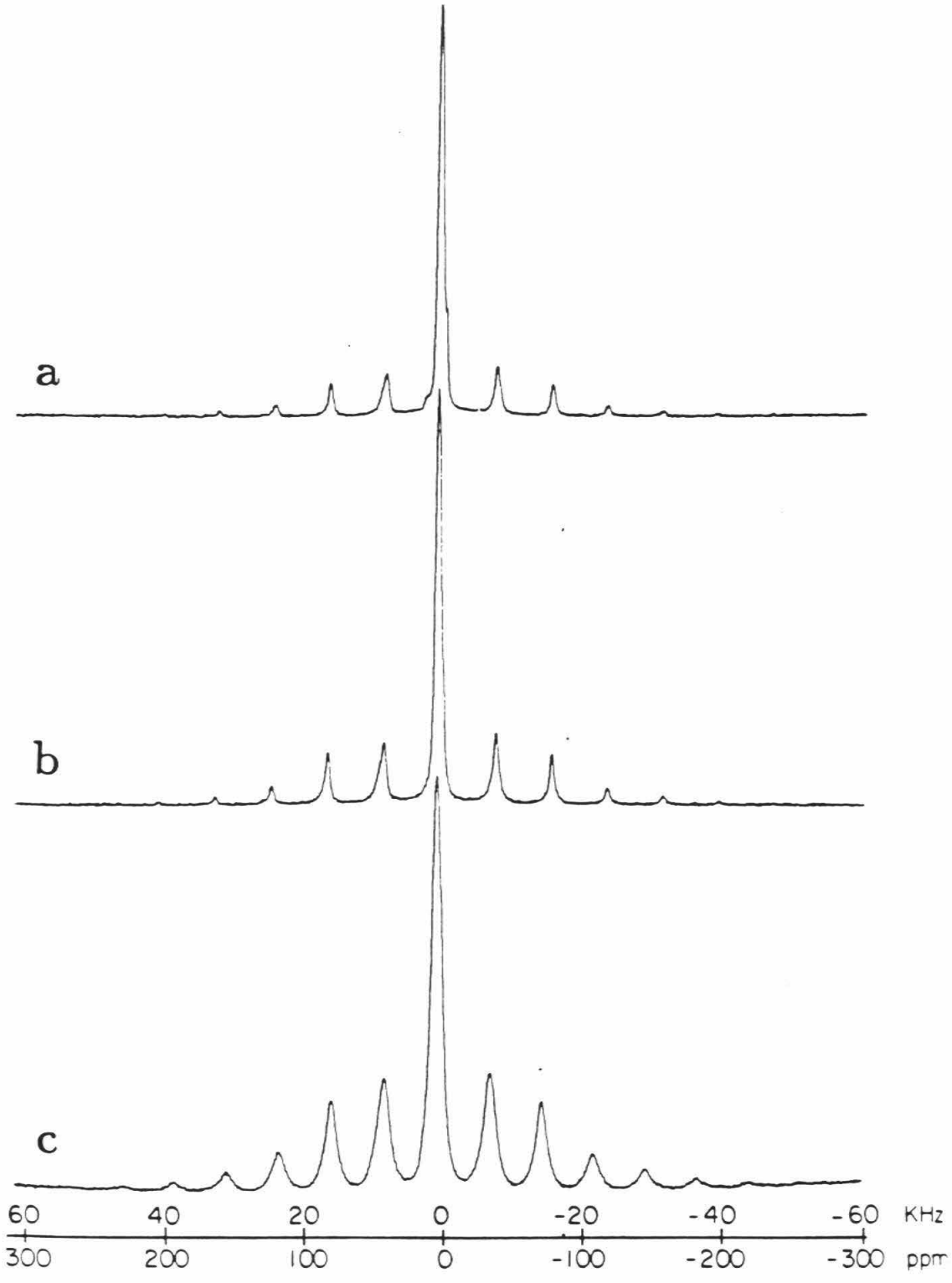

Figure 4

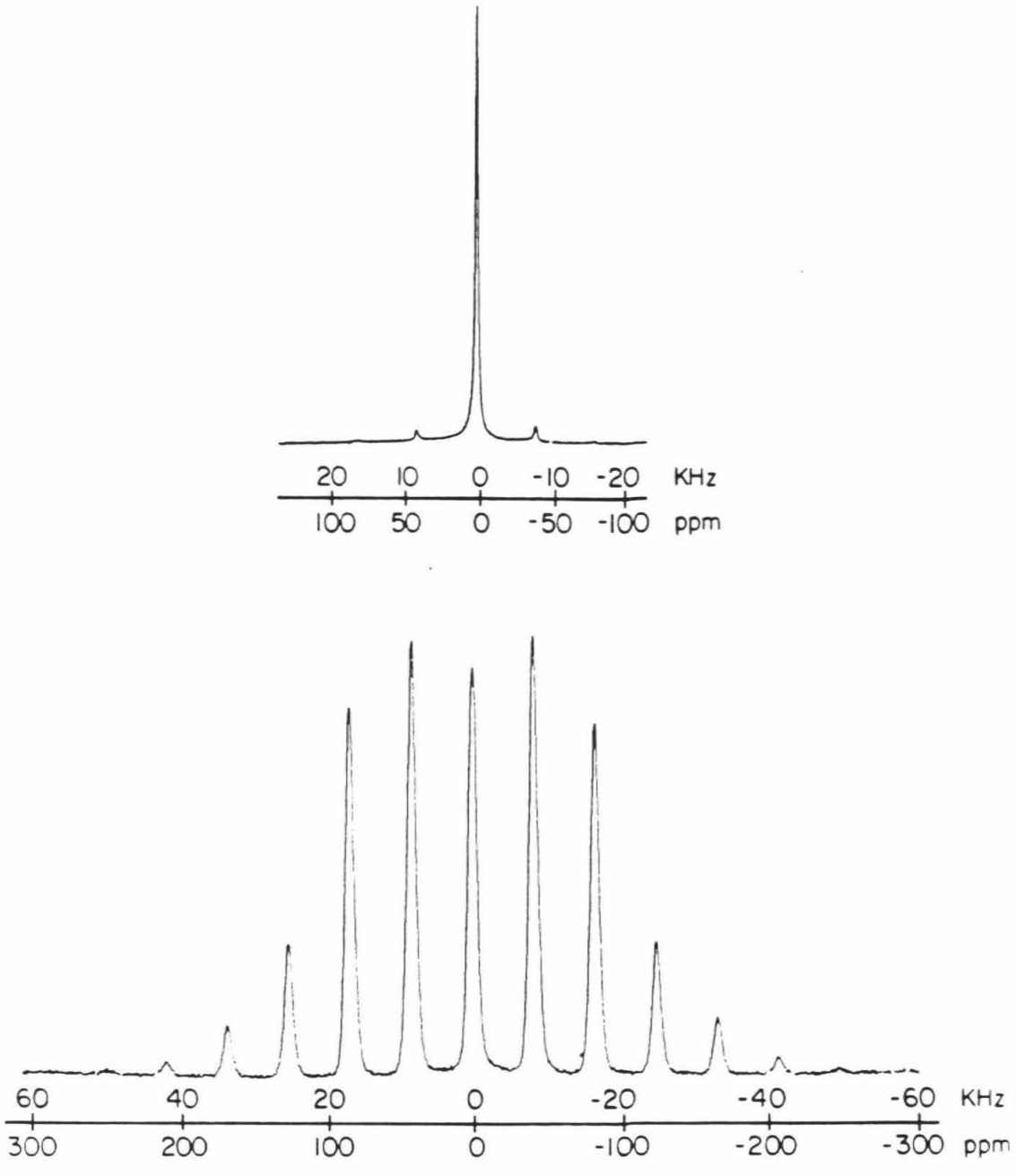
20 10 0 -10 -20 KHz
100 50 0 -50 -100 ppm
60 40 20 0 -20 -40 -60 KHz
300 200 100 0 -100 -200 -300 ppm

Figure 5

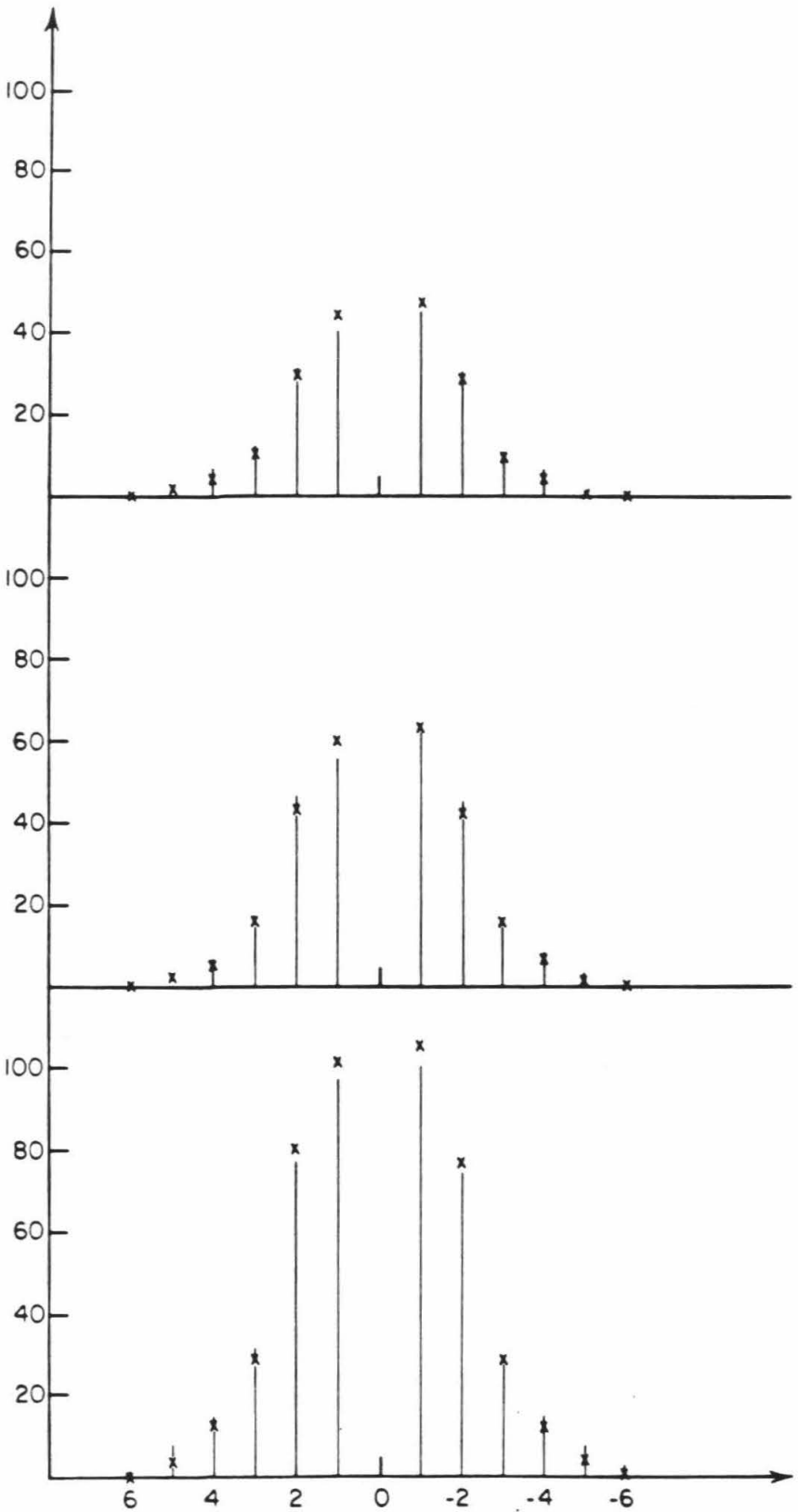

Figure 6a

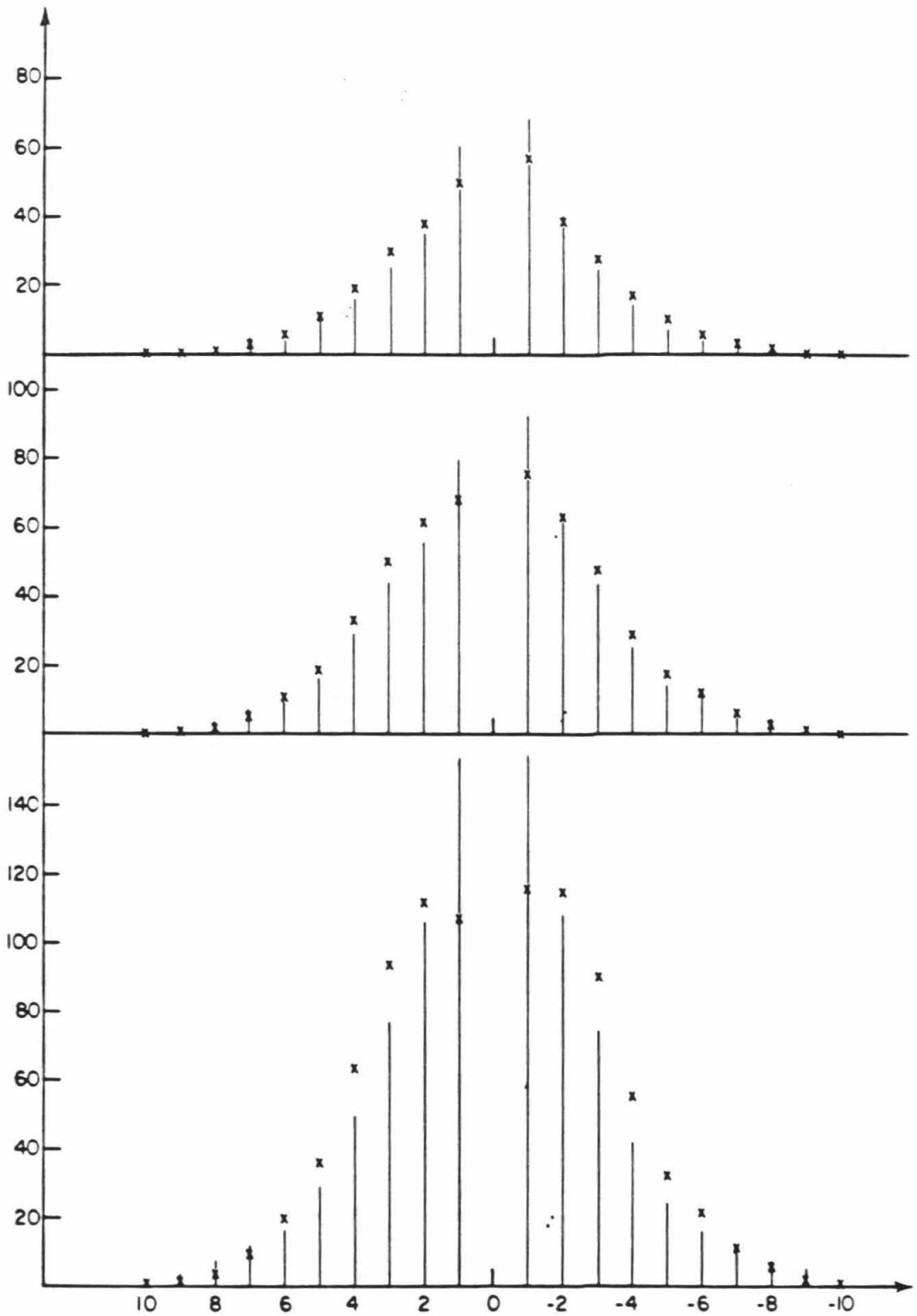

Figure 6b

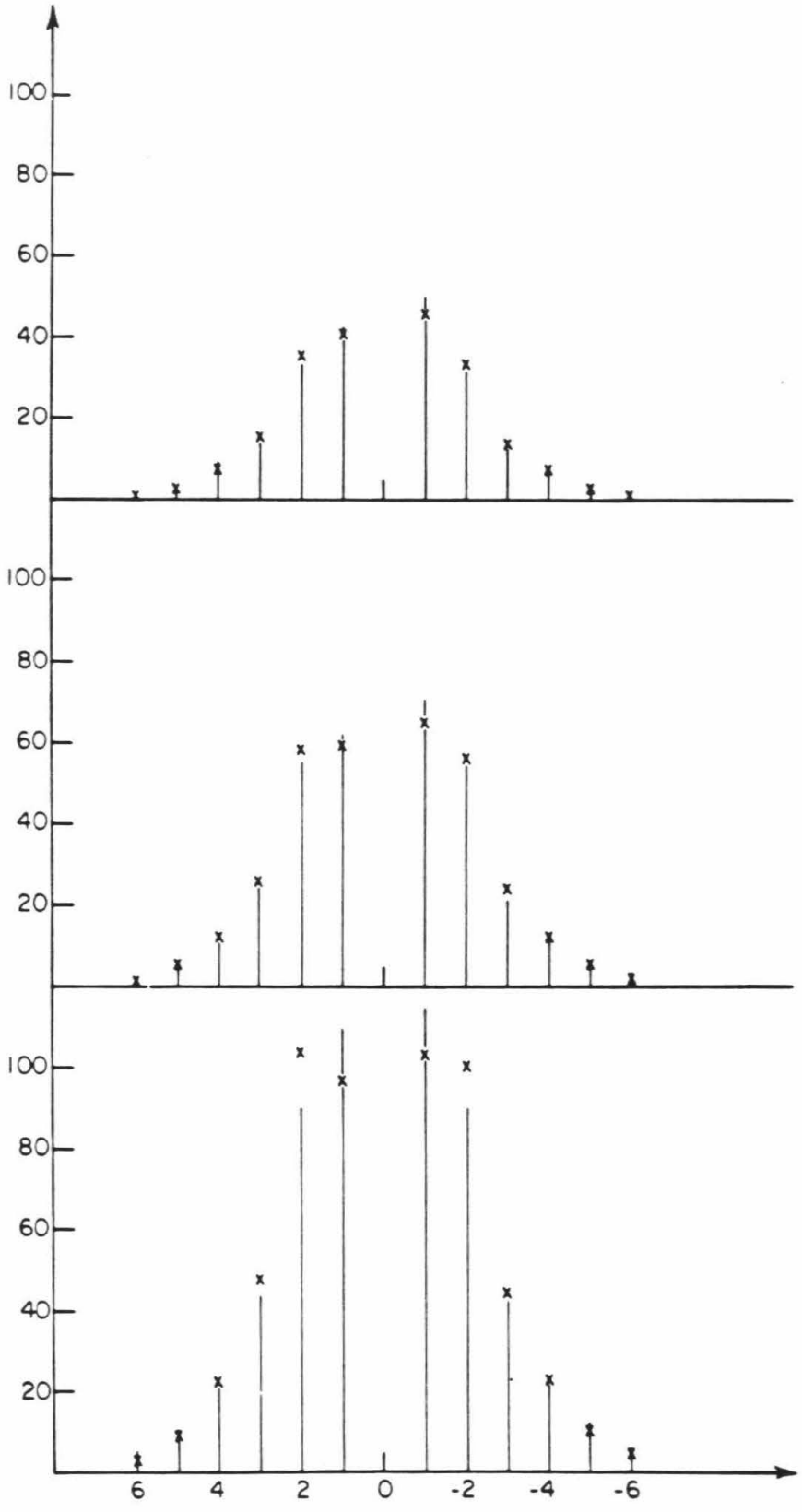

Figure 6c

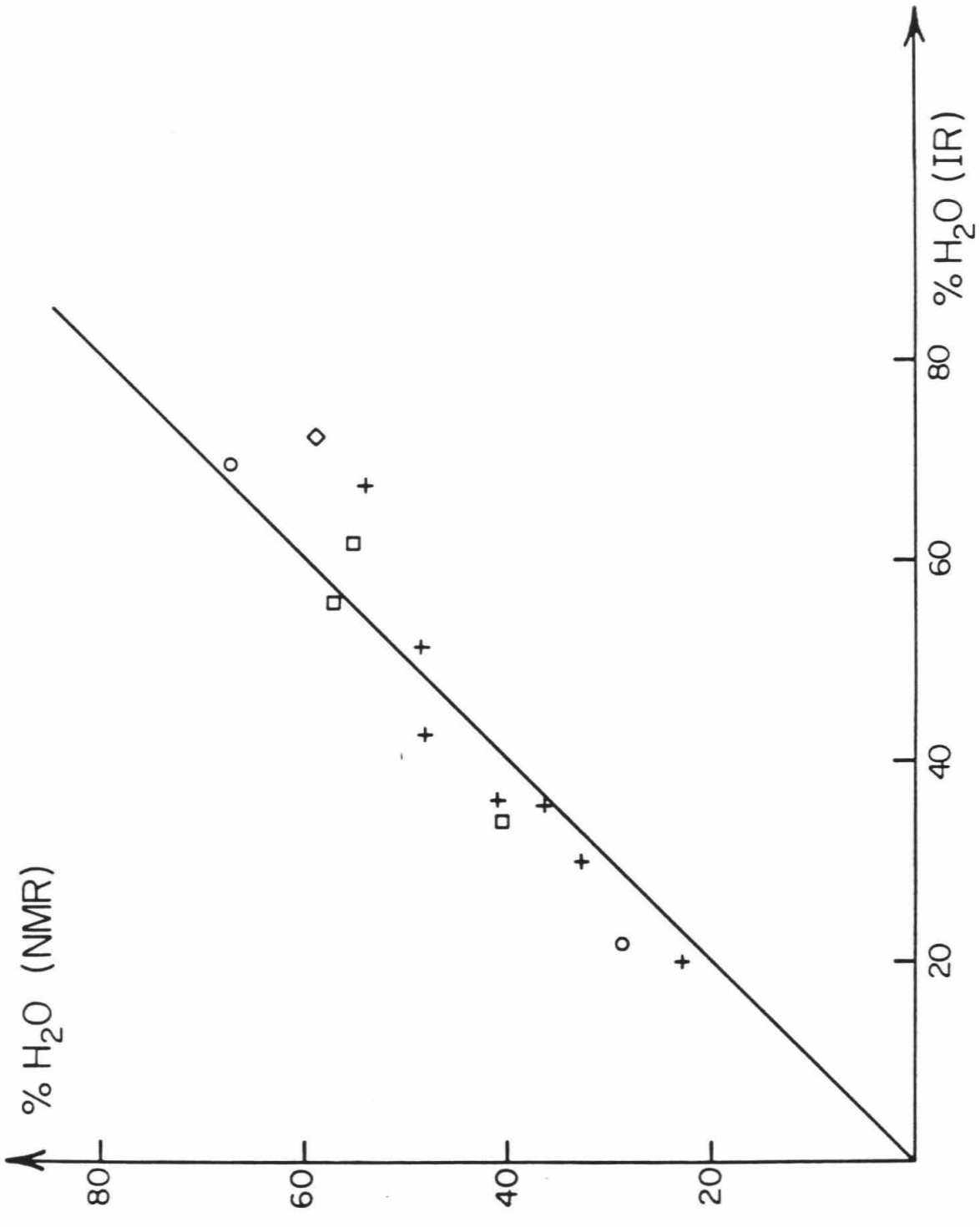

Figure 7

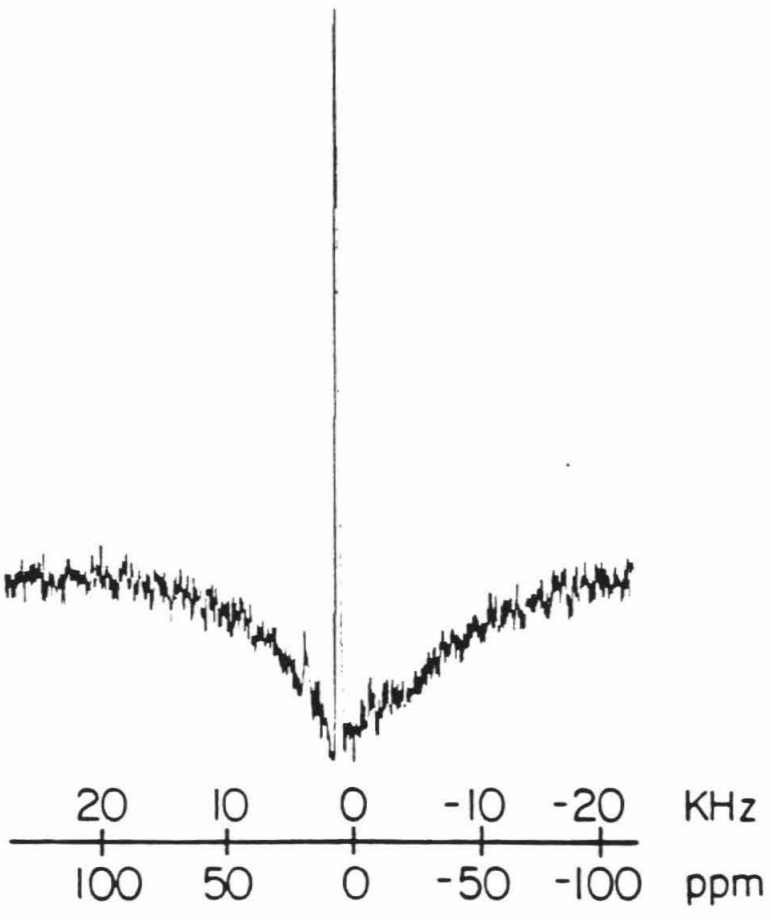

Figure 8

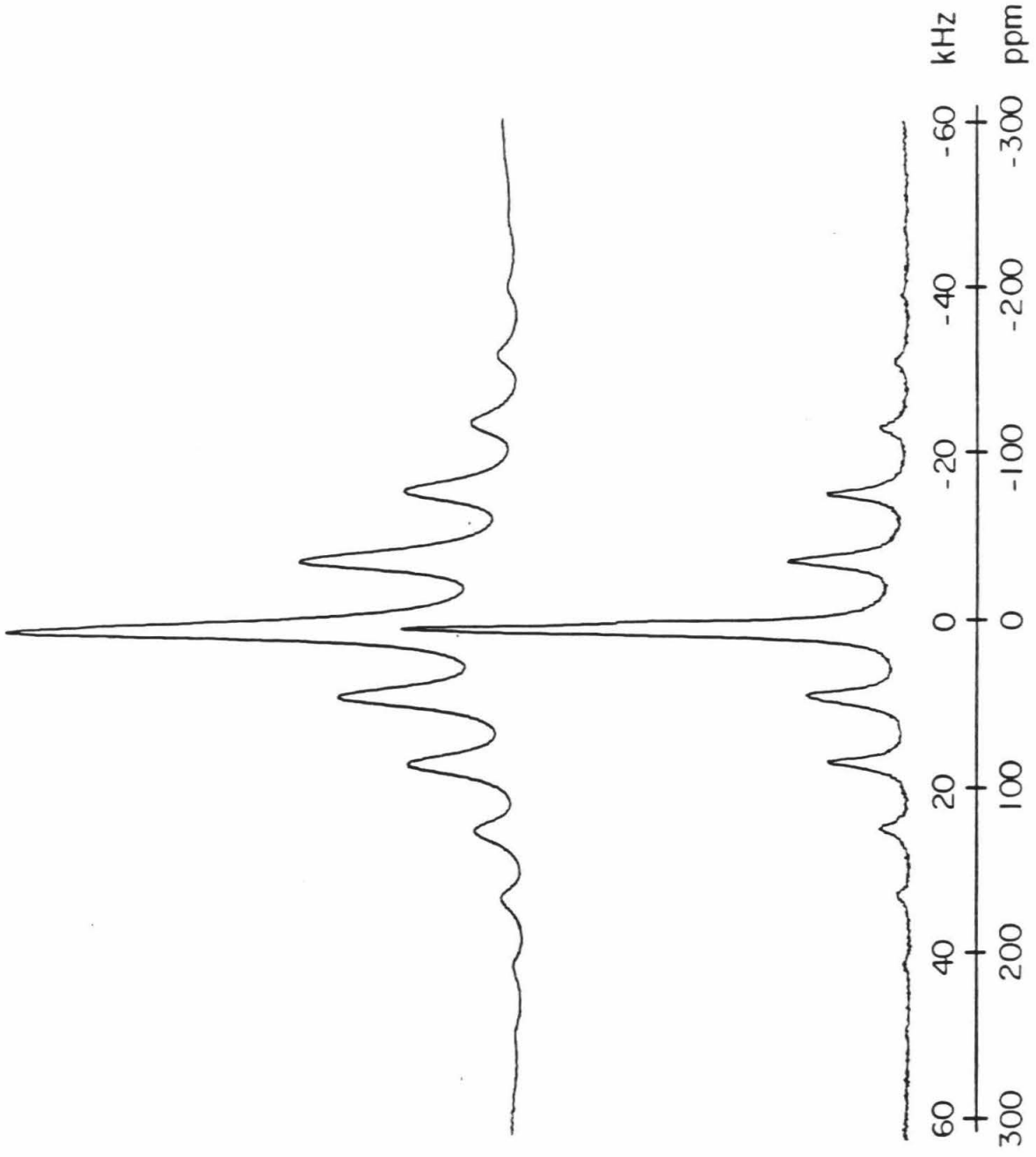

Figure 9a

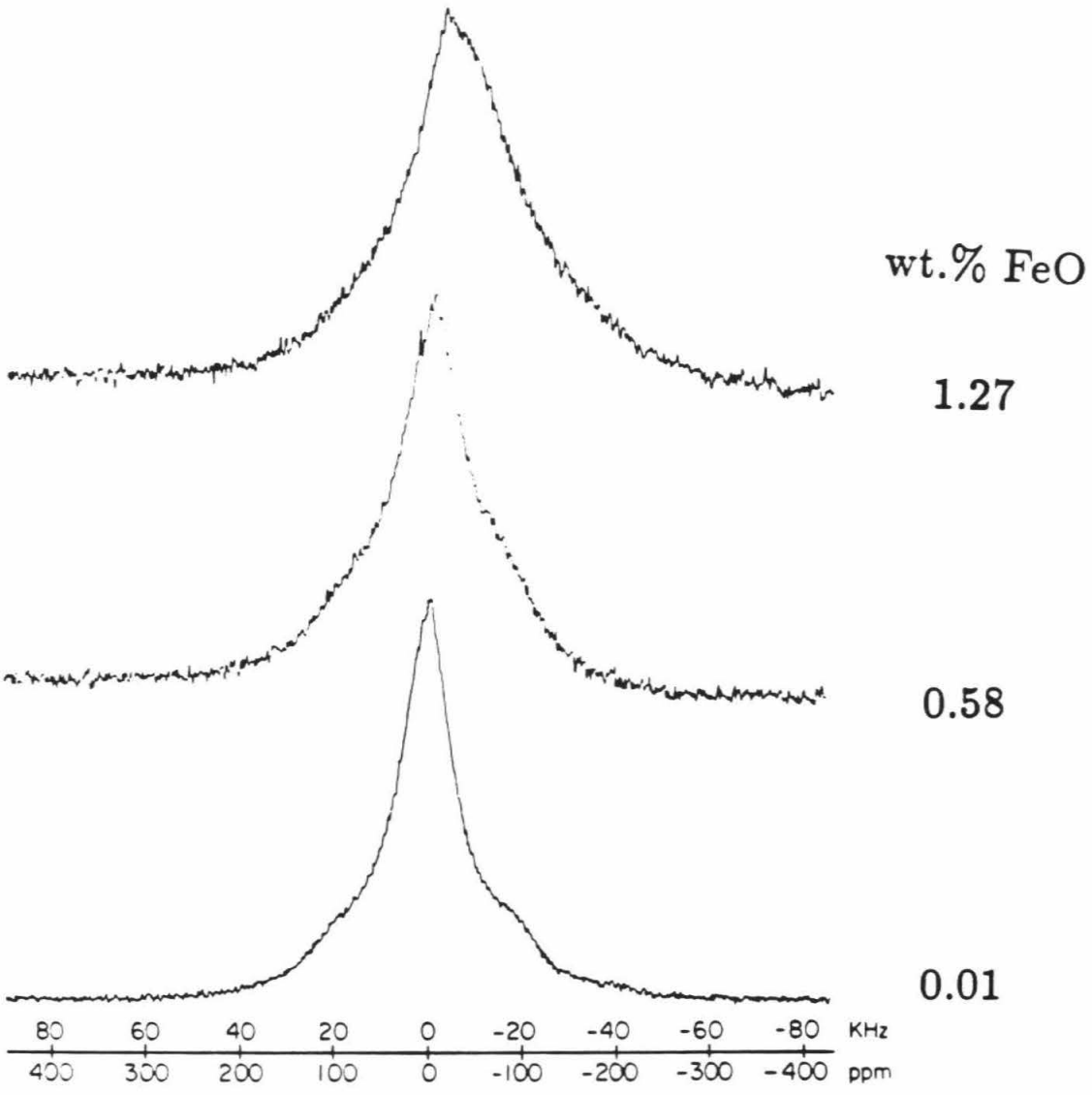
wt.% FeO
1.27
0.58
0.01
80 60 40 20 0 -20 -40 -60 -80 KHz
400 300 200 100 0 -100 -200 -300 -400 ppm

Figure 9b

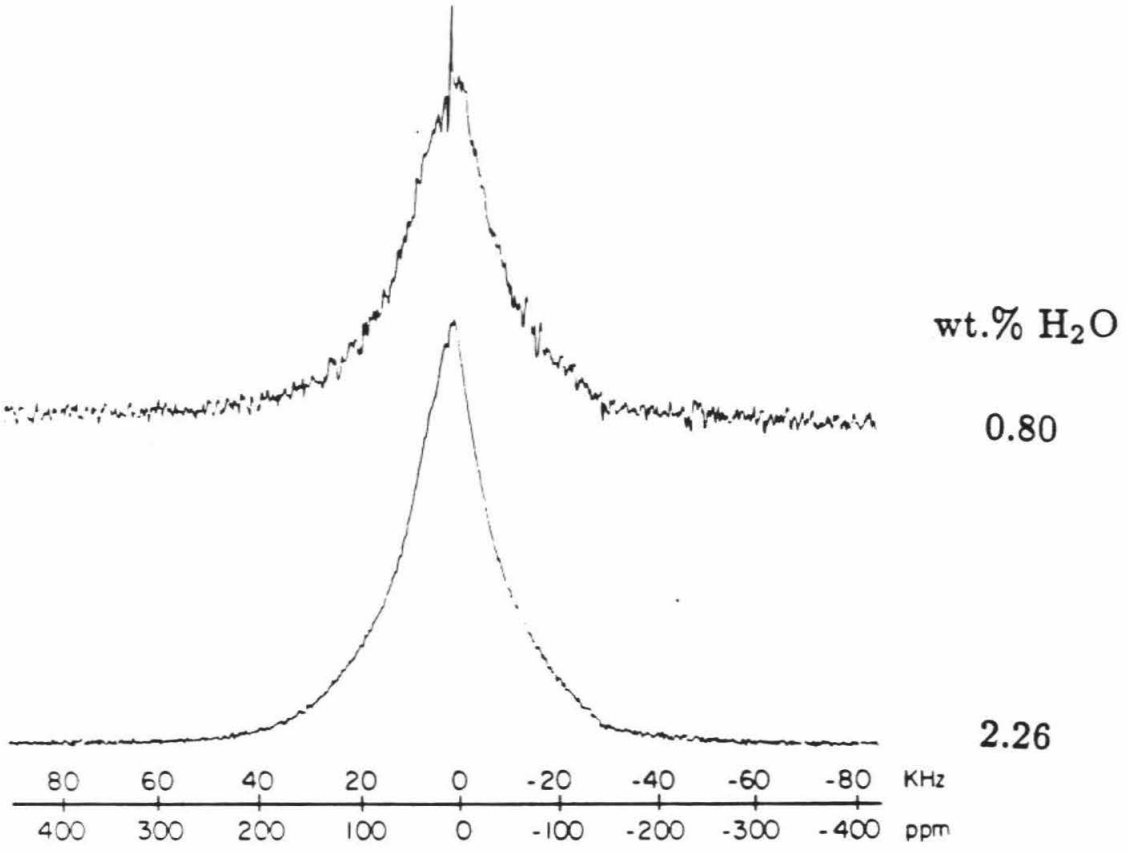
wt.% H_2O
0.80
2.26
80 60 40 20 0 -20 -40 -60 -80 KHz
400 300 200 100 0 -100 -200 -300 -400 ppm

Figure 9c

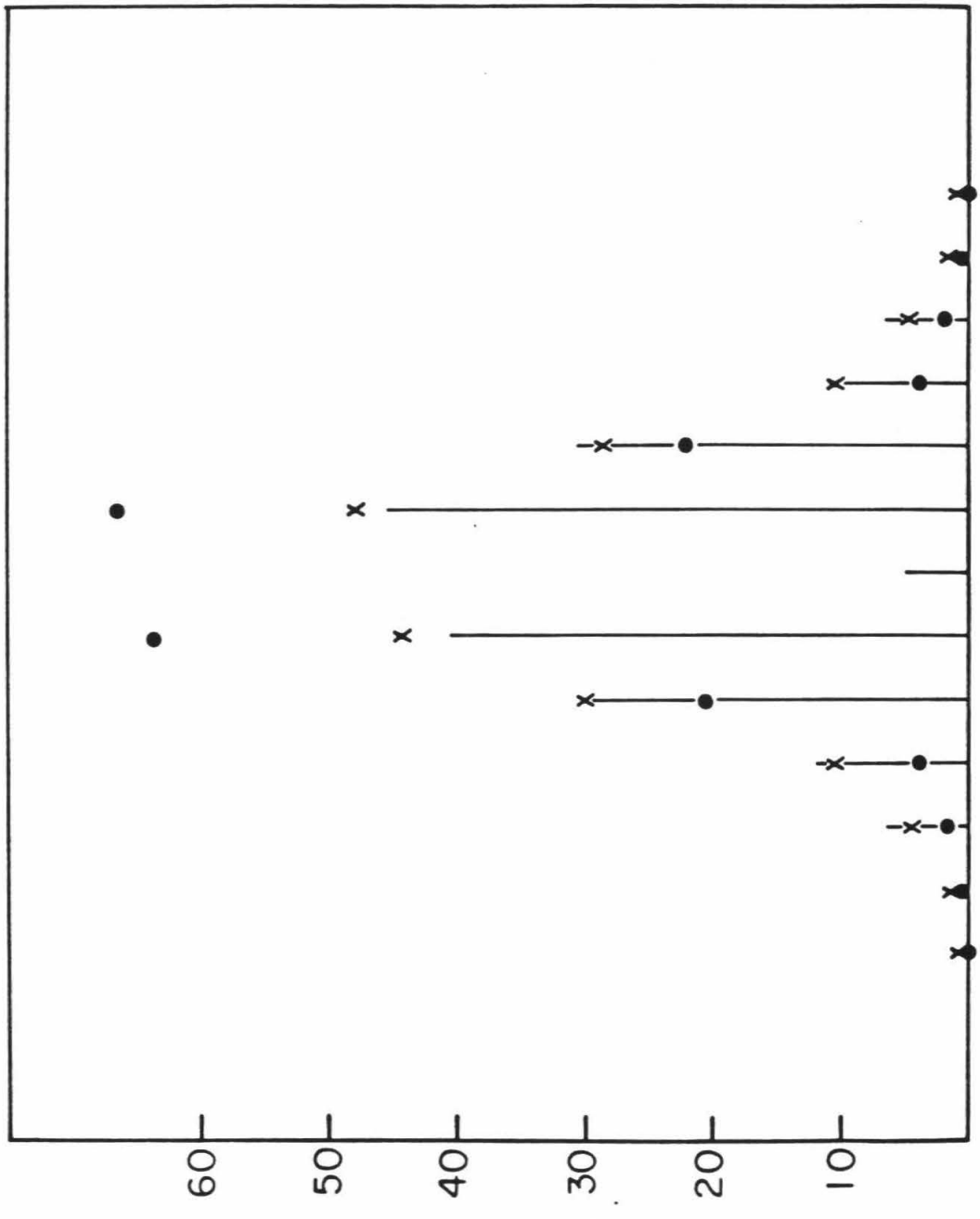

Figure 10

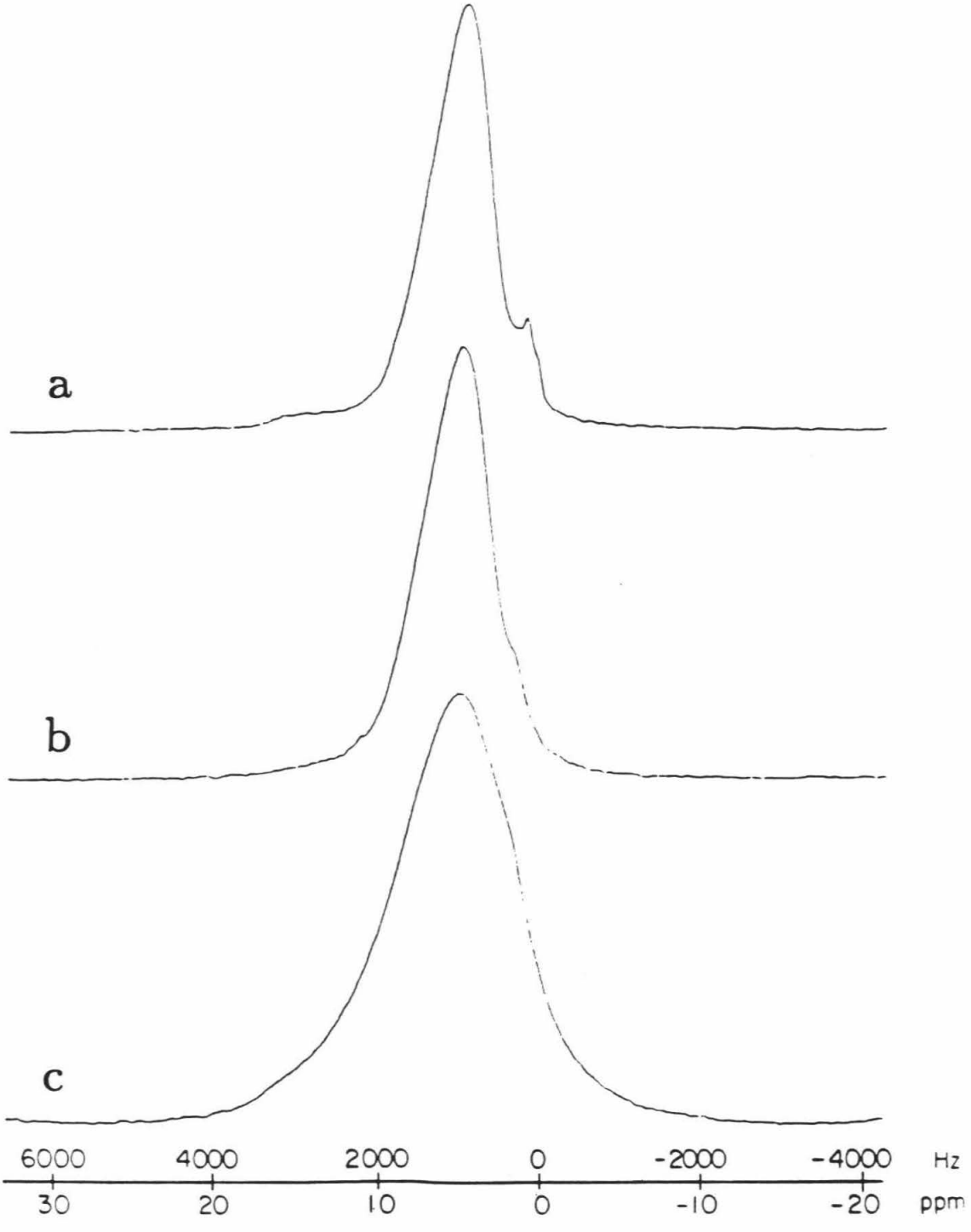

Figure 11

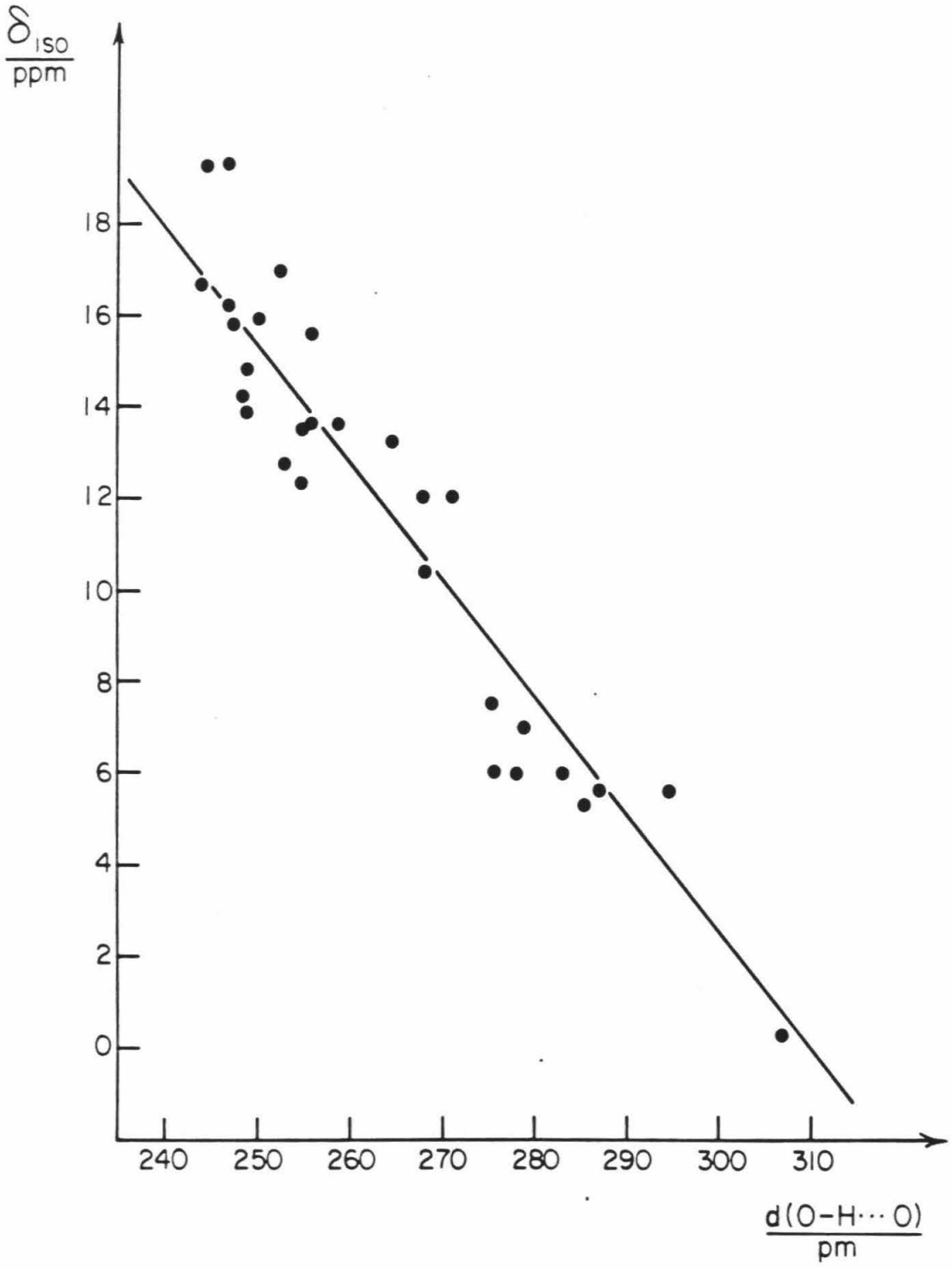
δ iso
ppm
18
16
14
12
10
8
6
4
2
0
240
250
260
270
280
290
300
310
d(O-H··· O)
pm

Figure 12